Development of Improved Connection Details for Voided Slab Bridges

Patrick C. Joyce

Thesis submitted to the faculty of the Virginia Polytechnic Institute and State University in partial fulfillment of the requirements for the degree of

MASTER OF SCIENCE

in

CIVIL ENGINEERING

Thomas E. Cousins, Chair

Carin L. Roberts-Wollmann

Ioannis Koutromanos

May 5, 2014

Blacksburg, VA

Keywords: Voided Slab, Sub-Assemblage, Shear Key, Fiber Reinforced Concrete

Development of Improved Connection Details

for Voided Slab Bridges

Patrick C. Joyce

ABSTRACT

Adjacent voided slab bridges (AVSB) are economical systems for short spans. They provide the advantages of having low clearances due to their small section depths, accelerated construction times, and high torsional stiffness. The current longitudinal connection detail, a partial depth grouted shear key, has been known to fail in many of these bridges. The failure leads to reflective cracking in the wearing surface which allows chloride laden water to seep down through the joint, where it corrodes the reinforcement and prestressing strand. Ultimately, the failed keys lead to costly repairs and bridge replacements sooner than their proposed lifespan.

This research project aimed to develop a more durable longitudinal connection detail by using sub-assemblages to test five alternate connections. The objective was to find a connection that abated all cracking in the shear key, thus removing the need for transverse post-tensioning. The tested connections employed alternate connection shapes and two different mix designs of fiber reinforced high strength concretes. The results showed that each tested connection outperformed the current detail.

The findings of this research indicate that the longitudinal connection detail of adjacent member voided slab bridges should be modified. The modified version should be a blockout with lap splice connection detail utilizing a nonproprietary fiber reinforced high strength concrete.

ACKNOWLEDGEMENTS

I would like to thank both Dr. Cousins and Dr. Roberts-Wollmann for giving me the opportunity to work on this project. This research project has been a very rewarding experience for me. I thank Dr. Cousins and Dr. Roberts-Wollmann for their guidance, recommendations, and extensive knowledge throughout the course of this project. I also thank Dr. Koutromanos for serving on my committee. I appreciate his advice on the finite element analysis that I performed for this project.

I also appreciate the constant support from Dave Mokarem. His advice and knowledge of correct laboratory practices were a big help. His unwavering comedic support contributed to the great working atmosphere at the structures lab. I owe much gratitude to both Dennis Huffman and Brett Farmer for their many hours spent contributing towards my project. I appreciate their kindness and generosity which they showed towards me every day at the structures lab.

I am extremely grateful for the efforts, support, and knowledge of Kedar Halbe. I am not sure if I would have completed this project without him. He was there to offer both his hand and advice whenever needed. I would also like to personally thank Paul Dyreng, William Collins, and Carrie Field for their help with my project. I am also thankful to the rest my fellow SEM graduate students that I shared my time with over the past two years, you all helped make this a very fun and enjoyable experience with many lasting friendships.

I owe a lot of thanks to all my friends and family for their constant support. My biggest thanks goes to my parents, Patrick and Kathy Joyce. Their unwavering support and guidance throughout my life has been more than I could ever ask for. I owe all of my successes to the hard work ethic they preached and instilled within me. A special thanks to Samantha Mingrone for putting up with me over the past two years and being crazy enough to follow me to Montana. Last but not least I would like to thank the rivers, streams, and trout for the stress relief. My time spent on the water allowed me to put things in perspective and bring order back to my life.

All photos by author, 2014.

Table of Contents

List of Figures

List of Tables

Introduction

Background

Adjacent voided slab bridges are comprised of rectangular beams that have two or three circular voids. Like other adjacent member bridges the beams are placed next to each other with a connection running longitudinally between the beams. This connection is typically a partial depth shear key that is filled with a high strength-low shrink grout. Figure 1 shows a general schematic of two voided slab beams and their shared shear key. These bridges are generally post-tensioned together in an attempt to compress the joints and to reduce reflective cracking along the joint. Adjacent voided slab bridges provide many advantages and are ideal systems for short span lengths. Voided slabs have a relatively small section depth which is beneficial, as overhead clearance can be an important factor for bridge construction. Another advantage of this system is the high torsional stiffness provided by the cross section. Perhaps the system's best advantage is that it allows for accelerated construction times.

Accelerated bridge construction is becoming a very popular technique due to the need to reduce traffic impacts and delays, while replacing a large number of the nation's aging bridges. The voided slab beams are precast offsite which allows for more quality control and thus a high quality concrete. Also with the precasting comes a much simpler and quicker superstructure construction. There would be no delays caused by concrete curing times since the beams can be cast ahead of time at the precasting plant. There would be no time wasted placing the reinforcement since this too would be done at the precasting plant. Also since the beams form a continuous top surface the topping material whether it be asphalt or concrete can just be placed on top of the beams. This characteristic negates the need to build and remove formwork which reduces the time of construction. This characteristic will reduce the cost of labor as well.

With these advantages and others the voided slab bridge system can be a very cost effective solution. This is especially true if there are small height clearances present at the site or tight time constraints for the construction. With all these advantages in mind the current shear key detail has proven to be a rampant flaw with these bridge systems since they were first put into use.

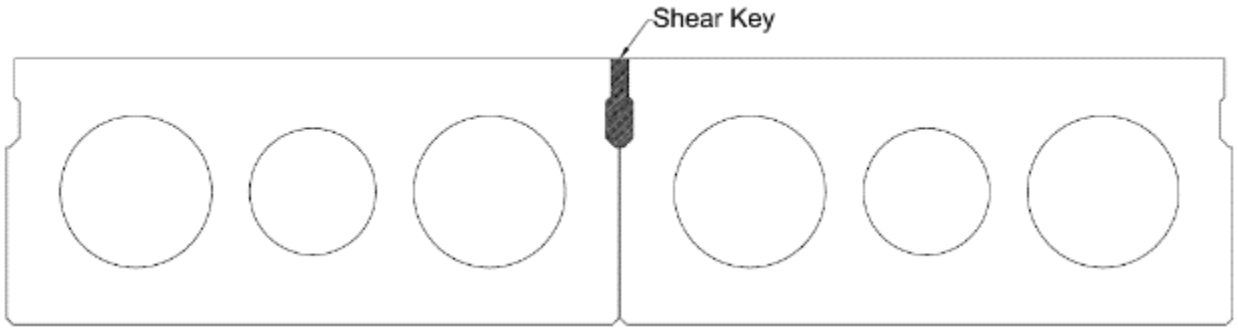

Figure 1: Schematic showing two voided slabs with shared shear key

The shear key not only serves as the longitudinal connection for the beams but it is responsible for transferring all of the vertical shear loads between the beams. This is an important structural component of these bridges because it distributes tire loads among adjacent beams and causes them to act compositely. This feature reduces deflections in the bridge. Unfortunately, it is the shear key that is the downfall of adjacent member bridges. Many adjacent member bridges show reflective cracking in the roadway surface that can be observed in Figure 2. Reflective cracking is attributed to failure in the shear key which is why the reflective cracking in Figure 2 runs longitudinally along the bridge.

Figure 2: Longitudinal Reflective Cracking in asphalt overlay

Initially, the reflective cracking is just a maintenance issue, but over time it decreases the overall durability of the bridge. As water leaks through the cracks carrying deicing salts and other substances it tends to corrode the transverse post-tensioning and reinforcement within the concrete. This causes concrete to spall off exposing and corroding more reinforcing bars. Ultimately, this leads to a deteriorated bridge that will need to be replaced, usually short of its

design life negating the cost effective advantages previously discussed. Luckily, the cracking rarely causes a sudden structural failure because the cracked shear key is still able to transfer load through mechanical interlock. Although, in some worst case scenarios the deterioration of the shear key is significant enough that little to no load is transferred between girders. This causes unexpected loads above the design limit on a single beam which can lead to a structural collapse.

Objective

With the numerous advantages provided by adjacent voided slab bridges it is of much interest to resolve the system's only major flaw, the longitudinal connection. In some DOTs and previous research projects the transverse post-tensioning and shear key size were altered in an attempt to decrease the amount of cracking in the shear key. These solutions decreased some of the cracking, yet in the end, the reflective cracking continued to occur on adjacent member bridges. The objective of this research is to develop more durable longitudinal connections for voided slab bridges that will abate all cracking. Another objective is to create a connection that will negate the need for transverse post-tensioning. Removing the post-tensioning requirements will dramatically decrease the cost and time to construct these adjacent member bridges. This is of much benefit when constructing a skewed bridge due to the complications of lining up the diaphragms needed for the post-tensioning.

The research looks into an alternate connection shape while utilizing the advantages of alternate materials like Kevlar reinforcement of the joint and through the use of fiber reinforced high performance concretes instead of grout. Some connections were also tested with a concrete topping. A total of six different connections were tested. Since it was not economically feasible to test six whole bridges, voided slab bridge sub-assemblages were used to test the various connections. The goal was to mimic the transverse stresses in the shear keys of the sub-assemblages that would be present in full scale bridges under service loads. Both cyclic and static loads were applied to the specimen to test the fatigue strength and the ultimate strength of each connection. The testing was performed in the Thomas M. Murray Structures lab at Virginia

Tech. Ultimately, the findings of this research will be presented to the Virginia Department of Transportation (VDOT) to help develop a more durable connection detail.

Organization

The next chapter of this thesis is the literature review that covers three topics. The first topic discusses shear key performance in adjacent member bridges across the country. The second topic looks into previous research done using ultra high performance concrete connections. The third topic discusses previous research that was performed using sub-assemblage testing. Following the literature review is a chapter on the specimens tested. It covers information on the geometry and other properties of the voided slab beam section as well as their construction. This chapter also discusses how the voided slab beam sections were constructed into sub-assemblages at the lab. Finally this chapter elaborates on each connection that was tested.

Following the specimen information is a chapter that delves into the finite element analysis performed for this research project. This includes a discussion on the full scale bridge model and a sub-assemblage model. After the finite element chapter is an experimental methods chapter. This chapter discusses all of the details about the test setup and instrumentation as well as the test methods and test schedule.

The next chapter is the results chapter which contains all of the pertinent data collected during the research. Following the results is a discussion chapter which expands on all of the important data and behavior that was noted during the testing. The discussion is summarized in the conclusion chapter and then recommendations are made in the final chapter. After the main body of the thesis is the listed references followed by the appendices. The appendices include the construction drawings, concrete mixes, and data that was either excessive or deemed unnecessary in order to make the said conclusions but are necessary for quality control purposes.

Literature Review

Shear Key Performance

A 2009 NCHRP survey showed that roughly two thirds of the states in America used adjacent member bridges and typically all used partial depth shear keys filled with a high strength-low shrink grout acting as the longitudinal connection between the beams (Russell, 2009). A majority of the respondents to this survey said to have had deterioration in the shear keys of their adjacent member bridges proving that this is a prevalent problem across the country. Through inspection of these bridges, the respondents have discovered a number of different issues. One common issue is reflective cracking in the wearing surface as seen in Figure 2. Concrete spalls on the underside of the beams around the joints was another typical response which is visible in Figure 3. Another issue is efflorescent staining collecting on the sides and undersides of the beams near the joints which can also be seen in Figure 3 as well. The staining noted above is most likely being caused by chloride-laden water that seeps through the reflective cracking in the joint (Russell, 2009). This water seepage has been known to corrode both the steel reinforcement and the prestressing strands sometimes even rupturing the prestressing strand. In some reports respondents described total loss of area in the prestressing strands next to the joint and even broken prestressing strands hanging from the underside of the bridge, noted in Figure 4.

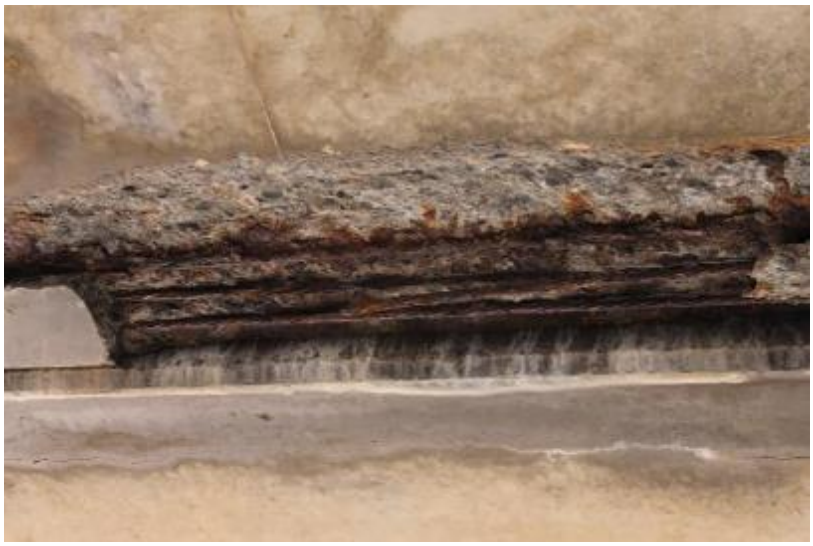

Figure 3: Concrete spalls, corroded prestressing strands, and staining under a shear key

Figure 4: Corroded prestressing strand hanging from large concrete spall near a shear key

The damage noted in the survey is most likely caused by cracking of the shear key which is due to a combination of tensile stresses initiated by temperature gradients, shrinkage, and live loads (Russel, 2009). The cracking is usually the result of a bond failure between the concrete and the grout. In some inspections that have taken place after the topping and beam elements have been removed, there have been observations of the grouted shear key falling cleanly out of the keyway leaving behind no parts that have bonded to the concrete (Gulyas et al., 1995). The shear key failure typically leads to relative displacements between adjacent girders causing failure of the topping waterproofing system (Huckelbridge et al., 1995). This allows the chloride and salt laden water to move down through the joint and capillary action wicks these corrosive materials into the concrete causing the corrosion of the reinforcement and prestressing strands (Gulyas et al., 1995). It is the corrosion that causes concrete spalling on the underside of the member. Severe corrosion of the prestressing strands may lead to concerns for the structural integrity of the bridge. For the most part, the cracked shear key will continue to transfer load between beams due to mechanical interlock. Although, in some severe cases the deterioration in the key is so great that there is no load sharing between adjacent beams causing unexpected loads in a single beam that can cause its failure.

As discussed above, most of the damage caused by cracked shear keys is either an aesthetic, a durability, or a maintenance issue which does not result in a structural failure but they would require costly repairs nonetheless. Sometimes, the only repair requirements are small concrete patches to the underside of the bridge. Other times the owner may have to remove the wearing course and replace the waterproofing membrane. In some cases the owner will have to remove the wearing surface, replace the distressed beams with news ones, and then place new joints (Gulyas et al., 1995). Ultimately, these issues will lead to a total bridge replacement occurring at a time frame much shorter than the expected design life of the bridge. An improved, more durable connection could solve the only major flaw attributed to adjacent member bridges. This improved connection would make adjacent member bridges a much more viable option for designers, and allow them to take advantage of all the upsides that these bridge systems provide.

Ultra High Performance Concrete Connections

The use of precast concrete bridge components is a very popular and successful approach for accelerated bridge construction. Aside from the economic advantages and accelerated construction times, the use of precast components could potentially result in higher quality, more durable bridges. Unfortunately, the required connections between the precast components often prove lacking, resulting in less than desirable overall system performance (Graybeal, 2011). These connections, which are typically grouted joints do not provide the durability needed to make these bridges viable options for designers. The grouted connection fails due to its inability to bond to the concrete. The use of grout tends to force connection sizes to be much larger than needed because of the large lap splice lengths required to develop the bars. Ultra High Performance Concrete (UHPC), whose mechanical and durability properties far exceed those of conventional concretes, allows the designer to enhance the performance of field-cast connections, thus allowing bridges composed of precast components to reach their true potential (Graybeal, 2011).

UHPC, a relatively new class of cementitious material, is one technology that is increasingly being considered to provide durability and longevity in highway infrastructures due to its advanced material behaviors (Graybeal, 2009). UHPC lacks any coarse aggregate with fine sand being the largest particle size. UHPC typically contains cementitious materials like fly ash

and silica fume. UHPC contains high cementitious material contents, low water to cementitious material ratios, and compressive strengths above 22 ksi (Graybeal, 2012). In order to compensate for the low water content a high range water reducer is needed to get the required workability. A crucial ingredient of UHPC is small steel fibers that increase the tensile capacity of the concrete. The steel fibers bridge across cracks giving UHPC a post-cracking tensile strength, which is a unique attribute not present in other cementitious materials. This post-crack tensile strength can be as high as 1.5 ksi (Graybeal, 2012).

Aside from increased material strengths, UHPC has many other characteristics that make it appealing for bridge connections. It is a very durable material due to its low permeability and its ability to resist cracking. The low permeability is attributed to the fine powders and chemical reactivity which creates an extremely compact matrix and a small, discontinuous pore structure (Perry and Royce, 2010). Since UHPC does not contain coarse aggregate, it does not exhibit early age microcracking common to conventional concrete (Graybeal, 2012). In fact, Graybeal (2011) has even shown that UHPC shows very tight to no cracking under loads through the testing of UHPC bridge topping connections under cyclic and static loads. This ability to resist the inflow of water gives the material a very high resistance to freeze-thaw cycles (Ozyildirim, 2011). This characteristic makes UHPC very advantageous to bridge construction since freeze-thaw cycles can severely degrade material that is exposed to the elements.

Another important attribute of UHPC that makes it advantageous to bridge connections is its ability to form very strong bonds. This gives it the ability to bond to the precast concrete and resist much higher tensile stresses than the grout could in the shear key. UHPC's bond capabilities also allow it to develop reinforcing bars over much shorter lap splice lengths when compared to grout or other concretes. Halbe ran splice tests showing that a proprietary UHPC called Ductal can develop No.4 reinforcing bars with 5 in. lap splices. The use of small lap splices can greatly reduce the connection size.

Through the use of high range water reducer, UHPC also acts as a self-consolidating concrete negating the need for vibrating or manual consolidation. The UHPC's flowable consistency allows it to be poured right into the joint or connections. The flowability allows for tight connections openings and optimized shapes that would otherwise not be attainable with normal concretes. In fact, Graybeal (2011) states that the UHPC connection concept allows for

small, simple connections without requiring post-tensioning or large volumes of field cast concrete.

Many research projects have shown that UHPC connections perform better than typical field-cast connections. One such research project performed by Graybeal (2012) looked into creating composite connections between precast concrete bridge decks and both steel and concrete bridge girders, though the use of UHPC. Figure 5 shows a schematic of the connection tested by Graybeal (2012) for steel girders. The original field-cast grouted connection provided a lot of congestion and fit up issues due to the need to connect multiple different elements that extended from both the girders and decks. UHPC's tensile and bond capacities were utilized instead of grout to avoid the congestion and fabrication issues. This novel connection detail resisted all cyclic and static loads applied during the testing program. In fact, Graybeal (2012) noted that no damage was observed in the composite connection and that during the final static test with the concrete girder, the member began to fail before the connection.

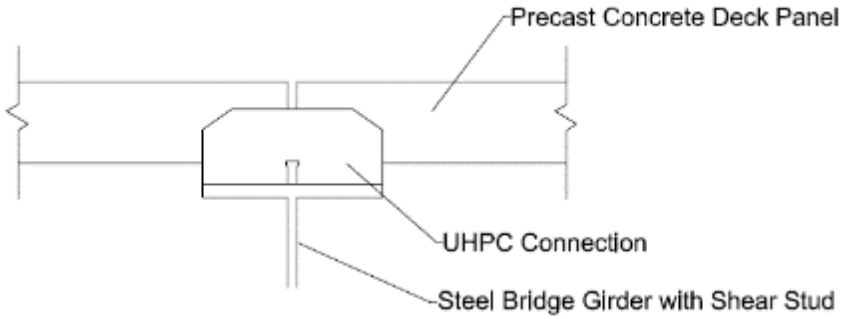

Figure 5: UHPC composite connection detail for steel girders used by Graybeal

In another research project run by the Federal Highway Administration (FHWA) the behavior of field-cast UHPC connections between precast deck panels was studied. Graybeal (2011) concluded that each of the four connection details tested in this FHWA study were anticipated to perform well in the field and that they surpassed the behavior of monolithic concrete decks. Also noted was that there were no cracks visible at the interface between the UHPC and the precast concrete. These research projects clearly show that UHPC has the capabilities to outperform the current connection standards for various precast bridge components.

UHPC bridge connections are slowly becoming an option for designers. As of early 2012 field-cast UHPC connections between precast bridge components have been implemented in 18 bridges in the United States and Canada. The one downfall holding UHPC back is its high costs as it can exceed five times the amount of normal concrete. The high upfront cost may be worth the investment since its durability will increase the design life of the bridge especially in the instances of adjacent member bridges where the connections are generally quite small and would not require a large amount of UHPC.

Sub-assemblage Testing

One economical way for research facilities to test multiple design ideas is to test a number of full-scale sub-assemblage models. For most researchers it would be far too expensive to test multiple full-scale full-bridge models, not to mention most facilities could not handle such large scale testing. While scaled models are a viable option it is not easy to recreate accurate representations that match the behavior of full-scale models. Senturk and Higgins (2010) noted that their own full-scale sub-assemblage models of reinforced concrete deck girder bridge bent caps realistically reflected their in-service counter parts. Scaled models are especially difficult with concrete because dimensions may become less than the typical construction tolerances allowed in concrete members (Hucklebridge and El-Esnawi 1997).

Full-scale sub-assemblage models can be extremely successful when paired with finite element modeling in order to recreate the behavior of whole models in the sub-assemblages. This can involve designing support conditions on the sub-assemblage that recreate the stiffness and behavior of the full model that is not present. This technique has been employed a number of times in bridge research where the three-dimensional behavior of the full bridge is simulated in sub-assemblages that typically only experience two-dimensional behavior.

Hucklebridge and El-Esnawi (1997) created their own sub-assemblage models of adjacent box beam bridges in an attempt to investigate the known problems with the shear key in these bridges. They were also trying to create a new shear key detail that would allow less relative displacement between girders. They had a total of six different connections to test and for the reasons discussed above decided to create full-scale sub-assemblage models that were 1 ft

long. They selected 1 ft long members because they believed most lateral load was transferred between shear keys within 1 ft of a concentrated load application. A schematic of their model can be seen in Figure 6. Hucklebridge and El-Esnawi (1997) created a full scale 3D finite element model and a model of their sub-assemblage in order to predict the desired stiffness in their supports that would simulate the actual 3D behavior of the bridge. They loaded their sub-assemblage on the top center flange with both cyclic loads, to test the fatigue life of the connection, and a static load to test the ultimate strength of the connection. Their sub-assemblage testing proved to be adequate and allowed them to conceive a new shear key detail that improved the load carrying capacity of the tested specimen when compared to the current shear key detail at the time.

Figure 6: Schematic of the three girder sub-assembly used by Hucklebridge and El-Esnawi

Hansen, Hanna, and Tadros (2012) also employed sub-assemblage models in order to improve the behavior of adjacent box beam bridges. They proposed an alternate post-tensioning system that contained tendons both high and low in the cross section in order to enhance the behavior of box beam bridges. They used a four box beam wide, 8 ft long sub-assemblage with two different loading scenarios to induce tension in both the top and bottom of the specimen. A schematic of their bottom tension setup can be seen in Figure 7. Hansen, Hanna, and Tadros (2012) chose to use a four beam wide sub-assemblage because it was the minimum number of beams that would accommodate their test setups. The 8 ft section depths were chosen because that is the spacing of their proposed post-tensioning. Hansen, Hanna, and Tadros (2012) also employed finite element modeling in order to recreate the full 3D behavior in their sub-assemblage model. They too employed both cyclic testing to test the fatigue strength of the sub-assemblage, and a final static loading to test the ultimate strength. Hansen, Hanna, and Tadros (2012) through the use of their sub-assemblage models were able to come up with a successful

detail that they believed had comparable performance to the current details but was more economical and practical.

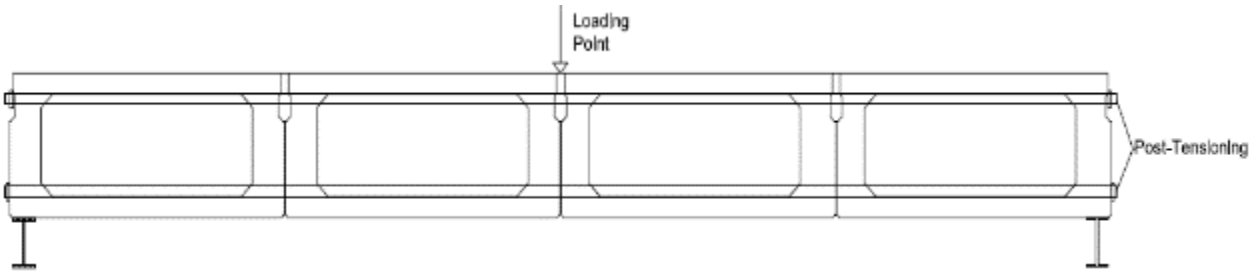

Figure 7: Schematic showing Hansen, Hanna, and Tadros' bottom tension setup

Summary

As seen in the NCHRP survey, shear key deterioration is a prevalent problem in adjacent member bridges throughout the country. Huckelbridge's and Gulyas' reports also discussed the problems that they discovered with the partial depth grouted shear key system. The problems discussed validates the need to improve the shear key connection, which is the objective of this project.

UHPC's advantage have made it a popular option for use in field-cast connections. In a few separate documents, Graybeal presented the material properties of UHPC and he also discussed UHPC's performance in laboratory tested field-cast connections. The numerous advantages of UHPCs were the reason they were chosen as an alternate connection filler material for this project, which will be discussed in greater detail in the following chapter.

The final section of the literature review presented two previous research projects that used sub-assemblage setups for laboratory bridge tests. The two projects had satisfactory performance of their setups. The sub-assemblages appeared to successfully represent the behavior of the full-scale bridges. These previous tests helped to endorse the sub-assemblage testing used in this research project, which is discussed in the Test Method chapter of this thesis.

Test Specimens

This chapter explains the geometry and characteristics of the specimens tested. The first section gives information on the voided slabs that were tested throughout this research project and how they were constructed. The following section discusses each different connection that was tested, the reasons for being tested, and how each connection was placed and or constructed. The final section describes how the sub-assemblages were formed in the lab.

Voided Slabs

The Virginia Department of Transportation (VDOT) uses a number of different reinforced concrete voided slab beams that vary in depth, width, and in the number of voids. One of VDOT's more typical sections, based on AASHTO's Voided Slab Type SIV-48, was tested for this research project. A dimensioned schematic of the type SIV-48 slab is provided in Figure 8. This voided slab has three circular voids with the outer two voids being 12 in. in diameter and the center void is 10 in. in diameter. The beam has an overall depth of 21 in. and is 48 in. wide. The beam's shear key is a 7 in. deep partial depth key and the exact dimensions are provided in Figure 9. The construction drawings including the rebar schedule and layout for the tested specimens are presented in Appendix A.

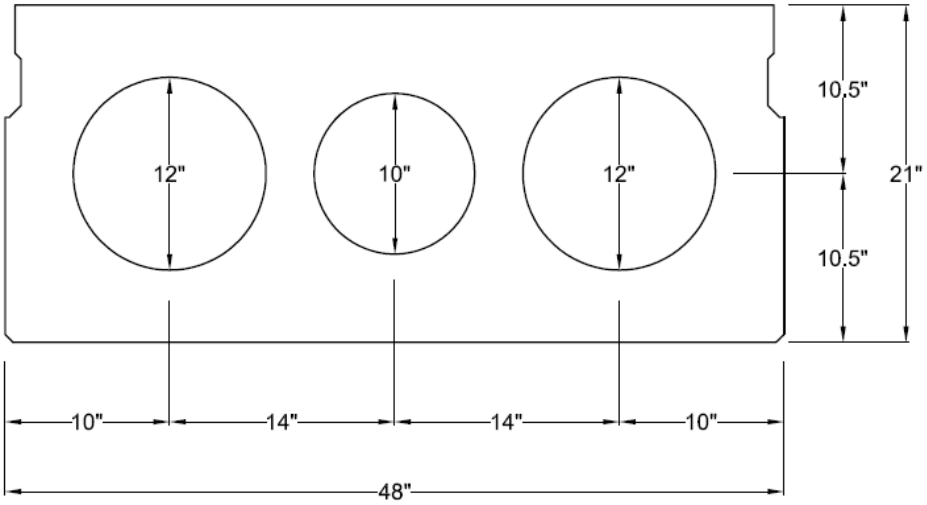

Figure 8: Dimensioned AASHTO voided slab type SIV-48

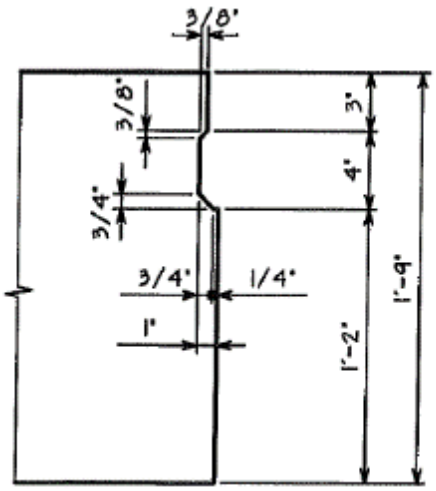

Figure 9: Detailed shear key dimensions for an AASHTO voided slab type SIV-48

The reinforced concrete beams tested as part of the sub-assemblages were 2 ft long sections. The whole sub-assemblage consisted of three voided slabs sections which represented a 2 ft long interior, midspan section from a typical adjacent member voided slab bridge. Lengths of 2 ft were chosen because this was believed to be the smallest length that would adequately represent behavior of the bridge while still being stable. At lengths shorter than 2 ft it was feared the specimens would too easily topple over. Each beam section weighed roughly 1600 lbs and consisted of class A5 concrete (5000 psi) and standard grade 60 reinforcement. Voided slab beams are typically prestressed but this was not relevant for the small 2 ft sections.

Voided slab bridges are typically transversely post-tensioned together at discrete points along the bridge as well. The subassemblages tested were not post-tensioned for a few reasons. The first reason is that the post-tensioning force is usually only effective near the point of application, but the effect is greatly reduced between the points of application. The second reason is that the goal for the project was to develop a durable connection that would negate the need for post-tensioning. Removing post-tensioning and its inherent solid concrete diaphragms would greatly reduce the construction time and costs. Moreover, since post-tensioned diaphragms provide transverse continuity only at discrete locations, the system becomes more susceptible to cracking and leakage (Hanna, Morcous, and Tadros 2011). Hanna, Morcous, and Tadros (2011) ran tests on adjacent member box beams without post-tensioned diaphragms and

concluded that getting rid of the post-tensioning while using alternate connections designs could be structurally superior and more economic then the current design.

The voided slab beam sections were constructed by Ross Prestressed Concrete, Inc. at one of their prestressing plants located in Bristol, TN. The internal circular voids were formed with wax coated cardboard cylinders. Each 2 ft section was formed between two pieces of plywood with threaded rods running through the voids to hold the plywood together. Figure 10 shows typical formwork with the tied reinforcement cage. Any other block-outs were formed with styrofoam that was wrapped with duct tape in order to prevent the styrofoam from absorbing water that was needed to hydrate the concrete. The forms were lined up in the prestressing beds as seen in Figure 11 which acted as the side walls for the beams. These side walls had an insert that formed the shear key.

Figure 10: Voided slab formwork and rebar cage

Figure 11: Voided slab forms sitting in prestressing beds

The concrete was batched and mixed onsite and then brought to the prestressing beds in a standard mixing truck. The concrete mix designs are presented in Appendix B. The slump and air content were checked prior to placement to make sure the concrete was adequate. Test cylinder that were 4 in. by 8 in. were cast for future material property testing. The concrete was then placed in a concrete skip which was lifted by a crane and then moved into a position above the formwork in order to drop the concrete into the forms. Figure 12 is a photo of the concrete being dropped from the skip. Two workers used pencil vibrators to consolidate the concrete from the top. Additional consolidation was provided by a vibrator which sat on the bottom of the side walls of the prestressing bed that could slide horizontally along the wall. After the forms were filled with concrete and consolidated properly, the tops of the beams, which were to receive a future concrete topping, were given a roughened rake finish, otherwise the tops of the beams were given a float finish. Figure 13 is a photo of the workers applying a finish to the beams. After the concrete was placed and finished the beams were covered with wet burlap and given a steam cure. It took three different concrete batches to make all of the specimens, and cylinders were made for each batch to be used in material testing. When the concrete reached a strength of 3500 psi the formwork was removed. The specimens were then shipped to the Thomas M. Murray Structures lab at Virginia Tech. Figure 14 is a picture showing a finished voided slab specimen.

Figure 12: Concrete being poured from the skip

Figure 13: Workers applying finishes to the concrete

Figure 14: Finished Voided slab specimen

Connections

There were a total of six different connections that were tested as part of this research project. The first connection tested was the current VDOT connection detail consisting of the 7 in deep shear key filled with grout. The second connection tested was the current grouted shear key detail with a Kevlar mesh placed on top of the connection. The third connection tested used

an alternate connection shape and a proprietary UHPC called Ductal made by Lafarge. The fourth connection used the same alternate connection shape but with a nonproprietary fiber reinforced very high performance concrete that was designed at Virginia Tech. The fifth and sixth connections were the same as the third and fourth but each with a concrete topping. Table 1 is a test matrix summarizing the six test specimens.

Table 1: Test matrix summarizing the specimens tested

	Specimens without Concrete Topping				Specimens with Concrete Topping	
Specimen #	Specimen 1	Specimen 2	Specimen 3	Specimen 4	Specimen 5	Specimen 6
Details	Existing partial depth shear key with grout filler	Existing partial depth shear key with grout filler and Kevlar mesh reinforcement	Partial depth key with discrete blockouts for drop-in splice bars with Ductal UHPC filler	Partial depth key with discrete blockouts for drop-in splice bars with nonproprietary VHPC filler	Partial depth key with discrete blockouts for drop-in splice bars with Ductal UHPC filler	Partial depth key with discrete blockouts for drop-in splice bars with nonproprietary VHPC filler

The VDOT connection standard was tested in order to assess the strength and behavior of the current detail. This acted as the standard against which all other connections were compared. As discussed before, the connection used the standard 7 in deep shear key which is shown in Figure 9. Prior to placing the joint the keyways were sandblasted and kept moist at surface saturated dry conditions in order to enhance the bond. This is standard VDOT practice and was carried out prior to each connection placement. The shear key was filled with a high strength low shrink grout, which according to VDOT's road and bridge specifications must conform to ASTM C1107 and has to develop a seven day compressive strength of at least 4000 psi. Bags of Quikrete's Non-shrink Precision Grout which complies with ASTM standards (ASTM C1107, 2013) were used as the grout material. Sample 2 in cubes of Quikrete's grout were made ahead of time to make sure that they would achieve a seven day compressive strength of 4000 psi. The sample cubes reached strengths in excess of 9 ksi at seven days confirming it was an acceptable grout. The dry mix from the bags was mixed with water to a flowable consistency in a pan style

concrete mixer and then placed in the joints. Figure 15 shows a cross section picture of the shear key after the grout has cured.

Figure 15: Hardened shear key from first specimen tested

The second connection used the current shear key detail with a Kevlar mesh epoxied to the top of the joint. The Kevlar-epoxy system creates a seal to prevent water leakage, is strong enough to transfer load, and can allow temperature and stress related deflections without cracking. These characteristics create a very durable material which is an imperative attribute for the shear key connection. Another advantage of this detail is that the current shear key detail could still be used. This means that the Kevlar-epoxy system could be easily used for repairs as well. All that needs to be done is to have the bridge's wearing surface removed and then place the Kevlar-epoxy system along the joints. Due to these possible advantages, the Kevlar-epoxy system was tested to see if it can abate cracking and transfer shear loads between beams.

The Kevlar used is a product made by Fortec Stabilization called Fortec 5680-BD Kevlar. According to Fortec the mesh is a bi-directional, highly durable material composed of dense Kevlar yarns. The ultimate strength listed by Fortec is 100 ksi. Figure 16 is a picture of the Kevlar mesh. The epoxy used is a two component mixture also developed by Fortec called E-bond 256. The epoxy has a rapid set time and a fast strength development. When cured the system creates a highly impermeable system. In order to construct this connection the shear key first had to be grouted and then given time to cure. Prior to placing the Kevlar, the area surrounding top of the shear key was sand blasted to enhance the bond with the Kevlar. The next step was to mix the epoxy by placing a one to one ratio of the resin component and the hardener

component into a clean container and mix for at least three minutes using a low speed drill with a mixing paddle. After thoroughly mixing the epoxy a layer was placed along the joint roughly as wide as the Kevlar mesh. The Kevlar mesh was then placed along the joint and firmly pressed into the epoxy layer with a paint roller brush until the epoxy oozed through the Kevlar. A coarse sand was then sprinkled on top of the Kevlar and epoxy. After the first layer of epoxy cured, a second layer was placed on top and then more of the coarse sand was sprinkled on top of that layer. The curing time for each layer was roughly 2 hours. Figure 17 is a picture of the finished Kevlar reinforced joint.

Figure 16: Picture of the Fortec 5680-BD Kevlar

Figure 17: Picture of Kevlar-Epoxy joint with coarse sand.

For the third connection tested, there were 6 in. deep and wide by 4 in. high blockouts formed into middle of the specimens at the top of the shear key. Figure 18 is an excerpt from the construction drawings used by the prestressing plant to build the specimens with the blockouts. The blockouts have exposed shear stirrups with which a dropped-in No.4 grade 60 reinforcing

bar is lapped when the blockouts from adjacent beams are lined up next to each other. Figure 19 is a picture of two adjacent blockouts with the tied in reinforcing bar. This blockout connection idea was proposed because it was thought that the lap splice connection is better suited to handle the transverse flexural stresses that occur across the joint. It was thought that this connection would cause composite action between the adjacent beams which would reduce cracking. Since the sub-assemblage represents a 2 ft section of a bridge, the spacing proposed for full scale implementation is 2 ft on center. There is research being done currently to see test the efficiency of this spacing. Hanna, Morcous, and Tadros (2011) did work using similar blockouts on adjacent member box beams. They too used lapped splice reinforcement connections inside of the blockout. In order to develop these lapped splices over short lengths they provided spiral confinement reinforcing with ¼ in wire. In order to negate the need for spiral reinforcement UHPC was used in this connection.

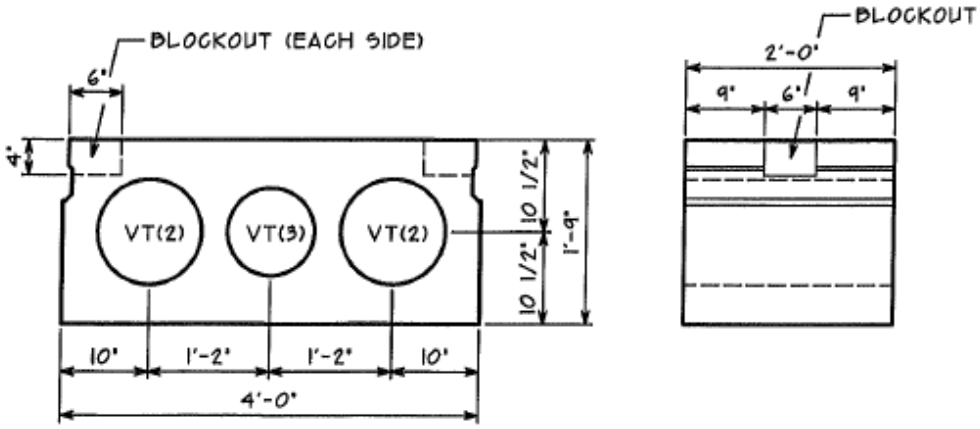

Figure 18: Construction drawing screenshot showing blockouts

Figure 19: Picture of Blockout with tied in lap splice bar before UHPC placement

Both the 7 in. partial depth shear key along with the blockouts described above were filled with a UHPC. As described above, UHPC is essential for this connection due to its ability to develop short lap splices. A grouted connection would need a much larger blockout in order to develop the reinforcement. UHPC is also preferred over grout for this connection due to the higher bond strength that it can form with concrete. Another reason UHPC is warranted for this connection is that it has higher tensile capacities than grout and has post cracking tensile capacity as well due to steel fiber reinforcement. The steel fibers also help to abate cracking caused by shrinkage and other stresses making it a durable material. The UHPC used in the third connection was a proprietary mix called Ductal that is manufactured by Lafarge. Ductal comes in a premix bag consisting of Portland cement, fine sand, silica fume, and ground quartz. The premix bag is mixed with water, a high range water reducer, and steel fibers. The steel fibers used were undeformed straight fibers that had a 0.008 in. diameter and were 0.5 in. in length. The steel fibers have a specified minimum tensile strength of 377 ksi. Lafarge lists the average compressive and flexural strength of Ductal as 29 ksi and 6.5 ksi, respectively.

The mixing procedure was a simple process that was provided by Lafarge. The mix quantities used to place the joint and the required material testing specimens can be found in Table 2, below. After weighing out the proper amount of materials the premix was placed in a pan mixer and was mixed dry for two minutes. The water and high range water reducer were combined and then slowly added to the mixing pan over the course of two minutes. The mixing continued until the UHPC turned into a self-consolidating paste. Then the steel fibers were slowly added to the pan. Mixing continued for another minute or two to make sure the steel fibers were well dispersed. After the mixing was finished the UHPC was placed in the joint. Since Ductal is self-consolidating it was a very flowable material. This made it very easy to place in the connection as it can just be poured into the joint without the need for any consolidation. Figure 20, is a picture of the cured Ductal filled joint.

Table 2: Ductal mix design used for third specimen and per cubic yd

Mix Quantity	1.45 ft^3	1.00 yd^3
Water (lb)	12.23	232.47
Ductal Premix (lb)	194.54	3699
Steel Fibers (lb)	13.83	262.98
High Range Water Reducer (lb)	2.73	51.84

Figure 20: Picture of cured UHPC joint

The fourth connection tested used the same specimens that were used for the third connection with the blockouts and lap splice connection. The difference with this connection is that instead of using Ductal, a nonproprietary mix designed at Virginia Tech was used to fill the joint. This mix was denoted as a very high performance concrete (VHPC). This connection was tested because Ductal is an expensive material. If the VHPC provided an adequate connection then it would be a more cost effective solution than using Ductal. The VHPC mix consisted of water, Portland cement, silica fume, fly ash, No.10 sand, ¼ in. limestone, a high range water reducer, and steel fibers. The steel fibers were Dramix ZP 305 hooked end fibers manufactured by Bekaert. They are roughly 1.18 in. long and have a diameter of 0.02 in.. From preliminary testing done at Virginia Tech the average twenty eight day compressive strength and flexural strength of the VHPC was 16 ksi and 2.3 ksi, respectively. The required volume for placing both the joints and material property specimens was 1.45 ft^3. The mix design used for this volume and per cubic yard is found in Table 3.

Table 3: VHPC mix design for fourth specimen and per cubic yard

Mix Quantity	1.45 ft^3	1.00 yd^3
Water (lb)	17.11	318.6
Cement (lb)	60.18	1120.5
Silica Fume (lb)	12.91	240.3
Fly Ash (lb)	12.91	240.3
#10 Sand (lb)	77.87	1449.9
1/4” Limestone (lb)	33.35	621
Steel Fibers (lb)	14.21	264.6
High Range Water Reducer (ml)	540	10000

After all of the materials were weighed, the sand and limestone were placed in the pan mixer with a little bit of water in order to control the dust. The sand and limestone were mixed until the materials were dispersed evenly. Next the cement was added, and then half of the remaining water was slowly poured into the mixer. The silica fume and fly ash were slowly added, followed by the rest of the water. The high range water reducer was added in increments until the desired consistency was achieved. Finally the steel fibers were added to the mixture. The Dramix fibers do not come shipped as single fibers instead a number are glued together. Figure 21 is a photo showing the fibers glued together. The mixture was allowed to mix until the fibers broke apart and dispersed evenly throughout the mix. When the mixing was complete the VHPC was placed in the joint. Just like the Ductal mix, the VHPC had a flowable consistency that allowed it to be poured into the joint without the need for consolidation.

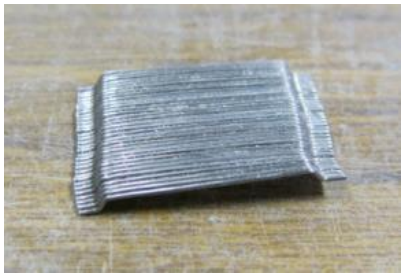

Figure 21: Picture showing the Dramix fibers which come glued together

The fifth and sixth connections tested were identical to the third and fourth connection with the addition of a 5 in. concrete topping on top of the specimen. In Virginia, adjacent member bridges can have an asphalt topping, a 5 in. thick concrete topping, or a 7.5 in. concrete topping depending on the average daily traffic (ADT) and the average daily truck traffic (ADTT). For relatively high traffic volumes (ADT>4000 and ADTT>200) VDOT requires the 7.5 in. topping. While bridges with relatively low traffic volumes (ADT<4000 and ADTT<100) require only an asphalt overlay. For bridges with ADTT between 200 and 100 a 5 in. deck is required by VDOT. It was not feasible to test both the 7.5 in. and 5 in. topping. The 5 in. topping was chosen because typically voided slab bridges receive a lower traffic volume so the 5 in. topping would be a more typical option in Virginia.

Sub-assemblages with toppings were tested to see how a topping could affect the behavior of the connection and to see if it could enhance the durability of the connection. A very

simple reinforcement mat had to be tied for the topping. Figure 22 shows the reinforcement mat detail that was used for the topping. Formwork for the topping had to be constructed that went around the perimeter of the sub-assemblage as well. Seventy-two hours after the joint was placed with its respective UHPC or VHPC the formwork for the joint was removed. Then the reinforcement mat was laid into place and the topping formwork built around it. Figure 23 is a picture of the sub-assemblage with the reinforcing mat and topping formwork prior to the placement of the topping. The local concrete mix plant, Conroc delivered A4 (4000 psi) concrete for the topping in one of their concrete trucks. The mix designs for the concrete can be found in Appendix B. Once at the lab, the concrete's slump was tested to make sure it was of the correct consistency. The concrete was then placed into the topping using the concrete skip carried by one of the two 5 ton overhead cranes present at the lab. The concrete was consolidated using a pencil vibrator and leveled off using a concrete screed. Following forty-eight hours, the formwork for the topping was removed. Figure 24 is a picture of the sub-assemblage with the topping on top.

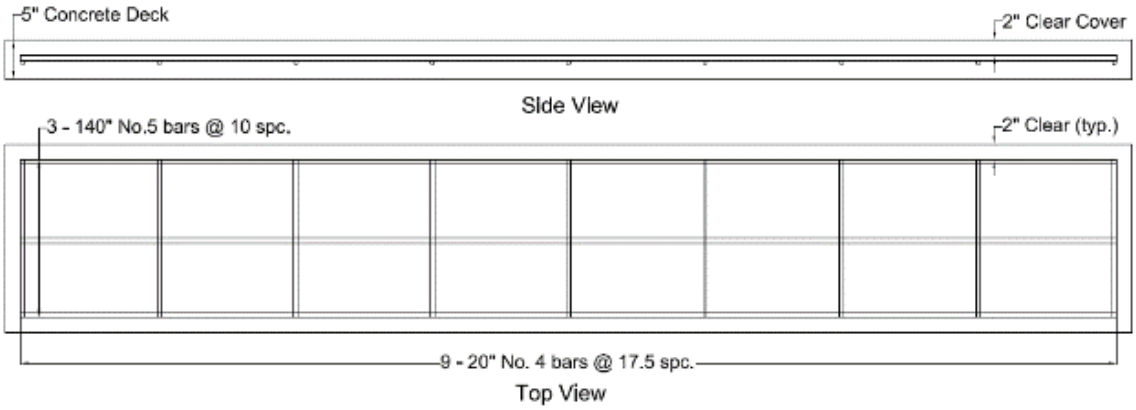

Figure 22: Topping reinforcement mat detail

Figure 23: Picture showing reinforcement mat in place and formwork for concrete topping

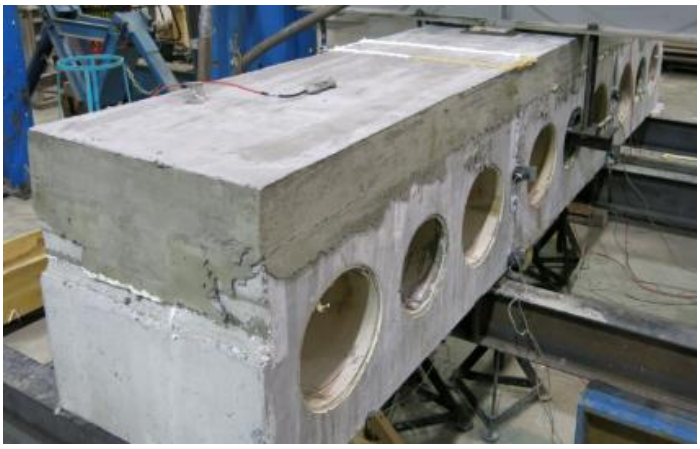

Figure 24: Picture showing concrete topping on top of sub-assemblage.

Sub-Assemblage Construction

Each connection was tested via its own sub-assemblage, which had to be assembled in the lab. As stated before, the sub-assemblages consisted of three voided slab specimens. This made 12 ft wide and 2 ft long sub-assemblages. Due to constraints in the test setup the sub-assemblage could not be moved into place whole. Each beam section had to be moved in separately and then connected with the appropriate connection. This required each of the six sub-assemblages to be positioned in the test setup right before joint placement.

The first step in the process was to sandblast the keyways of each voided slab specimen. This is standard practice conducted by VDOT. The sandblasting is done to clean the surface and expose the aggregate in order to enhance the bond with the joint filler material. The sandblasting was always done within twenty-four hours of joint placement. After sandblasting, the keyways were kept moist by spraying them with water, which was done frequently up until placement of the joint. This was done to achieve saturated surface dry (SSD) conditions on the surface of the concrete.

The next step was to move the center specimen into the test setup. Once lined up correctly in the horizontal directions the specimen was lowered by the overhead crane onto three screw-jacks. Then using the screw-jacks the center specimen was raised to the proper height and properly leveled. A thin strip of neoprene pad was attached using silicon, along the bottom of

both sides of the center specimen's keyway. The purpose of the neoprene pad was to prevent the joint filler material from leaking through the bottom of the joint. Prior to placing the exterior specimens into the test setup, three bearing pads had to be glued to the bottom of the slab at the points where the beams would rest on load cells. Three points of contact were used because this made it much easier to distribute the load evenly among the load cells. Two of the bearing pads went on the outsides of the interior edge and the other pad went on the center of the exterior edge. Then, using the crane, each exterior specimen was moved into the correct position next to the center specimen. When aligned properly the exterior specimens would be lowered onto their support beams.

The next step was to seal off the end of the shear keys with formwork. This was achieved by using two pieces of plywood placed at each end of the keyway. Then a threaded rod was run through each corner of the plywood. The top rods sat on top of the specimens and the bottom rods ran through the circular voids adjacent to the key. The bolts on each threaded rod were tightened down to seal the joint. The final step was to place the appropriate connection.

At the precast plant, the concrete sections were placed in three different batches, and each batch contained two specimens for each connection. In order to efficiently use the concrete cylinders that were casted, each sub-assemblage consisted of two specimens from one batch and third from another batch. Table 4, below shows what batches were used in each sub-assemblage. The south, middle, and north descriptors in the table headings refer to the direction in the lab that each section was located within the sub-assemblage.

Table 4: Concrete batch usage for each sub-assemblage

	South Section	Middle Section	North Section
Specimen 1 - Existing Detail	Batch 2	Batch 1	Batch 2
Specimen 2 - Existing Detail with Kevlar	Batch 1	Batch 3	Batch 3
Specimen 3 - Ductal UHPC Connection	Batch 1	Batch 2	Batch 1
Specimen 4 - VHPC Connection	Batch 3	Batch 2	Batch3
Specimen 5 - UHPC Connection with topping	Batch 1	Batch 2	Batch 1
Specimen 6 - VHPC Connection with topping	Batch 3	Batch 2	Batch3

Finite Element Analysis

This chapter presents the finite element modeling that was completed for this research project. All of the finite element modeling and analysis was completed using the commercial finite element analysis program Abaqus. The first section of this chapter discusses the modeling and analysis of a full scale adjacent member voided slab bridge. The second section presents the modeling and analysis of a sub-assemblage model. The final section talks about the mesh selection. The purpose of the finite element analysis (FEA) was to obtain the loading for the sub-assemblage that was necessary to recreate transverse stress conditions in the shear key equivalent to those seen in the full bridge under an AASHTO design truck loading.

Full Bridge Model

An excel sheet of all the VDOT maintained voided slab bridges along with plans for five different voided slab bridges were acquired from VDOT. From the plan sets and excel file, a typical VDOT voided slab bridge was developed and modeled using the commercial finite element analysis program Abaqus (Simulia 2013). The full bridge model was 35 ft in length and consisted of twelve voided slabs beams making it 48 ft wide. As per VDOT standards and the available plans, the exterior beams were modeled as solid rectangular beams without the circular voids. There were 2.5 ft solid end diaphragms incorporated into the model as well. VDOT's current standards call for transverse post-tensioning at mid span for spans shorter than 30 ft, at third points for spans between 30 and 60 ft, and at quarter points for spans longer than 60 ft. Transverse post-tensioning is also done at the ends of spans if the ends of the beams are not restrained from lateral movement. There was no transverse post-tensioning incorporated into the model since the goal of this research was to develop a connection that would remove the need for post-tensioning. A 1/8 in.- gap was assumed between the shear keys of adjacent beams for the model. Figure 25 is a screenshot from Abaqus of a section cut of the bridge model showing the voids.

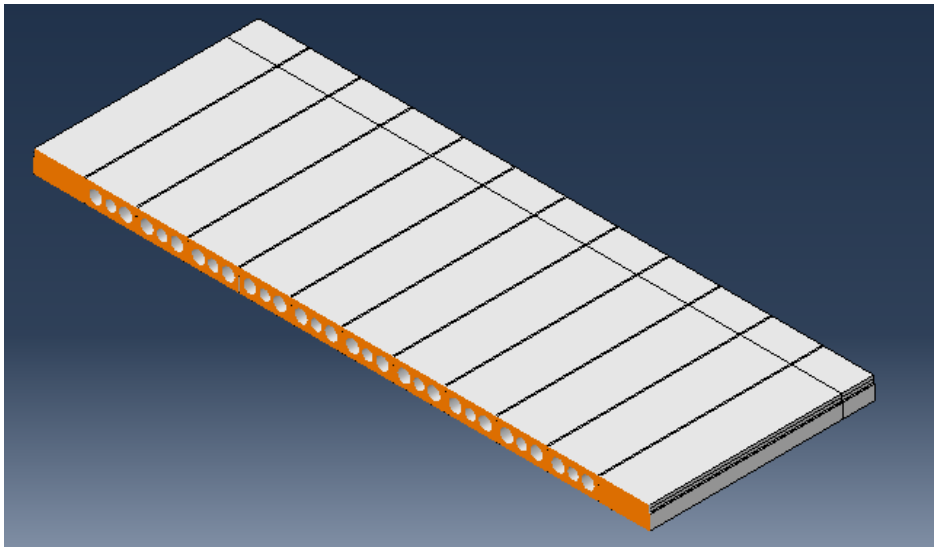

Figure 25: Screenshot from Abaqus showing a section cut of the full bridge model

The analysis performed was a linear elastic analysis used as a way to approximate the stress distribution and values in the shear key under an AASHTO design truck loading. Since it was a linear analysis it drastically simplified the model. All that was needed for the material characterization was the modulus of elasticity and Poisson's ratio. For the concrete used the in the voided slab beams the modulus of elasticity value used in the model was 4030 ksi. The modulus of elasticity approximation was obtained from the AASHTO equation for normal weight concrete and is presented below:

$$E_c = 57000\sqrt{f'_c}$$

For the grout used in the shear keys the modulus of elasticity value was taken from testing previously done on the grout. The value inputted to the model was 3270 ksi. The Poisson's ratio value for both materials was taken as 0.2.

As per the VDOT drawings, the model incorporated 6 in. long, 9 in. wide, and ½ in. thick bearing pads on all four corners of each voided slab beam. Modeling the stiffness of these bearing pads was important as Yazdani (2009) showed that this was imperative in order to achieve the actual bending behavior of the girders in the model. Yazdani (2009) used mechanics of materials and referenced AASHTO in order to derive equations for both the horizontal and vertical stiffnesses of the bearing pads. Figure 26 presents the bearing pad schematic for

Yazdani's equations and both the horizontal and vertical stiffness equations he derived are found below the schematic.

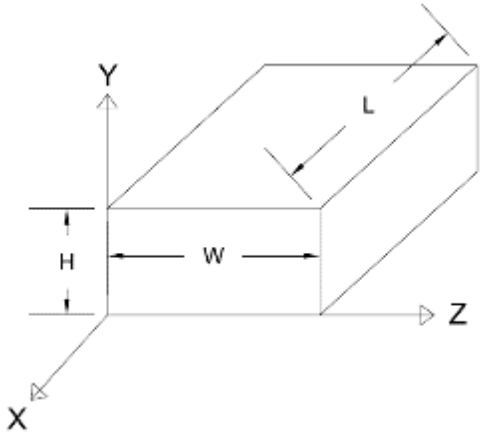

Figure 26: Bearing pad schematic for Yazdani's equations

Horizontal Stiffness, in lb/in:

$$k_{x,z} = \frac{E_c * L * W}{H}$$

Vertical Stiffness, in lb/in:

$$k_y = \frac{G * L * W}{H}$$

The Compressive Modulus of Elasticity is:

$$E_c = 6 * G * S^2$$

The Shape Factor Equation given in AASHTO is:

$$S = \frac{L * W}{2 * H * (L + W)}$$

The shear modulus, G was taken as 127.5 psi, as per AASHTO. The detailed calculations can be found in Appendix E. The horizontal stiffness value for the model's bearing pads was 13.77 kip/in and the vertical stiffness value found was 1070 kip/in. The horizontal stiffness was incorporated into the model via the spring function in Abaqus (Simulia 2013). The springs were attached to the corners of the model's bearing pads and then to the "ground" option in Abaqus (Simulia 2013), which acts as a fixed point. Since a spring was attached to each corner the stiffness value used for each was a quarter of the total horizontal stiffness from above. This was done for both horizontal directions making a total of eight springs per bearing pad. The vertical stiffness of the bearing pads was taken into account through Abaqus' (Simulia 2013) elastic foundation function. The elastic foundation function applies a uniform stiffness value over a selected area. The elastic foundation function was used instead of springs because it was thought

to give a more accurate presentation since it acts over a whole area instead of discrete points. For this function, the whole bearing pad was given a uniform vertical stiffness by dividing the calculated vertical stiffness value by the plan area of the bearing pad.

The bridge model was loaded with the AASHTO design truck which has three axles. The loading on the front axle is 8 kips and the loading on the back two axles is 32 kips each. The front two axles are spaced 14 ft apart and the back two can be spaced from 14 to 30 ft, but 14 ft was used for the model. Figure 27 is a schematic showing the axle spacing and loading for the AASHTO design truck. As per AASHTO, a 1.33 dynamic load factor was applied to the truck loads. For the model, the loading was distributed as a uniform pressure over tire patches that were 20 in. wide and 10 in. long, as per AASHTO. Influence line calculations were done to find out where the truck should be placed longitudinally along the bridge in order to produce the maximum moment. For this instance, the maximum moment occurred when the middle axle and the resultant of the three axle forces were equally spaced from the middle of the span. The truck was placed in the travel lane of the bridge where it was spanning one joint and thus had two tire loads directly adjacent to two other joints. A schematic showing this loading scenario is presented in Figure 28.

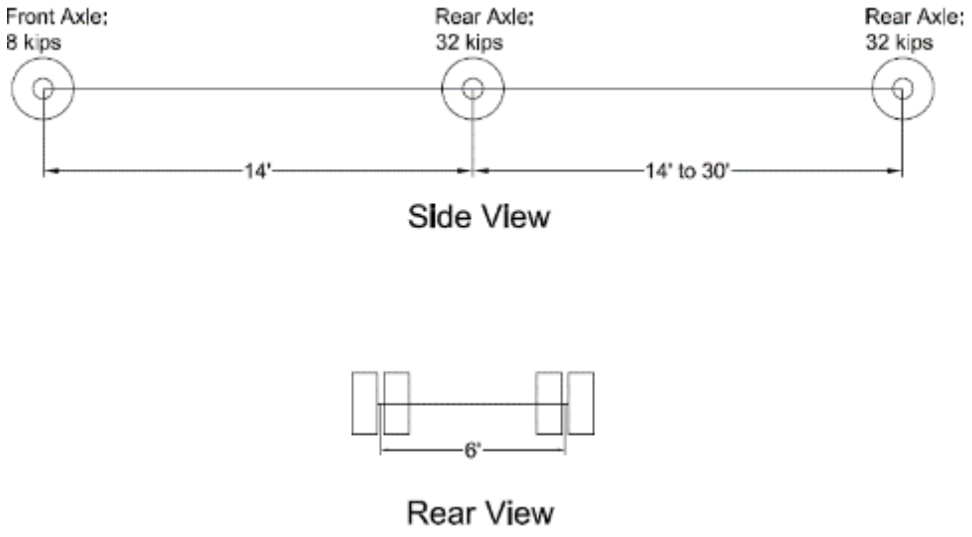

Figure 27: Sketch of AASHTO design truck dimensions and loads

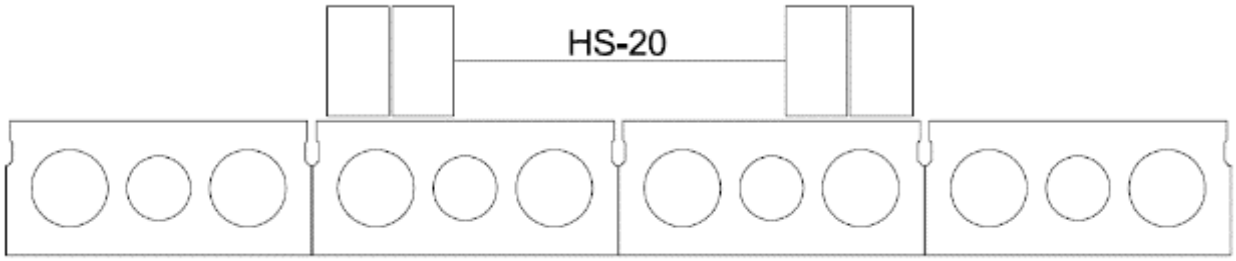

Figure 28: Loading scenario for Abaqus model

This loading resulted in a maximum displacement of approximately 0.19 in.. A screenshot from Abaqus (Simulia 2013) in Figure 29 below shows the deflected shape of the bridge, where the deformations have been magnified by a factor of 488. This screenshot shows that the end opposite of the loading lifts up a very minuscule amount. This is negligible because this would not occur in a real bridge. The reason it occurs in the model is because self-weight was not included in the model. The reason for doing this is because the focus of the model is on the shear key. The shear key would not carry any of the bridge's dead load since it is placed after the beams are in place. There was some concern that including the self-weight would affect the stress results in the shear key.

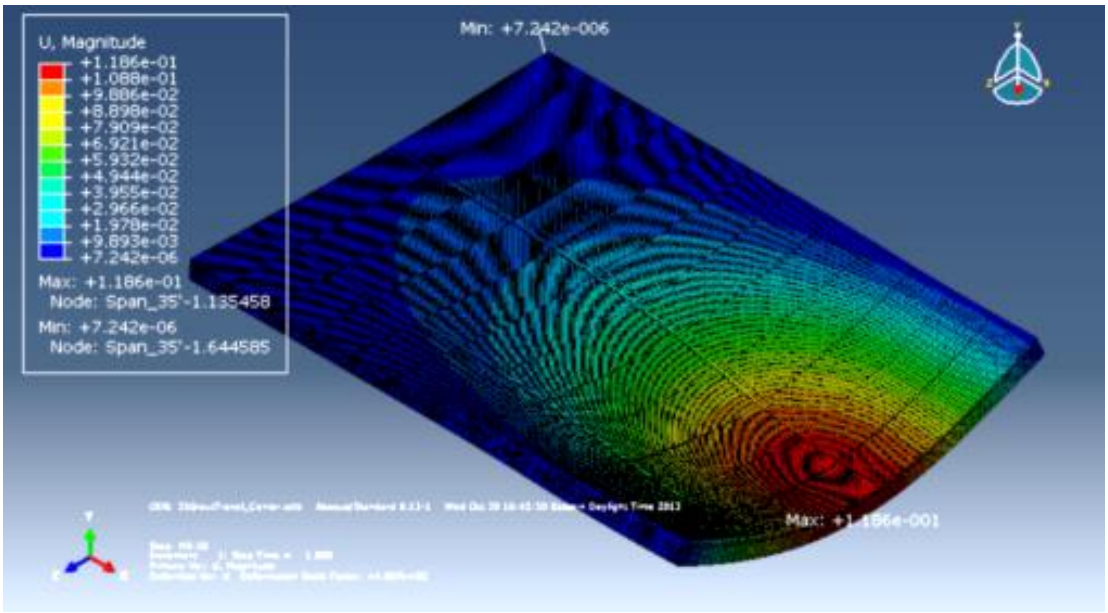

Figure 29: Screenshot from Abaqus showing the deflected shape of the bridge

A closer view of the deformed mesh indicates that the beams joints have opened with the largest separation occurring at the bottom of the beams. The max separation between adjacent beams was 0.0034 in. and the greatest vertical relative displacement between boxes was 0.0087 in.. Figure 30 is a screenshot from Abaqus (Simulia 2013) showing the zoomed in view at midspan of the exaggerated deformed shape.

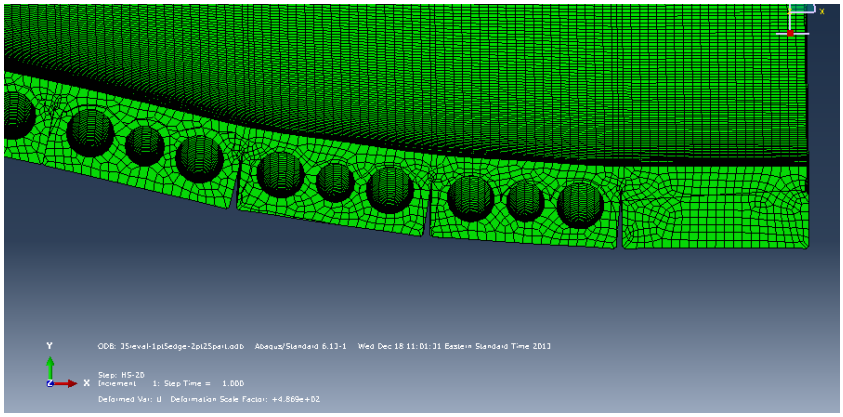

Figure 30: Screenshot from Abaqus showing relative displacements between voided slab

The shear key, which is of most interest, showed a maximum transverse stress of 0.393 ksi. A zoomed in cross section view of a shear key with the transverse stress distribution is shown in Figure 31. As seen in the cross section the bottom tip of the shear key experiences the greatest tensile stress and the tensile stress decreases as you move up the shear key. Eventually the tensile stress turns into a compressive stress near the top of the key.

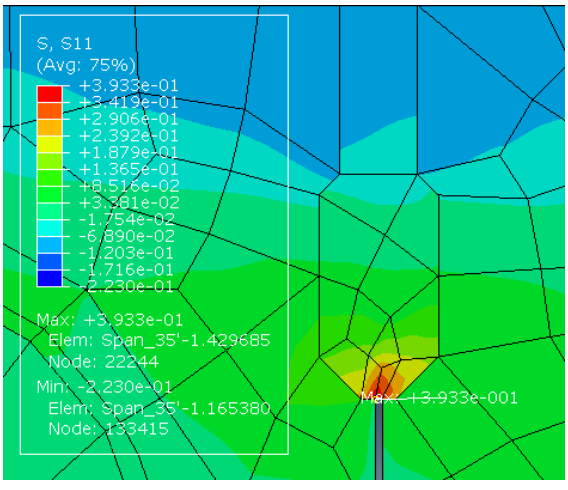

Figure 31: Screenshot showing transverse stresses in the shear key of the full bridge model

Sub-Assemblage Model

Just like the sub-assemblages tested, the sub-assemblage model consisted of three voided slab sections that were 2 ft long. Just as in the full bridge model, a distance between the beams sections of 1/8 in. was assumed. The analysis again was a linear elastic analysis and the material properties assigned in the sub-assemblage were the same as in the full bridge model. Also incorporated into the model were the four support beams that the exterior slabs sat on in the test setup. The support beams were used to represent the stiffness of the bridge that is missing in the sub-assemblage. This will be explained in further detail in the next chapter, experimental methods. The support beams found to be equivalent to the stiffness of the full bridge were four 8 ft long steel 8x15 I-beams. They were modeled using Abaqus' (Simulia 2013) wire shapes that acted as a beam center line model. The wire shape was given the section and material properties of a steel 8x15 I-beam. The beam lines were placed along the exterior and interior edges of the outside voided slab sections. In the test setup, there are two load cells placed on both of the interior support beams and one load cell placed on both exterior support beams. Again this will be discussed further in the next chapter, but these are the three contact points between the support beams and the outside voided slab sections. At these points of contact Abaqus' (Simulia 2013) "point to point" springs were used to connect the voided slabs to the support beams. At each point three different springs were added for each degree of freedom. The springs were given an arbitrary high stiffness value of 1x10^6 kip per inch so that there was no relative movement between the support beams and the voided slab sections. Since they were center line models the beam lines were placed at a distance of half the beam's depth plus the height of the load cells below the voided slab sections. The end conditions of the I-beams were modeled as pins that allowed no translational movement in order to reflect the condition of the test setup to be discussed in the next chapter. A screenshot of the overall model assembly from Abaqus (Simulia 2013) can be viewed in Figure 32.

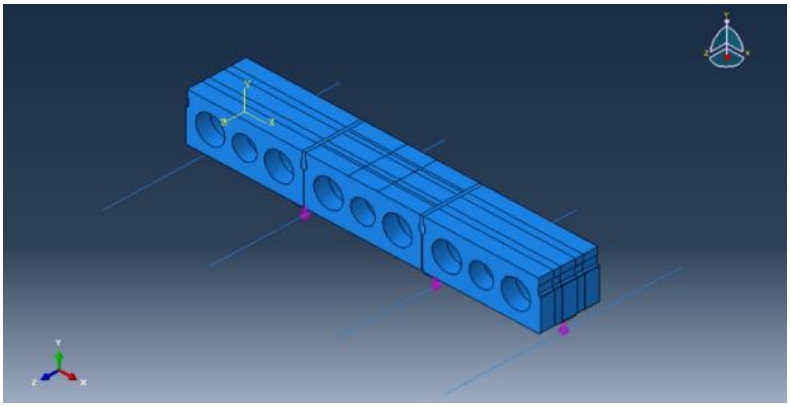

Figure 32: Screenshot of sub-assemblage assembly model in Abaqus

The sub-assemblage model was loaded by displacing a 12 in. by 6 in. section on the top of the middle section a set amount. This was done because in the test setup an actuator bearing against a 12 in. by 6in. rectangular plate on top of the middle section loads the sub-assemblage under displacement control. The displacement amounts were altered until one resulted in a transverse stress distribution in the shear keys that was similar to the one found in the full bridge model. A set displacement of 0.03 in. resulted in the most accurate match. This displacement resulted in a max transverse stress of 0.397 ksi compared to a max transverse stress of 0.393 ksi in the full bridge model. The distribution was very similar to the full bridge model as well, with the max tensile stresses occurring right at the bottom of the shear key and the stresses decreased upward along the shear key and ultimately turning into compressive stresses near the top of the key. Figure 33 is a screenshot of the stress distribution in the shear key from Abaqus.

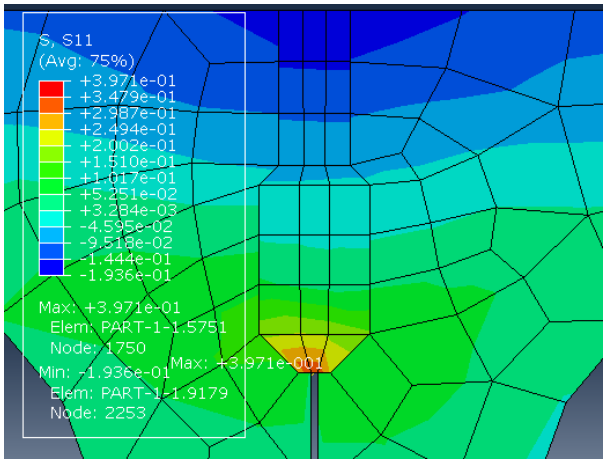

Figure 33: Screenshot showing the transverse shear stresses in the sub-assemblage's shear key

The overall sub-assemblage behavior was comparable to the full bridge model as well. The joints opened in a similar fashion with the largest gap at the bottom measuring 0.0046 in. compared to the 0.0037 in. opening in the full bridge model. A screenshot from Abaqus showing the deformed shape of the sub-assemblage is shown in Figure 34. Overall the sub-assemblage model proves that with the 8x15 support beams and under a controlled displacement of 0.03 in. the sub-assemblage will perform similarly to a 35 ft span adjacent voided slab bridge under an AASHTO design truck loading. The 0.03 in. displacement and 8x15 support beams were the main conclusion taken from the finite element analysis, and the displacement was used for both the static and cyclic tests which is explained further in the next chapter.

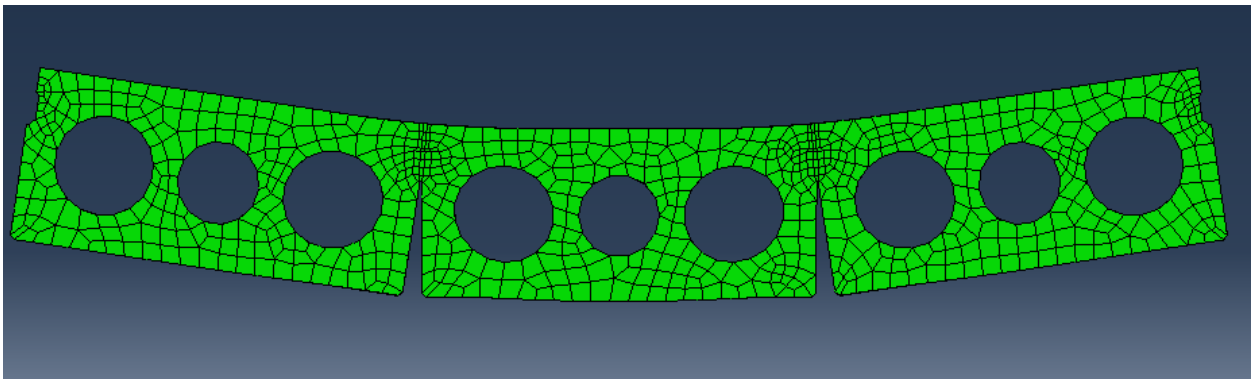

Figure 34: Screenshot showing the deformed shape of sub-assemblage model

Mesh Selection

For both the full bridge and sub-assemblage model 3D solid elements were used to mesh the models. In order to mesh the model in the approximate size of the elements to be used in the mesh had to be selected. For both models, the shear key was given smaller element sizes than the rest of the model. This was done for two reasons. The first reason is that the shear key was the focus of these models. The second reason for this strategy was to save time and computer memory during the analysis of the models. After the selecting the size of the elements, the automatic mesh generation was then used in Abaqus (Simulia 2013) to create the mesh.

The required mesh size was determined for the shear keys by repeating the analysis for varying shear key mesh sizes and determining whether the key quantities were converging to a constant value. The convergence checks were run on the sub-assemblage model because its

analysis took a fraction of the time and memory when compared to the full scale model. The convergence tests were run by starting with a coarse mesh size around the shear key and making it finer until the values converged. The values checked were the transverse stress values at the bottom of the shear key. The mesh of the rest of the model was held constant while the shear key mesh changed. Table 5 shows element sizes for the shear key and the transverse stress value at the shear key for each size. For these tests the element size of the rest of the model was held at 2.25 in.. The table shows that the stress values are converging to a value just under 0.4 ksi, and that an element size close to 1.0 in the key would lead to accurate results. Based on this convergence test, the element size selected was approximately 1 in. for the shear keys and approximately 2.25 in. for the rest of the model.

This element size was used for both models and resulted in 9,577 elements for the sub-assemblage and 553,371 elements in the full bridge. For both models the elements used reduced integration. The resulting analysis time for the sub-assemblage and full bridge model was approximately 2 minutes and 40 minutes, respectively.

Table 5: Result from convergence check

Shear Key Element size (in)	Transverse stress at the shear key's bottom (ksi)
2.5	0.536
2	0.419
1.5	0.401
1.0	0.397

In order to validate the use of a larger mesh size outside of the shear key an analysis was run using a mesh size of 1.5 for the whole specimen. The results gave a max transverse stress of 0.403 ksi. As seen in Table 5, when the shear key was sized as 1.5 in. while the rest of the specimen was held at 2.5 in. the stress was 0.401 ksi. This close comparison validated the use of different mesh sizes in order to speed up the analyses and save memory.

Experimental Methods

This chapter discusses the details of the tests run for this research project. The first section explains the pertinent details about the physical test setup. The second section lists all of the instrumentation used and discusses the importance of each instrument. The third section describes the test methods including setting up a test, running both cyclic and static tests, and the materials testing that was performed. The last section gives a breakdown of the testing schedule throughout this research project.

Test Setup

The six voided slab sub-assemblages that were fabricated and tested were designed to replicate the transverse bending found in a midspan section of a voided slab bridge. Boundary conditions were devised from the finite element analysis so that the behavior was more consistent with a full scale bridge. In order to mimic the stiffness of the rest of the bridge, the sub-assemblage rested on steel I-beams. The steel I-beams spanned 8 ft as this is the width of the reaction floor bays in the lab. Knowing their span, finite element analysis was used to find which size beam would provide the necessary stiffness to replicate the stiffness of the whole bridge. The finite element analysis is described in the previous chapter. Four 8x15 steel I-beams were used, two for each exterior voided slab running along both the inside edge and exterior edges of the voided slabs. The ends of the I-beams rested on pin style supports that only allowed rotation which would result in vertical deflection of the beams. Horizontal movement of the I-beams was not desired as this could cause rocking movements in the I-beams during cyclic loading. These end conditions were incorporated into the finite element model discussed previously. Stiffener plates were welded onto the I-beams at the supports and points of load applications in order to prevent web crippling during the final static testing of the sub-assemblages. The point of load application for the exterior I-beams was in the center and for the interior I-beams, the two points were located offset 9 in. from both sides of the center. These points are where load cells were placed which made contact with the bearing pads on the bottom of the voided slab sections.

The pin supports for the 8x15 steel I-beams were clamped down to steel members that bolted directly to the reaction floor. These steel members were bolted to the reaction floor. The exterior floor members were 9 ft long I-beams. The interior floor members were stub column sections that had plates welded on the top. All of the floor members were 14 in. high so as to provide the necessary height so that the sub-assemblage could be loaded properly.

The loading frame consisted of two columns that were bolted to the reaction floor, and were spaced 8 ft apart. Connecting the columns 10 ft above the reaction floor were two cross beams that were bolted to both columns. The hydraulic actuator used to load the specimen was bolted to the center of the cross beams, and was position vertically so as to load the sub-assemblages in the center.

The actuator used was a MTS Series 244 actuator with a 55 kip capacity which was powered by an MTS series 505.11 hydraulic pump. The actuator and pump were controlled by a MTS 407 controller. The actuator system was capable of applying both static and cyclic loads under either load or displacement control. Since the top actuator connection is a hinge, the actuator was braced by two angles near its bottom to keep it plum. Attached to the bottom of the actuator was a steel I-beam (spreader beam), which was clamped to the middle voided slab section. The spreader beam was connected to a T section that ran through the center void of the center voided slab. Half of a round HSS section was placed on top of the T section to better conform to the circular void. A thin neoprene pad was also placed on top of the HSS section in order to account for any imperfections on the concrete surface so that a uniform contact was kept between the HSS and the void. The purpose of clamping was to prevent the sub-assemblage from becoming out of phase during the cyclic loading. Figure 35, Figure 36, and Figure 37 are sketches detailing the test setup. Figure 38 is a picture of the test setup without a sub-assemblage present. The loading frame, actuator with spreader beam, floor sections, 8x15 I-beams, and loads cells are all present in this photo.

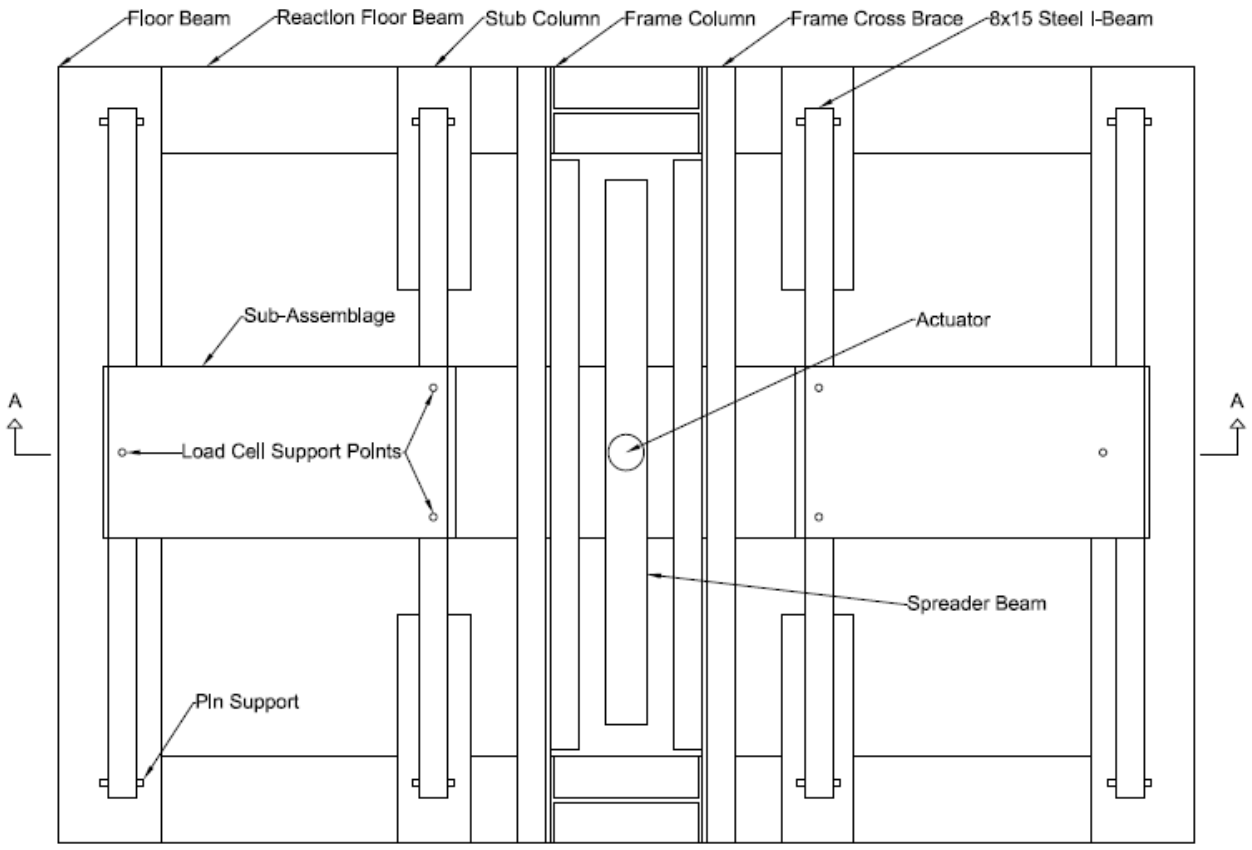

Figure 35: Top view of test setup

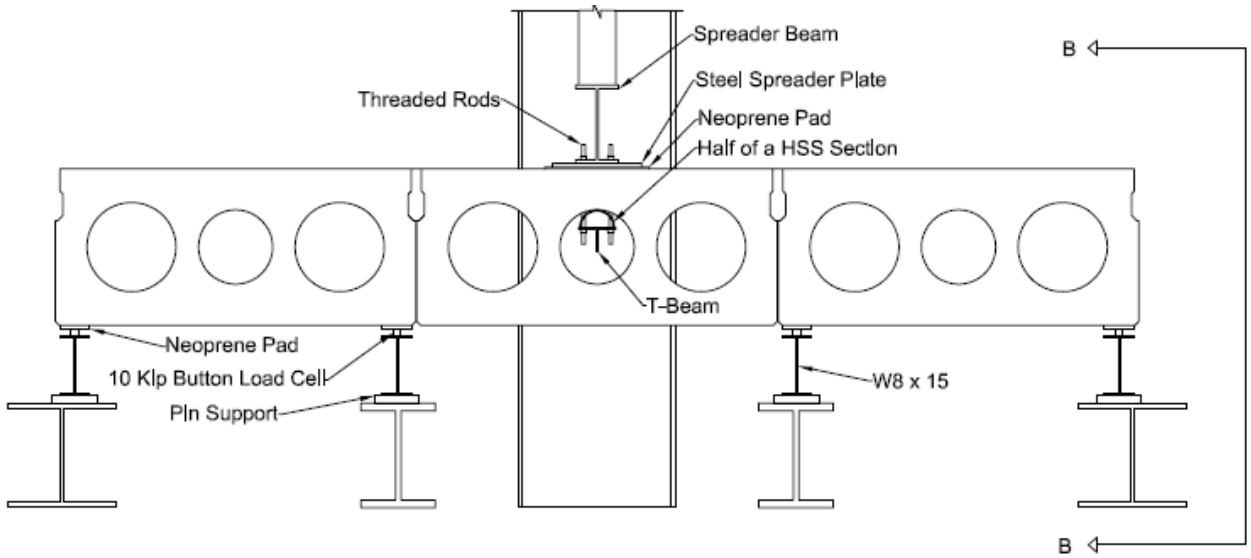

Figure 36: Detail A-A: Elevation view of test setup

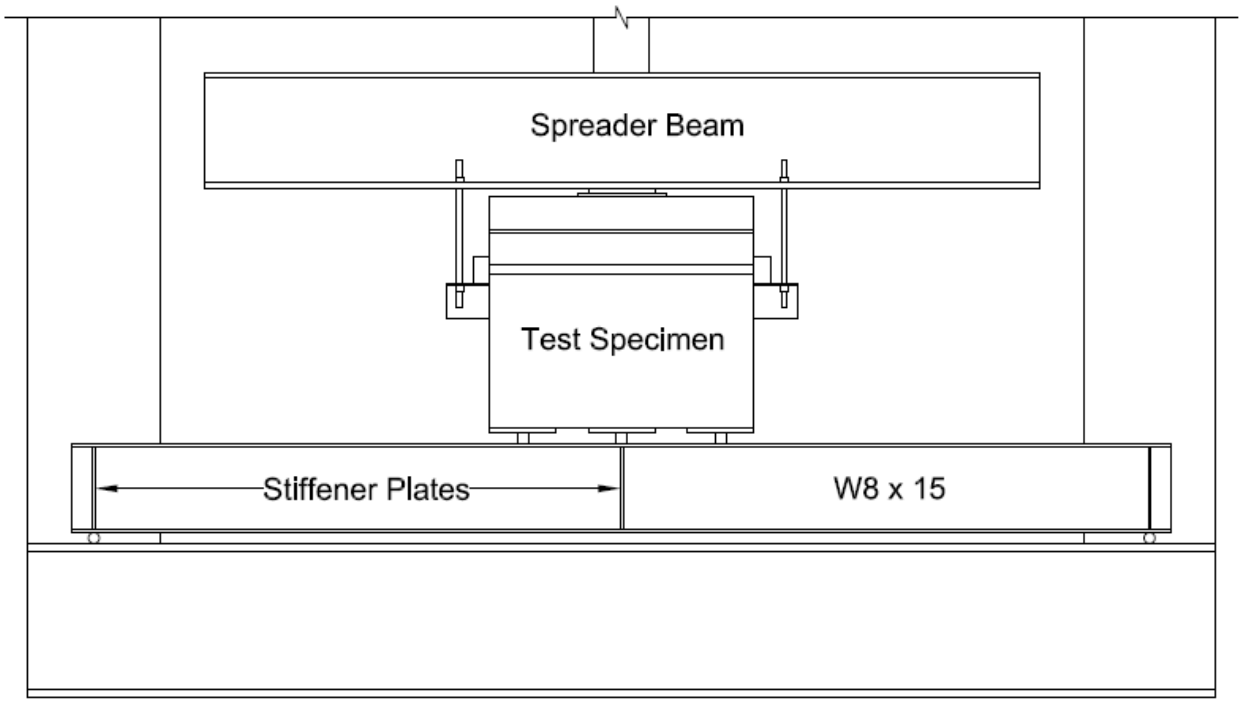

Figure 37: Detail B-B: End view of the test setup

Figure 38: Picture of test setup without specimen present

Instrumentation

Instruments were used to measure joint openings, concrete and steel strains, vertical deflections, and applied loads. All of the instruments were connected to a Vishay Measurements Group System 5000 data acquisition system, which collected data from each instrument at a rate of fifty scans per second.

Each 8x15 steel I-beam had strain gauges placed on both the top and bottom flanges. The purpose of these strain gauges was to show if the self-weight of the sub-assemblages and the loading from the actuator were being distributed symmetrically into the support beams. For the interior I-beams the strain gauges were placed at the middle of the beam. For the exterior I-beams they were placed two times the depth of the beam (16 in.) away from the middle as these beams were loaded in the middle and the loading could affect the strain values. The strain gauges used were Vishay model # CEA-06-250UN-350, which had 350 ohm resistance and had exposed solder tabs. The gauges were 0.415 in. long and 0.120 in. wide. The gauges were attached using an M-bond 200 adhesive, also manufactured by Vishay. The gauges were given a protective rubber coating to prevent damage or moisture infiltration.

Also placed on top of the I-beams were 10 kip button load cells. As described earlier one load cell was placed on the middle of the exterior I-beams and two were placed on interior beams 9 in. offset either side of the center. The load cells were crucial in making sure the voided slab sections were placed in the correct level position. The load cells were also used to monitor the loads being transferred from the actuator to the specimen and into the I-beams. Figure 39 is a sketch showing the location of the load cells. Figure 40 is a picture of an interior I-beam with the load cells placed above the stiffeners and the strain gauge in the center.

Figure 39: Sketch showing the location of load cells under the sub-assemblage

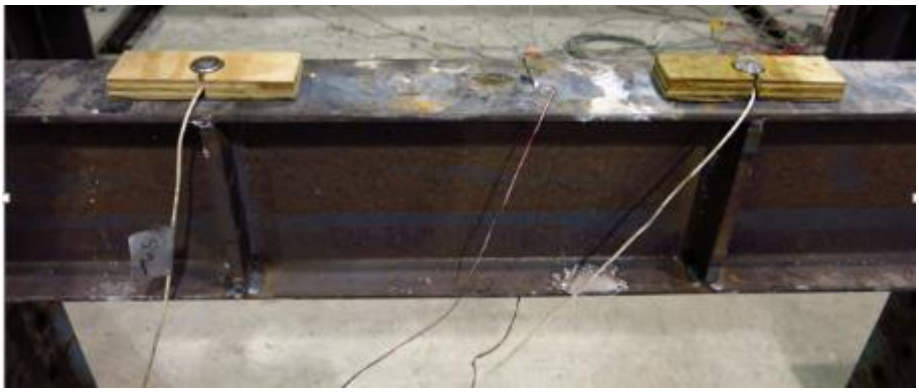

Figure 40: Picture of an interior I-beam with load cells and strain gauge

Joint opening during testing was the most important measurement taken. Joint openings were measured in two locations at each joint face. The first location was directly below the bottom of the shear key. The other location was at the base of the joint near the bottom of the voided slab sections. These openings were tracked through the use of horizontally placed Linear Variable Differential Transformers (LVDT). Short stroke LVDTs were used due to their precision and ability to capture small deflections. The LVDT at the base of the shear key was important because deflections here would imply cracking in the shear key. The LVDT at the bottom of the joint was important because it measured the opening of each joint. There were eight of these horizontally placed LVDTs in total, since there were two at each joint face with two faces per joint. A picture of one joint face with the LVDTs installed is presented in Figure 41. Figure 42 is a sketch showing the location of the 8 horizontal LVDTs.

Figure 41: Picture showing instrumented joint

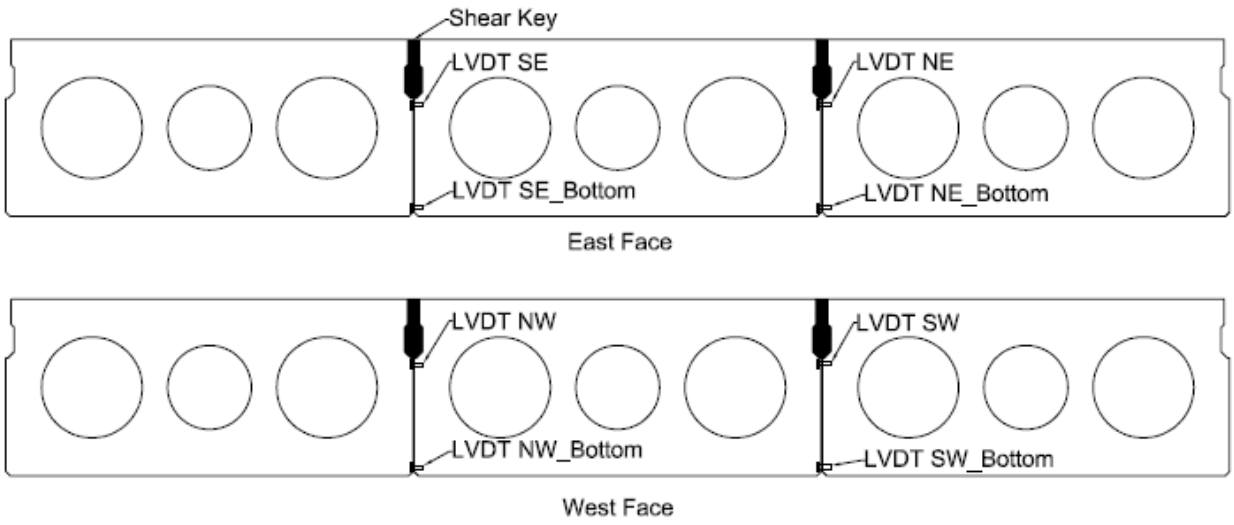

Figure 42: Sketch showing location of the horizontal LVDTs

Aside from the horizontally placed LVDTs, there were also six LVDTs used to measure vertical movements. Two of these vertical LVDTs were placed on both ends of the spreader beam, which is attached to the actuator. These LVDTs serve two purposes. First, there is an LVDT built into the actuator but the values it gives also include the small amount that the loading frame deflects, so these vertical LVDTs measure the deflection that the actuator directly imposes on the specimen. The second purpose is to make the sure the spreader beam is coming down in a level fashion and not providing an eccentric load to the specimen. The other four vertical LVDTs were placed under the exterior voided slab specimens to measure deflection. These LVDTs were placed next to both of the support I-beams and longitudinally in the middle of the specimens. Figure 43 is a sketch showing the location of the vertical LVDTs.

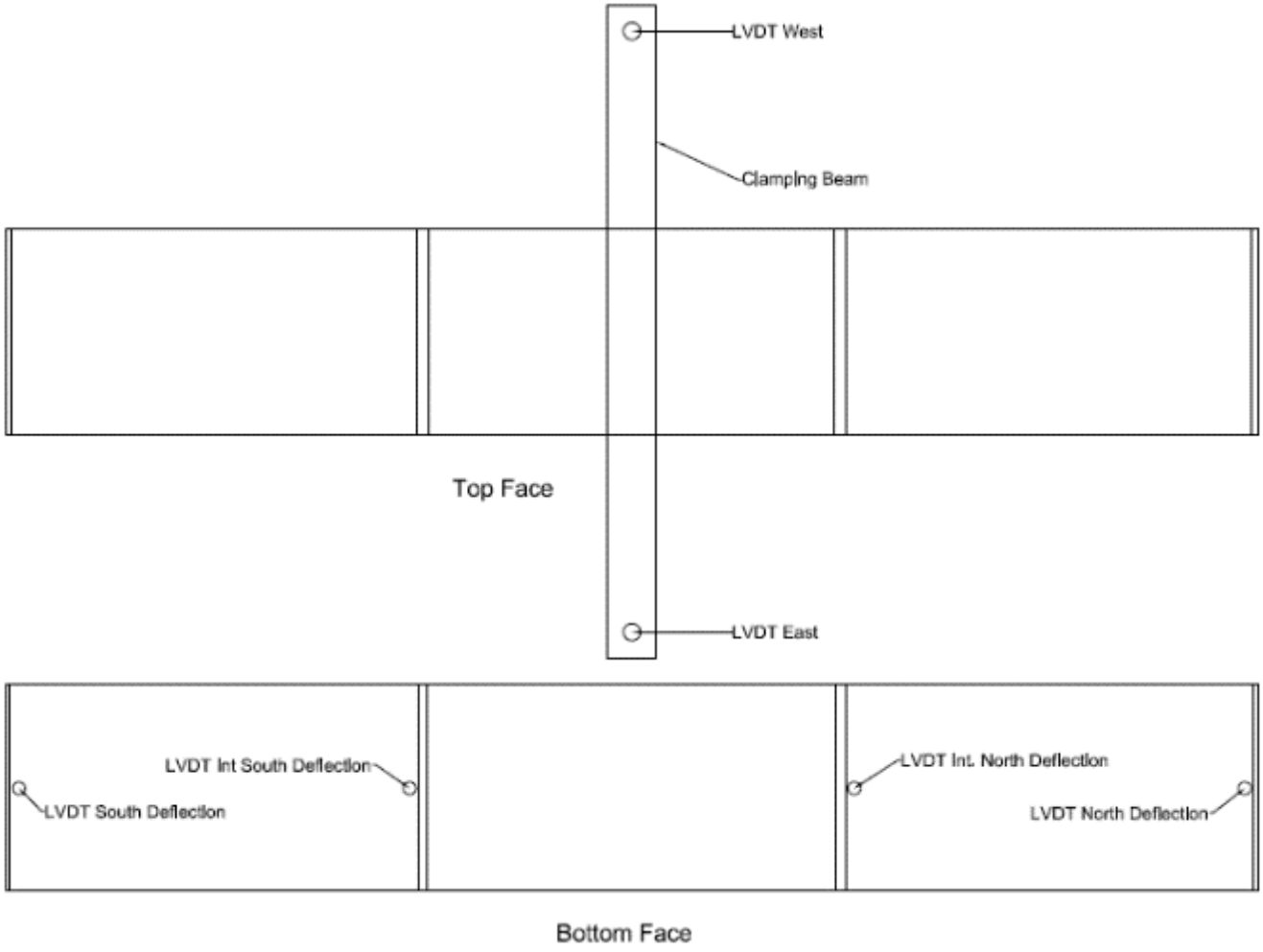

Figure 43: CAD sketch showing the location of the vertical LVDTs

The other instruments used in this setup were five of Bridge Diagnostics Inc's (BDI) strain transducers. These strain transducers are generally used for performing live load tests of full scale bridges, but they were also suited for the sub-assemblage tests. The Vishay strain gauges used on the steel I-beams were not appropriate for concrete surfaces. Two of the BDI strain transducers were centered on the top of the exterior voided slab sections. One could not be placed on top of the middle section because the spreader beam from the actuator was interfering with that location. The other three BDI strain gauges were centered on the underside of the each of the voided slab sections. These gauges were used to confirm the behavior that was expected to be seen in the members. The top of the specimens were expected to be in compression and underside of the member were expected to be in tension. Figure 44 is a sketch showing the location of the BDI transducers. Figure 45 is a picture of an installed BDI strain transducers.

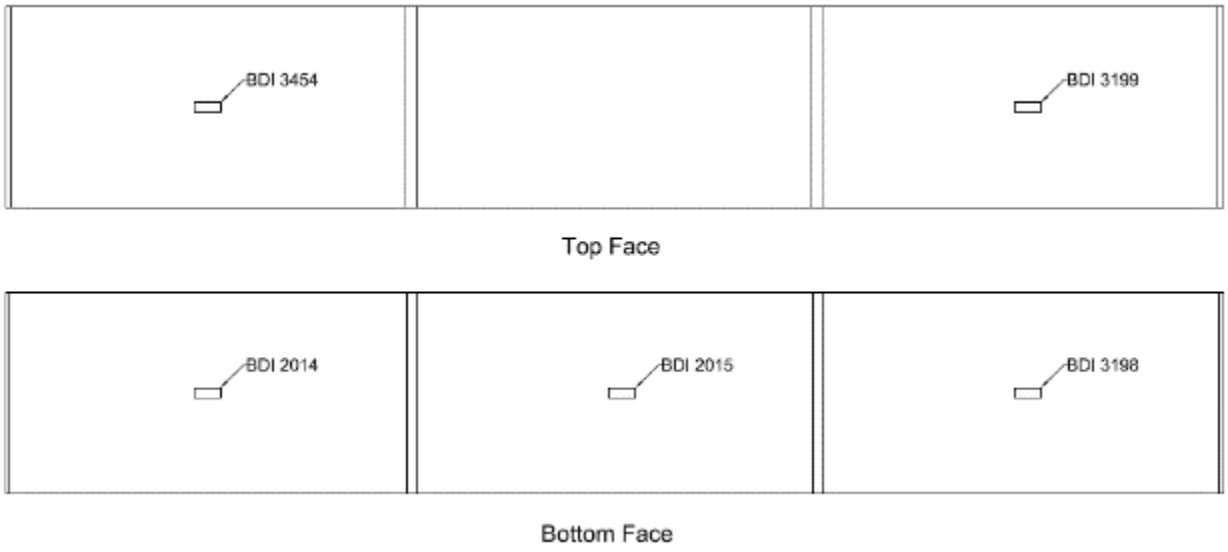

Figure 44: Sketch showing the location of the BDI gauges

Figure 45: Picture of BDI strain transducer

The LVDT and load cell built into the actuator were also wired into the data acquisition system. Although all of their data was collected, this data was mainly used to control the actuator via the 407 controller, which also gave a live output of both of these instrument's values. Overall the sub-assemblage was heavily instrumented, but all of the instruments proved to be useful in evaluating the behavior of both the connection and sub-assemblages. Figure 46 is a picture of a fully instrumented specimen positioned in the test setup.

Figure 46: Picture of fully instrumented specimen inside of test setup

Test Methods

The test methods were kept consistent throughout the project so that comparisons could be directly made between specimens. The connection formwork was removed four days after the connection was placed, and each test was started on the seventh day after the connection was placed. This was done to give adequate time for the connection material to cure properly and gain strength. The same loads and loading scheme were applied to each specimen as well. Each test took five days to finish.

Aside from testing the sub-assemblage, material testing was conducted for each specimen and connection. The connection material was tested on the first day of the specimen testing and on the last day of specimen testing. The voided slab concrete was only tested on the final day of testing. There was no need to test this concrete twice because it was already over 7 months old so the material properties would differ very little over the typical testing period of 5 days. For the voided slab concrete, 4 in. by 8 in. cylinders were cast at the time of placement according to ASTM standards (ASTM C192, 2013). These cylinders were tested for compressive strength (ASTM C39, 2014) and modulus of elasticity (ASTM C469, 2010). For the joint material, 4 in.

by 8 in. cylinders were also made for modulus testing. For compressive strength, 2 in. cubes were cast for the grout and UHPC but for the VHPC 4 in. by 8 in. cylinders were used for strength since it contained coarse aggregate.

Shrinkage bars were made for the joint material, in order to track the shrinkage properties of each material. For the grout and UHPC, 1 in. by 1 in. by 11 in. prisms were made and for the VHPC 3 in. by 3 in. by 11 in. prisms were made, again the difference being the coarse aggregate. Shrinkage readings were taken every day, starting four days after the connection was placed at the time when everything was demolded, and ending on the final day of testing.

Pull off tests were performed with the joint material and the voided slab concrete in an attempt to quantify the bond strength of the joint material to the voided slab concrete. These tests were performed by casting small cylindrical forms that were 2 in. in diameter and 1 in. high directly against the shear key of voided slab sections. The voided slab sections used for these tests were either previously tested exterior specimens that still had an unused joint or specimens that had yet to be tested. These surfaces were also sandblasted and kept moist prior to placement. In order to perform these tests a metal cap was epoxied to the concrete pull off specimens. An insert with a hook on the end was threaded into this metal cap. A tension load cell was hooked onto the insert and then pulled from the other end via a screw jack type device. Figure 47 is a picture of the setup. These pull off tests were run on the first day of testing and on the final day of testing. Table 6 summarizes the material testing performed for each specimen.

Figure 47: Picture of pull off test setup

Table 6: Summary of material test schedule

	Number of Tests and Specimen Size						
	1st Day of Testing			Last Day of Testing			Daily Testing
	Compressive Strength	Modulus of Elasticity	Pull Off	Compressive Strength	Modulus of Elasticity	Pull Off	Shrinkage
Voided Slab Concrete	No Test	No Test	No Test	2 - 4"x8" cylinders per batch	3 - 4"x8" cylinders per batch	No Test	No Test
Grout	3 - 2" cubes	3 - 4"x8" cylinders	2 - 2" dia. x 1" cylinders per batch	3 - 2" cubes	3 - 4"x8" cylinders	2 - 2" dia. x 1" cylinders per batch	2 - 1" by 1" by 11" beams
UHPC	3 - 2" cubes	3 - 4"x8" cylinders	2 - 2" dia. x 1" cylinders per batch	3 - 2" cubes	3 - 4"x8" cylinders	2 - 2" dia. x 1" cylinders per batch	2 - 1" by 1" by 11" beams
VHPC	3 - 4"x8" cylinders	3 - 4"x8" cylinders	2 - 2" dia. x 1" cylinders per batch	3 - 4"x8" cylinders	3 - 4"x8" cylinders	2 - 2" dia. x 1" cylinders per batch	2 - 3" by 3" by 11" beams

Before the sub-assemblage testing began, a few tasks were completed. First a 6 in. by 12 in. steel plate was put under the spreader beam to spread out the load. A neoprene pad was placed under the steel plate in order to create a smooth surface for uniform load distribution. The next task was to attach the spreader beam to the T-beam running through the center void via threaded rods. Attention was paid so that the bolts were snug tight and that the spreader beam was level. Failure to do so led to an eccentric loading which was easily visible during the cyclic loading as the spreader beam appeared to be rocking back and forth. After the center voided slab section was secured to the actuator, the three screw jacks, that were previously supporting the middle section, were lowered. This transferred all of the self-weight of the middle section into the actuator. The thin neoprene pads that were previously used to seal the bottom of the shear keys were removed so that they would not interfere with the test in anyway. Prior to starting the static test, the specimen was checked for cracks. Those that were found were marked and labeled "SH" for shrinkage so that these cracks could be differentiated from cracks observed during testing.

The displacement of the actuator was controlled during the tests. The testing regimen began with an initial static test. When clamping the actuator to the middle voided slab section it would lift the specimen a small amount leading to a tensile load in the actuator. So the first step

was to incrementally lower the actuator until the 407 controller showed zero load on the actuator. This point is referred to as the "zero point". At the "zero point" there is theoretically zero stress present in the joint. To start the static test the center voided slab was depressed at a slow rate by the actuator a total of 0.03 in.. This value was obtained from the finite element analysis. The analysis showed that under the setup's boundary conditions a displacement of 0.03 in. would result in the transverse stress distribution in the shear key equivalent to the distribution seen in the full scale bridge model under the AASHTO design truck loading. To finish the static test, the actuator was slowly backed off of the specimen allowing it to rebound back to the "zero point". After the static test the specimen was inspected for newly formed cracks.

After the first static test, cyclic tests were run in a logarithmic pattern, with a static test following each set to document the specimen's stiffness after each cycling increment. The first cycling increment was 10 cycles, then 100, 1,000, 10,000, and finally every 100,000 cycles up to a total of a million cycles. A million cycles was chosen because this was a close estimate of the number of expected truck loads during a bridge's lifespan. The cyclic tests were performed by first depressing the specimen 0.015 in.. Once at this point, the specimen was cycled between 0.03 in. and the zero point. Thus the span of the cycle was 0.03 in.. The frequency of the cycling was 3 hertz. Figure 48 is a graph showing the loading sine wave for three cycles, which the actuator followed during cyclic testing.

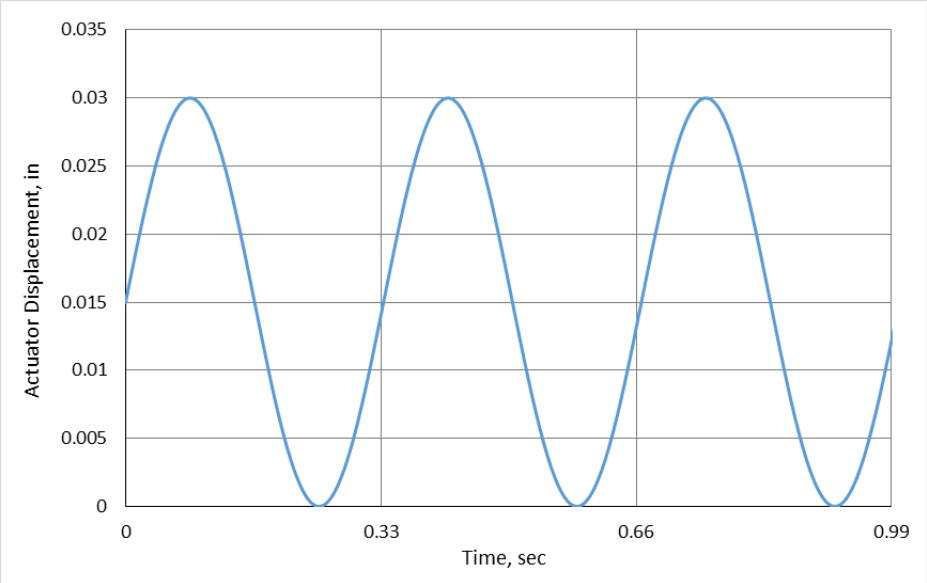

Figure 48: Loading curve for the actuator during cyclic testing

For those specimens that stayed intact for one million cycles and their subsequent static tests, a final static test was performed. For this test, the sub-assemblage was continuously displaced at a slow rate until failure occurred at one of the joints. At this point the testing of the sub-assemblage was terminated and the specimen was removed from the test setup.

Throughout testing water was ponded over the connection to see if the joints leaked. This was accomplished by creating a silicone dam around the joint and then ponding water on top of the joint during cycling. The specimen was then monitored to see if any water seeped through the joint.

Test Schedule

Table 7 presents a detailed schedule showing the test matrix for this research program. The current grouted shear key detail was tested first so that all other tests could be compared against the current standard. The second test was the current grouted shear key with the Kevlar reinforcement. The third specimen tested was the alternate connection shape with Ductal UHPC and the fourth specimen tested was the same alternate connection shape with the VHPC. The fifth and sixth specimens tested were the same as the third and fourth but with a concrete topping placed on top of the sub-assemblage.

Table 7: Test Schedule

	Specimen 1: Grouted Shear Key	Specimen 2: Kevlar Reinforced Grouted Shear Key	Specimen 3: Ductal UHPC connection	Specimen 4: VHPC connection	Specimen 5: Ductal UHPC with concrete topping	Specimen 6: VHPC with concrete topping
Joint Placement	1/24/2014	2/3/2014	2/17/2014	3/4/2014	3/17/2014	3/31/2014
Topping Placement (where applicable)	No topping	No topping	No topping	No topping	3/20/2014	4/3/2014
Start Test	1/31/2014	2/10/2014	2/24/2014	3/11/2014	3/24/2014	4/7/2014
End Test	1/31/2014*	2/15/2014	2/28/2014	3/15/2014	3/28/2014	4/11/2014

*First connection failed on first day of testing therefore was not able to be cycled to 1000000 cycles

Results

This chapter presents both the visual and recorded results from each test. The chapter is broken down into seven sections. One section to presents the data and observations for each specimen and a final summary section. The joint LVDT data is the main focus of each section, with additional data provided when necessary to support a hypothesis about the specimen's behavior. A summary of the material test data for each specimen is provided in each section as well. All supplementary data that was collected from the specimens and material tests has been provided in Appendix C and D, respectively. When appropriate, the axes of similar graphs were kept consistent between sections to make it easier to directly compare specimen behavior. The results form the basis for the discussion, conclusions, and recommendations presented at the end of this thesis.

Specimen 1: Current VDOT Grouted Partial Depth Shear Key

The finite element analysis showed that there would be high transverse tensile stresses in the shear key. Due to this analysis and with the knowledge that grout provides a low bond strength, it was presumed that the connection would fail in the early stages of testing. Prior to the start of the test, significant shrinkage cracks were observed on the top of both shear keys, even though the grout was specified as low-shrinkage. A picture of one of the shear keys with shrinkage cracks marked is presented in Figure 49.

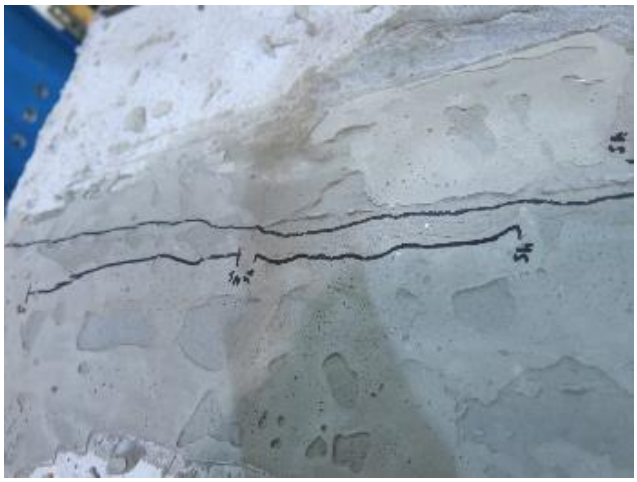

Figure 49: Top of shear key prior to testing showing marked shrinkage cracks

Due to the concern of an early failure, the first static test was run slowly, so that the shear keys could be checked for cracks more frequently. Figure 50 is a graph showing the data collected for the first static test from the four horizontal LVDTs, located at the bottom of each joint face. Cracks were first noted in the north side shear key at 0.02 in. actuator displacement, which is apparent in the graph below, from the jump in both north side LVDT values. Also apparent from the graph is that the south side shear key did not crack, and shows some closure when the north side cracked. This occurred because once the north side cracked the boundary conditions for the test setup changed. The middle and south section then acted rigidly while rotating about the cracked north shear key, which behaved like a hinge. The unloading portion of the first static test shows two things. The first is that the joints did not close, which was to be expected after cracking. The second thing is that the slope of the unloading portion of the curve is much shallower for the north side LVDTs when compared to their pre-cracking loading slope, which is also expected. Although significantly cracked, the northern shear key did not completely fail after the first static test, and could still hold load.

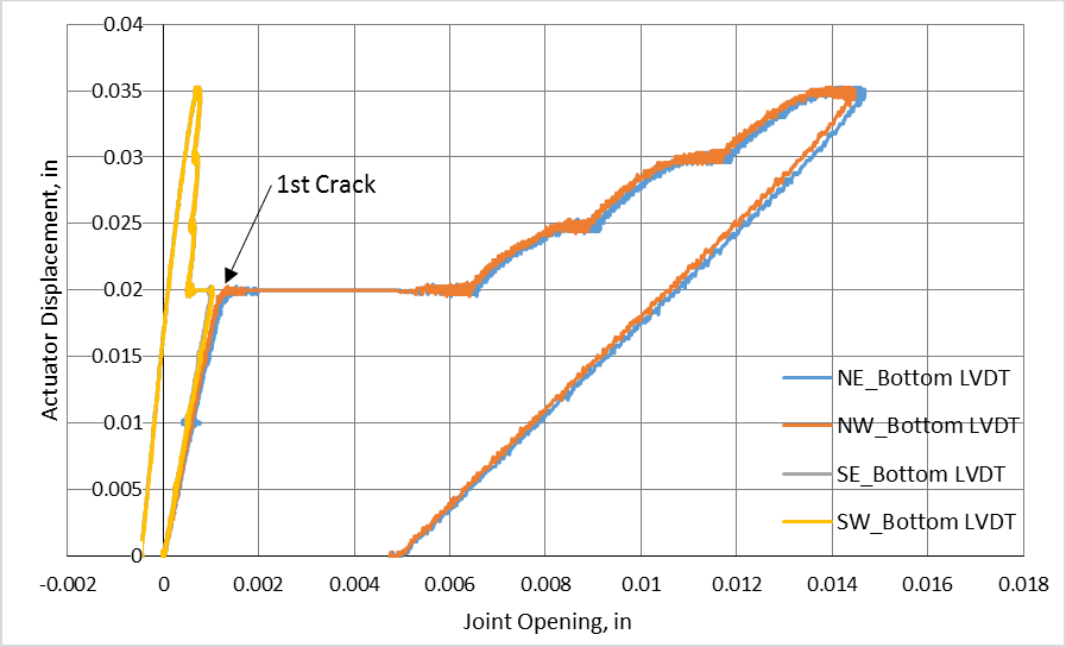

Figure 50: Joint openings versus actuator displacement for the first static test of specimen 1

Since the shear key had not completely failed, cyclic testing commenced. Complete failure of the northern shear key occurred at the 94th cycle. Figure 51 is a graph showing the data

collected during the first 100 cycles, via the horizontal LVDT located at the bottom of the north east shear key face. The graph shows that the key was intact until the 94th cycle when it drastically opened up. A large loss of load was also seen at this point signifying failure. Figure 52 is a picture of the failed joint which shows the flexural crack along the length of the shear key where it debonded from the middle specimen. Figure 53 is a picture of the bare shear key from the middle section. The picture shows that no grout pieces were left bonded to the precast concrete, which is indicative of the low bond strength between the grout and precast concrete.

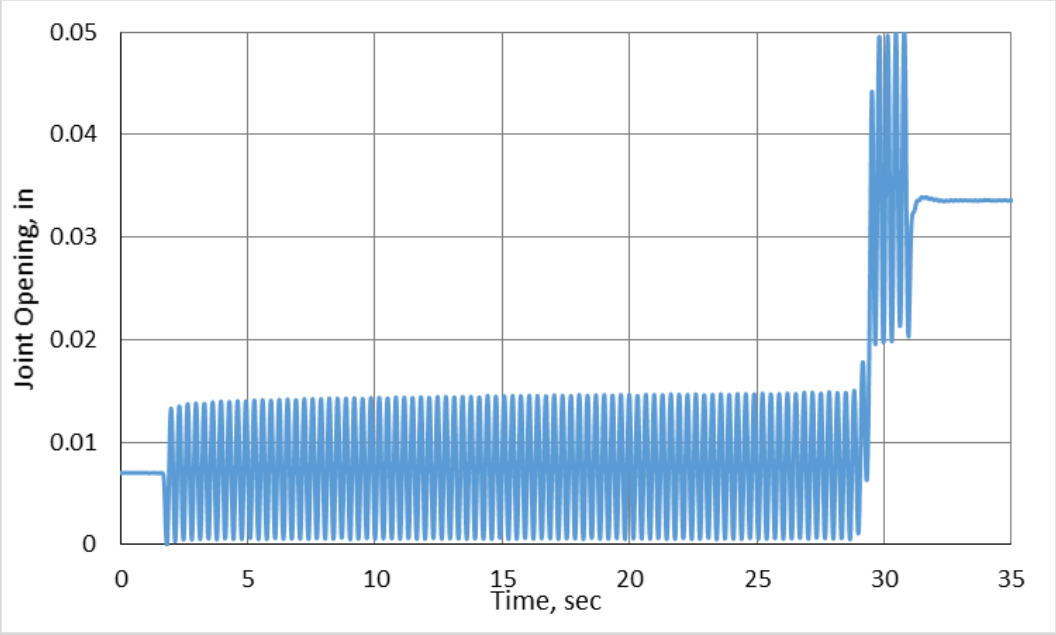

Figure 51: Graph showing north joint openings during the 100 cycle loading of specimen 1

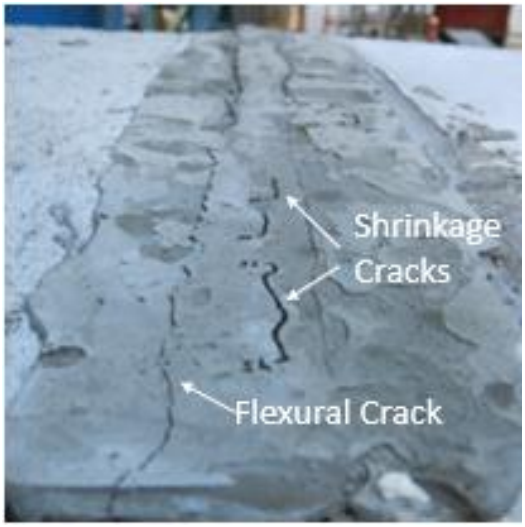

Figure 52: Damaged shear key of the first specimen

Figure 53: Shear key from middle section of the first specimen

Since failure occurred early in the testing regimen there was no opportunity to observe how the behavior degraded over the period of a million cycles. There was also no time to pond water on top of the joint, although it is apparent that water could easily leak down through the crack formed at the debonded surface. This quick failure also disrupted the material testing which was supposed to take place on the first and last day of testing. For this specimen material testing was only performed once. The first specimen was made of concrete sections placed during the first and second batches, so the material testing was performed accordingly. The material testing results are summarized in the Table 8 and Table 9, with all of the details being presented in Appendix D. Note the extremely low bond strength which was expected from the grout. Shrinkage values were also taken for two 1 in. by 1 in. by 12 in. shrinkage bars. All of the data is available in Appendix D, but what is noteworthy is that both bars had undergone 1000 microstrain by the start of testing. This was the probable cause for the shrinkage cracks described above.

Table 8: Compressive material properties for concrete and grout for specimen 1

Material	Average Compressive Strength (ksi)	Average Modulus of Elasticity (ksi)
Grout	7.71	2640
Batch 1 Concrete	7.00	5820
Batch 2 Concrete	6.59	5770

Table 9: Bond strength of grout to concrete for specimen 1

Base Material	Grout Age (days)	Average* Bond Strength (psi)
Batch 1 Concrete	7	49.3
Batch 2 Concrete	7	22.3

*Average of two tests per age per batch, typical for all bond data.

Specimen 2: Current VDOT Grouted Partial Depth Shear Key with Kevlar Reinforcement

As seen in the first specimen, the grout material in the second specimen provided low bond strength. Upon the first static test, although not visible due to the Kevlar-epoxy reinforcement covering the top of the key, it was assumed that the north shear key completely debonded from the middle specimen. Figure 54 is a graph showing the data collected for the first static test from the four bottom horizontal LVDTs. As seen in the graph, the north joint opening reached 0.016 in. in width. The south joint opened up to more than 0.005 in. before it closed due to the hinge action also seen and described in the first specimen. The large opening size on the north side validates the aforementioned assumption since the first specimen failed before the joint could open this much. Although the north shear key debonded, the Kevlar reinforcement prevented failure and was now responsible for all of the load transfer.

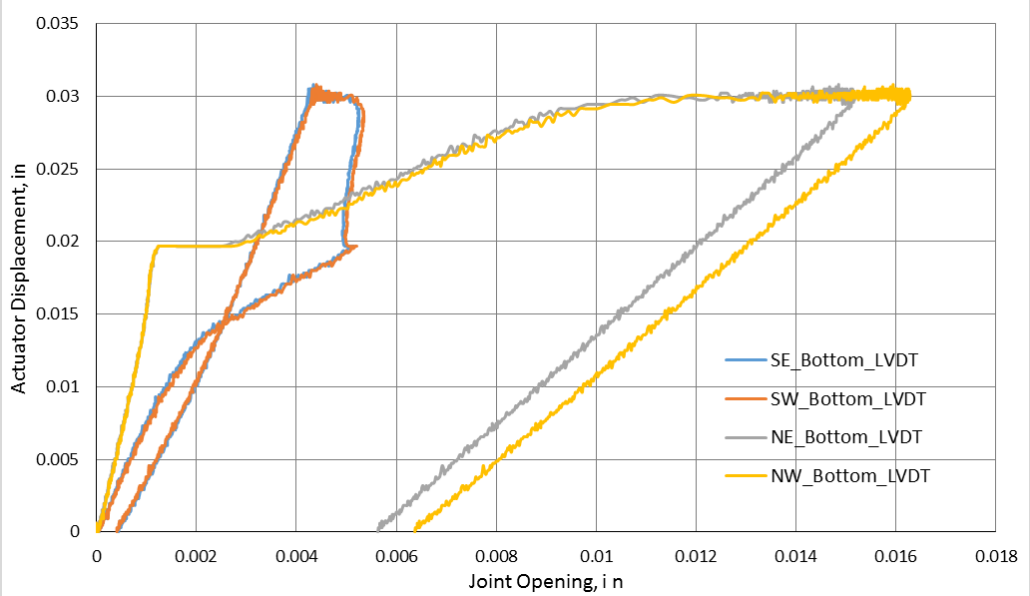

Figure 54: Graph showing the joint openings during the first static test of the specimen 2

The Kevlar reinforcement proved to be both durable and capable of transferring shear loads as the specimen successfully lasted a million cycles. Figure 55 and Figure 56 are graphs showing the north and south joint openings over the testing period. The data was collected during the static tests following each cycling regimen. Selected static test data was left off the graphs for ease of reading as data began to overlap. As seen in the graphs, the north joint following ten cycles of load, opened up to 0.012 in. in width. The joint opening closed throughout the cyclic regimen until it stabilized around 0.005 in., sometime after 10,000 cycles. The south joint originally opened up to around 0.004 in., and over the cyclic regimen the joint opened up until it stabilized around 0.007 in.. The reason for this behavior is due to the hinge action caused by the Kevlar reinforcement which acted as a pivot for rotation after the joint cracked. As described earlier, the north joint debonded in the first static test, which fully engaged the Kevlar reinforcement causing the north section to rotate. Although the south joint cracked during the first static test the full depth cracks at the north joint and subsequent rotation relieved stresses at the south joint. This prevented the south joint from developing full depth cracks and also minimized the amount of rotation. Throughout the cyclic testing the cracks in the south joint propagated which allowed more rotation at the south joint and thus a larger joint opening. This in turn minimized the amount of rotation seen at the north joint explaining why the north joint opening closed throughout the cycling regimen. The opening of the south joint and resultant closure of the north joint continued until the crack growth in the south joint propagated the full depth, which fully engaged the Kevlar reinforcement shortly after 10,000 cycles. At this point the behavior at both joints became constant showing no degradation through the final 900,000 cycles.

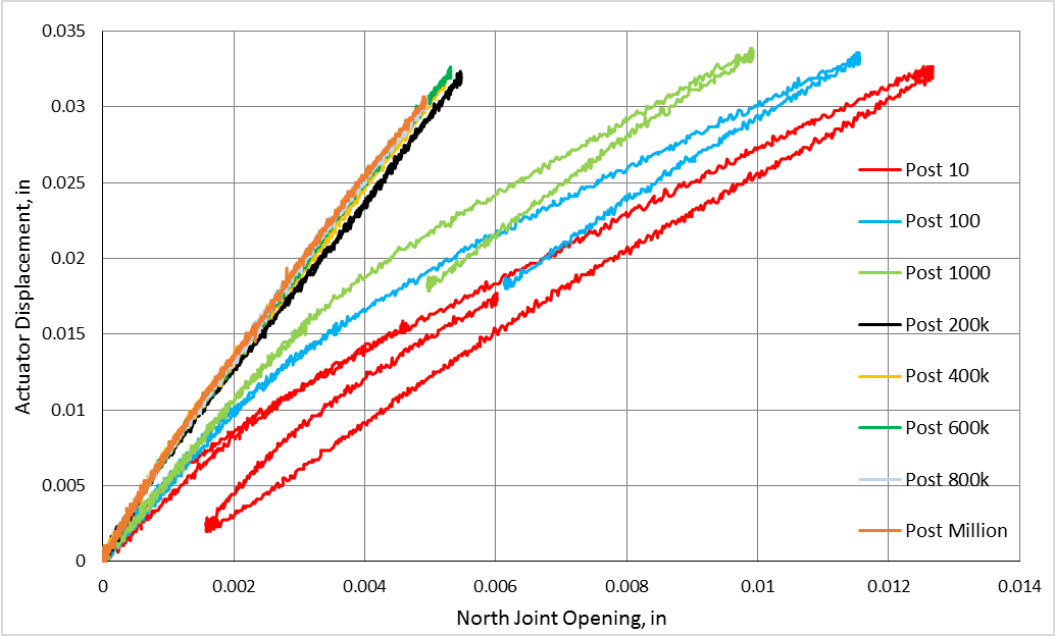

Figure 55: North joint opening for static tests following cyclic loading for specimen 2

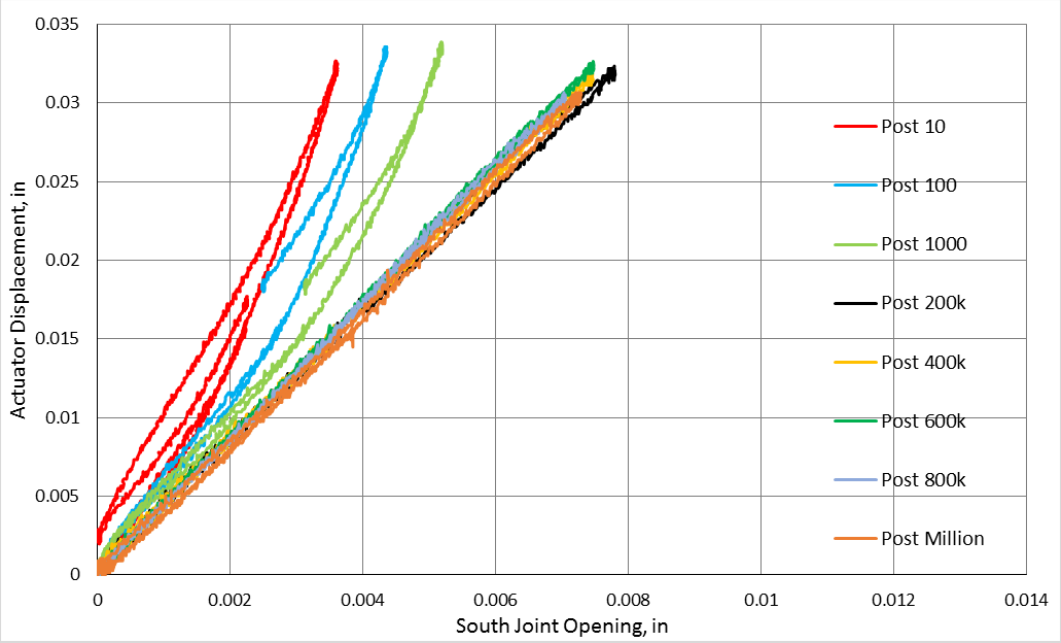

Figure 56: South joint opening for static tests following cyclic loading for specimen 2

Table 10 helps explain the behavior by providing the percentage of the load that went into the exterior beam load cell for every static test on both the north and south exterior support beams. If the beam section deflected straight down one would expect to see roughly 33% of the

total load in all three load cells, which is seen in the data prior to cracking. As the load on the exterior load cell decreases with the load increasing on the interior beam load cells it shows that the beam section is rotating. A schematic of such idealizations are presented in Figure 57 to help explain what is physically occurring. Table 10 shows that during the first static test only 2% of the load on the north specimen was going into its exterior support beam compared to 18% on the south side, showing that the north specimen was rotating more than the south side. These numbers converged during the following three static testing because the north began to rotate less as the south rotated more. The numbers stabilized after 10,000 cycles mirroring the behavior seen in the graphs. Figure 58 is a picture of the south section lifting off of the load cell during the final static test further verifying that the specimen was rotating.

Table 10: Percentage of load going into exterior load cells

	Percentage of Load on Exterior Support Beam Load Cell	
	South Side	North Side
First Static Test	18	2
Post 10	15	7
Post 100	14	7.5
Post 1000	14	9
Post 10000	7	11
Post 100000	10	12
Post 200000	11	12
Post 300000	11	12
Post 400000	11	12
Post 500000	11	12
Post 600000	11	12
Post 700000	11	12
Post 800000	11	12
Post 900000	11	12
Post 1000000	11	13

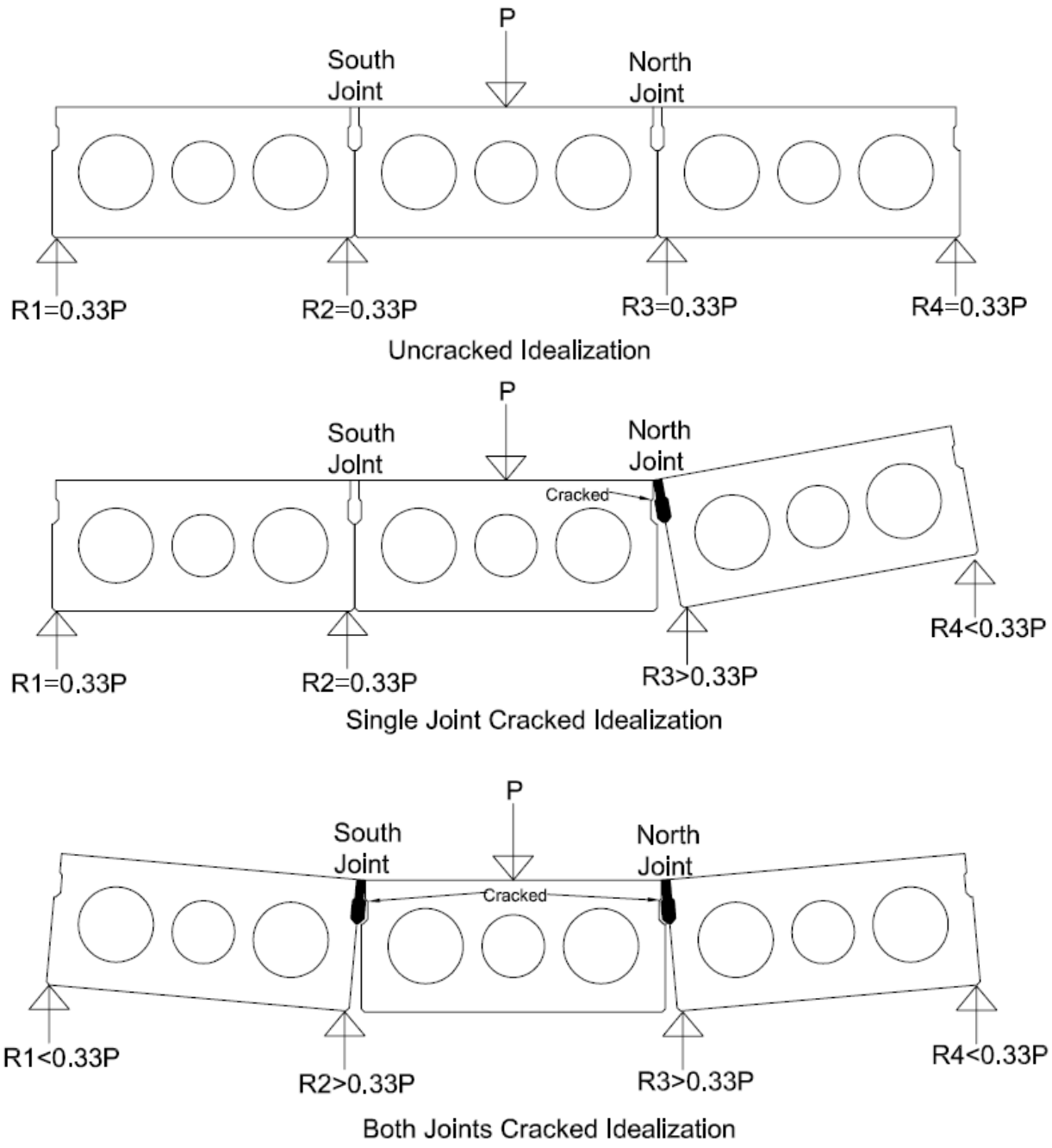

Figure 57: Schematic showing cracked idealizations

Figure 58: Uplift of south beam section at load cell

A final static test was conducted following the million cycles and the post million static test. Figure 59 is a graph of the joint openings during the final static test. The graph shows that both of the joint openings were consistent until 0.075 in. actuator displacement when the south joint underwent a loss of stiffness. At this point, the south joint continued to open and rotate while the north joint slightly closed. At a joint opening of 0.08 in. the south joint LVDT lost contact causing the vertical line seen on the graph. Figure 60 is a picture of the south joint showing the joint opening and loss of LVDT contact. Figure 61 is the load versus displacement plot for the final static test. During the final static test, the actuator displaced 0.487 in. and the maximum load was 13,200 lb. The graph shows that there was a sudden drop in load which occurred due to an abrupt failure of the specimen. The failure occurred when the Kevlar reinforcement, at the south joint debonded, destroying the connection between the south and middle section. Figure 62 is a picture looking down on top of the middle section showing where the Kevlar reinforcement popped off. Figure 63 is a picture of the intact Kevlar reinforcement that popped off as one whole piece.

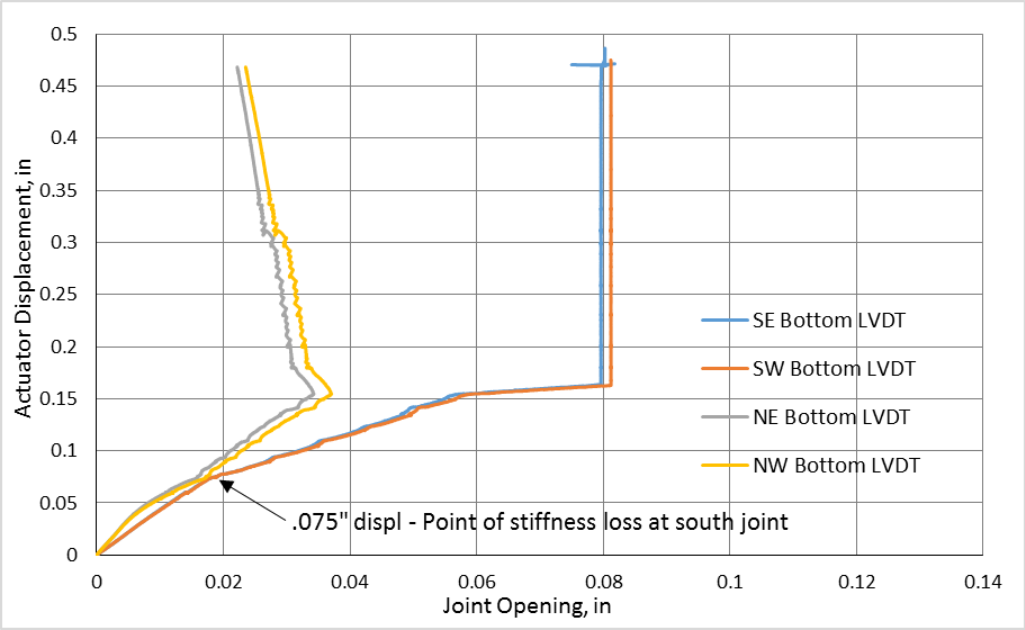

Figure 59: Graph of the joint opening data during the final static test of specimen 2

Figure 60: Picture of south joint of specimen 2 during final static test

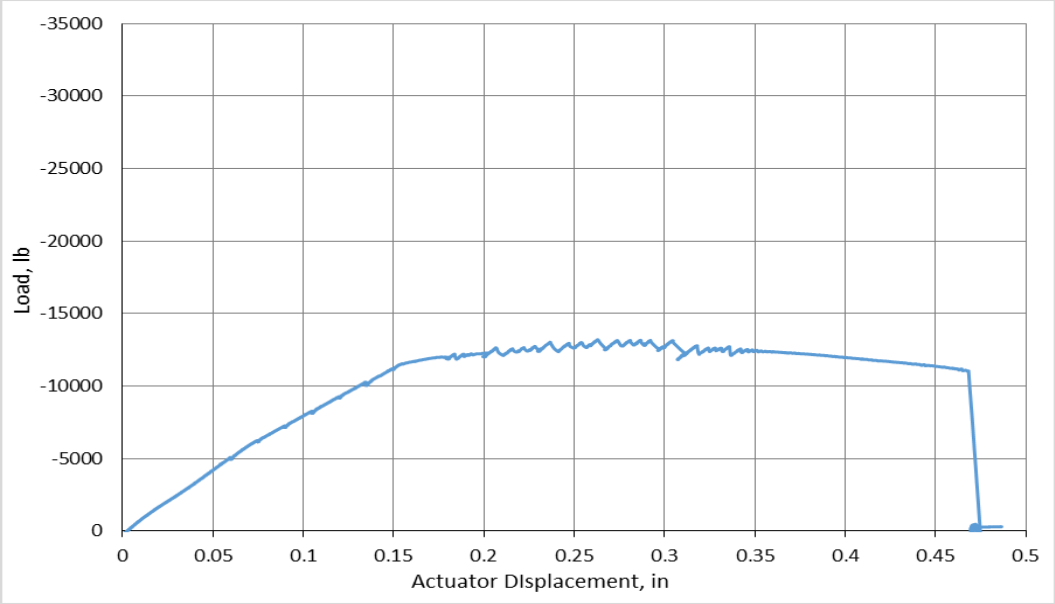

Figure 61: Load versus displacement plot for the final static test of specimen 2

Figure 62: Picture of the middle section at the joint showing where the Kevlar debonded

Figure 63: Picture of debonded, intact Kevlar reinforcement

Due to the longevity of the test, the water ponding test was performed three times. No water was observed leaking through the joint, and the water was left standing all three times until it evaporated. Also due to the longevity of the test, the full schedule of material testing was conducted on both the first and last day of testing. The second specimen was made of concrete sections placed during the first and third batches, so the material testing was performed accordingly. As expected, the grout bond strength was low. Figure 64 is a picture of a shear key after failure showing no traces of grout left bonded to the concrete. Table 11 provides a summary of the data from the pull off tests again showing low bond strengths. Although specified as non-shrink grout, shrinkage cracks were observed along both of the joints. These cracks can be seen marked prior to the placement of the Kevlar in Figure 65. Shrinkage was tracked using two 1 in. x 1 in. x 11 in. bars, and shrinkage strains measured 1000 microstrain by the start of testing in both bars and reached 1350 microstrain by the last day of testing. Table 12 summarizes the strength and modulus of elasticity for the grout and concrete. All of the material test data can be found in Appendix D.

Figure 64: Picture of failed shear key of specimen 2 with no traces of bonded grout leftover

Table 11: Summary of pull off test data for specimen 2

Base Material	Grout Age (days)	Average Bond Strength (psi)
Batch 1 Concrete	7	12.7
Batch 1 Concrete	15	15.9
Batch 3 Concrete	7	19.1
Batch 3 Concrete	15	17.5

Figure 65: Picture showing marked shrinkage cracks before placement of the Kevlar

Table 12: Summary of the strength and modulus data for the grout and concrete of specimen 2

Material	Average Compressive Strength (ksi)	Average Modulus of Elasticity (ksi)
Grout (1st day)	9.46	3800
Grout (Last day)	9.96	3940
Batch 1 Concrete	7.10	5540
Batch 3 Concrete	9.35	6840

Specimen 3: Ductal UHPC Connection

This connection was tested because it was thought that the UHPC would have a higher bond strength with the concrete and that the splice connection along with the blockouts would restrain the joint from opening. Both of these expectations proved true in the testing of the third specimen. The first static test showed no sign of cracking within the joints. Figure 66 is a graph showing the data collected for the first static test from the four horizontal LVDTs, located at the bottom of each joint face. The graph shows linear behavior for both the loading and unloading curves proving that there was no cracking at the joints. During this initial static test the largest joint opening measured 0.002 in. in width.

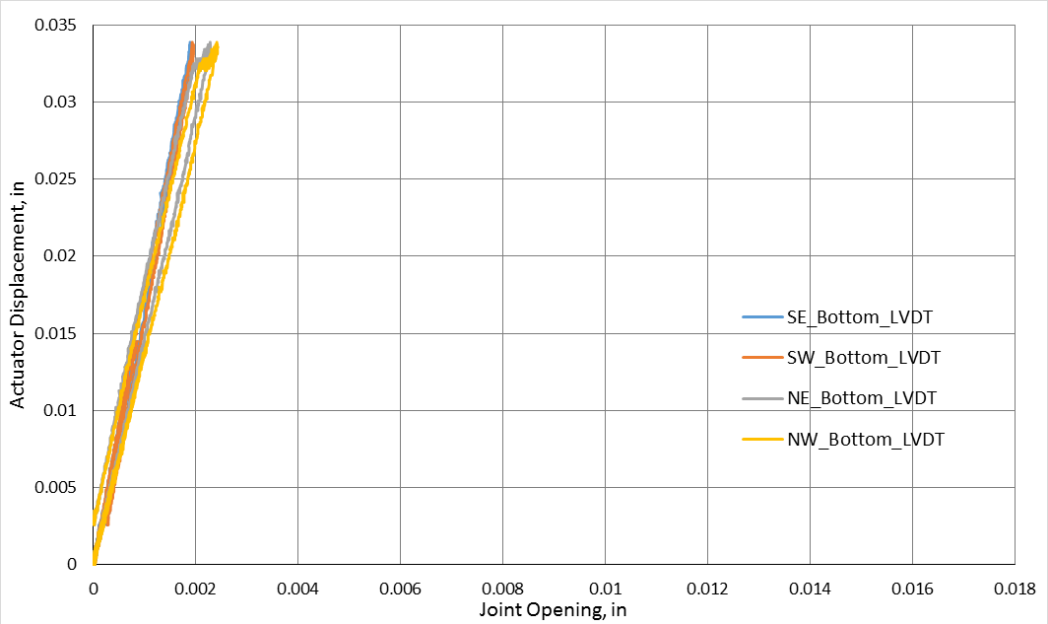

Figure 66: Graph showing the joint openings during the first static test of specimen 3

This connection proved to be durable as it endured one million cycles with small joint openings and no visible cracks at the shear key faces. Figure 67 and Figure 68 are graphs showing the north and south joint openings over the testing period. Selected static test data was left off the graphs for ease of reading as data began to overlap. As seen in the graphs, the north joint retained its linear behavior through the first 1,000 cycles. Between 1,000 and 10,000 cycles cracks were assumed to have formed in the north key leading to joint opening. Figure 69 and Figure 70 are graphs of the exterior north load cell for the 1,000 and 10,000 cycles, respectively. The graph for 1,000 cycles shows a fairly constant span for the load throughout the cycles but graph for the 10,000 cycles shows a drop in load signifying that a crack has formed. Following 10,000 cycles Figure 67 shows that the north joint's stiffness degrades over the remainder of the cyclic regimen. The graph of the south joint shows no cracking and no degradation of stiffness throughout the testing regimen. Once the north joint cracked it relieved stress in the south joint. The UHPC's bond was strong enough so that the relieved stress was not capable to cause cracking through a million cycles. Although the results show cracking, there were no visible cracks on any of the joint faces.

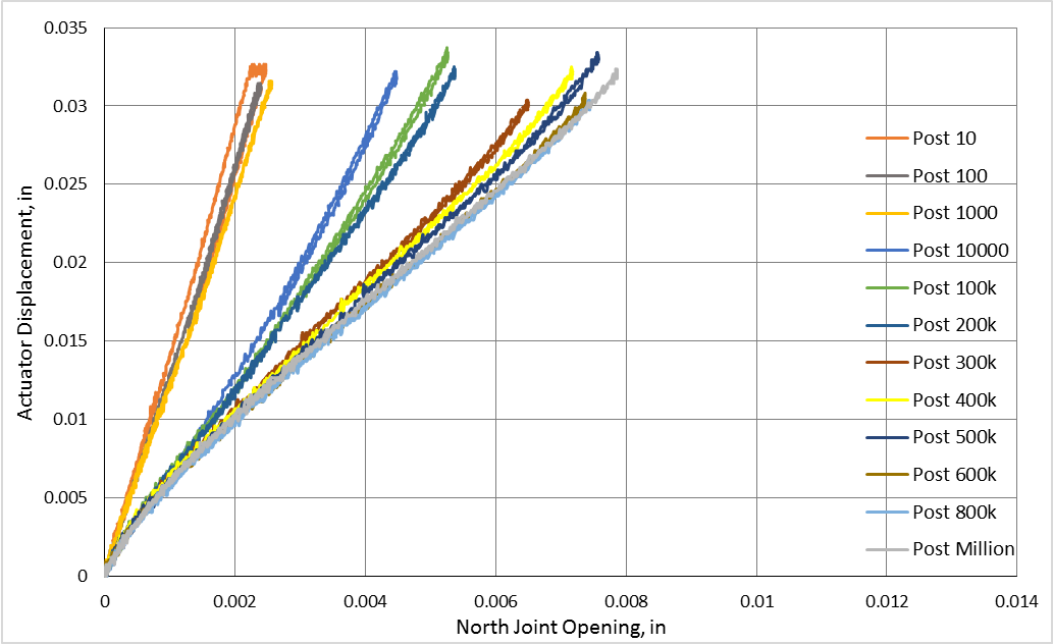

Figure 67: North joint opening for static tests following cyclic loadings for specimen 3

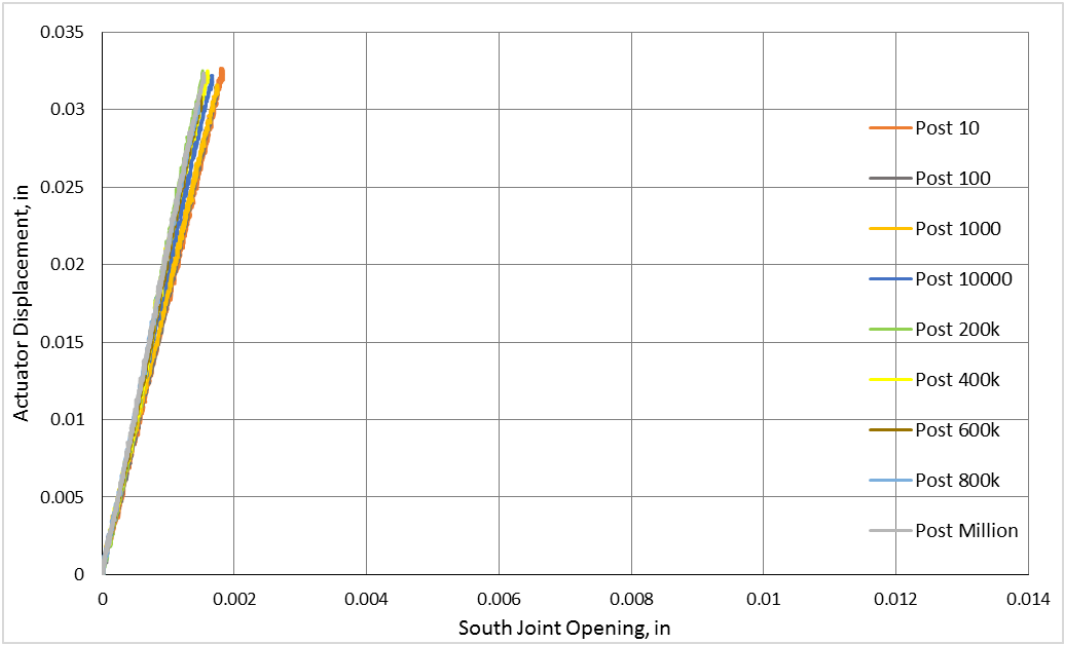

Figure 68: South joint opening for static tests following cyclic loadings for specimen 3

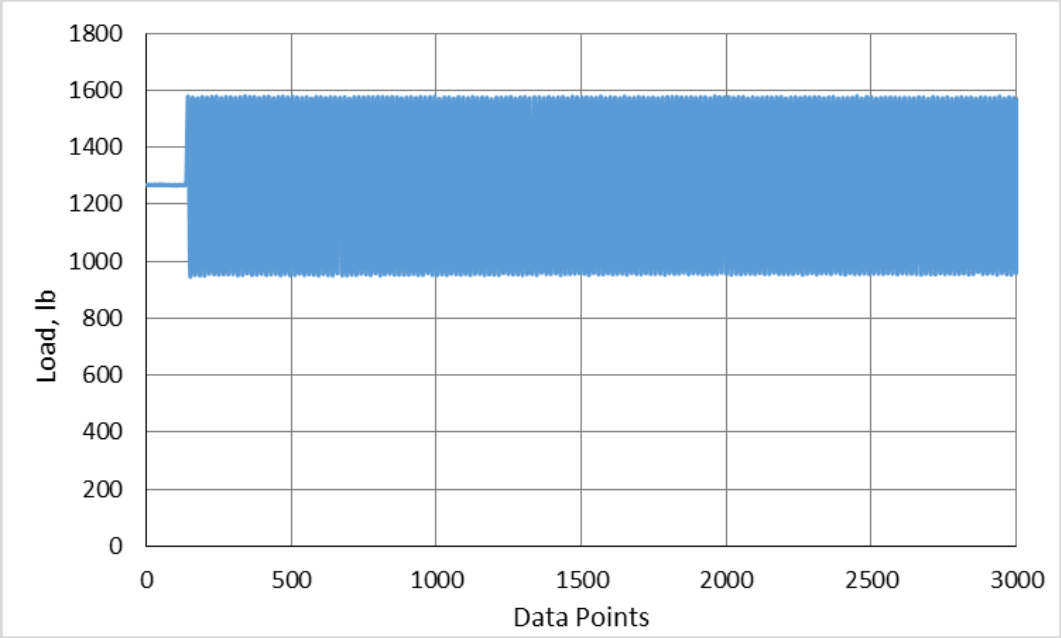

Figure 69: Graph showing data for exterior north load cell during specimen 3's 1,000 cycles

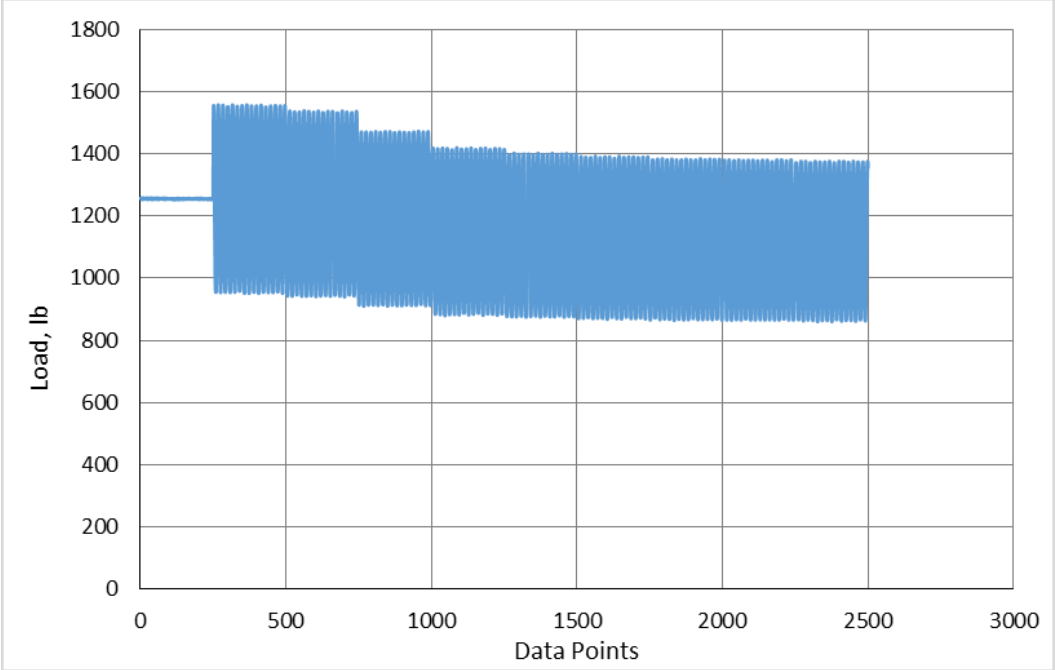

Figure 70: Graph showing data for exterior north load cell during specimen 3's 10,000 cycles

A final static test was conducted following the million cycles and the post million static test. Figure 71 is a graph of the joint openings during the final static test. As seen in the graph the south joint acted linear and remained uncracked until close to 0.1 in displacement of the

actuator. At this point the south side cracked and the joint opened up. The south side opening widened quickly and this caused the north joint to partially close, as seen in the graph. The south joint LVDTs lost contact at 0.12 in. of opening and this is represented in the graph by the vertical lines at the end of the south LVDT data.

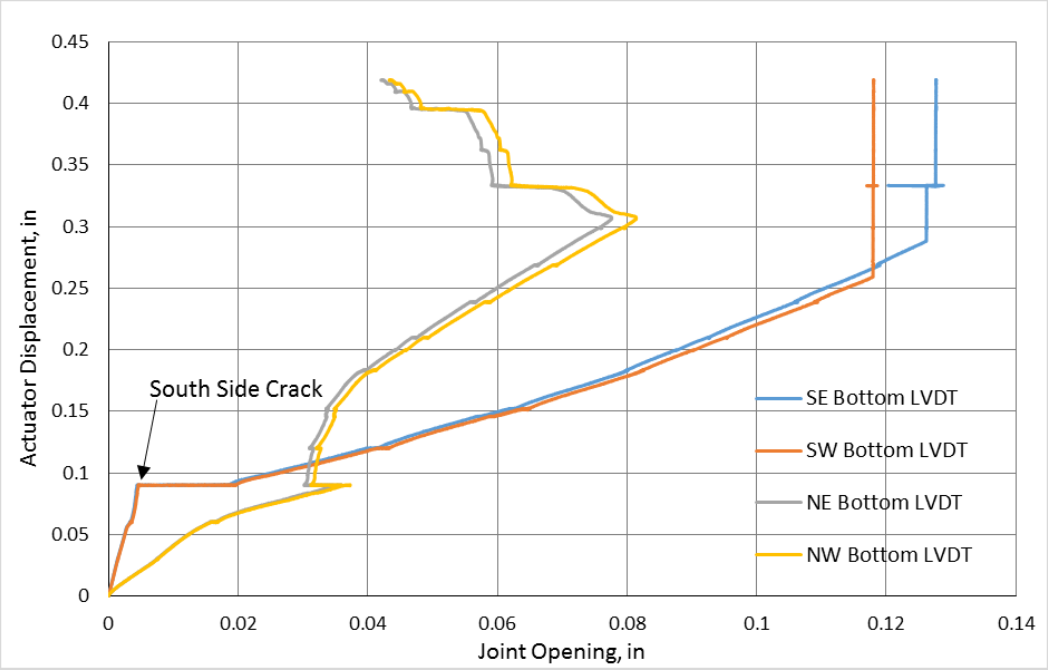

Figure 71: Graph of the joint opening data during the final static test of specimen 3

Figure 72 shows the load versus displacement plot for the final static test. The peak load was 25,200 lb and was attained around 0.3 in. of actuator displacement. At this point the specimen would not hold load suggesting a failure. The load continued to drop as the actuator was taken to 0.42 in. displacement, at which point the test was stopped. Also noted at a displacement of 0.3 in. was that the cracks around the south joint faces extended out of the UHPC and into the concrete. Figure 73 is a picture showing these cracks. At this point, only the concrete above the extended crack was in compression and with such a small area the concrete began to spall and crush leading to the drop in load. Figure 74 is a picture showing the crushed concrete. Figure 75 is a picture of cracks crossing the UHPC joint at the blockout. These cracks may be either shear or bond related, but the specific cause is unknown.

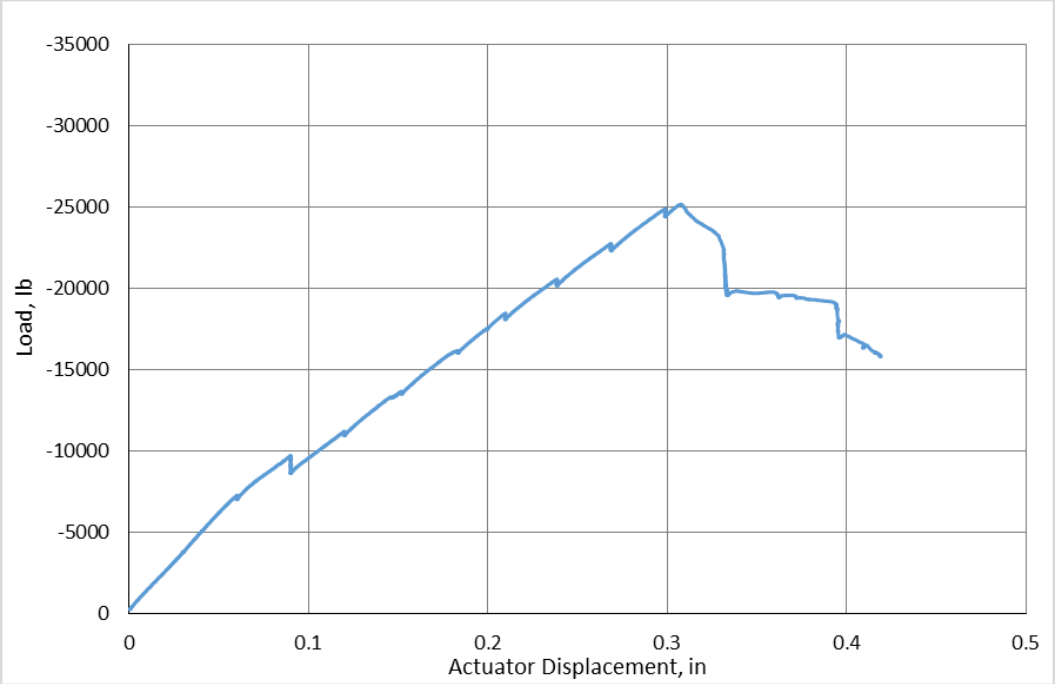

Figure 72: Load versus displacement plot for the final static test of specimen 3

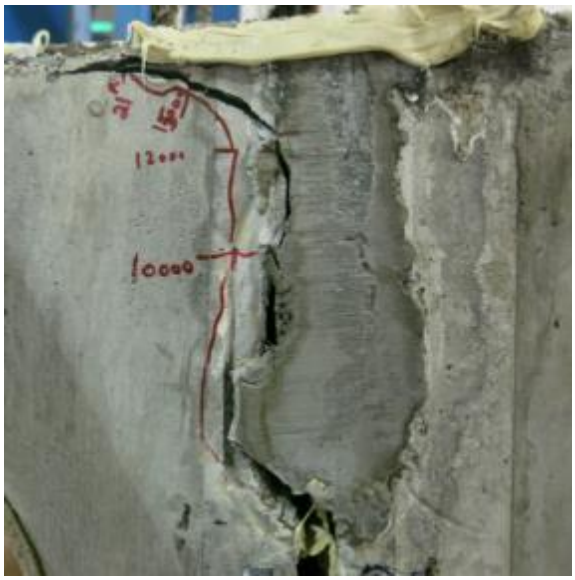

Figure 73: Picture showing the cracked south shear key of specimen 3

Figure 74: Picture of concrete crushing and concrete spalls on top of specimen 3

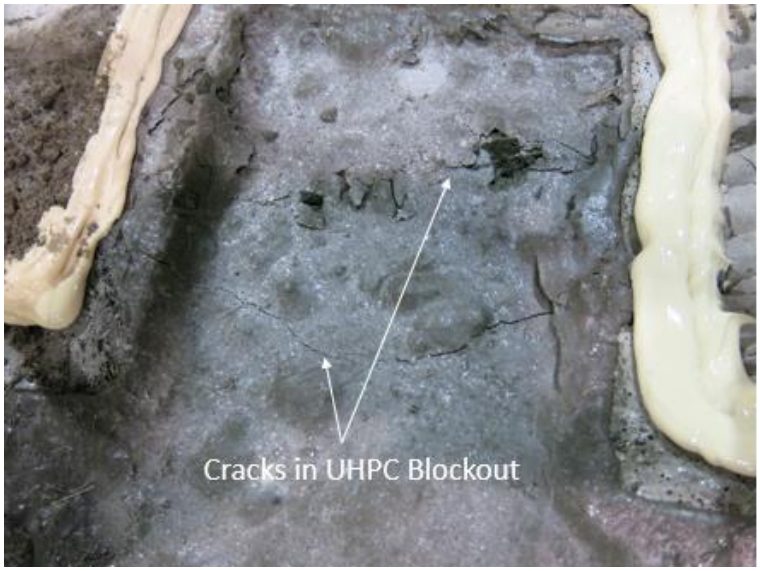

Figure 75: Picture looking down on UHPC blockout showing cracks run across the blockout

Due to the longevity of the test, the water ponding test was performed three times. No water was observed leaking through the joint, and the water was left standing all three times until it evaporated. Also due to the longevity of the test, the full schedule of material testing was conducted on both the first and last day of testing. The third specimen was made of concrete sections placed during the first and second batches, so the material testing was performed accordingly. The pull off tests showed that the UHPC had high bond strengths. During the pull

off tests some of the UHPC bond specimens ripped pieces of concrete with it showing that the bond strength could actually be stronger than the tensile capacity of the concrete. A picture showing this is found in Figure 76. Table 13 provides a summary of the data from the pull off tests showing the high bond strengths. There were no shrinkage cracks observed around the UHPC joint. Shrinkage was tracked using two 1 in. x 1 in. x 11 in. bars, and shrinkage strains from the bars measured at 210 microstrain for bar 1 and 260 microstrain for bar 2 at the start of testing. On the last day of testing the strain measured 320 and 380 microstrain. Table 14 summarizes the strength and modulus of elasticity for the UHPC and concrete. All of the material test data can be found in Appendix D.

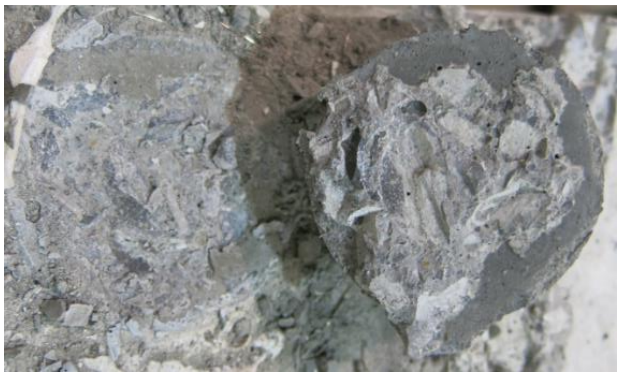

Figure 76: Picture showing a pull off specimen that pulled concrete off with it

Table 13: Bond strength data for the UHPC for specimen 3

Base Material	UHPC Age (days)	Average Bond Strength (psi)
Batch 1 Concrete	7	220
Batch 1 Concrete	12	210
Batch 2 Concrete	7	240
Batch 2 Concrete	12	310

Table 14: Summary of strength and modulus values for UHPC and concrete for specimen 3

Material	Average Compressive Strength (ksi)	Average Modulus of Elasticity (ksi)
UHPC (1st day)	11.3	7240
UHPC (Last day)	15.5	7780
Batch 1 Concrete	7.16	5340
Batch 2 Concrete	7.28	5810

Specimen 4: VHPC Connection

This connection was tested to see if the nonproprietary VHPC could provide similar performance to Lafarge's UHPC, but at a lesser cost. The results from specimen 4 show that the VHPC also has high bond strengths and can perform well as the joint filler material. The initial static test showed no signs of cracking with linear behavior in both the loading and unloading curve of the joint LVDTs. This graph is made available in Figure 77. The largest joint opening measured was 0.002 in..

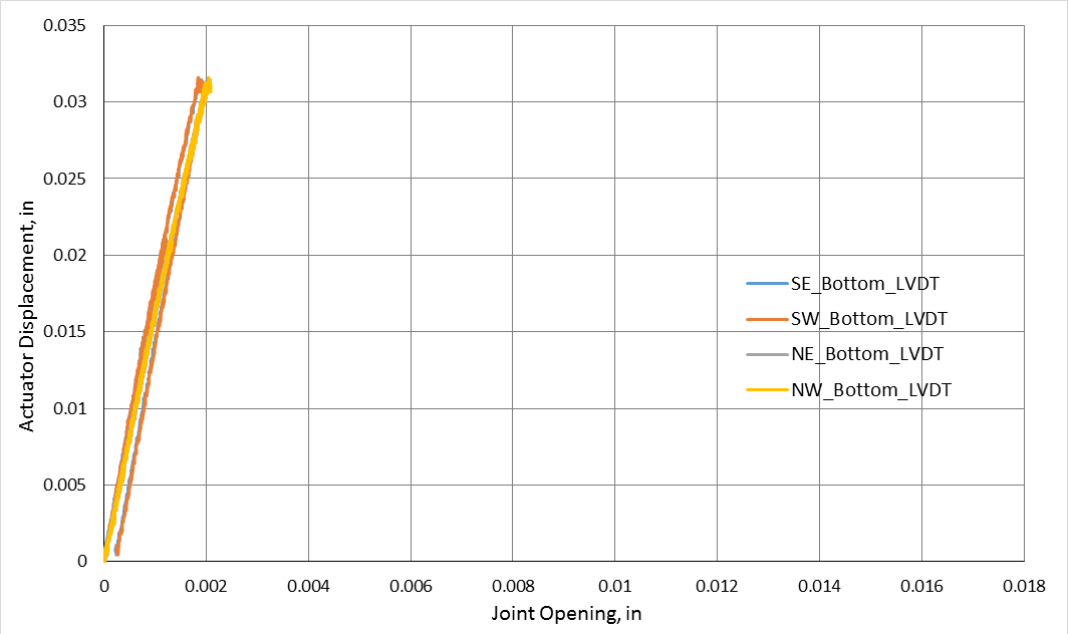

Figure 77: Graph of the specimen 4's initial static test showing data from the joint opening

The VHPC proved to be a durable material as there was no stiffness degradation observed over a million cycles. Figure 78 and Figure 79 are graphs showing the north and south joint openings over the testing period. Most of the data overlapped, so after the post 1000 cycle static test other static test's data was left off of the graph for ease of reading. As seen in the graphs, the data left still overlaps signifying no change in behavior throughout the testing regimen. There were also no observed cracks on either joint after a million cycles which agrees with the data. The largest opening that was measured throughout the testing regimen was 0.003 in., which took place on the north joint.

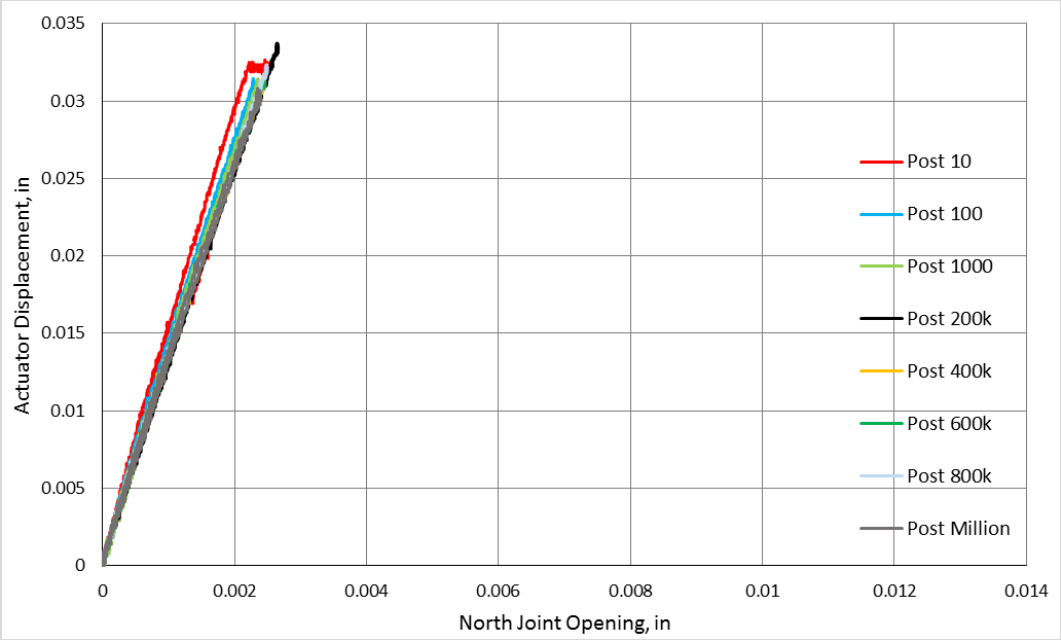

Figure 78: Specimen 4's north joint opening throughout the test regimen

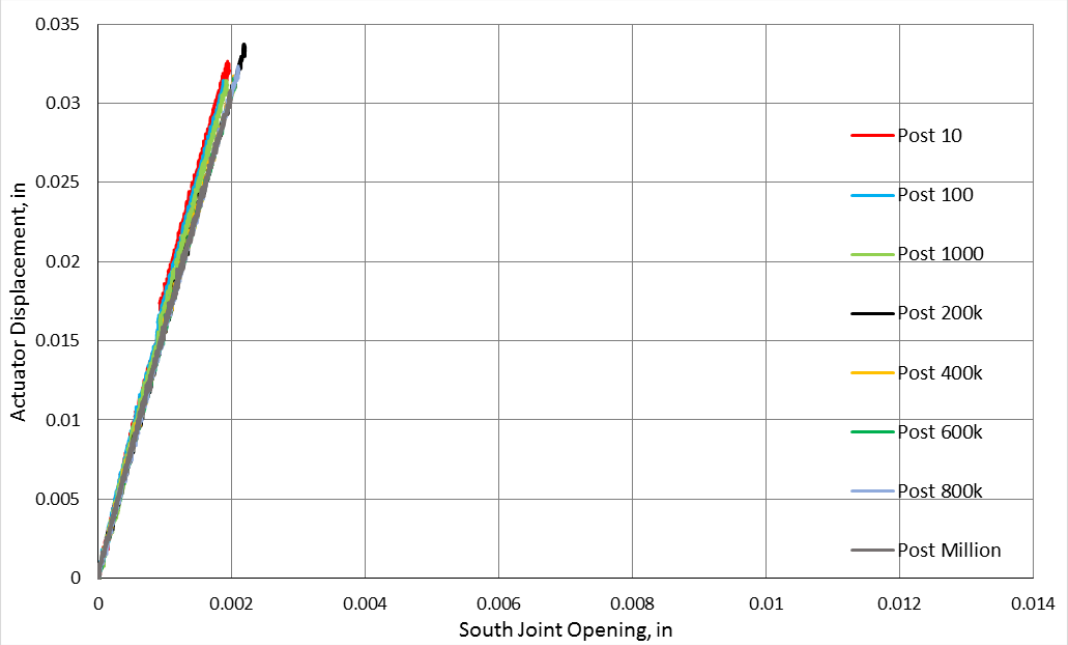

Figure 79: Specimen 4's south joint opening throughout the test regimen

A final static test showed that the VHPC connection also had a high strength. The final static test had to be stopped before the connection failed, for two reasons. The first reason was that a few load cells were close to their 10 kip capacity. The second reason was that the interior

8x15 steel I-beams were showing signs of lateral torsional buckling, and since they were needed for future tests their strength could not be compromised. The max load reached before the test had to be stopped was 32400 lb., which took place at an actuator displacement of 0.44 in.. Figure 80 is a graph of the load versus displacement plot for the final static test. As seen in the graph, the slope of the line had not begun to flatten out at the point when the test was stopped. This signifies that the specimen could still have taken more load.

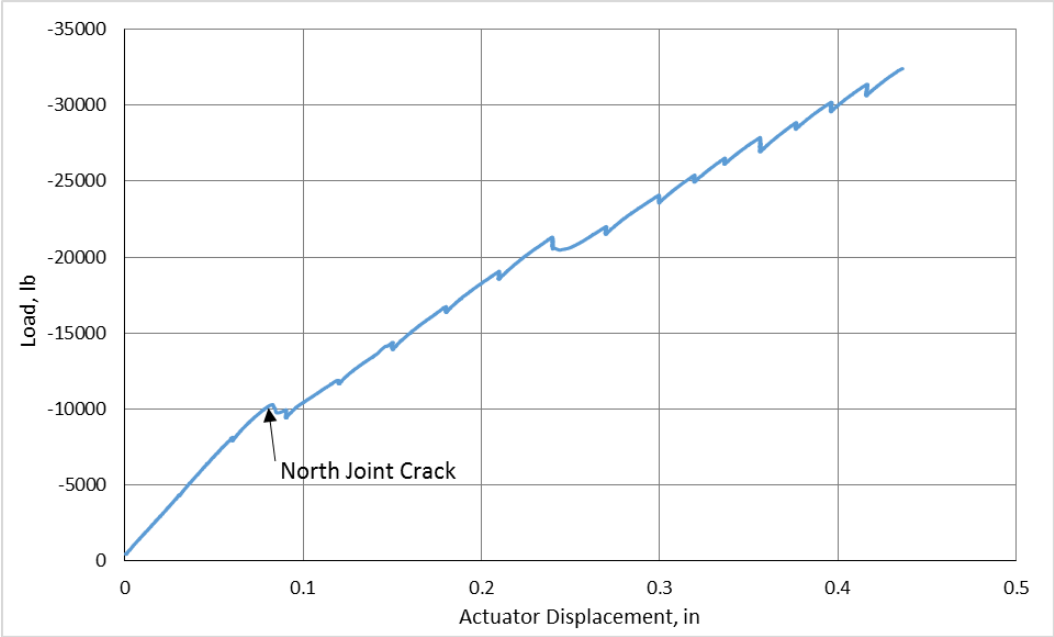

Figure 80: Load versus displacement plot for the final static test of specimen 4

Figure 81 is a graph showing the joint openings during the final static test. The north joint remained linear and uncracked until close to 0.09 in. actuator displacement. It was at this point during the test that the load dropped which can be seen in Figure 80. Cracks were observed on both faces of the north joint at this point. The south joint remained linear and uncracked until close to 0.25 in. actuator displacement at which point cracks were observed in the south joint. Before the LVDTs lost contact the largest joint opening measure 0.123 in. in width. The cracks on all four keys' faces propagated along the joint interface for a short distance (<3 in.) before the cracks propagated into the voided slab concrete. Figure 82 is a picture showing this behavior. Reflecting shear cracks were also seen on top of the middle voided slab section at the south joint. A picture of this is shown in Figure 83. As seen in the picture the

marked cracks were propagating so that they would avoid the VHPC blockout, which makes sense because it is the stronger material. Also noted was a splitting crack in the south blockout that ran parallel to the splice bar. This crack is shown marked in Figure 84. The likely cause of this crack was due to dowel action in the splice bar that was being relied on to help transfer the shear force across the joint.

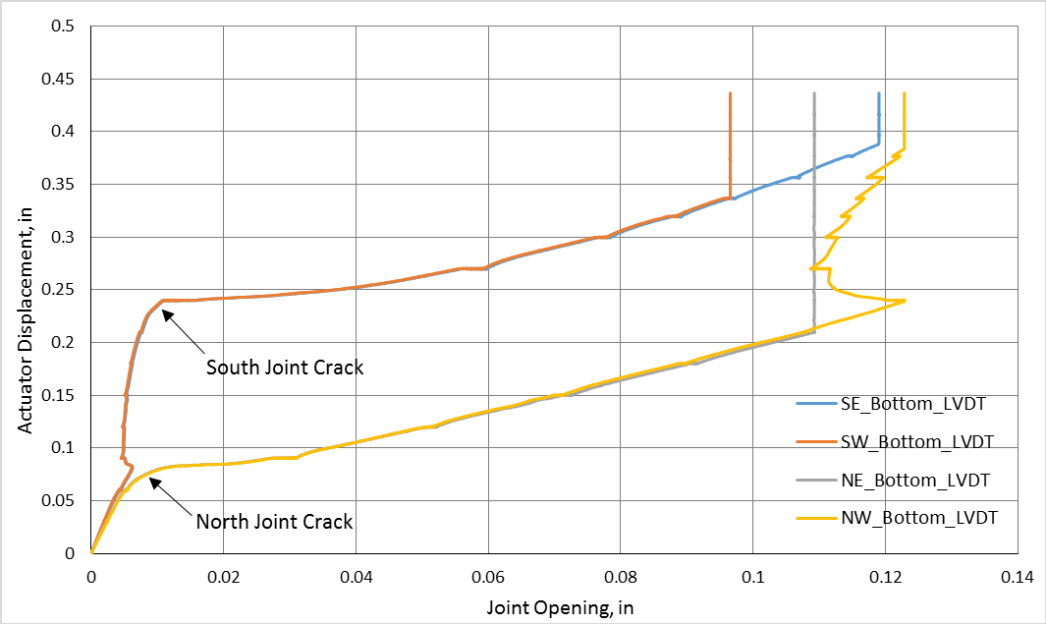

Figure 81: Joint openings during final static test for specimen 4

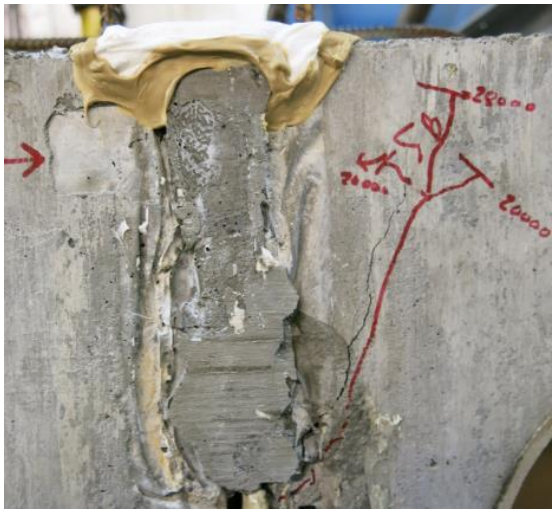

Figure 82: South joint showing the crack behavior during the final static test of specimen 4

Figure 83: Picture showing reflective cracks on the middle section near the south joint

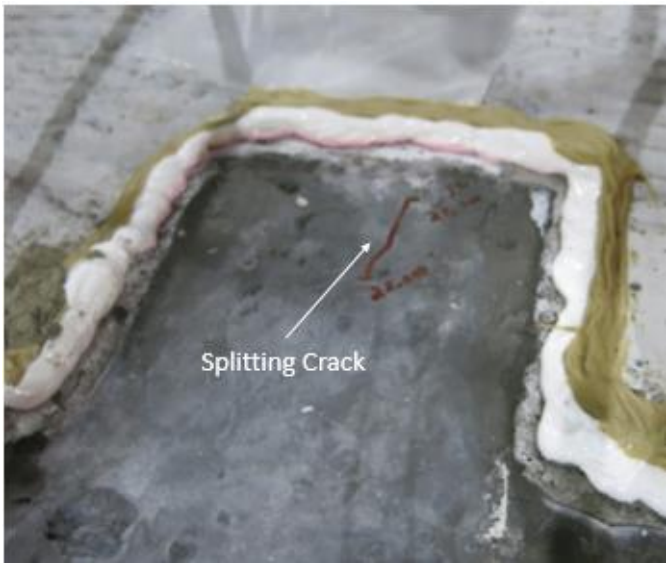

Figure 84: Picture showing splitting crack on south blockout

Throughout the cyclic regimen, water was ponded on top of the joint three times with no observed leakage through the joint. Since the test lasted one million cycles, the full schedule of material testing was conducted on both the first and last day of testing. The fourth specimen was constructed of concrete sections placed during the second and third batches with the material testing being conducted accordingly. The pull off tests showed the high bond strengths provided

by the VHPC. Some specimens pulled of pieces of the concrete with it, showing that the bond strength was higher than the tensile capacity of the concrete. Figure 85 is a picture of a specimen showing the bonded concrete pieces. Table 15 provides a summary of the data from the pull off tests. Shrinkage was traced using two 3 in. x 3 in. x 11 in. bars. On the first day of testing bar 1 measured 166 microstrain and bar 2 showed 172 microstrain. On the last day of testing bar 1 underwent 279 microstrain while bar 2 had 258 microstrain. Table 16 summarizes the strength and modulus of elasticity for the UHPC and concrete. All of the material test data can be found in Appendix D.

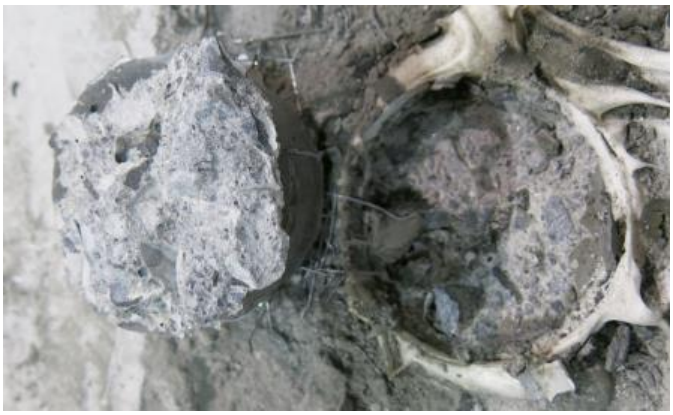

Figure 85: Picture of a VHPC pull off specimen with bonded concrete stuck to specimen

Table 15: Pull off test summary for specimen 4

Base Material	VHPC Age (days)	Average Bond Strength (psi)
Batch 2 Concrete	7	210
Batch 2 Concrete	15	220
Batch 3 Concrete	7	190
Batch 3 Concrete	15	240

Table 16: Compressive and modulus data summary for specimen 4

Material	Average Compressive Strength (ksi)	Average Modulus of Elasticity (ksi)
VHPC (1st day)	12.4	5420
VHPC (Last day)	13.9	5560
Batch 2 Concrete	7.58	5930
Batch 3 Concrete	10.6	6860

Specimen 5: Ductal UHPC Connection with Concrete Topping

The sub-assemblages were tested with concrete toppings to see how the concrete topping would affect the behavior as concrete toppings are required under higher traffic volumes. The results show that the topping made the system stiffer. During the initial static test there was no cracking observed in either joint. Figure 86 is a graph of the joint openings during the initial static test. The graph shows linear behavior for both the loading and unloading portions of the curves. The max joint opening during the initial static test measured 0.001 in. in width.

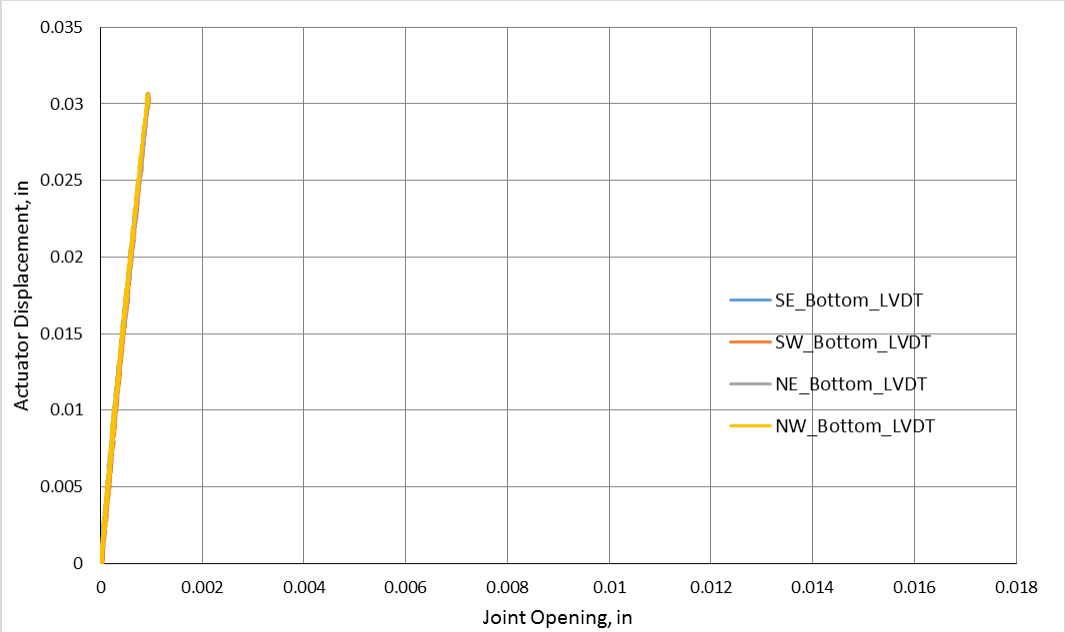

Figure 86: Graph of the joint openings during the initial static test of specimen 5

The joint did not open further during the cyclic regimen either, with the largest opening measured throughout the million cycles as 0.001 in. in width. Figure 87 and Figure 88 are graphs showing the joint openings during the static tests following each cyclic test. The data overlapped itself so a number of the static tests' data was let off of the graphs. As seen in the graphs there was no stiffness degradation throughout the cycling regimen, and there were no observed cracks on any of the joints throughout the cycling regimen.

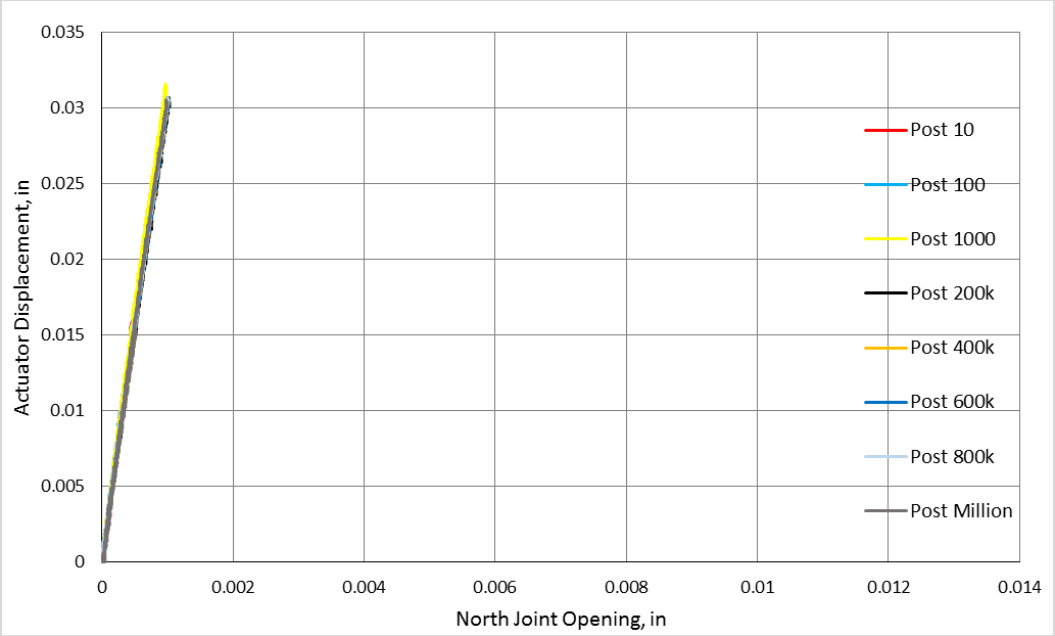

Figure 87: Graph of the north joint openings following cyclic tests for specimen 5

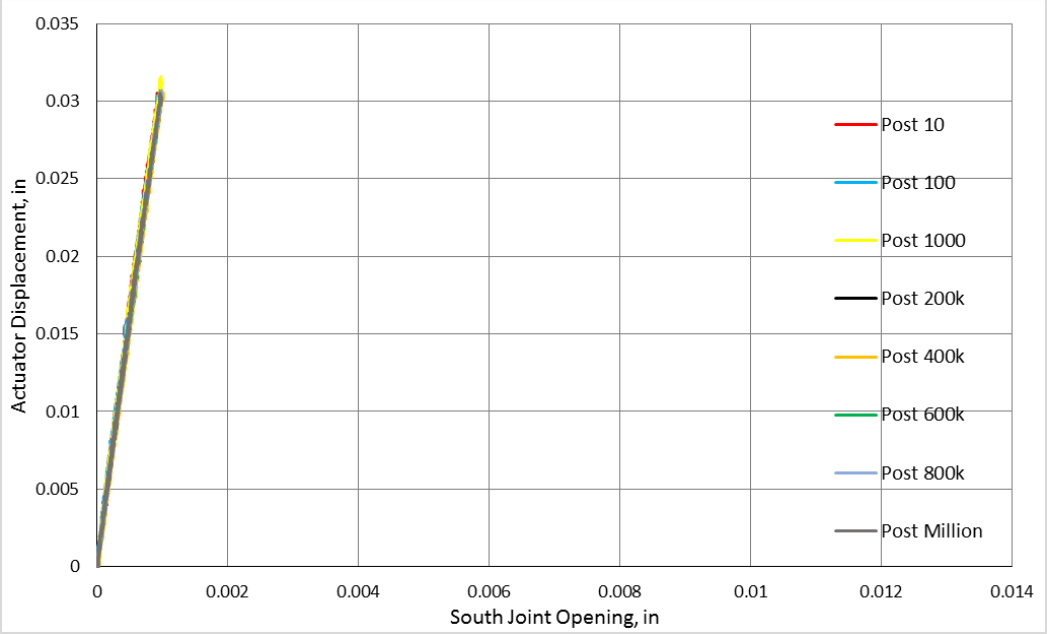

Figure 88: Graph of the south joint opening following cyclic tests for specimen 5

A final static test showed that the added topping helped with the ultimate strength of the specimen as the max load reached was 33,000 lb, which took place at an actuator displacement of 0.390 in.. It was at this point that the test had to be stopped for fear of destroying the load

cells as they were reaching their 10 kip capacity. Figure 89 shows the load versus displacement plot for the final static test. The graph shows that the specimen had relatively linear behavior until close to 0.12 in. actuator displacement when the joints cracked as noted on the plot. The graph shows that the end slope was still relatively close to the initial slope signifying that the specimen could still take more load.

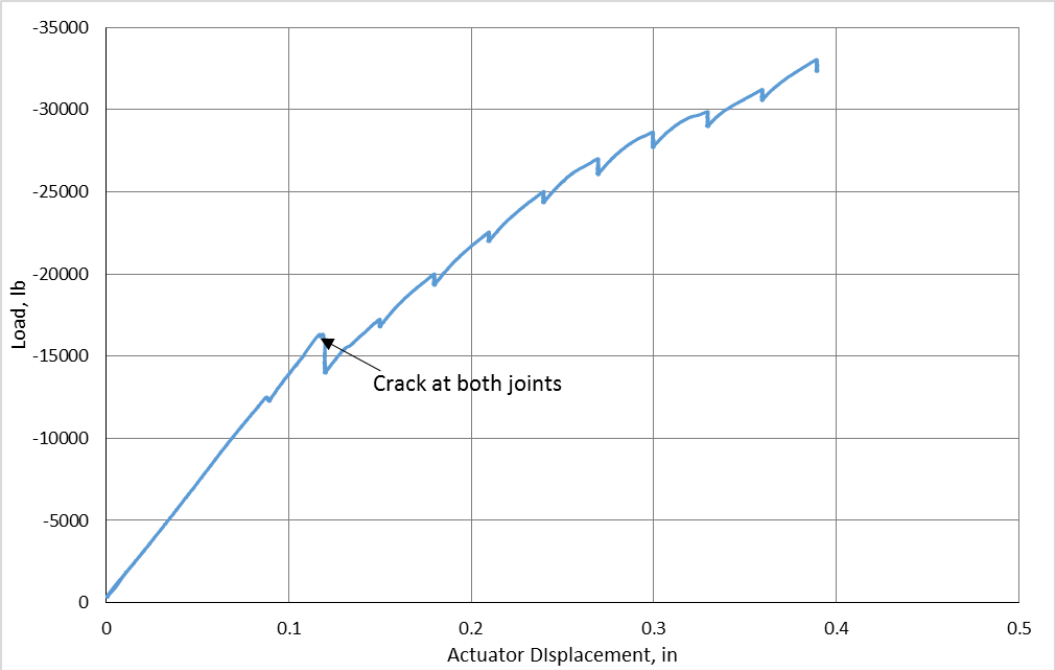

Figure 89: Load versus displacement plot for the final static test of specimen 5

Figure 90 is a plot showing the joint openings for the final static test. The largest joint opening measure on the south joint before the LVDTs lost contact was 0.125 in. in width. As seen in the graphs all four joints cracked at the same time. Cracks were observed on all key faces at 0.12 in. actuator displacement. At an actuator displacement of 0.15 in. cracks were noted at the interface between the concrete topping and the joint. These cracks propagated towards the middle of the sub-assemblage along the interface between the topping concrete and the precast voided slab concrete. The cracks on the joint interface propagated up the key and then near the top of the joint the joint crack propagated into the previously formed crack between the topping concrete and voided slab concrete. Eventually the cracks along the interface between the topping and voided slab traveled vertically through the topping. One reason for it not to continue running horizontally is because near the middle there was extra compressive forces

holding the topping and voided slabs together due to the clamping of the spreader beam to the voided slab. Figure 91 and Figure 92 shows pictures of the cracking patterns noted above.

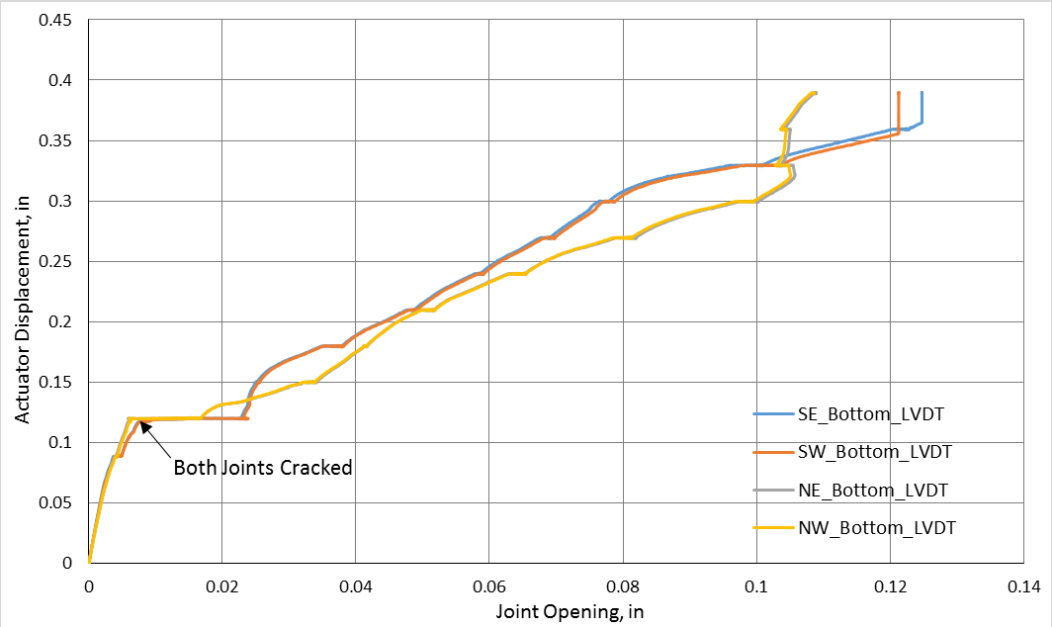

Figure 90: Graph of the joint openings during the final static test of specimen 5

Figure 91: South joint showing typical cracking pattern observed during final static test

Figure 92: Close up showing cracking along topping voided slab interface

The water ponding tests was performed three times with no leakage observed. The full schedule of material tests were run with extra tests being run for the concrete topping. The fifth specimen was constructed of concrete specimens placed during the first and second batches. The pull off tests showed high bond strength for the UHPC, which is summarized in Table 17. Some of the pull off specimens removed concrete showing that the bond strength was stronger than the tensile strength of the concrete. Shrinkage was tracked using two 1 in. x 1 in. x 11 in. bars. On the first day of testing bar 1 measured 264 microstrain and bar 2 showed 296 microstrain. On the last day of testing bar 1 underwent 317 microstrain while bar 2 had 341 microstrain. Table 18 summarizes the strength and modulus of elasticity for the UHPC, topping concrete, and voided slab concrete. All of the material test data can be found in Appendix D.

Table 17: Pull off data summary for specimen 5

Base Material	UHPC Age (days)	Average Bond Strength (psi)
Batch 1 Concrete	7	100
Batch 1 Concrete	12	220
Batch 2 Concrete	7	180
Batch 2 Concrete	12	270

Table 18: Compressive strength and modulus data summary for specimen 5

Material	Average Compressive Strength (ksi)	Average Modulus of Elasticity (ksi)
UHPC (1st day)	11.6	6300
UHPC (Last day)	14.3	7050
Topping Concrete (1st Day)	3.78	4240
Topping Concrete (Last Day)	4.50	5090
Batch 1 Concrete	7.60	5600
Batch 2 Concrete	7.24	5630

Specimen 6: VHPC Connection with Concrete Topping

The topping and VHPC connection led to a very stiff section. During the initial static test there was no cracking observed in any of the four joints faces. The largest joint opening during the first test measured 0.001 in. in width. Figure 93 is a graph of the joint openings during the first static test. As seen in the graphs both the loading and unloading curves remained linear confirming that there was no cracking.

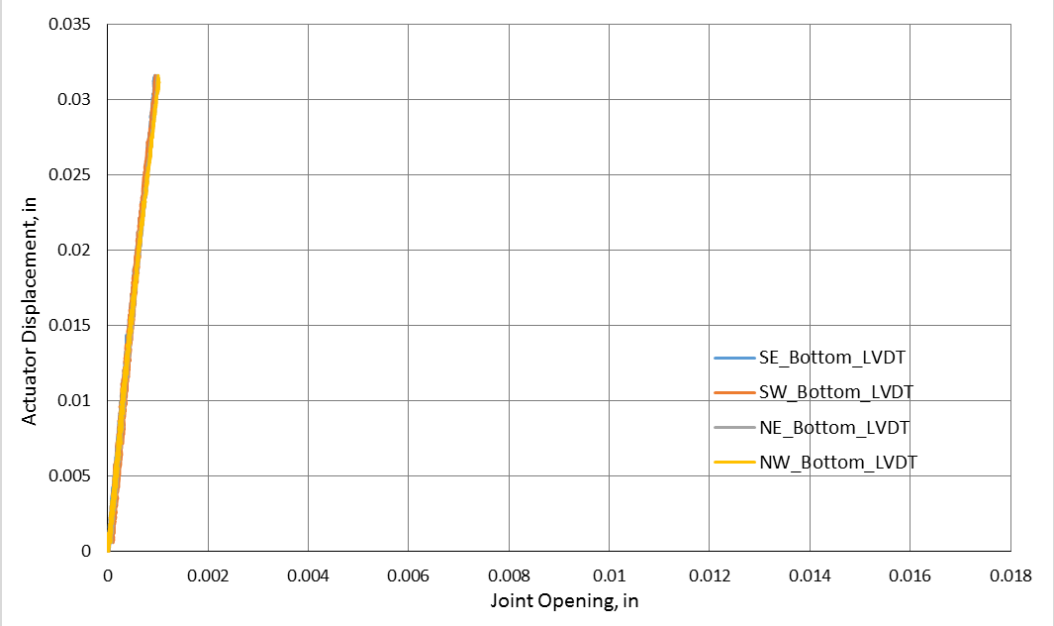

Figure 93: Joint opening during the first static test of specimen 6

The joints did not crack during the cyclic regiment either, with the largest opening measured as 0.001 in. in width. Figure 94 and Figure 95 are graphs showing the joint openings during the static tests following each cyclic test. The data overlapped itself so a number of tests were left off the graph. As seen in the graphs the slope of the lines remained constant throughout the tests signifying that there was no stiffness degradation.

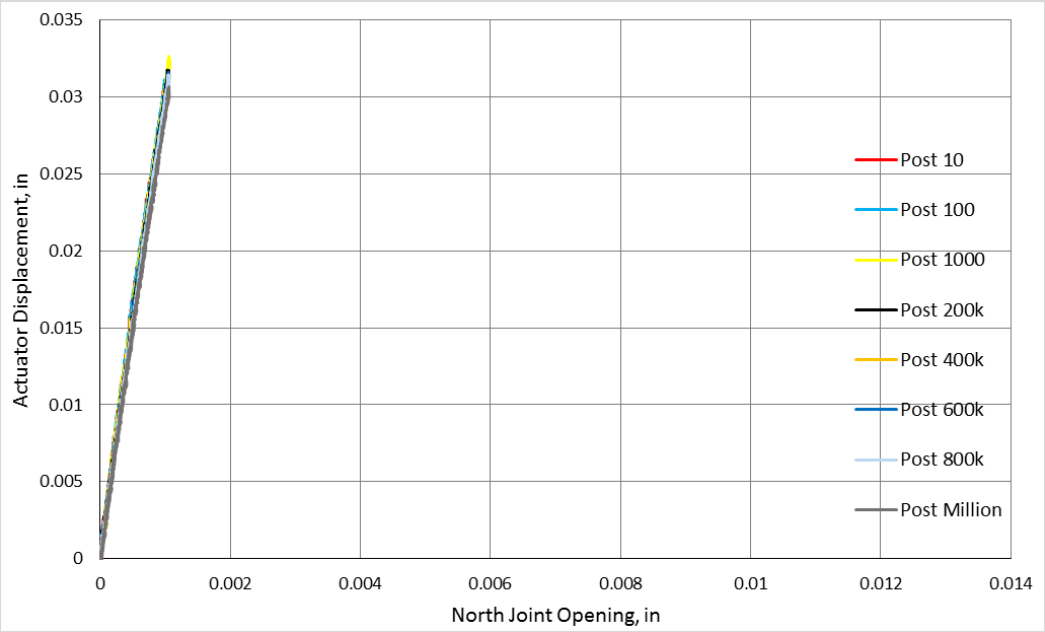

Figure 94: North Joint openings throughout cyclic regimen of specimen 6

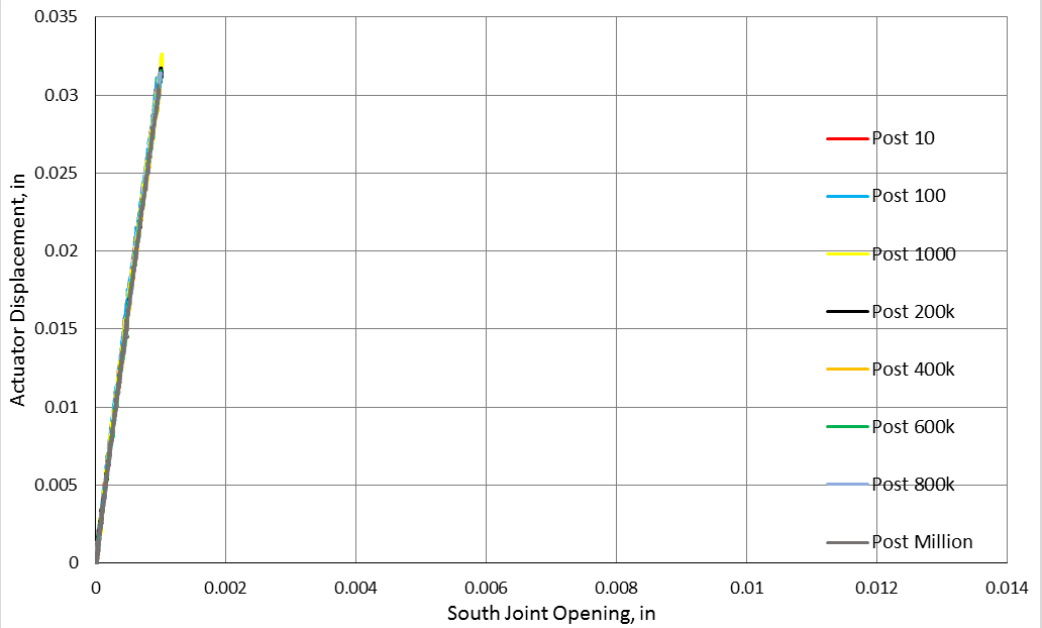

Figure 95: South joint opening throughout cyclic regimen of specimen 6

During the final static test the max load reached was 35,000 lb, which took place at an actuator displacement of 0.375 in.. It was at this point that the test had to be stopped for fear of destroying the load cells as they were reaching their 10 kip capacity. Figure 96 shows the load versus displacement plot for the final static test. The graph shows that the specimen had relatively linear behavior until close to 0.12 in. actuator displacement when the north joint cracked as noted on the plot. The cracking of the south joint, which took place around 0.27 in. actuator displacement is marked on the plot as well. The graph shows that the end slope had not yet flattened out signifying that it was capable of taking more load.

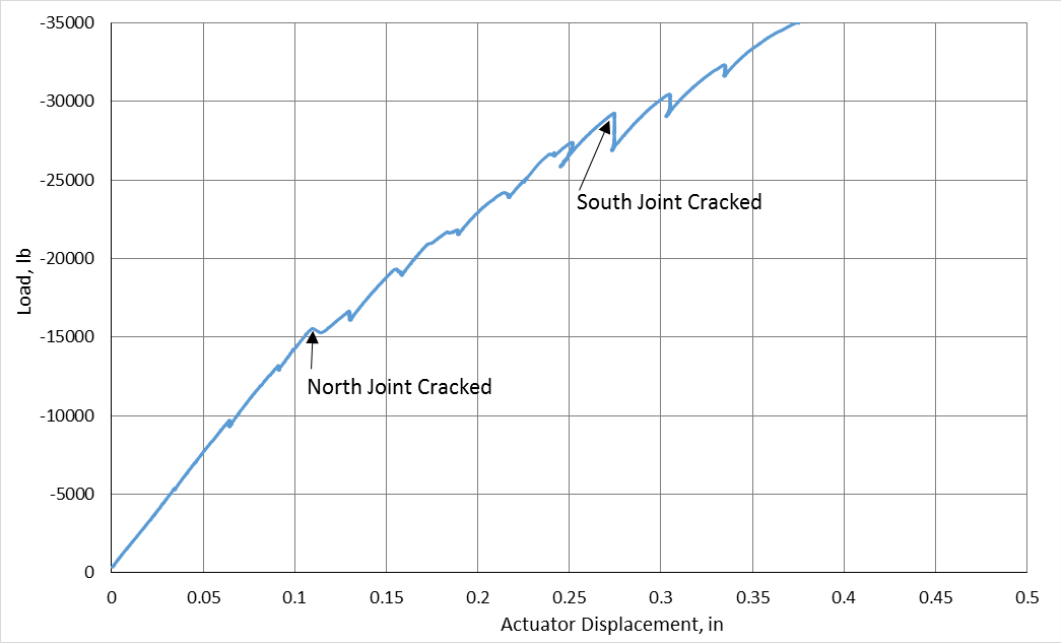

Figure 96: Load vs displacement plot for specimen 6's final static test

Figure 97 is a plot showing the joint openings for the final static test. The largest joint opening measure on the south joint before the LVDTs lost contact was 0.122 in. in width. As seen in the graphs the north joint cracked first at 0.12 in. actuator displacement. The cracks observed on the north joint were full depth cracks. There were also cracks at the interface between the concrete topping and the joint on the north side at this time. Cracking occurred on the south joint at 0.27 in. actuator displacement. At this time, full depth cracks were observed in the key and cracks were also observed at the topping joint interface. The topping-joint interface cracks on both the south and north side, propagated towards the middle of the sub-assemblage

along the interface between the topping concrete and the precast voided slab concrete. Eventually the cracks along the interface traveled vertically through the topping. One reason for it not to continue running horizontally is because near the middle there were extra compressive forces holding the topping and voided slabs together due to the clamping of the spreader beam to the voided slab. Figure 98 shows pictures of the cracking patterns noted above.

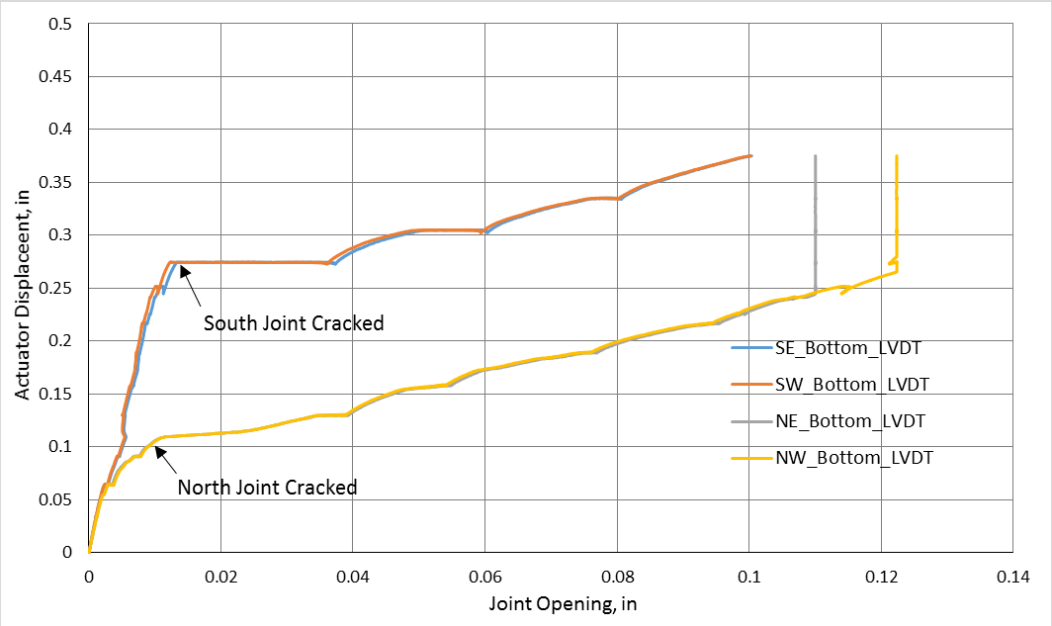

Figure 97: Joint openings during final static test of specimen 6

Figure 98: Typical cracking pattern for specimen 6 key

The water ponding tests was performed three times with no leakage observed. The full schedule of material tests were run with extra tests being run for the concrete topping. The sixth specimen was constructed of concrete specimens placed during the second and third batches. The pull off tests showed high bond strength for the VHPC, which is summarized in Table 19. Some of the pull off specimens removed concrete showing that the bond strength was stronger than the tensile strength of the concrete. Shrinkage was tracked using two 1 in. x 1 in. x 11 in. bars. On the first day of testing bar 1 measured 320 microstrain and bar 2 showed 293 microstrain. On the last day of testing bar 1 underwent 400 microstrain while bar 2 had 373 microstrain. Table 20 summarizes the strength and modulus of elasticity for the UHPC, topping concrete, and voided slab concrete. All of the material test data can be found in Appendix D.

Table 19: Pull off test summary for specimen 6

Base Material	VHPC Age (days)	Average Bond Strength (psi)
Batch 2 Concrete	7	201
Batch 2 Concrete	12	258
Batch 3 Concrete	7	166
Batch 3 Concrete	12	204

Table 20: Compressive and modulus data summary for specimen 6

Material	Average Compressive Strength (ksi)	Average Modulus of Elasticity (ksi)
VHPC (1st day)	11.3	5130
VHPC (Last day)	12.10	5280
Topping Concrete (1st Day)	3.65	3900
Topping Concrete (Last Day)	4.36	4530
Batch 2 Concrete	6.72	5830
Batch 3 Concrete	9.53	6860

Summary of Results

Table 21 gives a brief summary of the results found for each specimen. It shows the relative behavior of the six specimens based on their ability to last a million cycles, their ultimate strength, and whether they passed the ponding tests. Further detailed comparison are found in the discussion chapter.

Table 21: Summary of specimen testing

	Specimen 1: Grouted Shear Key	**Specimen 2: Kevlar Reinforced Grouted Shear Key**	**Specimen 3: Ductal UHPC connection**	**Specimen 4: VHPC connection**	**Specimen 5: Ductal UHPC with concrete topping**	**Specimen 6: VHPC with concrete topping**
Complete Million Cycles	No (94 cycles)	Yes	Yes	Yes	Yes	Yes
Max Load/ Service Load Ratio	1	4.4	7.2	8.5*	7.7*	8.1*
Avg Bond Strength (psi)	35	17	260	230	240	230
Initial Cracking Point with Load	Cracked during initial static test at 1,260 lb	Cracked during initial static test at 2,330 lb	Cracked during the 10,000 cycle regimen at 3,500 lb	Cracked during final static test at 10,300 lb	Cracked during final static test at 16,300 lb	Cracked during final static test at 15,300 lb
Failure	Yes, grouted north key debonded	Yes, both grouted keys debonded and Kevlar debonded on south key	Yes, concrete crushing on south key	No, test had to be stopped before failure	No, test had to be stopped before failure	No, test had to be stopped before failure
Ponding Results	N/A	No Leakage	No Leakage	No Leakage	No Leakage	No Leakage

*Specimens 4, 5, and 6 could not be failed so these should not be compared against each other, but what is important is that all three underwent maximum loads much larger than their service loads.

Discussion

The discussion chapter is broken down into eight sections. The first part discusses the accuracy of the finite element model. The next topic discussed is the materials used for the joint filler material and how their properties compared. The third section is a comparison of the results from each specimen. The following four sections discusses each general connection type; the current partial depth grouted shear key, the current detail with Kevlar reinforcement, the blockout connection type, and the specimens with toppings. The final section is a summary of the discussion.

Finite Element Model

As explained earlier in this thesis, finite element analysis was used to find the displacement of the sub-assemblages that would recreate transverse stress conditions in the shear keys equivalent to a 35 ft bridge span under an AASHTO design truck loading. Both a full scale model and a sub-assemblage model were recreated in Abaqus, and as seen previously in the finite element chapter, the sub-assemblage results matched up with the full scale model when under a 0.03 in. displacement. In order to justify using this displacement criteria for each specimen, the accuracy of the finite element model was validated using the data from the first specimen.

The overall behavior seen in the model was similar to the behavior seen in the actual test for specimen 1. Both the model and specimen showed that the exterior sections rotated away from the middle section as the joints opened up. There was global displacement downwards, but due to the rotation about the shear keys, the outside of the exterior sections deflected less than the interior. For both the model and the actual specimen the tops of the voided slabs underwent transverse compression strains while the bottoms underwent transverse tension strains.

Since the finite element analysis was a purely linear elastic model, the results could only be compared to the tested specimen prior to cracking. As seen in the results chapter, the first

specimen cracked at 0.02 in. actuator displacement, so the comparison had to take place before this point. Table 22 compares results from the finite element model to actual results obtained from specimen 1 at 0.01 in. actuator displacement.

Table 22: Comparison between FEA model and specimen 1

	Finite Element Model	Specimen 1 Results
Joint Opening (in)	0.001	0.001
Exterior Section Bottom Transverse Strain (με)	1.8	1.2
Middle Section Bottom Transverse Strain (με)	6.4	5.0
Outside of Exterior Section Deflection (in)	0.005	0.004

The comparison shows that the results from both the model and specimen 1 were similar. The small difference are assumed to be negligible when considering the accuracy of the instruments at such small values. Although small differences are expected when dealing with a non-uniform material like concrete. The instruments used for this data were the horizontal LVDTs on the joints, the vertical LVDTs under the specimen, and the BDI strain transducers on the bottom of the sections. The values from the BDI strain transducers from the tops of the specimen were not provided because the values from both the model and instruments were fractions of a microstrain. Although they both did report compression strains.

In conclusion, the similar behavior and results between the first specimen and the model validated the accuracy of the finite element model. This validation endorsed the use of the 0.03 in. displacement for both the static and cyclic loading regimens. Consequently, this displacement was used for the remainder of the test specimens.

Joint Material Comparison

Non-shrink grout, Lafarge's Ductal UHPC, and a non-proprietary VHPC were the three materials used as joint filler material. Material testing was performed on all three materials at the start and end of each test. The properties tested were bond strength, shrinkage, compressive

strength, and modulus of elasticity. Table 23 below gives a summary of the material properties for each joint filler material on both the first and last day of testing.

Table 23: Summary of joint filler materials' properties

First Day of Testing					
Filler Material	Avg. Comp. Strength (ksi)	Avg. Mod. Of Elasticity (ksi)	Avg. Bond Strength (psi)	Std. Dev of Bond Strength	Avg. Shrink. Strain
Grout	8.59	3220	25.9	16	0.00097
UHPC	11.4	6770	183	61	0.00026
VHPC	11.8	5280	190	46	0.00024
Last Day of Testing					
Grout	9.96	3940	16.72	3.1	0.0013
UHPC	14.9	7410	251	57	0.00034
VHPC	12.9	5420	228	30	0.00033

Bond strength is the most important property for the joint filler material. The pull off tests did not give the most precise data as seen with the large standard deviation values, but when directly comparing values, Table 23 shows that grout has a relatively low bond strength while both the UHPC and VHPC have comparable high bond strengths. As seen in previous figures, some UHPC and VHPC pull off specimens pulled pieces of concrete out of the voided slabs sections, showing that their bond strengths could actually be stronger than the tensile strength of the concrete. This was never seen in any of the grout pull off specimens. The pull off tests were not the only testament to these findings. The specimens utilizing grouted connections developed full length cracks in the shear key at relatively low loads, while the UHPC and VHPC connections took much higher loads before developing cracks in the key. The bond of the grout to the precast concrete was so low that upon failure the entire shear key could be removed leaving no pieces bonded to the concrete. Figure 99 is a picture of such a key. The low bond strength of the grout is one of the reasons for the poor performance by the specimens employing a grouted connection.

Figure 99: Fully intact shear key after failure of bonded connection

Table 23 shows that the shrinkage strains are almost an order of magnitude higher in the grout compared to both the UHPC and VHPC. Shrinkage is another important material property of the joint filler material because high shrinkage strains like those seen in the grout will lead to higher stresses at the concrete-filler material interface. Other proof of the high shrinkage strains were the shrinkage cracks that developed at the grout concrete interface seen in both specimens 1 and 2. There were no shrinkage cracks observed in either of the UHPC or VHPC specimens.

The summary table shows that both the UHPC and VHPC had relatively high and comparable compressive strengths. The grout too had high compressive strengths when compared against normal concrete, but it was not as strong as the UHPC or VHPC. The table also shows that the grout had a relatively low modulus of elasticity value. The UHPC had the highest modulus value while the VHPC had a slightly lesser modulus value than the UHPC, but it was still much higher than grout's modulus.

Table 24 below gives the material costs per cubic yard of each material. The costs are just an estimate and can vary depending on the location where the material is being procured. The table shows that UHPC is by far the most expensive of the three, while the grout and VHPC have comparable costs.

Table 24: Prices estimate for filler materials

Material	Price per Cubic Yard
Grout	$770
UHPC	$2,500
VHPC	$1,000

In summary, the material properties of the non-shrink grout are inferior to both the UHPC and VHPC. The grout's low bond strength and high shrinkage strains lead to its poor performance seen as the joint filler material for specimens 1 and 2. The UHPC and VHPC have very comparable properties, but the UHPC is more than twice the cost of the VHPC. The high bond strengths seen from both materials lead to good performance as joint filler materials in specimens 3 through 6.

Connection Comparison

Directly comparing the data from each specimen is imperative to analyze the relative performance of each connection. The following section will compare the specimen's performance and behavior during the initial static test, the cyclic regimen, and the final static tests. The initial static test was important because it showed how the uncracked connection would respond to an AASHTO design truck loading. This test showed the initial stiffness of each specimen and the connection's ability to abate joint opening under a heavy load. Figure 100 is a graph of the north joint openings from each specimen during their first static test.

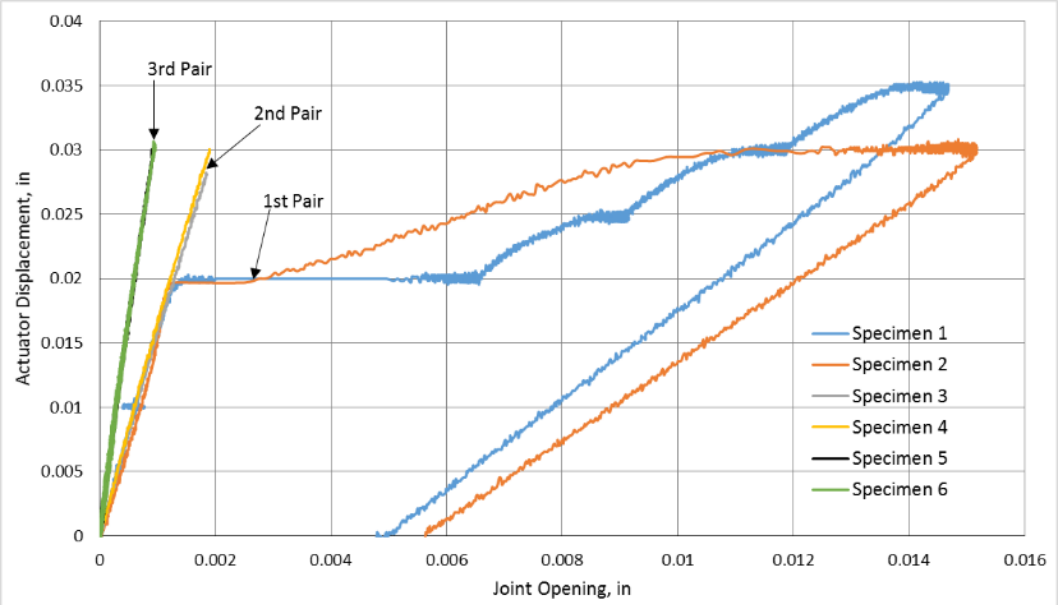

Figure 100: Graph of joint openings for each specimen during initial static test

The graph shows that the first pair of specimens, the second pair of specimens, and the third pair specimens all had similar joint opening behavior during the first static test. The first two specimens, which used a grouted key, underwent cracking around 0.02 in. actuator displacement. Both grouted specimens allowed joint openings over 0.014 in. The second pair, which utilized fiber reinforced high strength concretes and the blockout design, did not have cracking in the joint showing linear behavior for the full loading sequence. Both specimens allowed joint openings close to 0.002 in.. The final pair of specimens, which had concrete topping, did not crack and allowed joint openings close to 0.001 in.. As seen in the graph, the first two specimens had similar joint openings as the third and fourth specimens until 0.02 in. actuator displacement. This is expected as prior to cracking all four specimens were experiencing linear behavior and utilizing the same moment arm with which to combat the rotation about the joint. Once the flexural stresses became too high the grout bond failed leading to the large joint opening in the first two specimens. The specimens with the topping had the advantage of a larger moment arm due to the 5 in. thick topping, which lead to the smallest joint opening values and the stiffer system.

Table 25 gives the initial system stiffness for each specimen during the initial static test. In order to compare the initial stiffness values, they were calculated prior to cracking at an actuator displacement of 0.015 in.. As expected, the two specimens with the topping gave the highest overall system stiffness values. The first specimen gave the lowest stiffness value, which is also expected. Specimens 2, 3, and 4 all have similar initial stiffness values, although after cracking specimen 2 would have a much lower value.

Table 25: Initial system stiffness values

	Actuator Displacement (in)	Load (lb)	System Stiffness (kip/in)
Specimen 1	0.015	1180	79
Specimen 2	0.015	1680	112
Specimen 3	0.015	1700	113
Specimen 4	0.015	1780	119
Specimen 5	0.015	1950	130
Specimen 6	0.015	1990	133

The loads at which the joints cracked are important because it shows the connection's ability to abate cracking. Table 26 summarizes the cracking loads for each specimens' joints.

As explained in the results section, due to the boundary conditions of this setup once one joint failed stresses were relieved at the opposite joint. This is the reason that for most tests one joint would fail much earlier than the other joint. In order to compare the cracking loads, it makes more sense to look at the lower of the two values. As expected Specimens 5 and 6 had similar cracking loads, which were higher than Specimens 3 and 4, which too had similar cracking loads. Specimens 1 and 2 had the lowest values.

Table 26: Cracking load for each specimens' joints

	Cracking Load (lb)	
	South Joint	North Joint
Specimen 1	Cracked During cycling	1,260
Specimen 2	Cracked during cycling	2,330
Specimen 3	9,700	Cracked during cycling
Specimen 4	21,200	10,300
Specimen 5	16,300	16,300
Specimen 6	27,300	15,300

The purpose of the cyclic regimen was to determine the relative durability and cyclic load strength of each connection. It was important to see whether cracks would form under repeated AASHTO truck loadings in an attempt to equate how the connection would perform throughout a bridge's lifespan. The propagation of formed cracks was also checked to see whether they would stabilize at some point or continue to grow to the full depth. Aside from crack observation at the joint faces, the joint openings were also tracked to see how the system's behavior may have degraded throughout the cycling. Table 27 gives the max joint opening during the first static test and the max joint opening following a million cycles.

Table 27: Joint opening changes throughout tests

	First Static Test		Post Million Cycle Static Test	
	Max North Joint Opening (in)	Max South Joint Opening (in)	Max North Joint Opening (in)	Max South Joint Opening (in)
Specimen 2	0.016	0.005	0.005	0.008
Specimen 3	0.002	0.002	0.008	0.002
Specimen 4	0.002	0.002	0.002	0.002
Specimen 5	0.001	0.001	0.001	0.001
Specimen 6	0.001	0.001	0.001	0.001

Specimen 1 was left off the table since it failed during the 94th cycle thus no degradation could be tracked. Specimens 4, 5, and 6 proved to be durable as they showed no changes in joint openings throughout the cycling regime signifying that there was no degradation after a million AASHTO design truck loadings. With linear behavior seen throughout a million cycles it can be assumed that a higher stress would be needed to initiate cracking in the joints for specimens 4, 5, and 6. As expected, there were no cracks visually observed on any of the joints for either of specimens 4, 5, or 6 throughout the cycling regimen. As shown in the results chapter the north joint of specimen 3 cracked between 1,000 and 10,000 cycles. At this point the joint opened up from 0.002 in. to 0.004 in.. The crack then propagated, but eventually stabilized as the joint opened up to 0.008 in. during the last 400,000 cycles. Although cracked, it was not a full depth crack and no water leaked through the joint during the repeated ponding tests. The second specimen's north joint closed up while the south joint opened up throughout the cyclic regimen. This behavior was explained in full detail in the results section. The second specimen had full depth cracking observed on all four joints faces indicating that only the Kevlar reinforcement was holding the specimens together. Once fully engaged, the Kevlar reinforcement did not degrade during the final 900,000 cycles, as the joint openings stabilized after 1,000 cycles. Although each joint had full depth cracks the epoxy used to lay down the Kevlar created a waterproof seal, which prevented any of the ponded water from seeping down through the joint.

To summarize the cyclic testing results, specimens 2 through 6 were all durable enough to withstand one million cycles of an AASHTO design truck. Specimens 2 through 6 passed the ponding tests as no water was observed to leak through any of the joints. Specimen 4, 5, and 6 had ideal behavior showing no signs of cracking as the joint openings did not change throughout

testing. Specimen 3 had one joint develop a crack, but specimen 3 still showed acceptable behavior as the crack stabilized and did not propagate up the entire height of the shear key. Specimen 2 had the poorest relative behavior with full depth cracks forming in each joint.

While the behavior under service level cyclic loads is probably the most important aspect to consider when comparing each connection, the strength can also be useful. The stresses induced during the final static tests were much larger than those seen under normal traffic considerations, but it is beneficial to see how the connection would react when over-loaded. Figure 101 is a graph of the load versus displacement plots for specimen 2 through 6 during their final static tests.

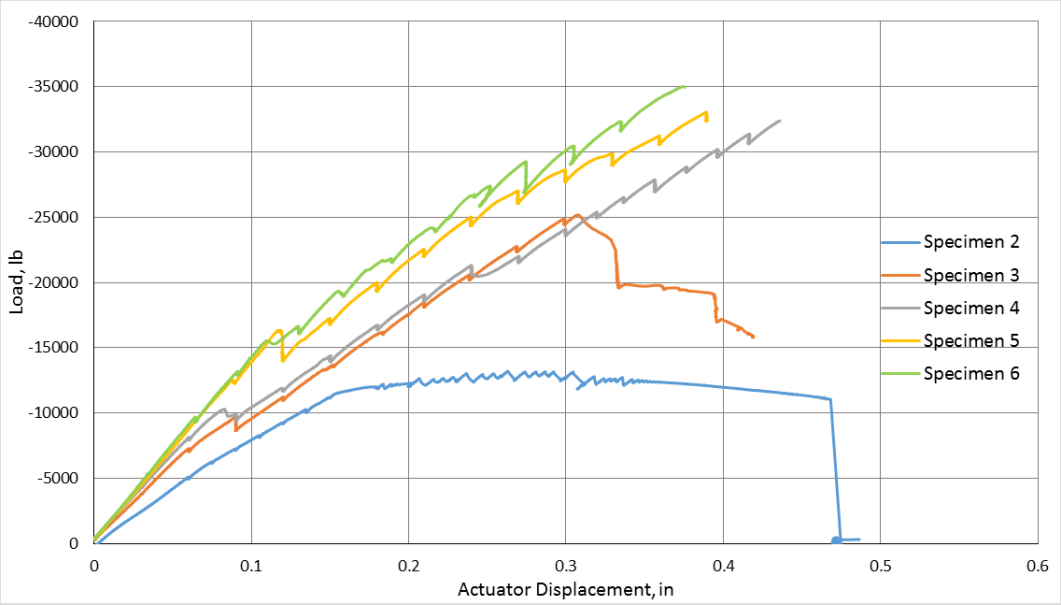

Figure 101: Load vs. displacement plots for the final static tests

Specimen 1 was again left off of this graph as it did not have a final static test for it failed during cycling. During the final static tests only specimens 2 and 3 could be tested to failure. As seen in the graph, specimen 2 experienced a sudden failure and it ceased to take more significant load after reaching 12,000 lb. Specimen 3 ceased to take load after 25,000 lb but did not undergo a sudden failure, portraying good post-peak behavior. The other three tests reached loads greater than 30,000 lb, but had to be stopped before failure for fear of destroying both the load cells and support beams. Specimens 5 and 6 were the stiffest systems while specimens 3 and 4 had slightly less comparable stiffness values. Specimen 2 was the least stiff specimen.

The exact stiffness values are hard to calculate due to the cracking that occurred during the final static tests.

During the final static test, the failure of specimen 2 was a sudden failure of the bond of the Kevlar to the precast concrete. Along with specimen 1, these were the only connection failures seen. During specimen 3's final static test the precast concrete started crushing due to compression loads near the tops of the joints, which lead to its loss of load. At higher loads during specimen 4's final static test, shear cracks started to develop in the concrete. This shows that when employing the blockout connection type, the connection is no longer the weakest link in the system because the voided slab sections started to fail before the connection. Graybeal, also saw this behavior while testing field-cast UHPC connections, where damage occurred to the precast specimens before damage was noted in the connection (2012).

Looking at the results from this research project leads to a few main points. The current grouted detail was the poorest performing connection tested. The Kevlar reinforcement joint performed much better than the grouted joint, but was outperformed by both the blockout connection specimens. Both specimen 3 and 4 showed similar behavior and results while utilizing two different types of fiber reinforced high strength concrete filler materials, although specimen 4 performed slightly better. Specimens 5 and 6 showed that an added concrete topping will enhance the overall stiffness of the system and will reduce joint openings. The following four sections will further discuss observations, pros, and cons of each connection type.

Current VDOT Grouted Partial Depth Shear Key

The results from specimen 1, which tested the current VDOT grouted shear key detail, confirmed the problems associated with partial depth grouted shear keys. The key geometry provides a small moment arm with which to prevent rotation, and the grout used as the filler material provides a low bond strength with the precast concrete. These two major functionality issues lead to cracks at the interface between the grout and the concrete at relatively low stresses.

For specimen 1, cracks in the shear key first occurred at 0.02 in. actuator displacement. This was only 66% of the desired displacement to reach transverse stress levels in the key

equivalent to an AASHTO design truck loading. Specimen 2, which also employed the use of the grouted partial depth shear key albeit with the addition of Kevlar reinforcement, showed cracking in the shear keys around 0.02 in. actuator displacement as well.

These results shows that partial depth grouted shear keys will crack under loads less than the design live load, since AASHTO calls for a design live load of a design truck or tandem plus a lane load. This leads to the assumption that most voided slab bridges' shear keys crack shortly after being put into service. The mechanical interlock due to the geometry of the shear key will continue to transfer portions of the shear load between adjacent beams. This behavior was seen in the first specimen as after the north key completely debonded during the 94th cycle, the north side load cells continued to register load during the remainder of the test.

So as discussed in the beginning of this thesis, the cracking is not a major safety concern, although if let go for too long the deterioration can lead to an unsafe structure. The upfront issues are when the cracks allow chloride laden water to seep down through the joint. The wide surface cracks seen on the top of the joint after specimen 1's failure would easily allow water to seep through carrying corrosive materials that would deteriorate both the concrete and reinforcement. Overtime this would lead to costly repairs and eventual replacement. Figure 102 is a picture of the crack on top of the joint.

Figure 102: Crack on top of the first specimen after failure

In summary the results and behavior from specimen 1 mirror the concerns and observations expressed by the DOTs that responded to the 2009 survey done by NCHRP referenced in the literature review of this thesis. The first specimen validated the need for an improved longitudinal connection for voided slab bridges.

Kevlar Reinforced Grouted Shear Key

The Kevlar reinforced joint provides many advantages that the current detail does not provide. The first advantage is that the Kevlar-epoxy system is stiff enough to transfer high shear loads between adjacent beams leading to better load sharing between adjacent beams. Once full depth cracks formed on both keys during testing, the Kevlar became fully engaged and the three section system acted symmetrical with even load distribution going into both the north and south section. The ability to transfer high loads means that the Kevlar-epoxy system could undergo higher stresses than the normal grouted joint leading to a higher ultimate strength.

Another advantage of the Kevlar system is that it is a much more durable system then the current detail as it was able to withstand the full million cycles of the AASHTO design truck loading. Once the Kevlar was fully engaged the system stabilized with the joint openings remaining constant for the final 900,000 cycles of loading. The epoxy resin showed no signs of cracking under the loads as it held water during three ponding tests.

With these improvements on the current detail being stated, there are still a number of disadvantages and concerns with this connection. The first concern comes from the fact that the test was performed over a period of five days in a fairly constant mild temperature. It is not known if the epoxy will degrade or break down over the period of a bridge's lifespan. The degradation could come from its reaction to the number of substances and chemicals it would come in contact with or from the large number of freeze thaw cycles it would have to endure. A second disadvantage with this connection type is that it didn't prevent the joint from cracking. This is because the Kevlar didn't do anything to prevent rotation about the joint, and acted like a hinge which failed to transfer moment across the beams. As seen in the test, both joints had full depth cracks formed in the shear keys early in the testing regimen. So if the epoxy did develop cracks in its matrix, water would surely seep down into the joint causing the same damage seen with the current detail.

A third disadvantage of this system is that the failure type is a brittle one that happens abruptly when the bond between the Kelvar-epoxy system and the precast concrete fails. There were no outward signs of distress before the failure which could warn inspectors or the public

about the possible safety hazard of the bridge. This leads to fears that if the bridge became overloaded it may undergo a structural collapse before being noticed.

In conclusion, the Kevlar reinforced joint is a definite improvement on the current detail, but does not abate cracking of the joint which is a main objective of the new connection. This connection type seems better suited as a repair method for current bridges. The Kevlar-epoxy system can be placed over distressed joints if there is fear in the lack of load sharing between adjacent beams. This repair method could be a fix that pushes a bridge replacement by a few years. The actual placing of the Kevlar reinforcement is not a complicated or time consuming process. It would only require a few workers, and would only need a few hours to fully cure so the bridge could be opened to traffic quickly.

Blockout Connections with Fiber Reinforced High Strength Concretes

Specimens 3 and 4 used the blockout with lapped splice connection design using Ductal's UHPC and the nonproprietary VHPC, respectively. Both specimens and materials produced comparable results, with each providing the same advantages. The connections proved to be very durable lasting all million cycles without developing full depth cracks in any of the shear keys. They also had a high ultimate strength surviving such high loads that damage started to be inflicted onto the voided slab sections.

The filler material being either UHPC or VHPC was one of the main advantages of this connection. The high bond strengths, which were an order of magnitude stronger than the bond strength provided by the grout, significantly enhance the behavior of this connection. The high bond strengths resist cracking at stresses much higher than the grout would be able to resist. This prevents joint rotation as the whole shear key depth is intact to resist the moment, and thus transfer the moment across the connection improving load distribution. The use of UHPC and VHPC are essential to this connection for they are required to develop the lap splice over a 6 in. length.

The lapped splice and blockout connection design enhance both the shear and moment transfer between adjacent beams. As seen in the results, this connection design greatly reduces

joint openings and inter-girder displacements, which causes adjacent beams to efficiently share the loads and deflect together. These advantages result in a connection that abates cracking in the joints leading to a durable connection capable of transferring loads throughout the lifespan of a bridge.

Constructability wise this connection would not require many more man hours than the current detail. The blockouts would be built in at the precast concrete plant. Although extra care would be needed in the fabrication so that the blockouts line up within at least 2 in. of each other to allow the splice bar to be tired in place. The beams would then be set in place on site just as in the current practice. The small amount of additional work would then follow as workers would need to tie in the lap splice bars across the blockouts. The joint material would then be placed just as it is done for the current detail, albeit with some extra material to fill the blockouts.

Unlike the Kevlar reinforced connection failure, the failure of this connection style would show signs of distress before collapsing. Seen in specimen 3 the concrete started to crush and spall off of the voided slab sections, and in specimen 4 there were shear cracks running through the voided slab section. Although failure is unlikely to occur as these bridges are generally controlled by displacement during design, so the beams would have to be greatly overloaded in order to cause the observed damage. Aside from showing outward signs of damage both the VHPC and UHPC have post-peak behavior due to the fiber reinforcement leading to ductal failures instead of brittle ones.

In summary, the blockout connection design was the most successful connection tested. It prevented joint rotation, abated cracking in the joint, proved to be durable, and had a high ultimate strength. If the blockouts were spaced along the length of the bridge every 2 ft as proposed it would negate the need for any transverse post-tensioning for there would be no joint cracking to compress. With such similar behavior seen between specimens 3 and 4 it makes more sense to use VHPC as the filler material as it is nonproprietary and less expensive. Albeit the VHPC connection would still be more expensive than grout, it is assumed that the overall lifecycle cost will be lower since there will be less repairs and a longer lifespan for the bridge.

Behavior of Specimens with Topping

As described in the test specimen section, for an ADTT between 200 and 100, Virginia requires a 5 in. concrete topping, for an ADTT over 200 a 7.5 in. topping is required, and for an ADTT less than 100 only an asphalt overlay is required. The two specimens tested with 5 in. concrete toppings, which too employed a blockout connection type with UHPC and VHPC, respectively, showed similar behavior and results. The added topping further decreased the joint openings seen in the blockout connection without toppings. The topping also created a much stiffer system.

The topping improves the behavior due to the 5 in. of extra concrete depth. This added height provides a larger depth to transfer the shear loads between specimens. This added height also increased the moment arm with which to transfer moments between specimens. This attribute increased the load sharing between beams and furthers the composite action between adjacent beams that was seen with the blockout connection type. The topping also adds to the durability of the blockout connection with an added concrete layer creating a barrier between the joint and water, deicing salts, or other chemicals.

The ultimate strength of the specimens with concrete topping was too high to see what the failure mode may be, for both tests had to be stopped for fear of destroying the load cells. Since the topping was the weakest material, it is assumed that the failure would begin here with some type of concrete crushing or shear cracks. This failure would also shows signs of distress prior to structural collapse.

The only downfall is that the added topping will have higher construction costs and the curing time would delay the bridge opening. This is unavoidable on any bridge type though as the topping is required under certain traffic volumes explained earlier. In the end, the topping will create a stronger, stiffer, more durable bridge when paired with the blockout connection design.

Summary

The objective of this research was to develop a more durable longitudinal connection for voided slab bridges that would abate cracking along the shear key and thus negate the need for transverse post-tensioning. Other metrics that were considered when judging the adequacy of each connection was constructability, cost, ultimate strength, and the failure mode.

The partial depth grouted shear key was tested as a control measure to compare the alternate connections against the current practice. As expected, the specimen was not durable nor did it abate cracking as it failed after 94 cycles of loading. The Kevlar reinforced joint was an improvement upon the current detail proving to be capable of lasting a million cycles and not complicating the construction. The Kevlar reinforced joint did not actually prevent cracking in the key, nor was it capable of transferring moment. It also had a much lower ultimate strength than specimens 3 through 6, and its brittle failure mode should be avoided.

Both blockout out connection specimens performed well proving to be very durable with both lasting a million cycles without full depth cracks. The construction of this connection would not be difficult either with the blockouts being formed at the precast plant, and the only extra work being the tying of the lapped reinforcement bars. The failure mode was desirable as the connection turned out to be stronger than the precast concrete sections themselves. From the tests performed, Specimen 4 which utilized the VHPC proved to be the slightly better option of the two blockout specimens. The UHPC specimen did form partial depth cracks in one of the joints during cycling while the VHPC joint did not. The VHPC also had a higher ultimate strength. Although with such similar behavior and results the main deciding factor between the two is that the VHPC would be cheaper to procure.

When traffic volume requires a concrete topping, the blockout connection with the VHPC filler material makes the best pair. The test results for specimen 5 and 6 were very similar, but specimen 6 which utilized the VHPC pair had just slightly better results. As stated before though, the cheaper VHPC is the driving factor in the decision.

Conclusions

.

The findings and experimental observations in this research have led to the following conclusions:

- The non-shrink grout develops too low of a bond strength with precast concrete to be an adequate shear key filler material because of the high flexural stresses seen in the shear keys. The grout also has higher shrinkage values than both the UHPC and VHPC
- Ductal's UHPC and the nonproprietary VHPC prove to be much better joint filler material for this adjacent voided slab system as it develops much higher bond strengths with the precast concrete.
- The current VDOT longitudinal connection detail using the partial depth grouted shear key is a poor connection as it develops full depth cracks under relatively low stresses, allowing water to seep through reflective cracking in the wearing surface, which leads to corrosion of the concrete and reinforcement.
- The Kevlar reinforced grouted shear key is an improvement upon the current detail as it is durable and capable of transferring shear loads, but it did not meet all of the objectives of this research project as it did not prevent joint cracking, was not successful in transferring moments across adjacent beams, and had a brittle failure mode.
- The blockout connection with lapped splice bar is the optimal longitudinal connection as it abates cracking and successfully transfers both shear and moment across adjacent beams even under high loads. By abating cracks in the joint, it will also negate the need for transverse post-tensioning.
- An added concrete topping will improve behavior by decreasing the amount of joint openings and creating a stiffer more durable system.
- Although producing similar results, the VHPC is a more viable option than the UHPC as the joint filler material as it produced slightly better results, but more importantly is it the less expensive material.

Recommendations

The following is a list of recommendations based on the conclusions of this research project:

- VDOT should implement the blockout with lap splice connection design using the VHPC as a filler material for the new longitudinal connection detail of adjacent member voided slab bridges
- Upon implementing this connection detail, VDOT should consider negating the need for transverse post-tensioning. One of the current purposes of the transverse post-tensioning is to compress the reflective cracking, but there will not be an extensive amount of cracking with the new connection detail. If construction could be completed without the assistance of the post-tensioning, then negating the need for the post-tensioning would reduce both the cost and time of construction.
- VDOT should use the Kevlar reinforcement as a repair method for current distressed shear keys that no longer transfer loads between adjacent beams properly.
- Further research should be done to see if the blockout spacing in the connection detail of 2 ft center to center is the most efficient spacing.
- Further research should be performed to test the connection's behavior under stresses caused by temperature gradients, for this will cause higher stresses than the live loads.

References

Abaqus, I. (2013). "Abaqus/Standard User's Manual." Dassaults Systemes.

American Association of State Highway Transportation Officials (AASHTO). AASHTO LRFD Bridge Design Specifications, Sixth Edition. Washington, D.C.: 2012.

ASTM Standard C39, 2014, "Standard Test Method for Compressive Strength of Cylindrical Concrete Specimens," ASTM International, West Conshohocken, PA, 2014, DOI 10.1520/C0039_C0039M, www.astm.org.

ASTM Standard C192, 2013, "Standard Practice for Making and Curing Concrete Test Specimens in the Laboratory," ASTM International, West Conshohocken, PA, 2013, DOI 10.1520/C0192_C0192M, www.astm.org.

ASTM Standard C469, 2010, "Standard Test Method for Static Modulus of Elasticity and Poisson's Ratio of Concrete in Compression," ASTM International, West Conshohocken, PA, 2010, DOI 10.1520/C0469_C0469M-10, www.astm.org.

ASTM Standard C1107, 2013, "Standard Specification for Packaged Dry, Hydraulic-Cement Grout (Nonshrink)," ASTM International, West Conshohocken, PA, 2013, DOI 10.1520/C1107_C1107M, www.astm.org.

Graybeal, Benjamin, (2011). Behavior of Field-Cast Ultra-High Performance Concrete Bridge Deck Connections Under Cyclic and Static Structural Loading, Report No. FHWA-HRT-11-023, Federal Highway Administration, McLean, VA.

Graybeal, Benjamin, (2011). "Fatigue response in bridge deck connection composed of field-cast ultra-high-performance concrete." Transp. Res. Rec., 2251, 93-100.

Graybeal, Benjamin, (2006). Material Property Characterization of Ultra-High Performance Concrete, Report No. FHWA-HRT-06-103, Federal Highway Administration, McLean, VA.

Graybeal, Benjamin, (2012). Ultra-High Performance Concrete Composite Connections for Precast Concrete Bride Decks, Report No. FHWA-HRT-12-042, Federal Highway Administration, McLean, VA.

Graybeal, Benjamin, (2009). "UHPC Making Strides." Public Roads, 72(4) 17 Federal Highway Administration, McLean, VA.

Hanna, Kromel, Morcous, George, and Tadros, Maher, (2011) "Adjacent Box Girders without Internal Diaphragms or Post-Tensioned Joints." PCI Journal. 56(4), 51-64.

Hansen, Jenna, Hanna, Kromel, and Tadros, Maher, (2012) "Simplified Transverse Post-Tensioning Construction and Maintenance of Adjacent Box Girder Bridges." PCI Journal. 57(2), 64-79.

Huckelbridge, Arthur, El-Esnawi, Hassan, (1997) Evaluation of Improved Shear Key Designs for Multi-Beam Box Girder Bridges, Report No. FHWA-OH-97-009, Federal Highway Administration, McLean, VA.

Huckelbridge, Arthur, El-Esnawi, Hassan, Moses, Fred, (1995) "Shear key performance in multibeam box girder bridges." J. Perform. Constr. Facil., 9(4), 271-285.

Gulyas, Robert, Wirthlin, Gregory, and Champa, Jeffrey, (1995). "Evaluation of keyway grout test methods for precast concrete bridges." PCI Journal, 40(1), 44-57.

Ozyildirim, Celik, (2011). Evaluation of Ultra-High-Performance Fiber-Reinforced Concrete, Report No. VCTIR 12-R1, Virginia Center for Transportation Innovation and Research, Charlottesville, VA.

Perry, Vic, and Royce, Mathew, (2010). Innovative Field-Cast UHPC Joints for Precast Bridge Decks (Side-by-Side Deck Bulb-Tees), Village of Lyons, New York: Design, Prototyping, Testing, and Construction.

Russell, Henry, (2009). "Adjacent Precast Concrete Box Beam Bridges: Connection Details. A Synthesis of Highway Practice." Report NCHRP-SYN-393, Transportation Research Board, Washington, DC.

Senturk, Ekin, and Higgins, Christopher, (2010). "Evaluation of Reinforced Concrete Deck Girder Bridge Bent Caps with 1950s Vintage Details: Laboratory Tests." ACI Struct. Journal. 107(5), 534-543.

Virginia Department of Transportation (VDOT). Road and Bridge Specification. Richmond, VA.: 2007.

Yazdani, Nur, Eddy, Scott, and Cai, Chun, (2000). "Effect of Bearing Pads on Precast Prestressed Concrete Bridges." Journal of Bridge Engineering, ASCE. 5(3), 224-232.

Appendix A: Voided Slab Construction Drawings

REV.	DATE	BY	DESCRIPTION
1	5-16-13	CR	KEYWAY

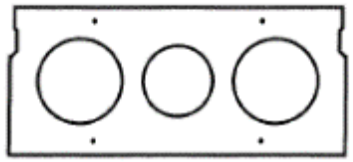

SPECIMEN 1

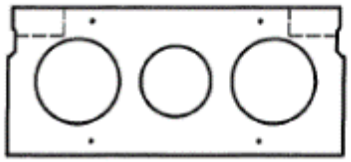

SPECIMEN 2

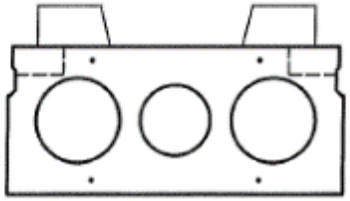

SPECIMEN 3

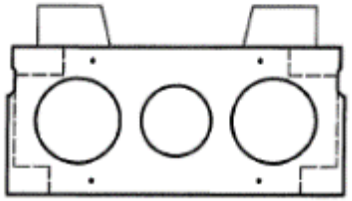

SPECIMEN 4

GENERAL NOTES

1. CONCRETE USED IN SPECIMEN FABRICATION SHALL BE CLASS A5 HAVING A MINIMUM 28 DAY COMPRESSIVE STRENGTH OF 5000 PSI. CONCRETE SHALL HAVE A MINIMUM COMPRESSIVE STRENGTH OF 3500 PSI PRIOR TO REMOVAL FROM FORMS.

2. DEFORMED REINFORCING BARS SHALL CONFORM TO THE REQUIREMENTS OF ASTM A615 GRADE 60.

3. INTERNAL VOIDS SHALL BE FORMED WITH EITHER EXPANDED POLYSTYRENE OR WAX COATED CARDBOARD.

4. TOPS OF BEAMS WHICH SHALL RECEIVE A FUTURE CONCRETE TOPPING SHALL HAVE A ROUGHENED RAKED FINISH. OTHERWISE TOPS OF BEAMS SHALL BE GIVEN A FLOAT FINISH.

VOIDED SLAB SCHEDULE

BEAM	LENGTH	C.Y.	TONS	QTY
SPECIMEN 1	2'-0"	0.36	0.79	6
SPECIMEN 2	2'-0"	0.36	0.79	6
SPECIMEN 3	2'-0"	0.36	0.79	6
SPECIMEN 4	2'-0"	0.36	0.79	3
TOTALS	42 LF	7.56 C.Y.	16.59 Tons	21

ROSS PRESTRESSED CONCRETE, INC.
P.O. BOX 6299
KNOXVILLE, TENNESSEE 37914
PHONE NO. (865) 524-1485
FAX NO. (865) 637-0831
www.rossprestress.com

PROJECT
VIRGINIA TECH
BOX BEAM AND
VOIDED SLAB PROJECT
P.O.#P2470683

STATION NO. --
COUNTY --
CONTRACTOR --
ARCHITECT/ENGINEER --

VT VOIDED SLAB PROJECT

DRAWN BY	CHECKED BY	RPC JOB NO.
R	RAM	813-18
SCALE	DATE	DRAWING NO.
NTS		VT-VA-13B 1 OF 6

REV.	DATE	BY	DESCRIPTION
1	5-16-13	CR	KEYWAY, VSLB2 and VSLB3 Bars

BILL OF MATERIALS

PIECE	QTY	DESCRIPTION	LENGTH
VSLB1	210	#4 BENT BAR	7'-7"
VSLB2	18	#4 STRAIGHT BAR	5'-10"
VSLB3	18	#4 BENT BAR	7'-0"
VSLB4	84	#4 STRAIGHT BAR	1'-11"
VT(2)	42	12" DIA. VOID	2'-6"
VT(3)	21	10" DIA. VOID	2'-6"
LL2	42	1/2" DIA. STRAND LIFTING LOOPS	

NOTES:
1. BAR DIMENSIONS ARE OUT TO OUT UNLESS NOTED OTHERWISE.
2. STANDARD CRSI DETAILS SHALL APPLY UNLESS NOTED OTHERWISE.

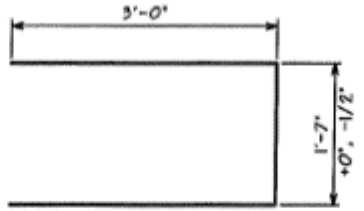

VSLB1

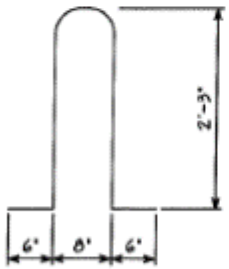

LL2

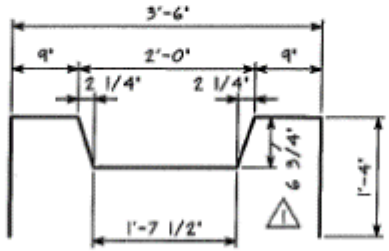

VSLB3

KEYWAY IS LOCATED ON BOTH SIDES OF ALL SLABS.

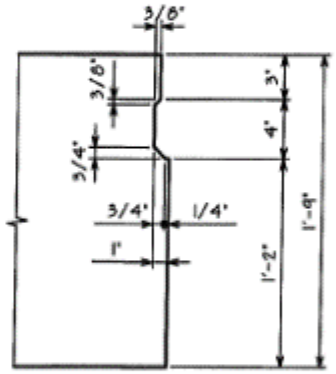

1 KEYWAY

ROSS PRESTRESSED CONCRETE, INC.
P.O. BOX 6299
KNOXVILLE, TENNESSEE 37914
PHONE NO. (865) 524-1485
FAX NO. (865) 637-0831
www.rossprestress.com

PROJECT
VIRGINIA TECH
BOX BEAM AND
VOIDED SLAB PROJECT
P.O.#P2470683

STATION NO. --
COUNTY --
CONTRACTOR --
ARCHITECT/ENGINEER --

STEEL DETAILS, BOM, KEYWAY

DRAWN BY	CHECKED BY	RPC JOB NO.
R	RAM	813-18
SCALE	DATE	DRAWING NO.
NTS		VT-VA-138 2 OF 6

VT-52

REV.	DATE	BY	DESCRIPTION
1	5-15-13	CR	KEYWAY CLEARANCE

BILL OF MATERIAL PER SLAB	
PIECE	QTY
VSLB1	10
VSLB4	4
VT(2)	2
VT(3)	1
LL2	2

STEEL REINF. ASSEMBLY 'A'

SEE SHEET 2 FOR KEYWAY DETAIL

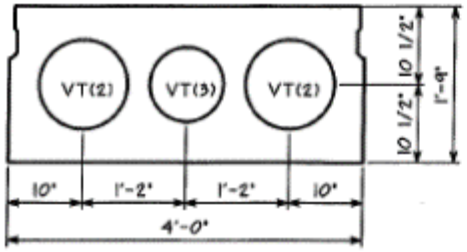

SECTION
SHOWING PHYSICAL PROP.

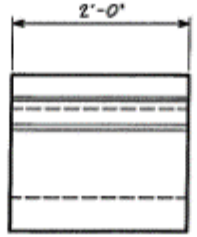

LONG. ELEV.
SHOWING PHYSICAL PROP.

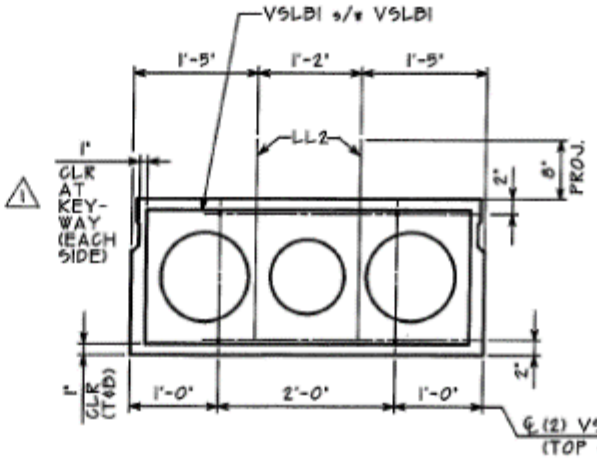

SECTION
SHOWING STEEL REINF.

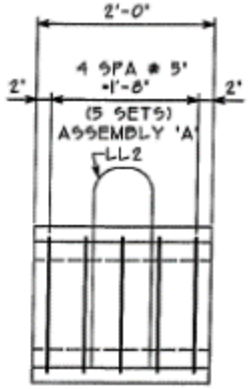

LONG. SECT.
SHOWING STEEL REINF.

ROSS PRESTRESSED CONCRETE, INC.
P.O. BOX 6299
KNOXVILLE, TENNESSEE 37914
PHONE NO. (865) 524-1485
FAX NO. (865) 637-0831
www.rossprestress.com

PROJECT
VIRGINIA TECH
BOX BEAM AND
VOIDED SLAB PROJECT
P.O.#P2470683

STATION NO. --
COUNTY --
CONTRACTOR --
ARCHITECT/ENGINEER --

VOIDED SLAB SPECIMEN 1

DRAWN BY	CHECKED BY	RPC JOB NO.
R	RAM	B13-18
SCALE	DATE	DRAWING NO.
NTS		VT-VA-13B 3 OF 6

VT-93 151

REV.	DATE	BY	DESCRIPTION
1	5-16-13	CR	KEYWAY. CLEARANCE

BILL OF MATERIAL PER SLAB	
PIECE	QTY
VSLB1	10
VSLB2	1
VSLB4	4
VT(2)	2
VT(3)	1
LL2	2

STEEL REINF. ASSEMBLY 'A'

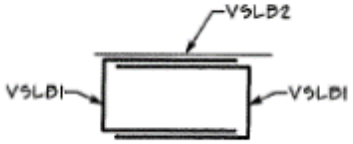

STEEL REINF. ASSEMBLY 'B'

SEE SHEET 2 FOR KEYWAY DETAIL

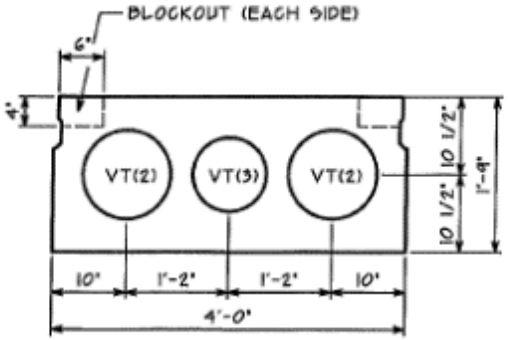

SECTION
SHOWING PHYSICAL PROP.

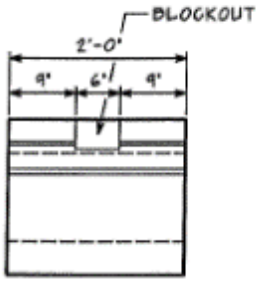

LONG. ELEV.
SHOWING PHYSICAL PROP.

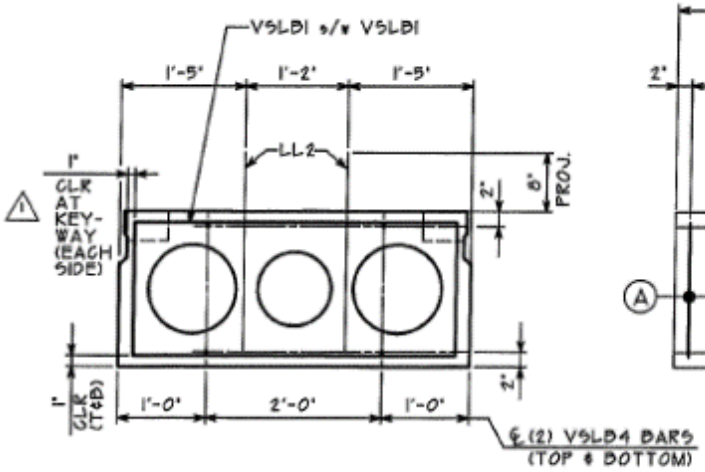

SECTION
SHOWING STEEL REINF.

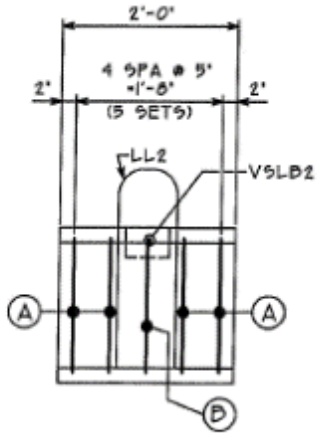

LONG. SECT.
SHOWING STEEL REINF.

ROSS PRESTRESSED CONCRETE, INC.
P.O. BOX 6299
KNOXVILLE, TENNESSEE 37914
PHONE NO. (865) 524-1485
FAX NO. (865) 637-0831
www.rossprestress.com

PROJECT
VIRGINIA TECH
BOX BEAM AND
VOIDED SLAB PROJECT
P.O.#P2470683

STATION NO. --
COUNTY --
CONTRACTOR --
ARCHITECT/ENGINEER --

VOIDED SLAB SPECIMEN 2

DRAWN BY	CHECKED BY	RPC JOB NO.
R	RAM	B13-18
SCALE	DATE	DRAWING NO.
NTS		VT-VA-138 4 OF 6

VT-54 (2)

REV.	DATE	BY	DESCRIPTION
1	5-16-13	CR	KEYWAY CLEARANCE

BILL OF MATERIAL PER SLAB	
PIECE	QTY
VSLD1	10
VSLD2	1
VSLD3	2
VSLD4	4
VT(2)	2
VT(3)	1

STEEL REINF. ASSEMBLY 'A'

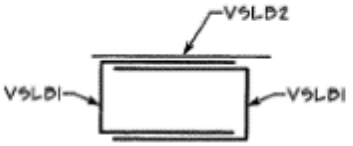

STEEL REINF. ASSEMBLY 'B'

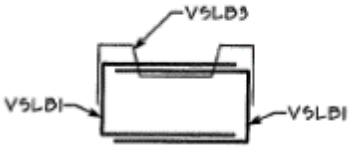

STEEL REINF. ASSEMBLY 'C'

SEE SHEET 2 FOR KEYWAY DETAIL

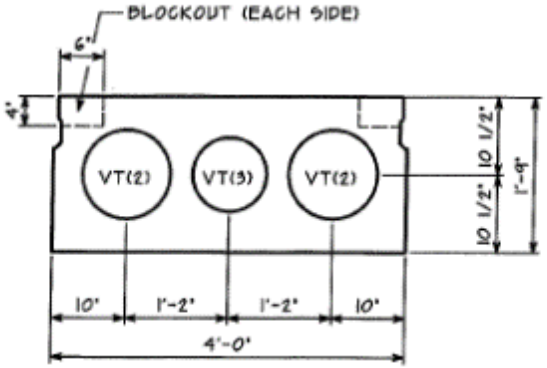

SECTION
SHOWING PHYSICAL PROP.

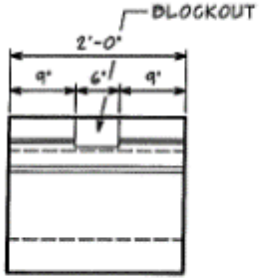

LONG. ELEV.
SHOWING PHYSICAL PROP.

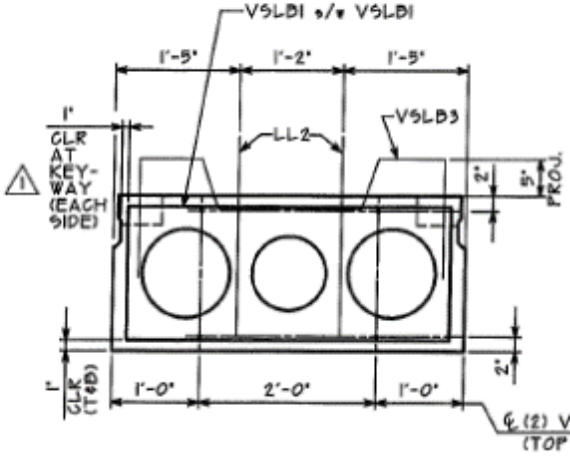

SECTION
SHOWING STEEL REINF.

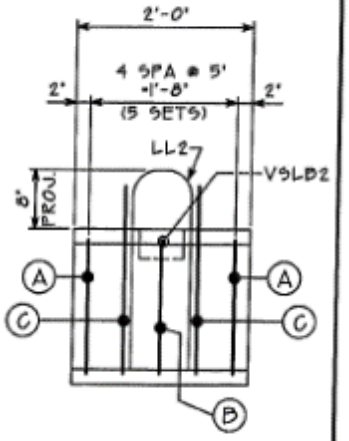

LONG. SECT.
SHOWING STEEL REINF.

ROSS PRESTRESSED CONCRETE, INC.
P.O. BOX 6299
KNOXVILLE, TENNESSEE 37914
PHONE NO. (865) 524-1485
FAX NO. (865) 637-0831
www.rossprestress.com

PROJECT
VIRGINIA TECH
BOX BEAM AND
VOIDED SLAB PROJECT
P.O.#P2470683

STATION NO. --
COUNTY --
CONTRACTOR --
ARCHITECT/ENGINEER --

VOIDED SLAB SPECIMEN 3

DRAWN BY	CHECKED BY	RPC JOB NO.
R	Ram	B13-18
SCALE	DATE	DRAWING NO.
NTS		VT-VA-138 5 OF 6

VT-96 152

REV.	DATE	BY	DESCRIPTION
1	5-16-13	CR	KEYWAY CLEARANCE

BILL OF MATERIAL PER SLAB	
PIECE	QTY
VSLD1	10
VSLD2	2
VSLD3	2
VSLD4	4
VT(2)	2
VT(3)	1
LL2	2

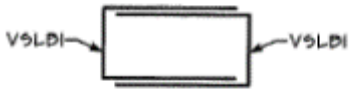

STEEL REINF. ASSEMBLY 'A'

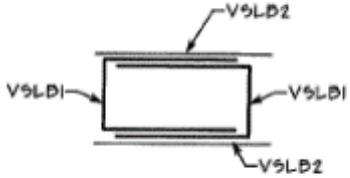

STEEL REINF. ASSEMBLY 'B'

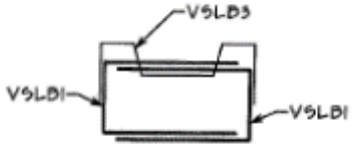

STEEL REINF. ASSEMBLY 'C'

SEE SHEET 2 FOR KEYWAY DETAIL

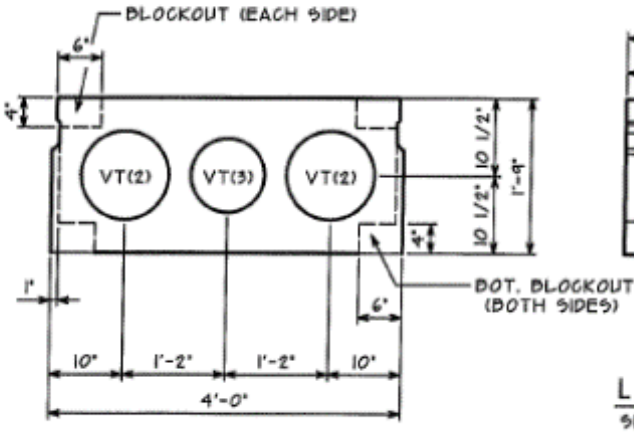

SECTION

SHOWING PHYSICAL PROP.

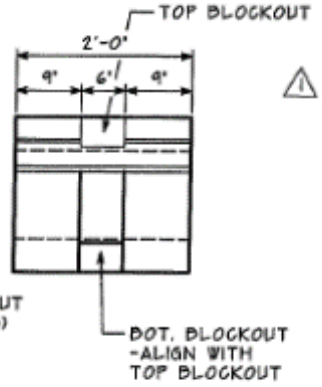

LONG. ELEV.

SHOWING PHYSICAL PROP.

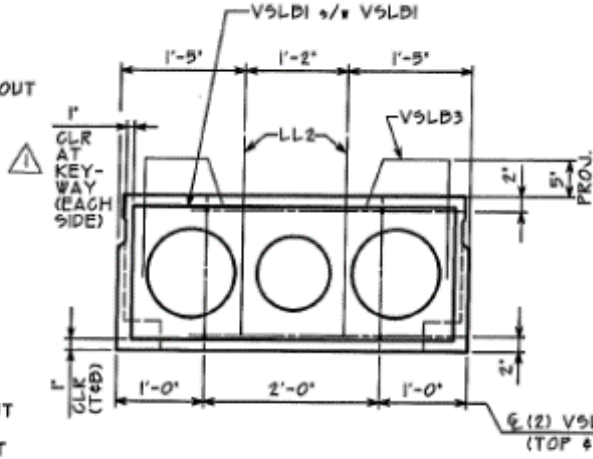

SECTION

SHOWING STEEL REINF.

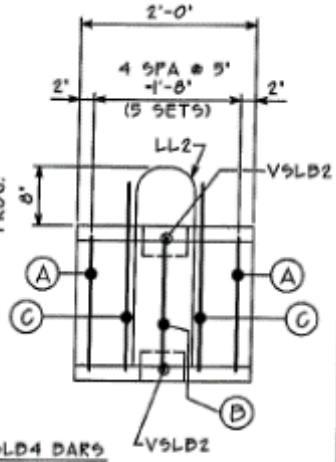

LONG. SECT.

SHOWING STEEL REINF.

ROSS PRESTRESSED CONCRETE, INC.
P.O. BOX 6299
KNOXVILLE, TENNESSEE 37914
PHONE NO. (865) 524-1485
FAX NO. (865) 637-0831
www.rossprestress.com

PROJECT
VIRGINIA TECH
BOX BEAM AND
VOIDED SLAB PROJECT
P.O.#P2470683

STATION NO. --
COUNTY --
CONTRACTOR --
ARCHITECT/ENGINEER --

VOIDED SLAB SPECIMEN 4

DRAWN BY	CHECKED BY	RPC JOB NO.
R	Ram	B13-18
SCALE	DATE	DRAWING NO.
NTS		VT-VA-138 6 OF 6

Appendix B: Concrete Mix Designs

Batch 1:

PULL WEIGHT SUMMARY BASED ON MOISTURE

25-Jun-13

MIX NO: Virginia Pull (BRISTOL PLANT)

Item	SSD (1 C.Y.)	
Cement	635	POUNDS
Fine	1452	POUNDS
Coarse	1744	POUNDS
Water	30.0	GALLONS
200N	25.0	OUNCES
S. Fume	0.0	POUNDS
Air Ent	3.0	OUNCES
Super	45.0	OUNCES

Free Moist F.A.= 2.7 Percent
Free Moist C.A.= 2.8 Percent
Total Free Moist= 10.6 Gal./CY

Batch 2:

PULL WEIGHT SUMMARY BASED ON MOISTURE

28-Jun-13

MIX NO: VIRGINIA (BRISTOL PLANT)

Item	SSD (1 C.Y.)	
Cement	635	POUNDS
Fine	1452	POUNDS
Coarse	1744	POUNDS
Water	30.0	GALLONS
200N	30.0	OUNCES
S. Fume	0.0	POUNDS
Air Ent	3.0	OUNCES
Super	45.0	OUNCES

Free Moist F.A.= 4.4 Percent
Free Moist C.A.= 1.9 Percent
Total Free Moist= 11.6 Gal./CY

*Batch 3 mix design was never received from Ross Prestress, but it is assumed the mix design was the same as the first two mixes.

Specimen 5 Concrete Topping Mix Design:

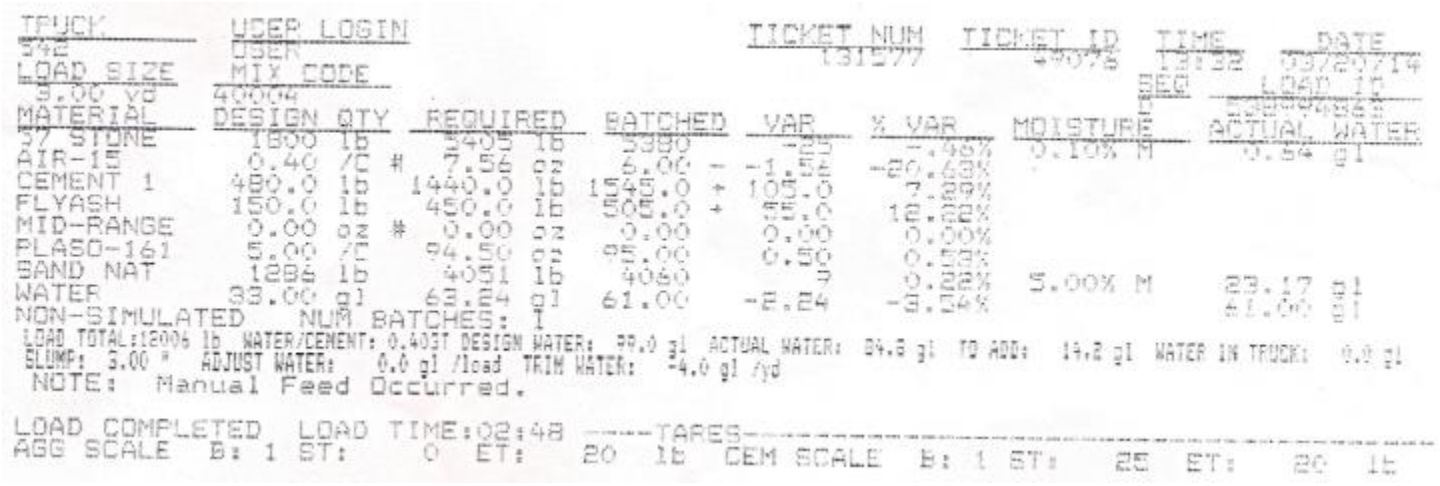

TRUCK	USER LOGIN			TICKET NUM	TICKET ID	TIME	DATE
542	USER			131277	490748	13:32	03/20/14
LOAD SIZE	MIX CODE					SEQ	LOAD ID
3.00 YD	40004					1	20140320-5

MATERIAL	DESIGN QTY	REQUIRED	BATCHED	VAR	% VAR	MOISTURE	ACTUAL WATER
57 STONE	1800 lb	5405 lb	5380	-25	-0.46%	0.10% M	
AIR-15	0.40 /C #	7.56 oz	6.00 -	-1.56	-20.63%		0.54 gl
CEMENT 1	480.0 lb	1440.0 lb	1545.0 +	105.0	7.29%		
FLYASH	150.0 lb	450.0 lb	505.0 +	55.0	12.22%		
MID-RANGE	0.00 oz #	0.00 oz	0.00	0.00	0.00%		
PLAS0-161	5.00 /C	94.50 oz	95.00	0.50	0.53%		
SAND NAT	1286 lb	4051 lb	4060	9	0.22%	5.00% M	23.17 gl
WATER	33.00 gl	63.24 gl	61.00	-2.24	-3.54%		41.00 gl

NON-SIMULATED NUM BATCHES: 1

LOAD TOTAL:12006 lb WATER/CEMENT: 0.403T DESIGN WATER: 58.0 gl ACTUAL WATER: 64.8 gl TO ADD: 14.8 gl WATER IN TRUCK: 0.0 gl
SLUMP: 5.00 " ADJUST WATER: 0.0 gl /load TRIM WATER: -4.0 gl /yd
NOTE: Manual Feed Occurred.

LOAD COMPLETED LOAD TIME:02:48 -----TARES-----
AGG SCALE B: 1 ST: 0 ET: 20 lb CEM SCALE B: 1 ST: 25 ET: 20 lb

Specimen 6 Concrete Topping Mix Design:

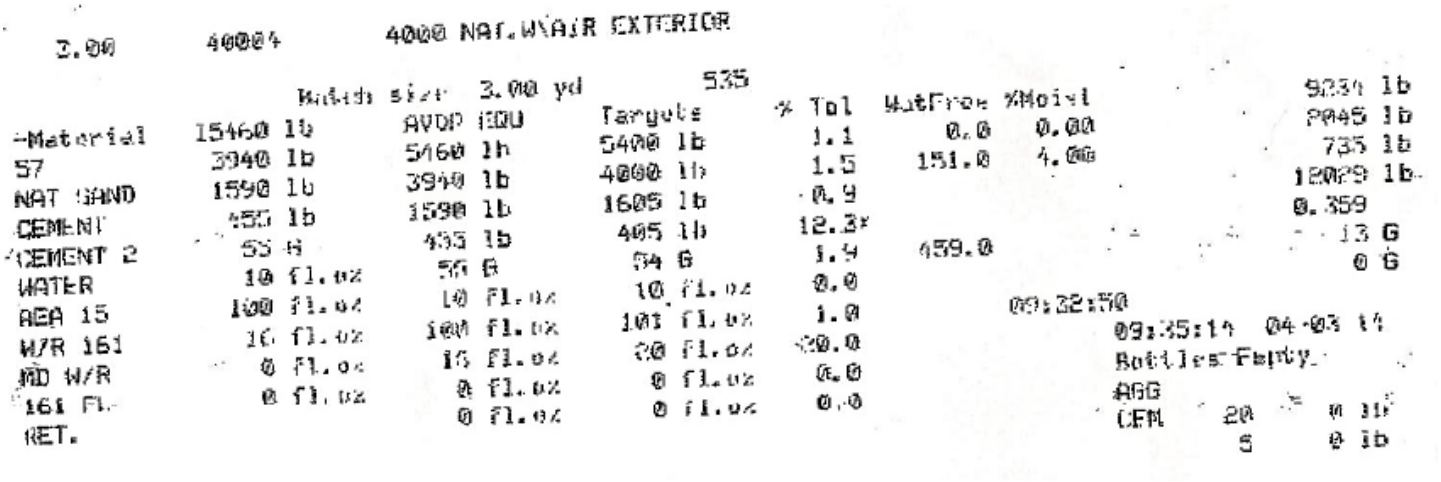

2.00 40004 4000 NAT.W\AIR EXTERIOR

Batch size 3.00 yd 535

-Material		AVDP IDEU	Targets	% Tol	WetFree	%Moist	
57	15460 lb	5160 lb	5400 lb	1.1	0.0	0.00	9234 lb
NAT SAND	3940 lb	3940 lb	4000 lb	1.5	151.0	4.00	2045 lb
CEMENT	1590 lb	1590 lb	1605 lb	0.9			735 lb
CEMENT 2	455 lb	433 lb	405 lb	12.3*			12029 lb
WATER	55 G	56 G	54 G	1.9	459.0		0.359
AEA 15	10 fl.oz	10 fl.oz	10 fl.oz	0.0			13 G
W/R 161	100 fl.oz	100 fl.oz	101 fl.oz	1.0			0 G
MID W/R	16 fl.oz	16 fl.oz	20 fl.oz	-20.0			
161 FL-	0 fl.oz	0 fl.oz	0 fl.oz	0.0			
RET.	0 fl.oz	0 fl.oz	0 fl.oz	0.0			

09:32:50
09:35:14 04-03 14
Bottles Empty
AGG
CEM 20 0 lb
5 0 lb

Appendix C: Supplementary Data

Appendix C contains all of the supplementary data collected during tested that wasn't put into the results section. There are six sections in Appendix C, one for each specimen. Where appropriate each section is broken down into three subsections. One for data collected during the first static test, a second for all the static tests ran throughout the cycling regimen, and a third for the final static test. The supplementary data comes from the four vertical LVDTs that measured deflection on the underside of the two exterior section, and also from the six 10 kip button loads cells that sat under the exterior sections. Similar to the results sections, data was left off of the graphs when it overlapped other data sets making the graphs difficult to read. The axes of similar graphs are kept the same size throughout Appendix C so that the results between specimens can be easily compared.

Specimen 1: Current VDOT Grouted Partial Depth Shear Key

First Static Test:

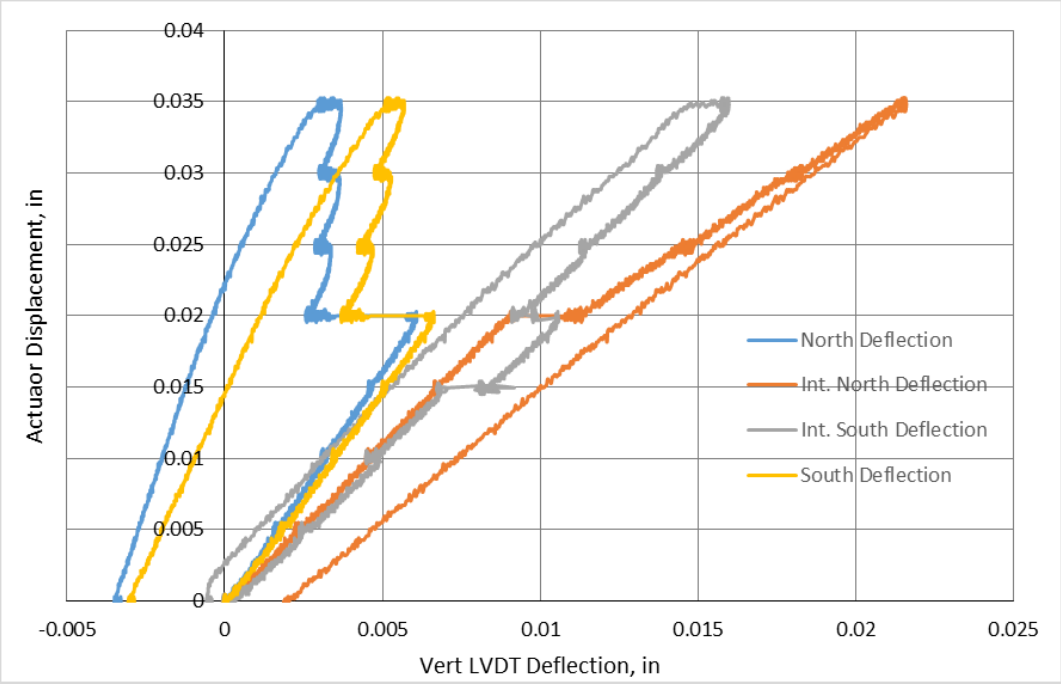

Figure 103: Vertical LVDT deflection during initial static test of specimen 1

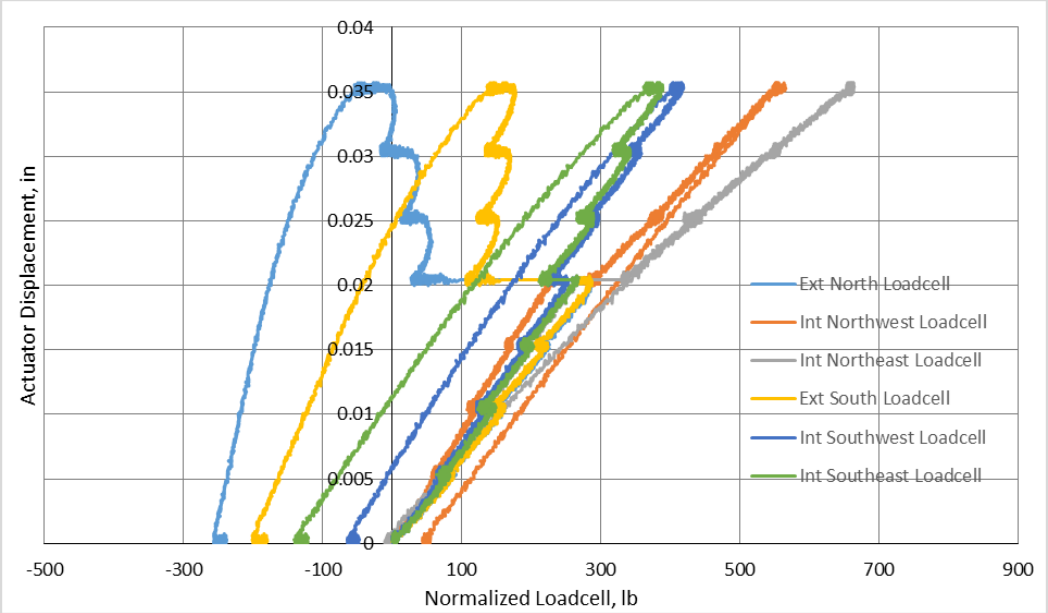

Figure 104: Normalized load cell values during initial static test of specimen 1

Since the first specimen failed before it could reach 100 cycles there is no other supplemental data available.

Specimen 2: Current VDOT Grouted Partial Depth Shear Key with Kevlar Reinforcement

First Static Test:

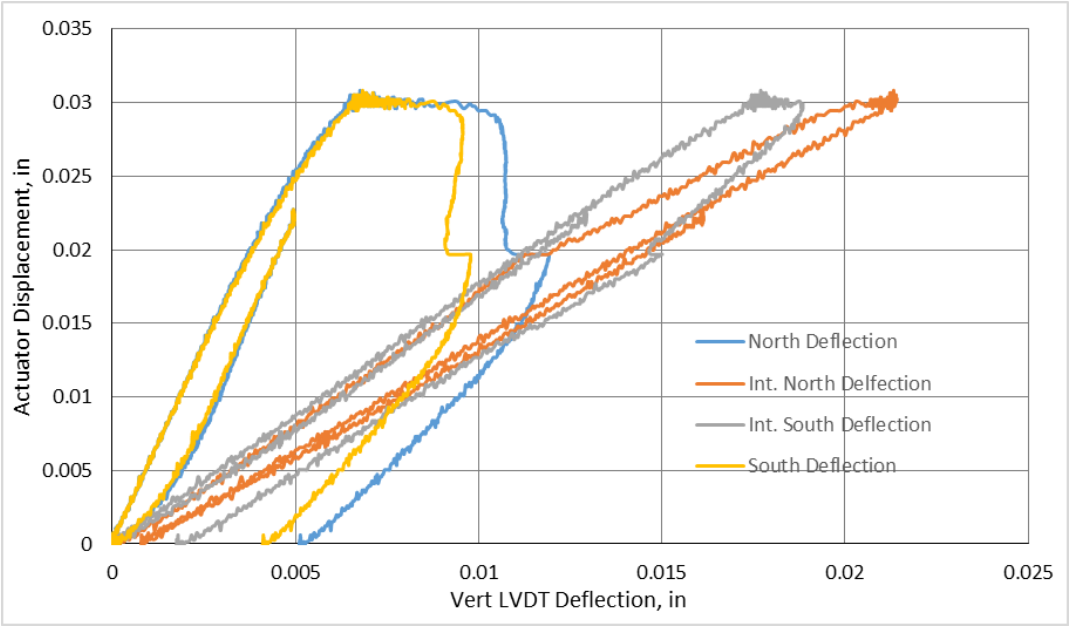

Figure 105: Vertical LVDT deflection during initial static test of specimen 2

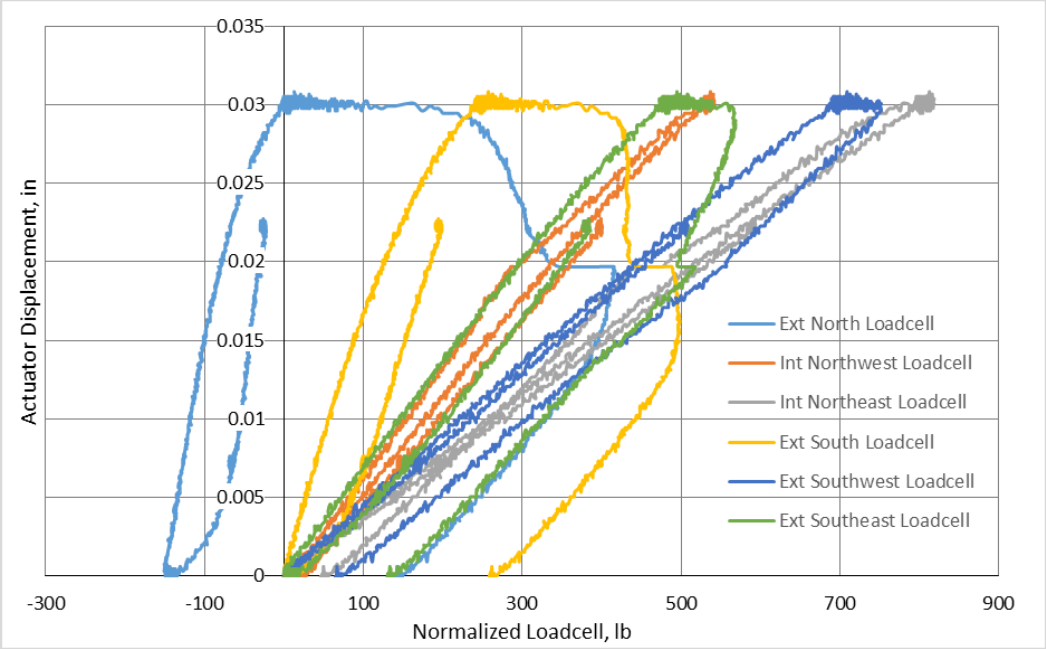

Figure 106: Normalized load cell values during initial static test of specimen 2

Static Tests following each Cyclic Test:

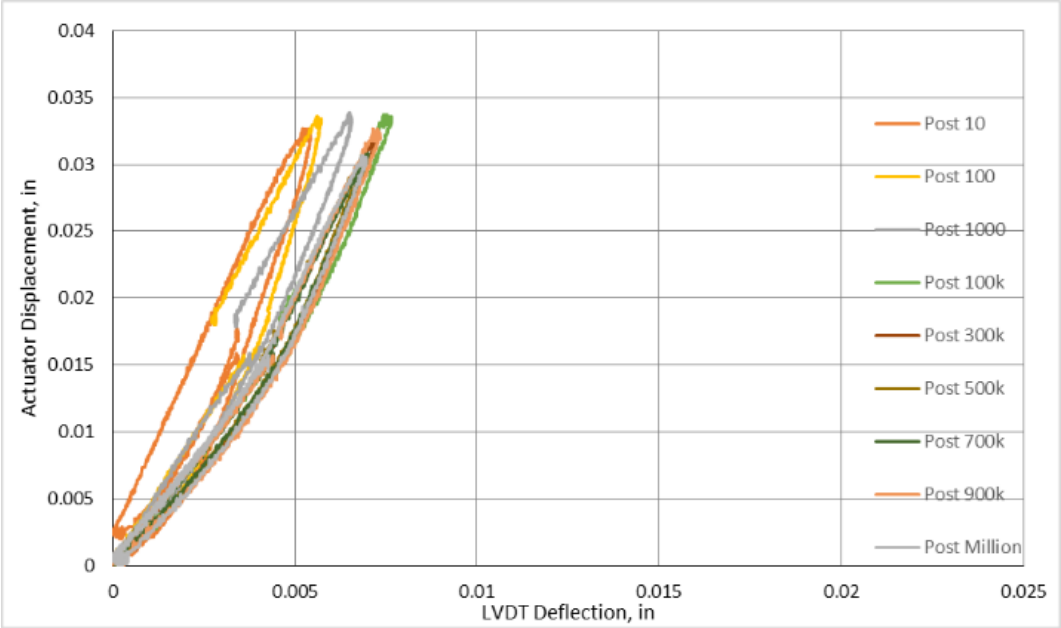

Figure 107: Exterior north vertical LVDT deflection for each cyclic test for specimen 2

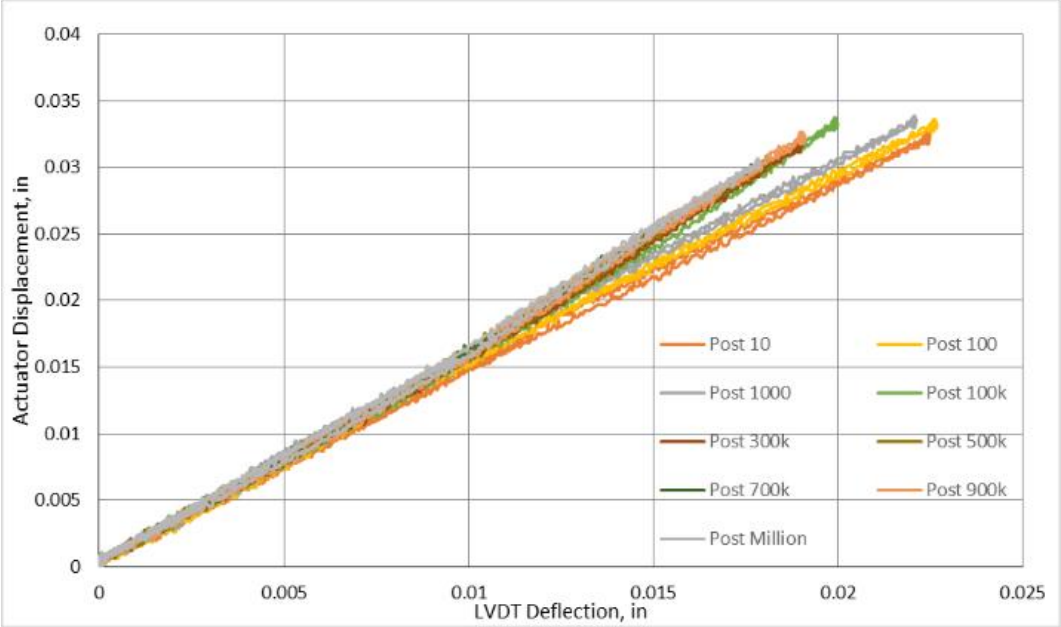

Figure 108: Interior north vertical LVDT deflection for each cyclic test for specimen 2

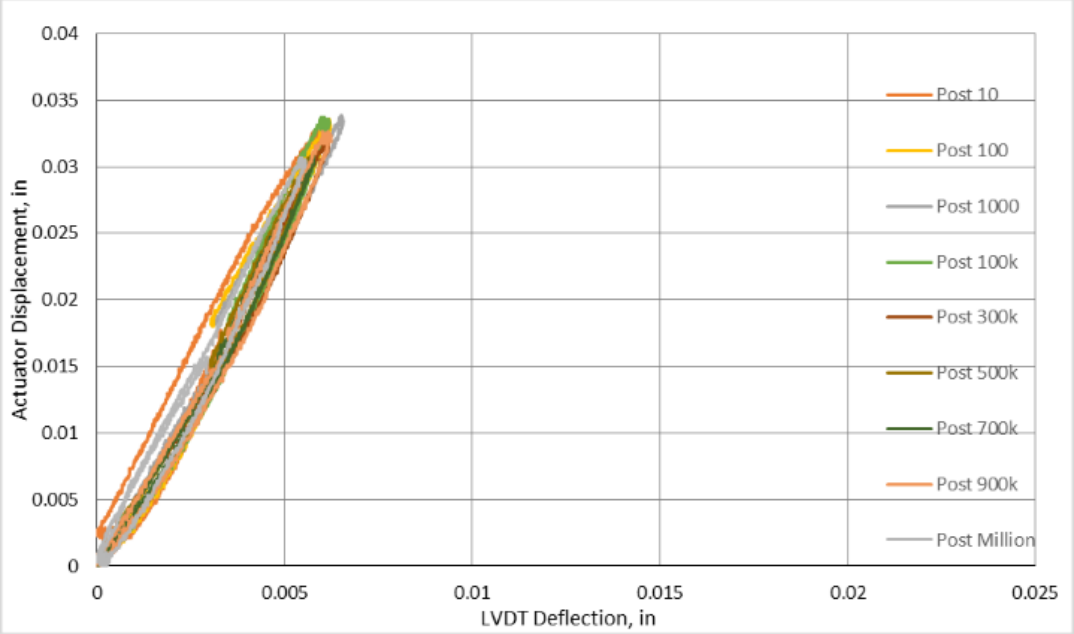

Figure 109: Exterior South vertical LVDT deflection for each cyclic test for specimen 2

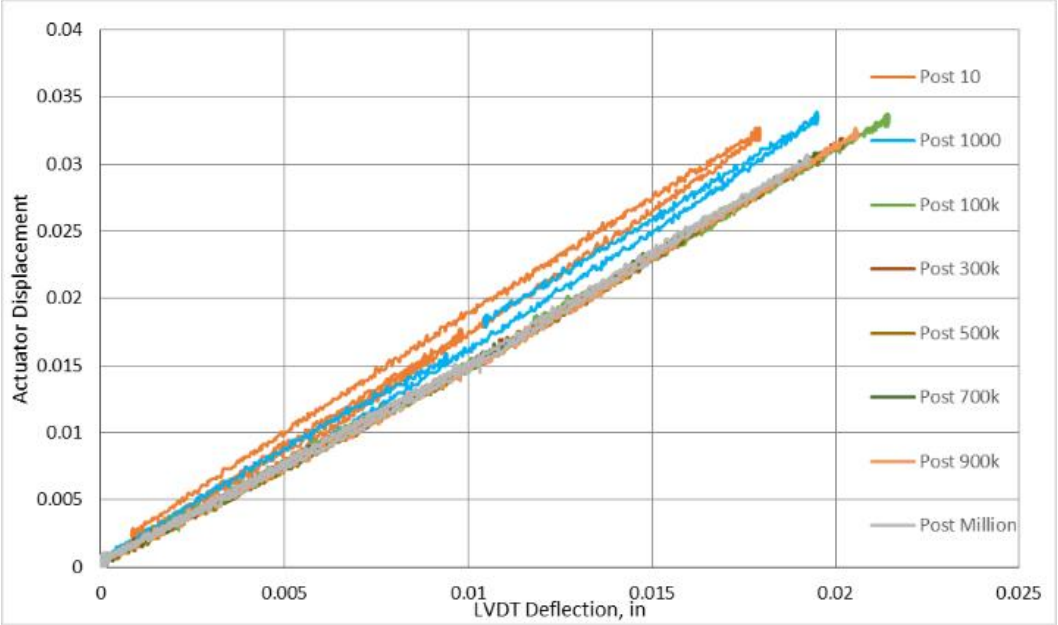

Figure 110: Interior South vertical LVDT deflection for each cyclic test for specimen 2

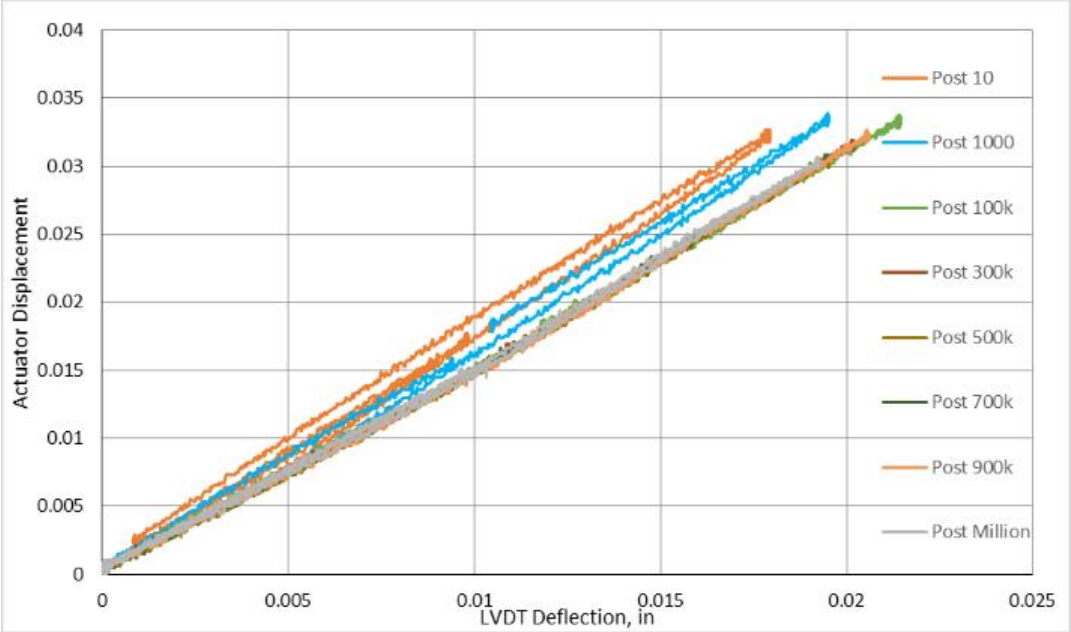

Figure 111: Normalized exterior north load cell following cyclic regimens for specimen 2

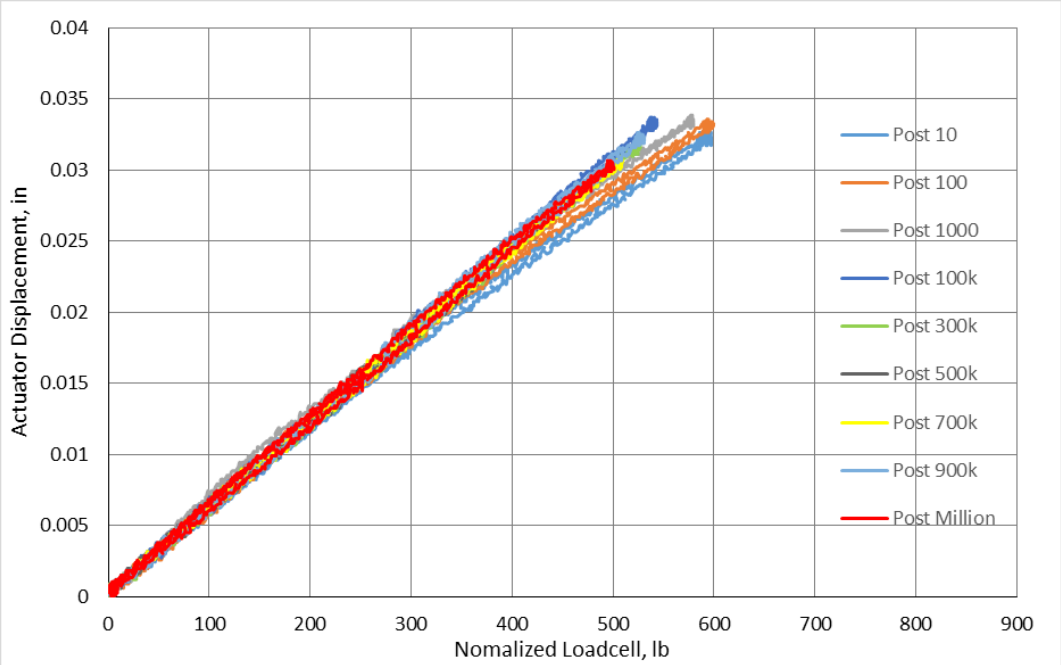

Figure 112: Normalized interior northwest load cell following cyclic regimen for specimen 2

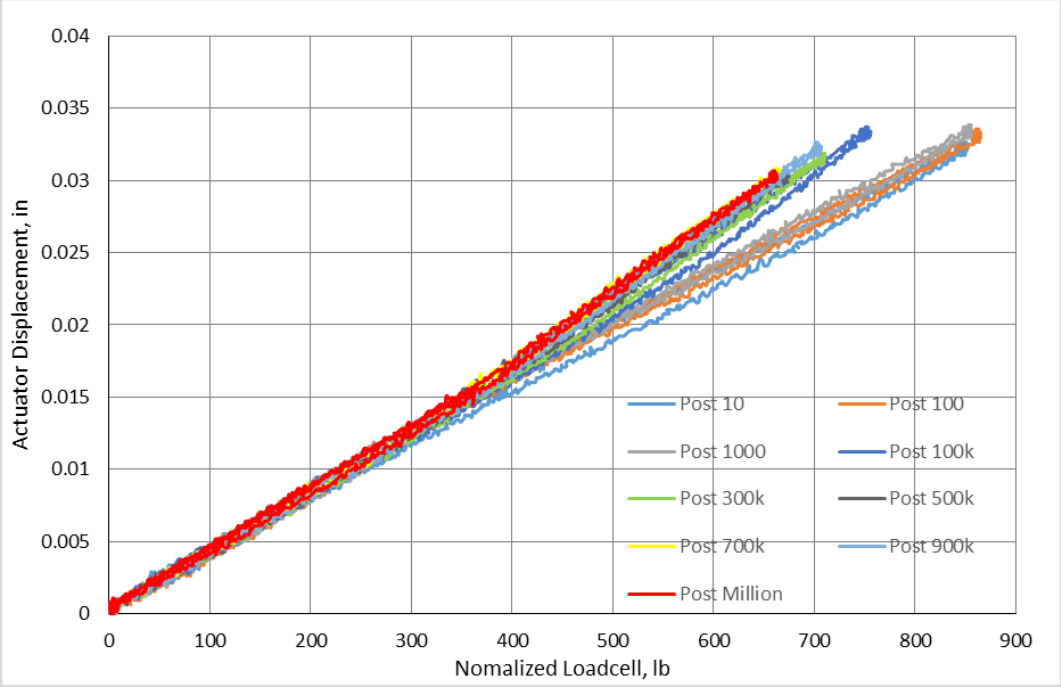

Figure 113: Normalized Interior northeast load cell following cyclic regimen for specimen 2

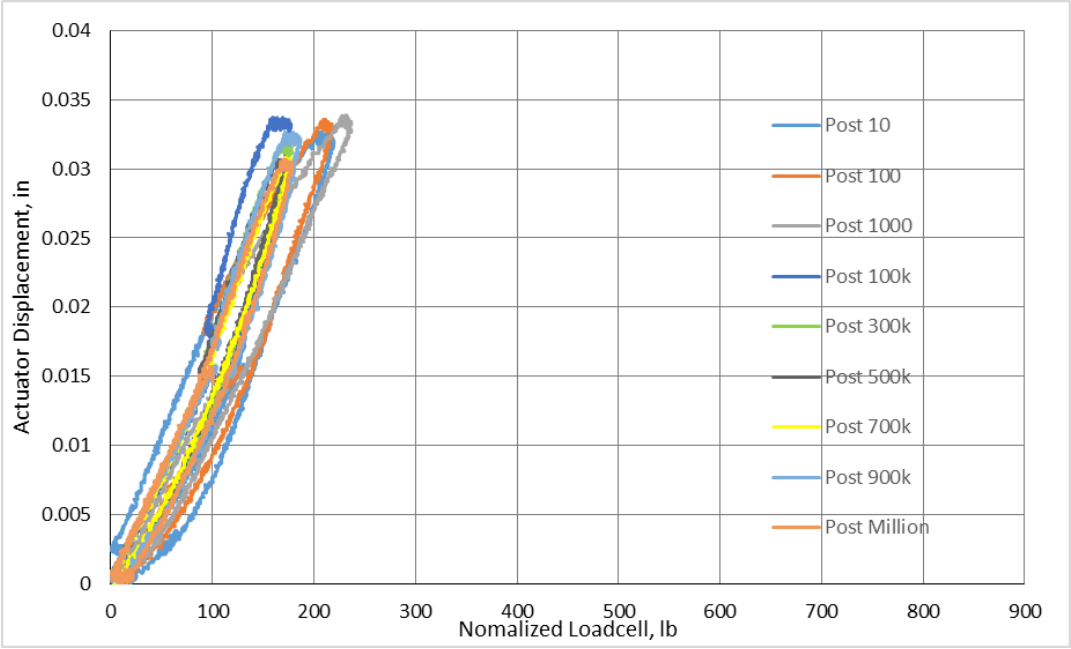

Figure 114: Normalized exterior south load cell following cyclic regimen for specimen 2

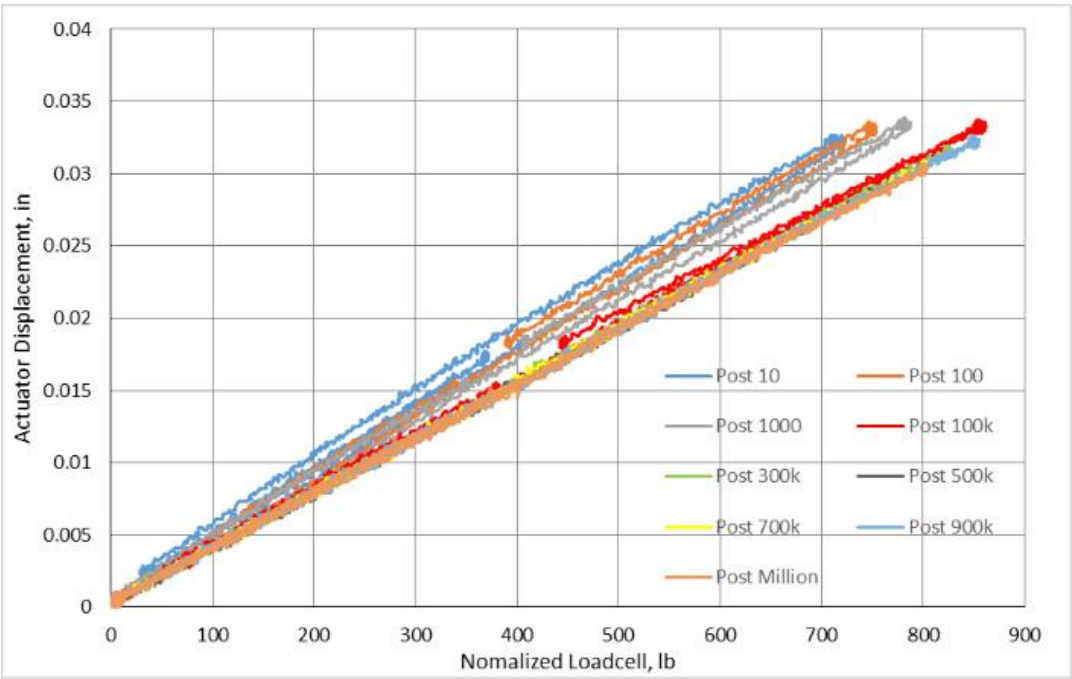

Figure 115: Normalized interior southwest load cell following cyclic regimen for specimen 2

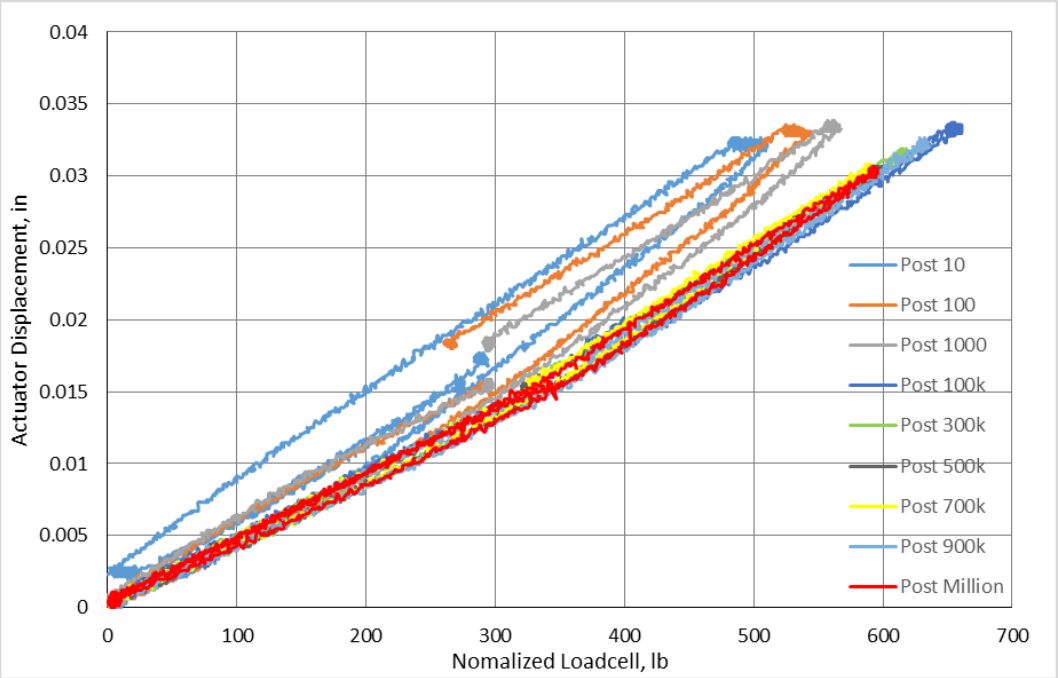

Figure 116: Normalized interior southeast load cell following cyclic regimens for specimen 2

Final Static Test:

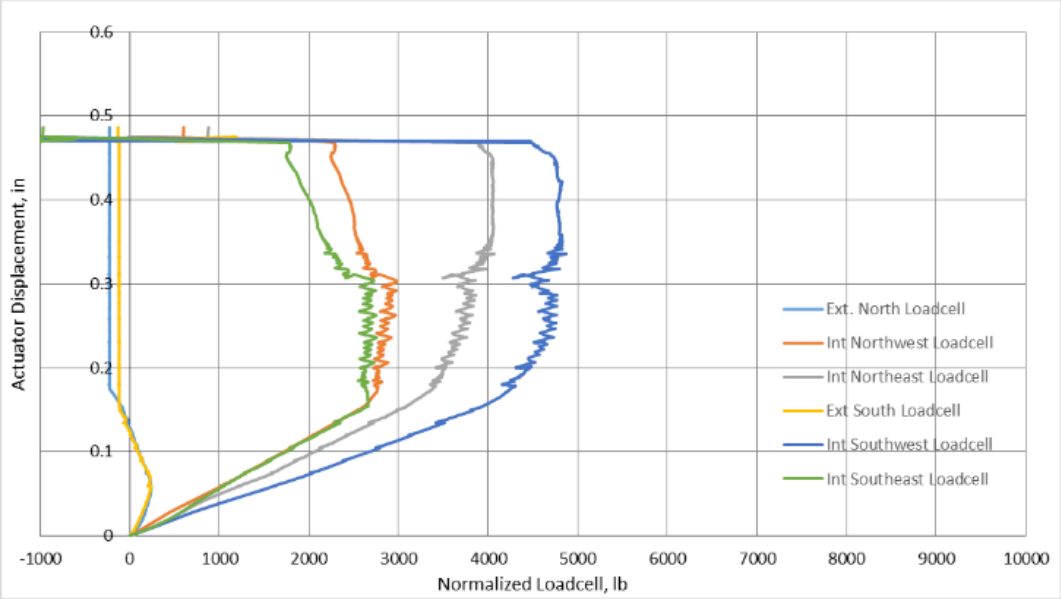

Figure 117: Normalized load cell data for the final static test of specimen 2

Specimen 3: Ductal UHPC Connection

First Static Test:

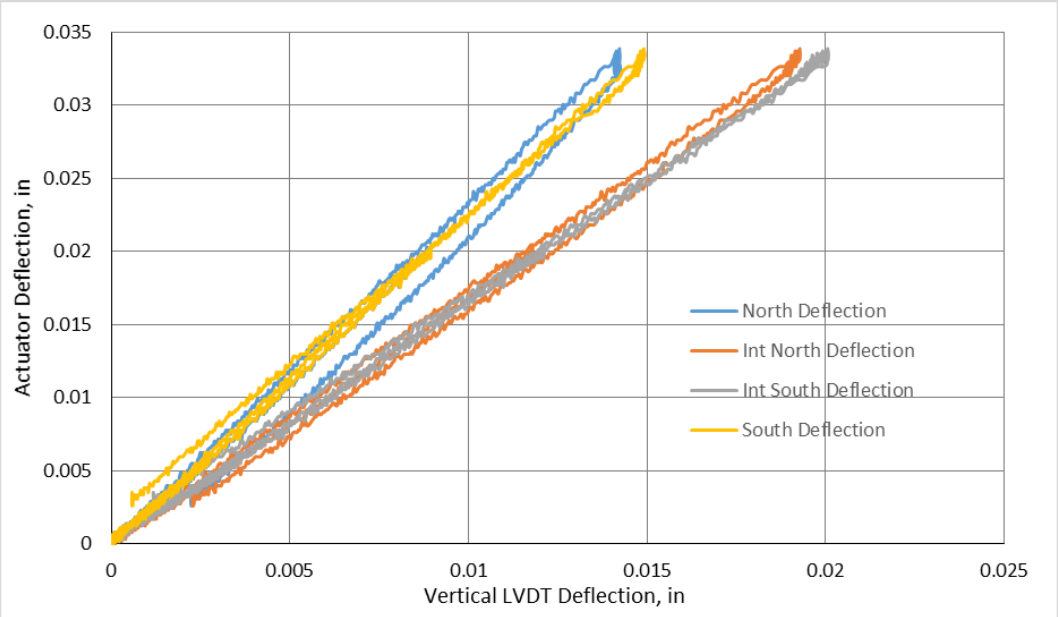

Figure 118: Vertical LVDT deflection during initial static test of specimen 3

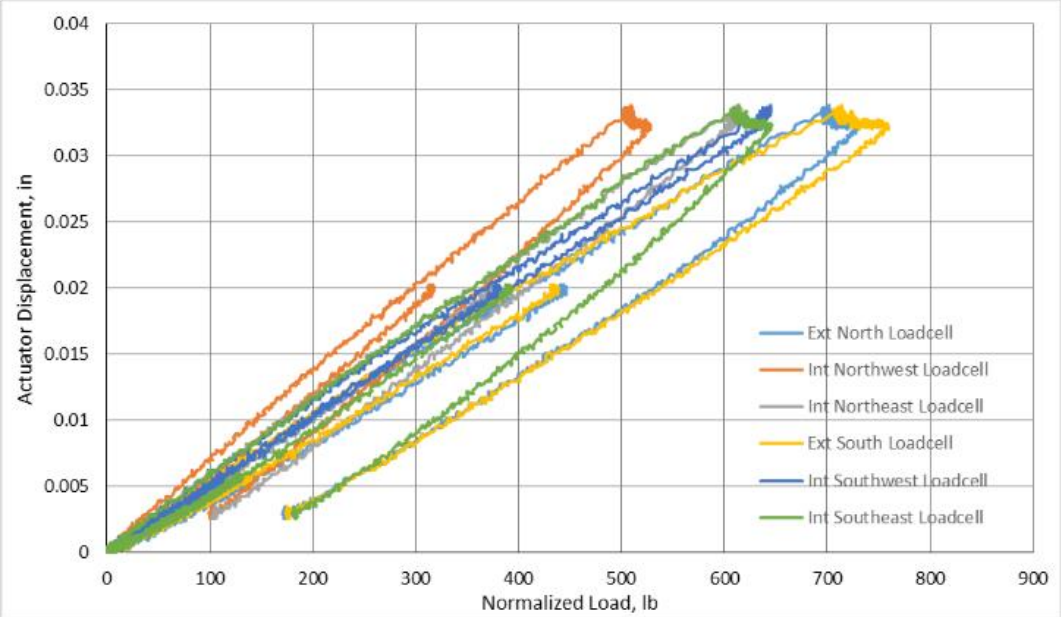

Figure 119: Normalized load cell values during initial static test of specimen 3

Static Tests following each Cyclic Test:

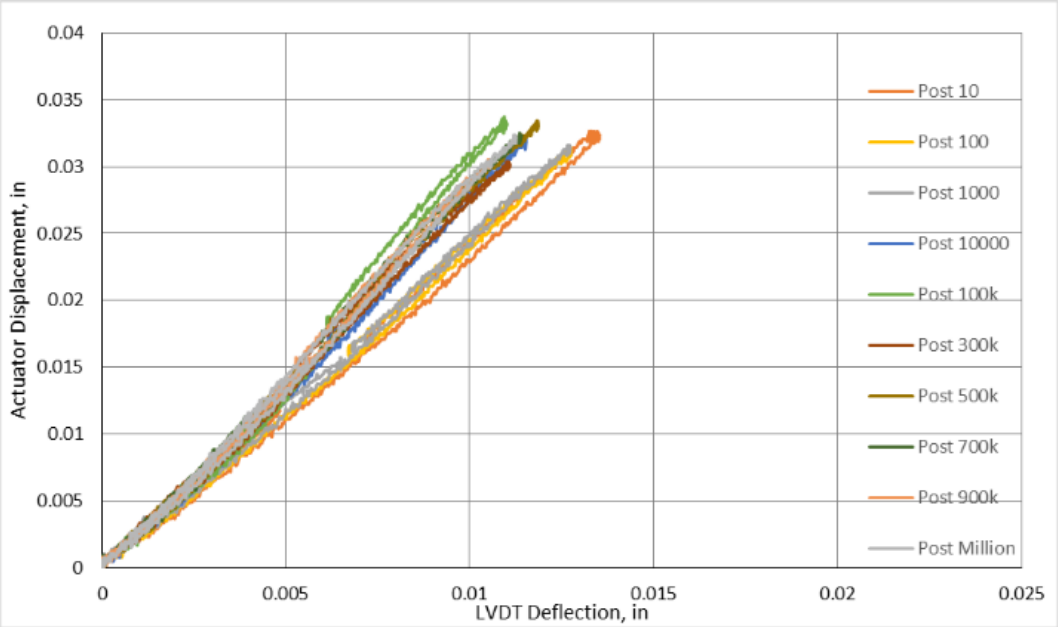

Figure 120: Exterior North vertical LVDT deflection for each cyclic test for specimen 3

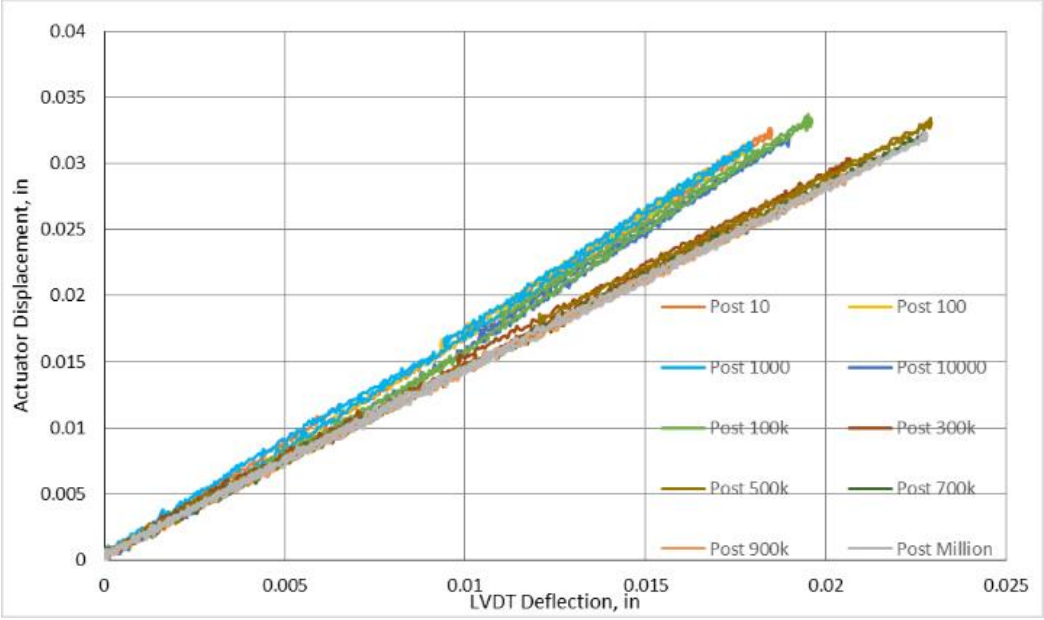

Figure 121: Interior North vertical LVDT deflection for each cyclic test for specimen 3

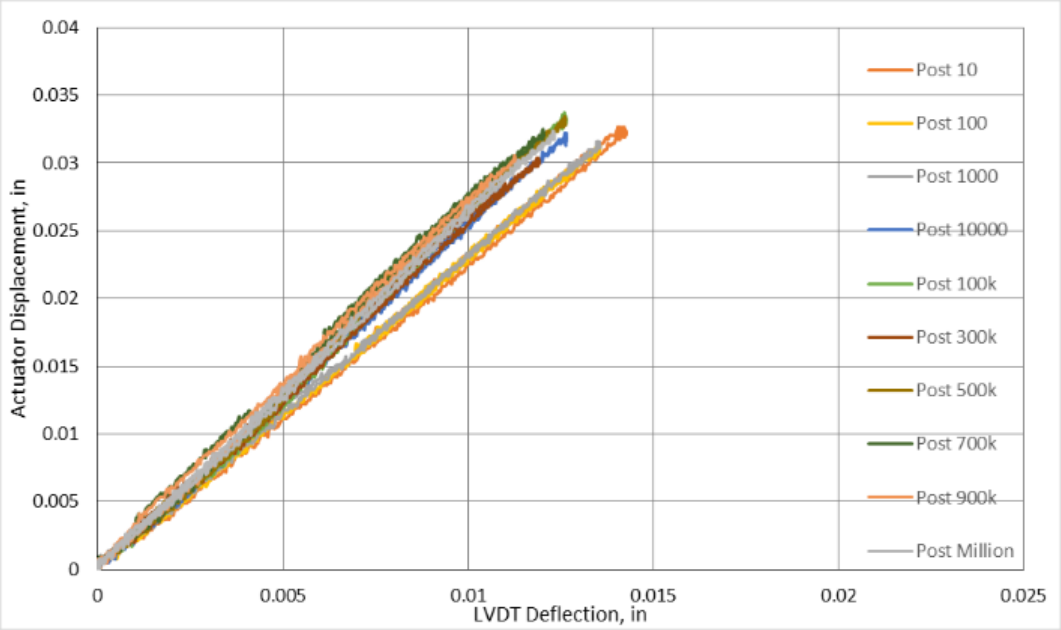

Figure 122: Exterior South vertical LVDT deflection for each cyclic test for specimen 3

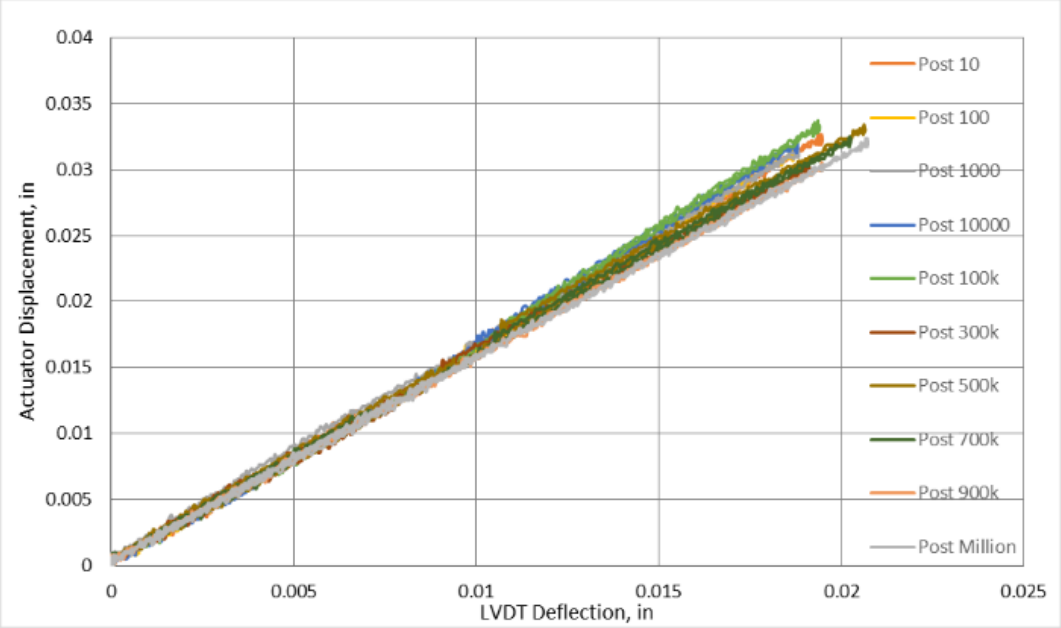

Figure 123: Interior South vertical LVDT deflection for each cyclic test for specimen 3

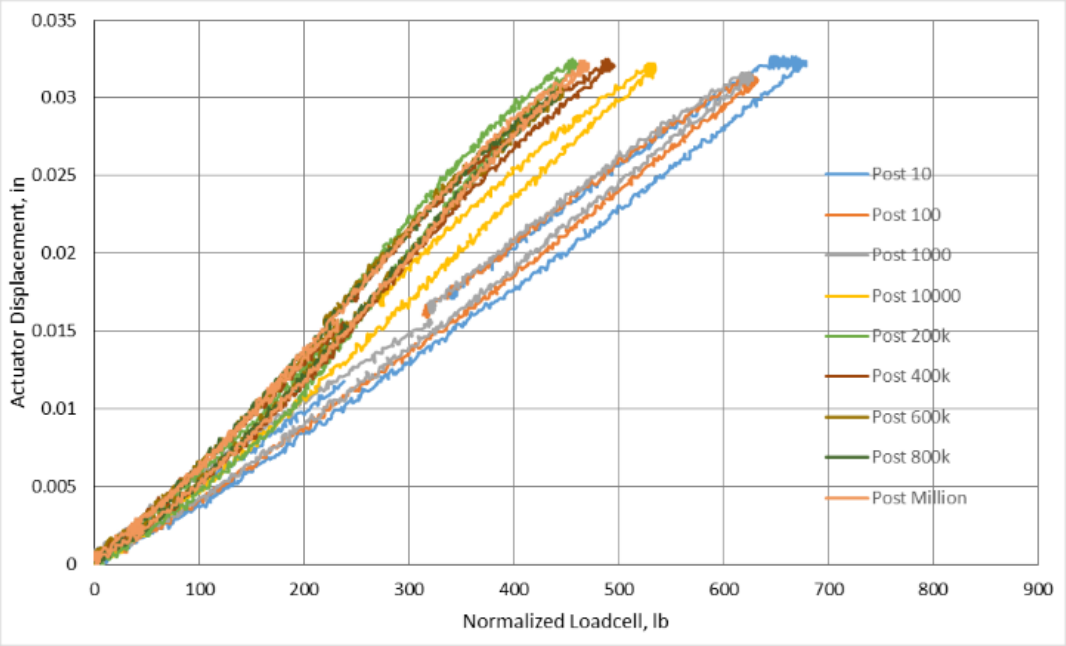

Figure 124: Normalized exterior north load cell following cyclic regimens for specimen 3

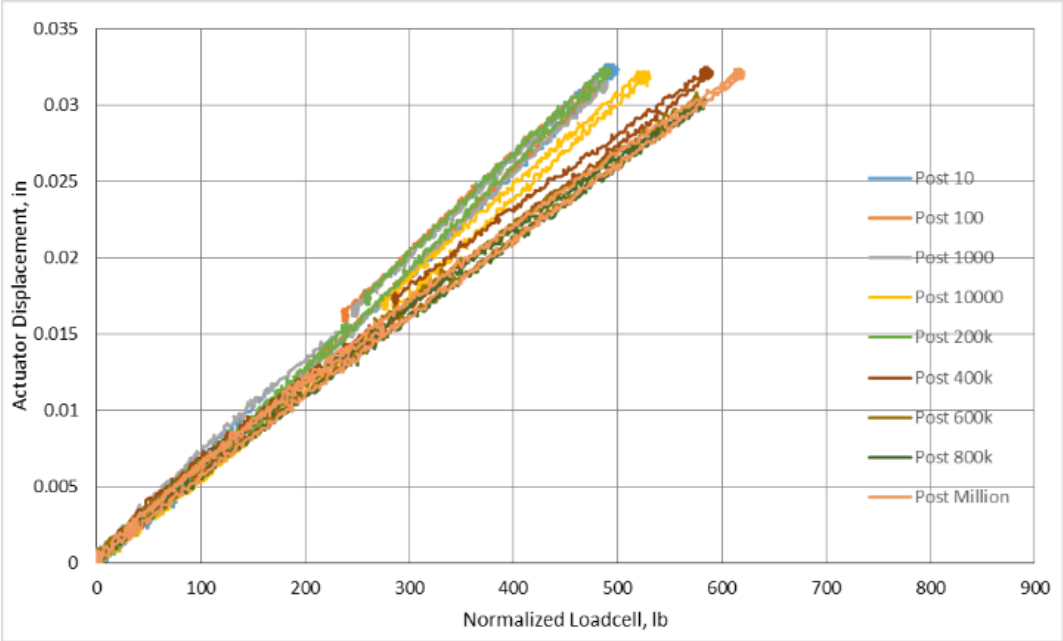

Figure 125: Normalized interior northwest load cell following cyclic regimen for specimen 3

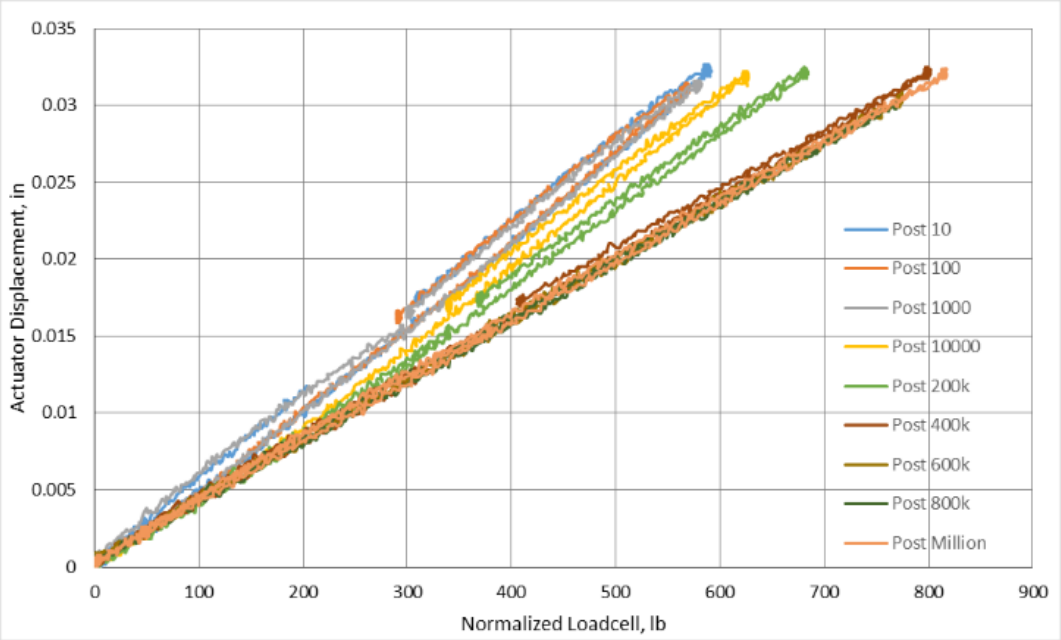

Figure 126: Normalized exterior northeast load cell following cyclic regimens for specimen 3

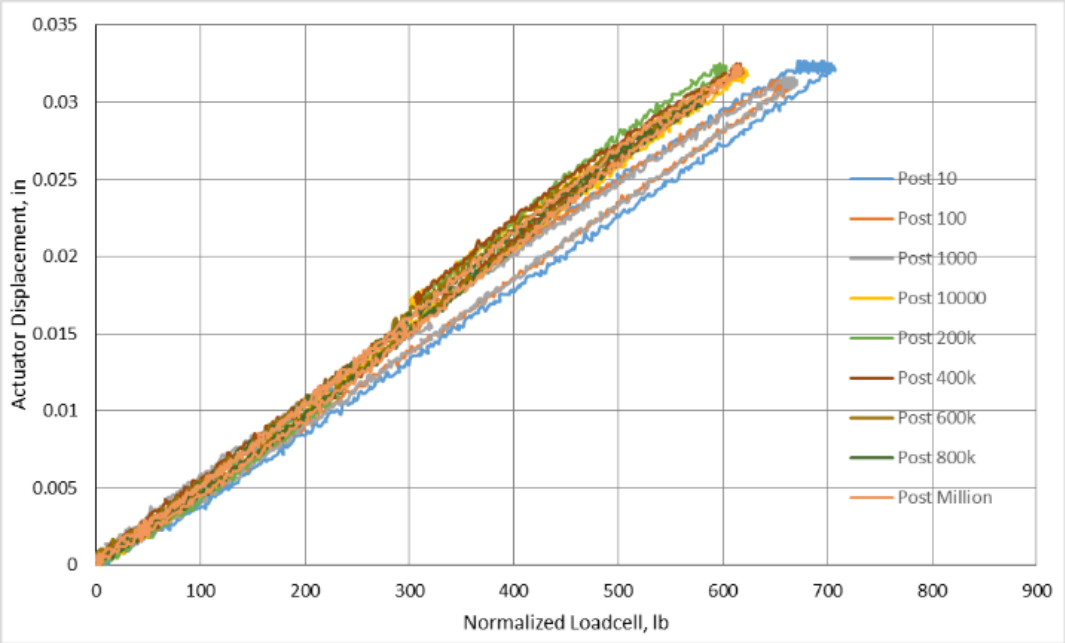

Figure 127: Normalized exterior south load cell following cyclic regimens for specimen 3

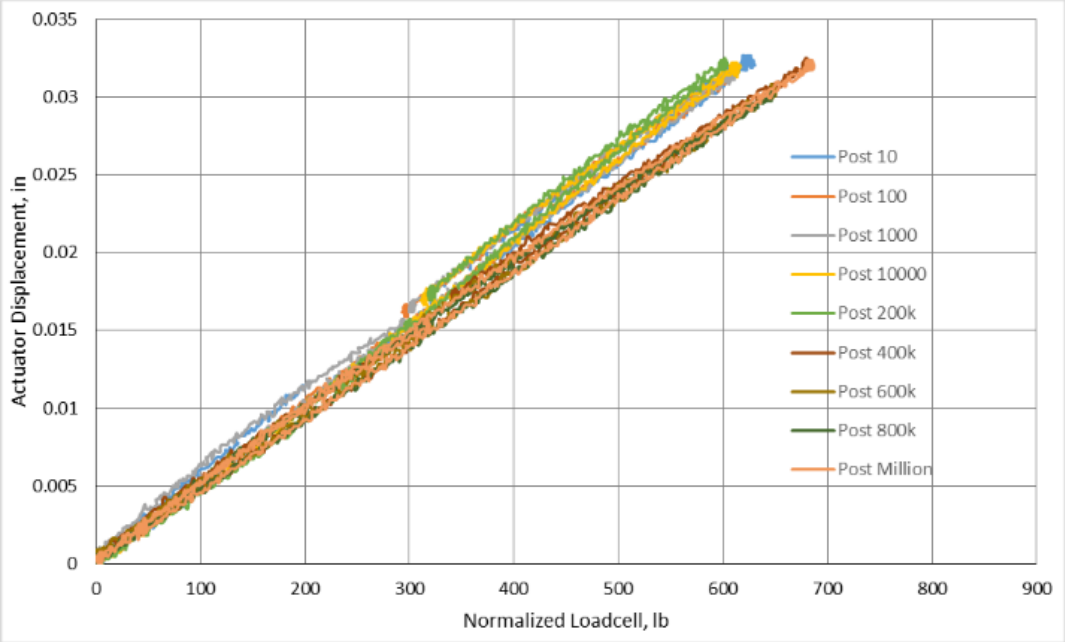

Figure 128: Normalized interior southwest load cell following cyclic regimen for specimen 3

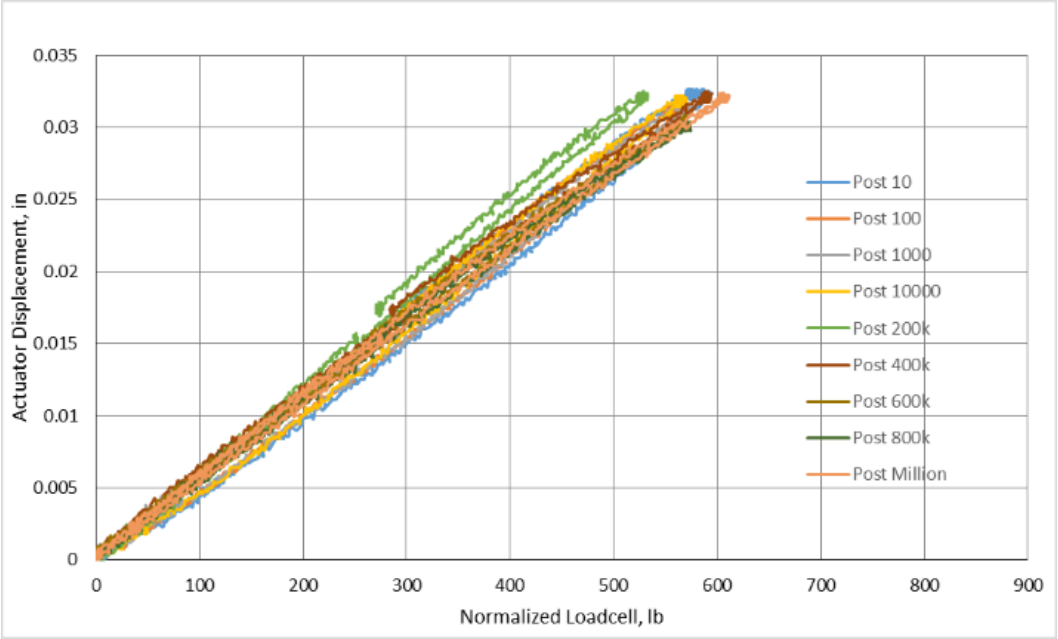

Figure 129: Normalized interior southeast load cell following cyclic regimens for specimen 3

Final Static Test:

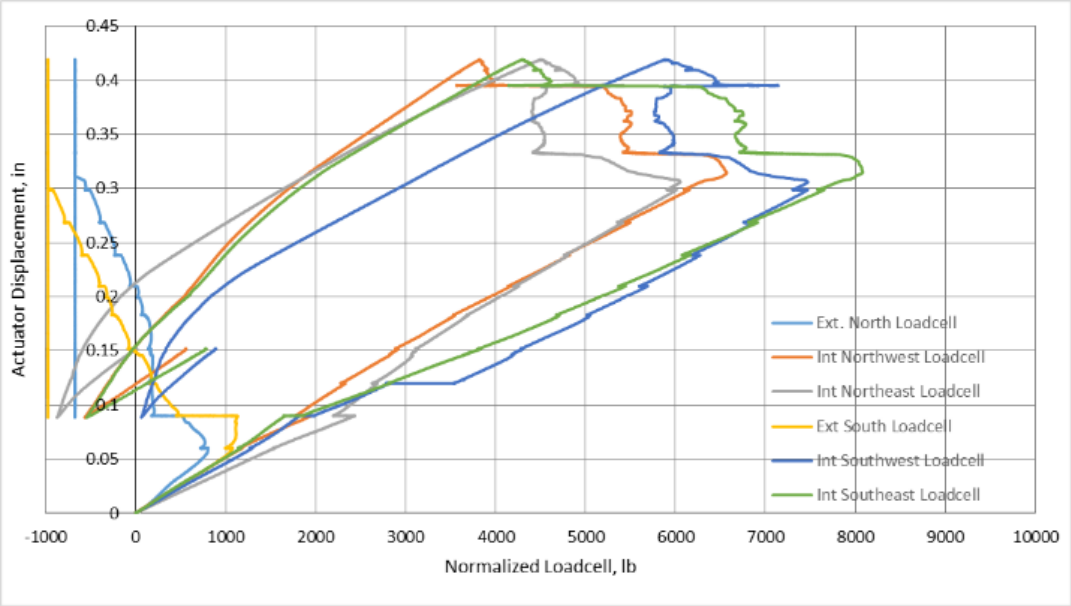

Figure 130: Normalized load cell data for the final static test of specimen 3

Specimen 4: VHPC Connection

First Static Test:

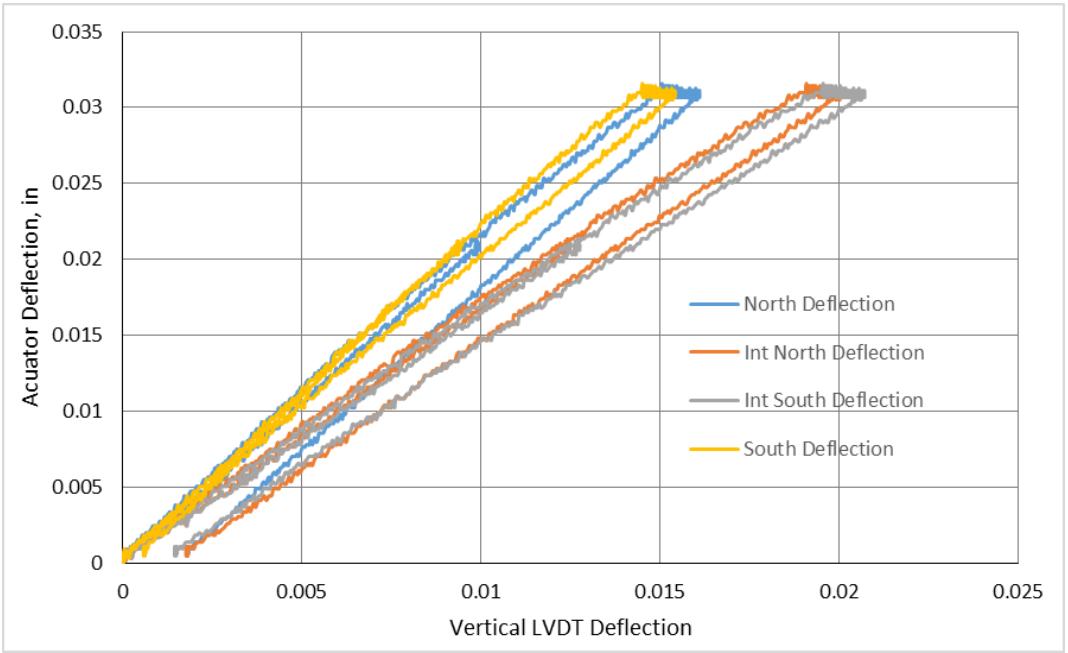

Figure 131: Vertical LVDT deflection during initial static test of specimen 4

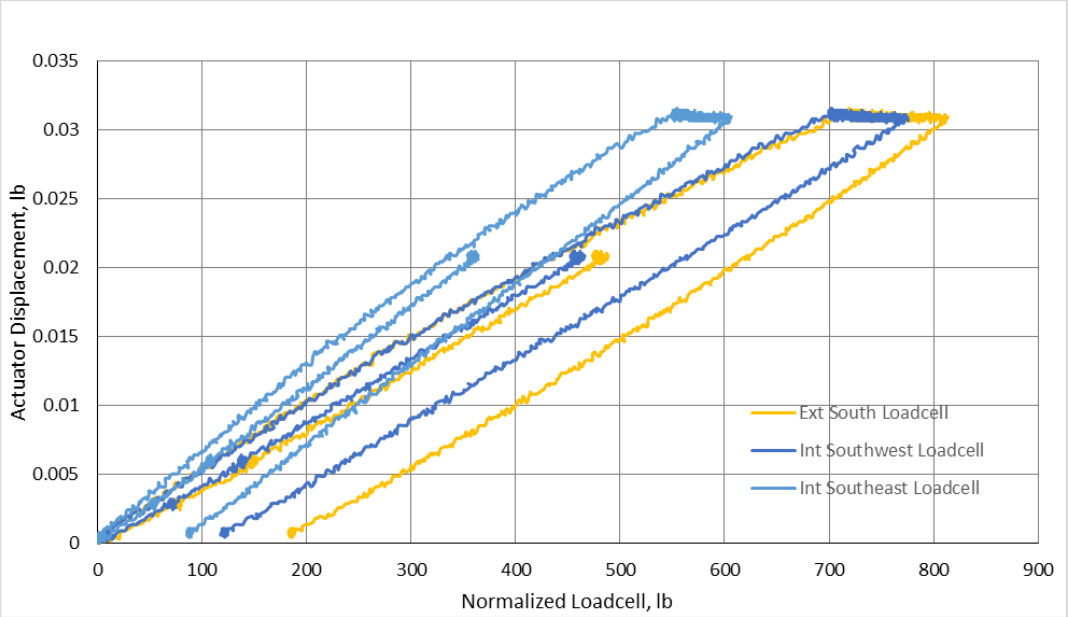

Figure 132: Normalized load cell values during initial static test of specimen 4.
Note North Load cells were not functioning during initial static test

Static Tests following each Cyclic Test:

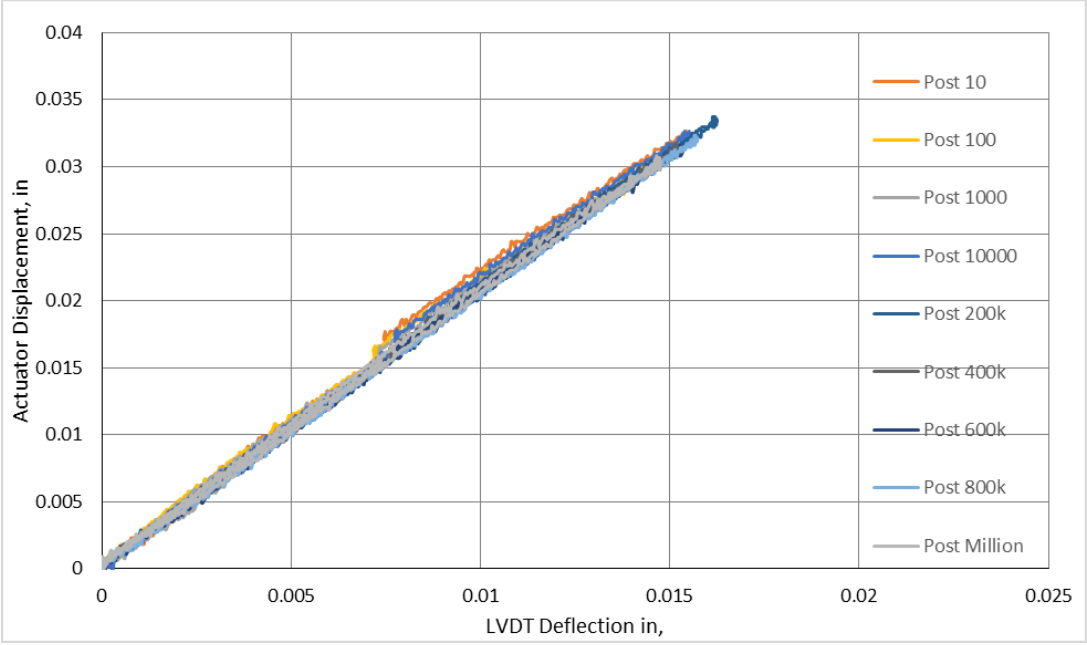

Figure 133: Exterior North vertical LVDT deflection for each cyclic test for specimen 4

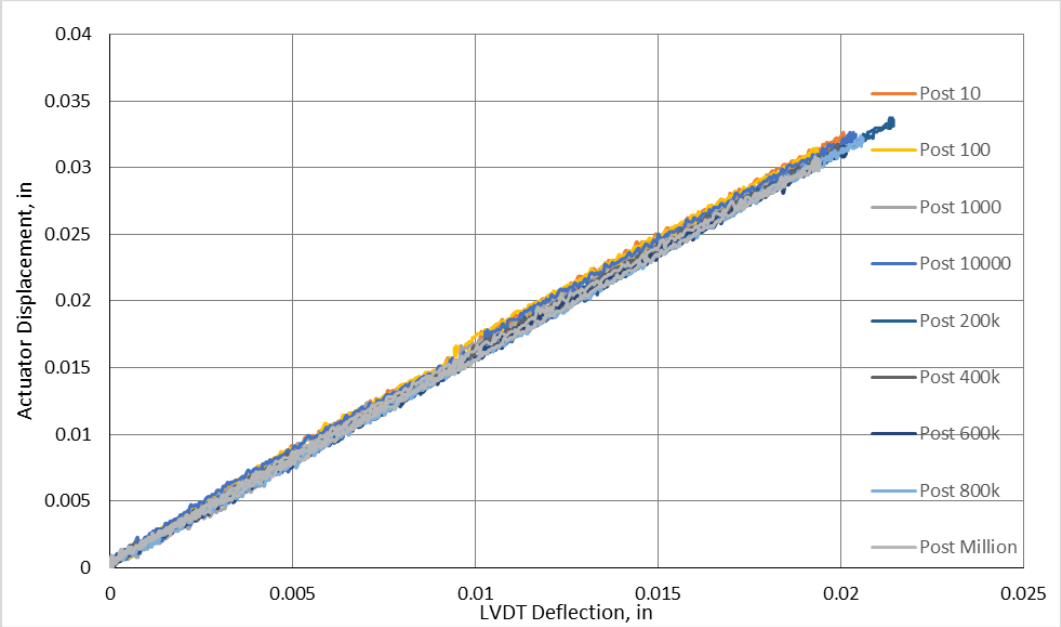

Figure 134: Interior North vertical LVDT deflection for each cyclic test for specimen 4

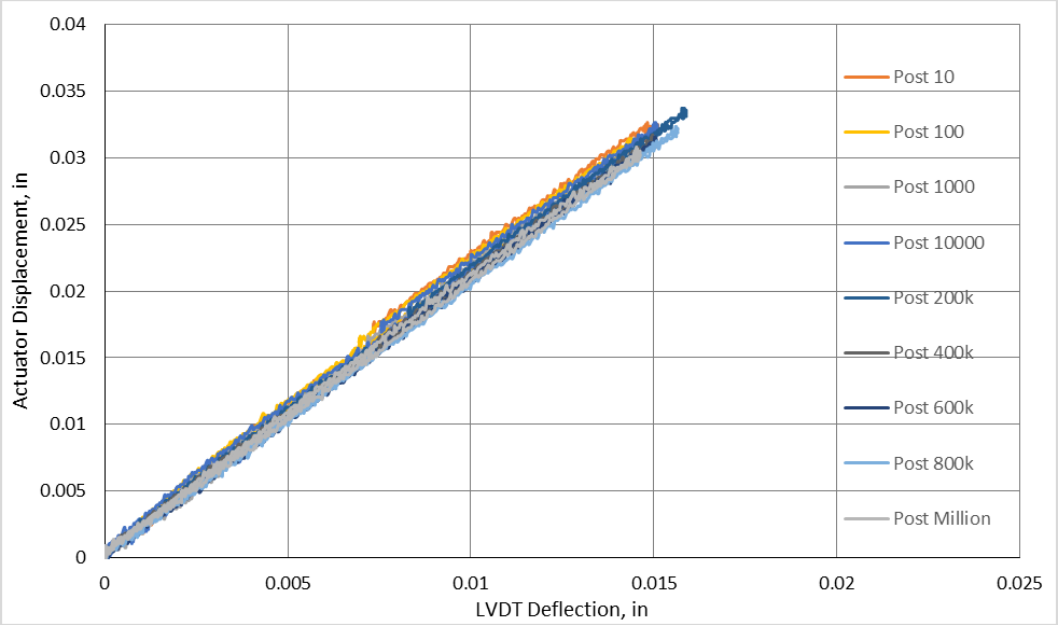

Figure 135: Exterior South vertical LVDT deflection for each cyclic test for specimen

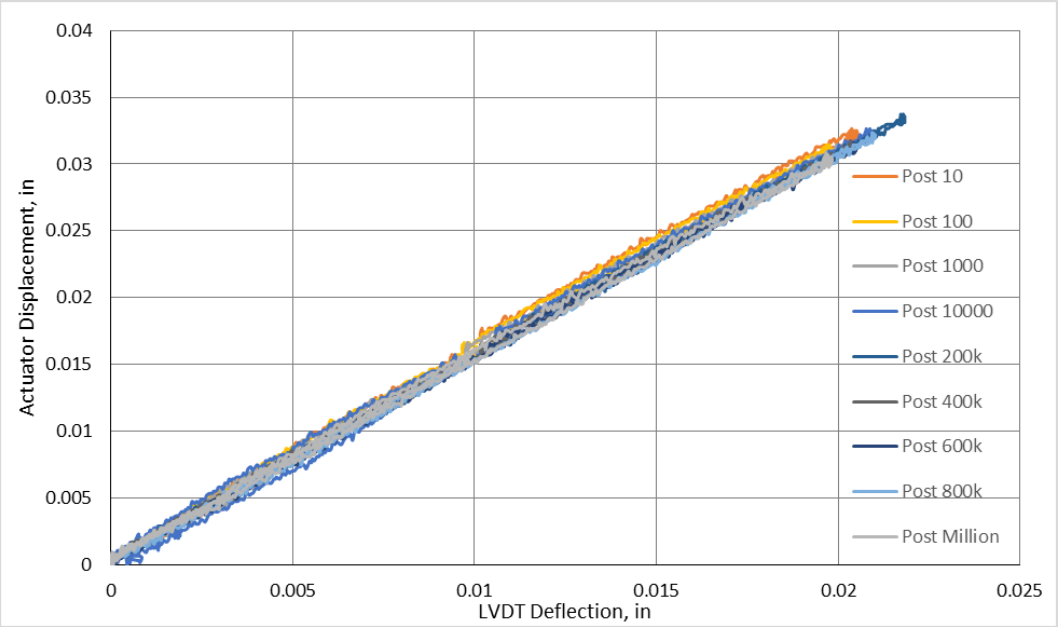

Figure 136: Interior South vertical LVDT deflection for each cyclic test for specimen 4

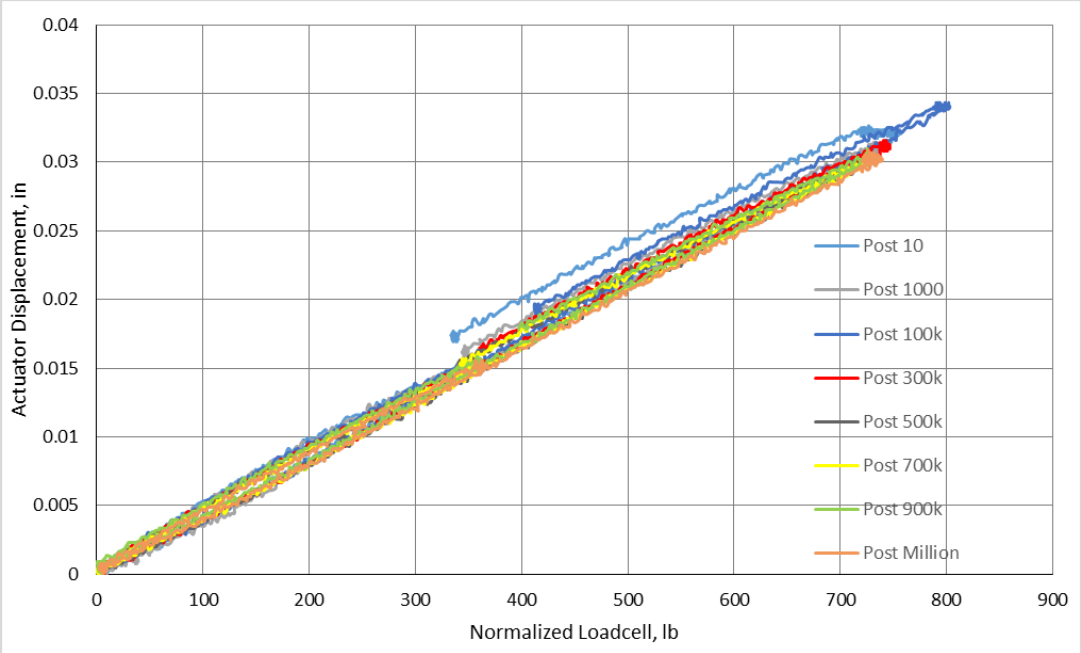

Figure 137: Normalized exterior north load cell following cyclic regimens for specimen 4

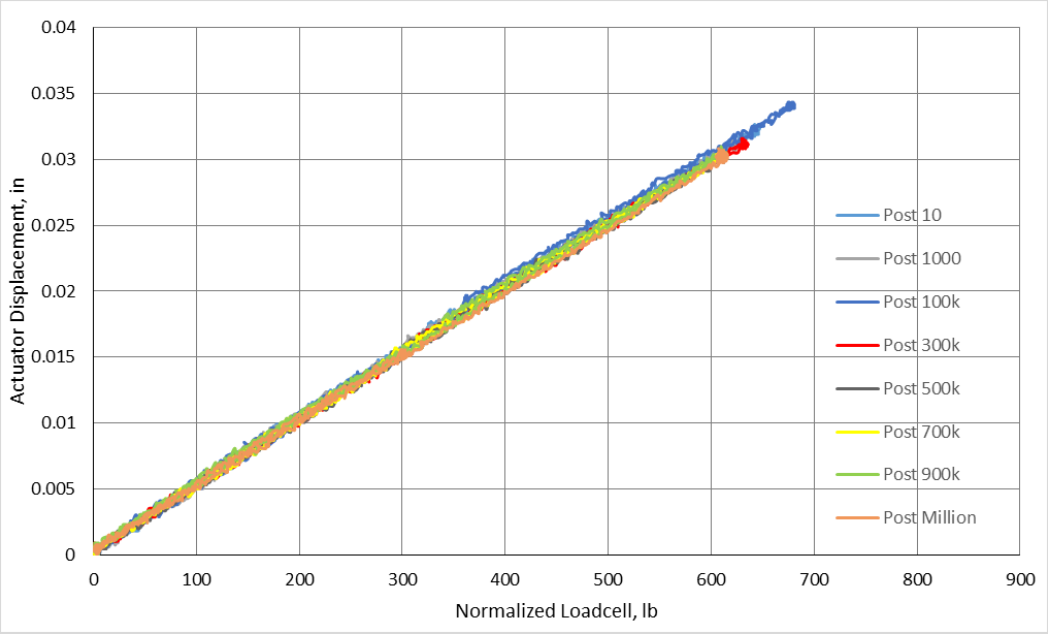

Figure 138: Normalized interior northwest load cell following cyclic regimen for specimen 4

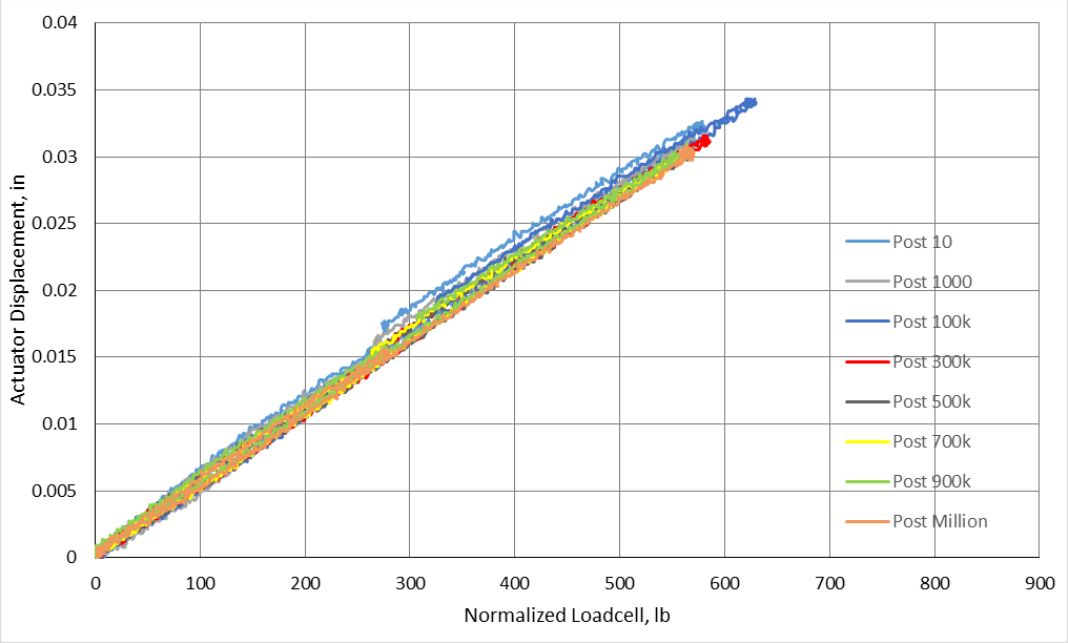

Figure 139: Normalized interior northeast load cell following cyclic regimens for specimen 4

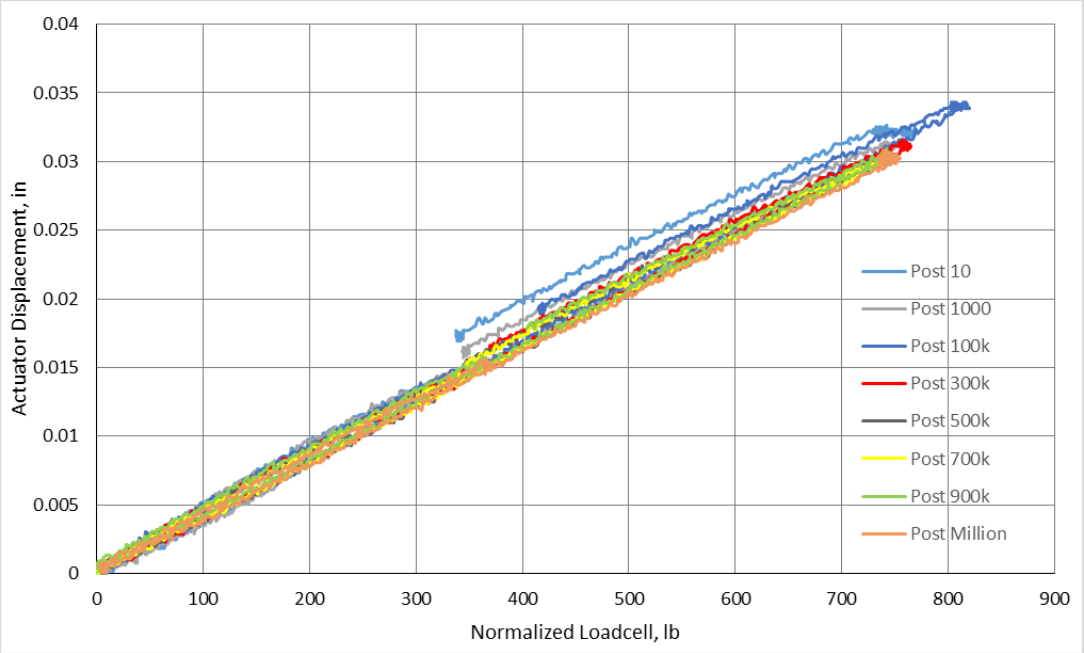

Figure 140: Normalized exterior south load cell following cyclic regimens for specimen 4

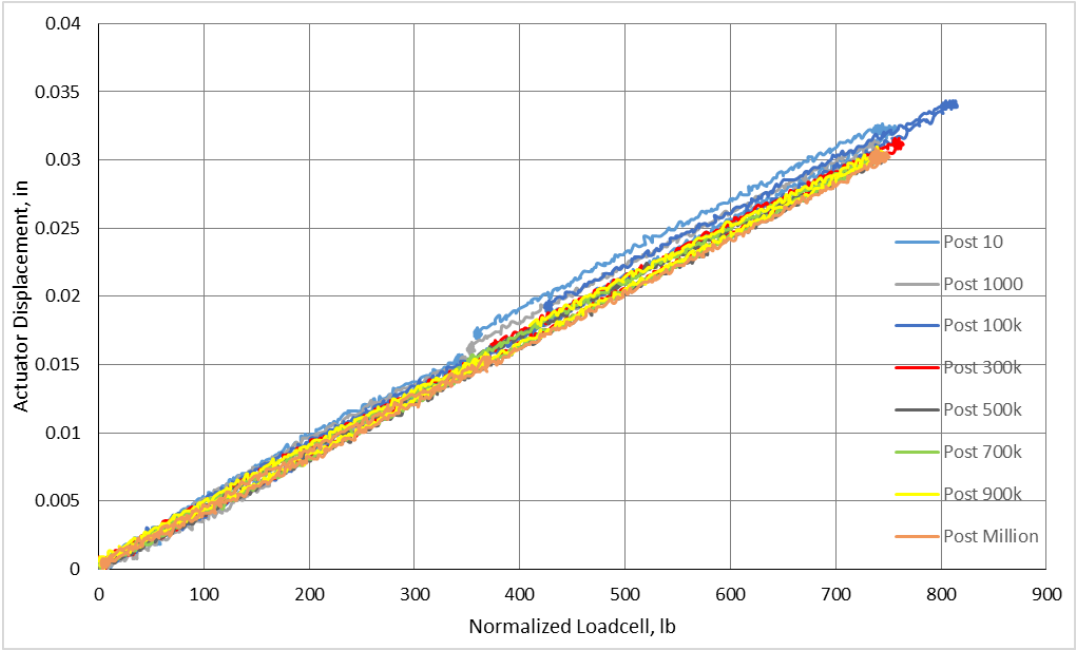

Figure 141: Normalized interior southwest load cell following cyclic regimen for specimen 4

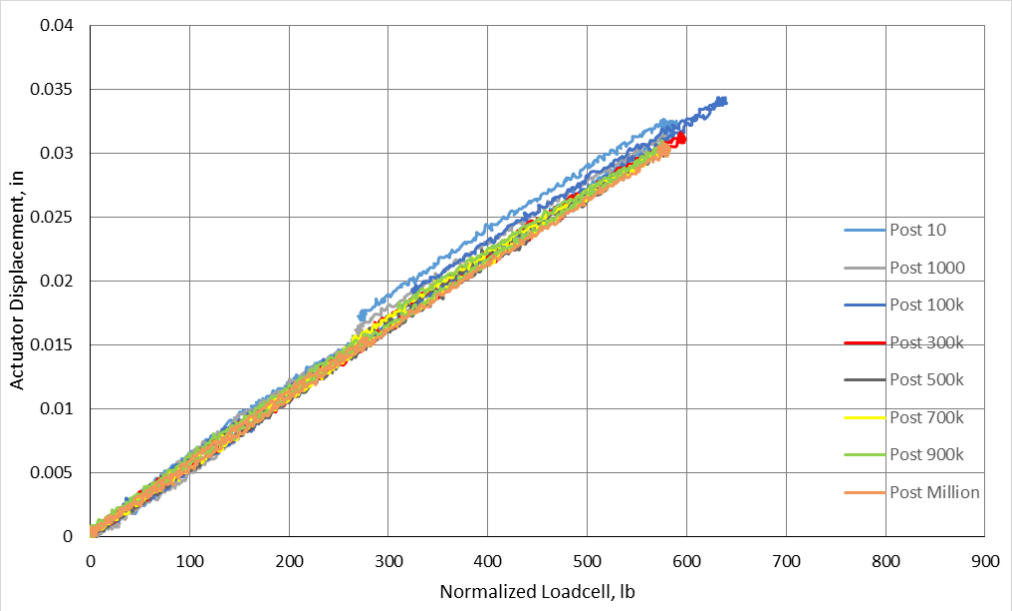

Figure 142: Normalized interior southeast load cell following cyclic regimens for specimen 4

Final Static Test:

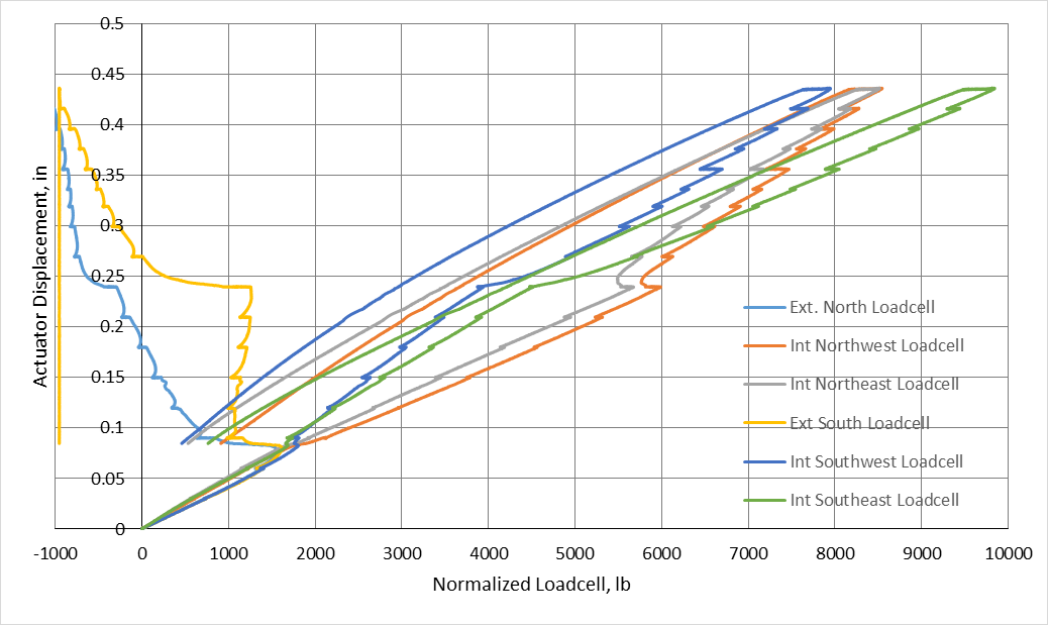

Figure 143: Normalized load cell data for the final static test of specimen 4

Specimen 5: Ductal UHPC Connection with Concrete Topping

First Static Test:

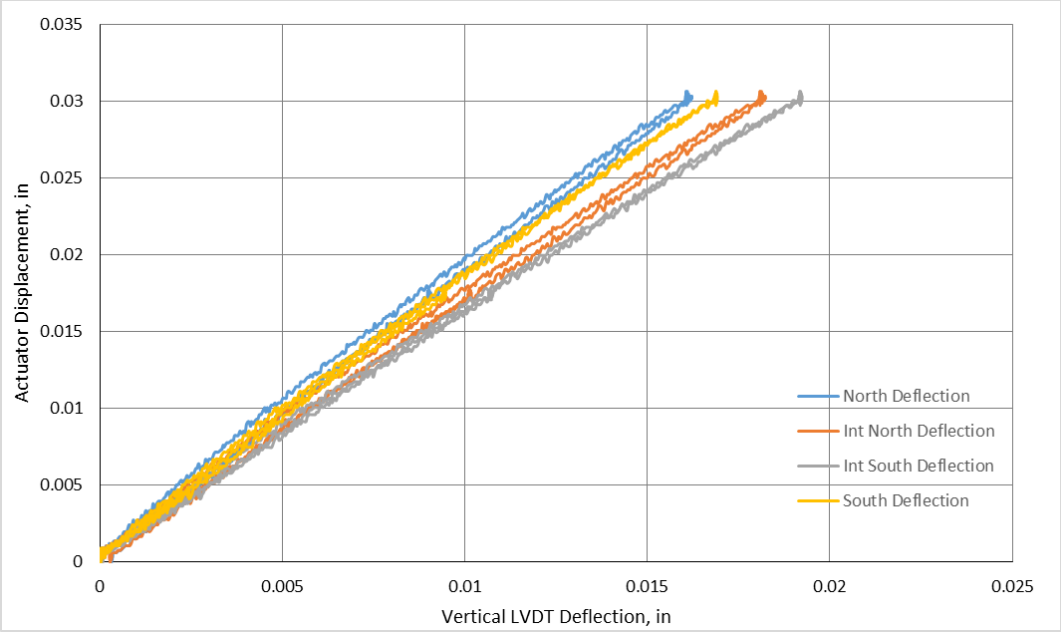

Figure 144: Vertical LVDT deflection during initial static test of specimen 5

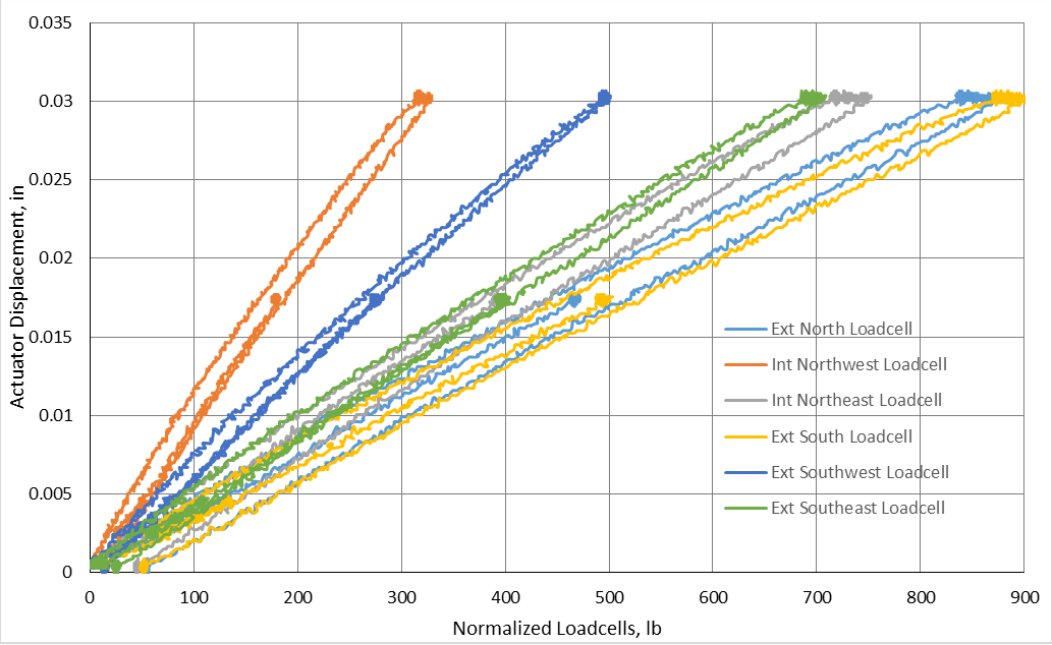

Figure 145: Normalized load cell values during initial static test of specimen 5.

Static Tests following each Cyclic Test:

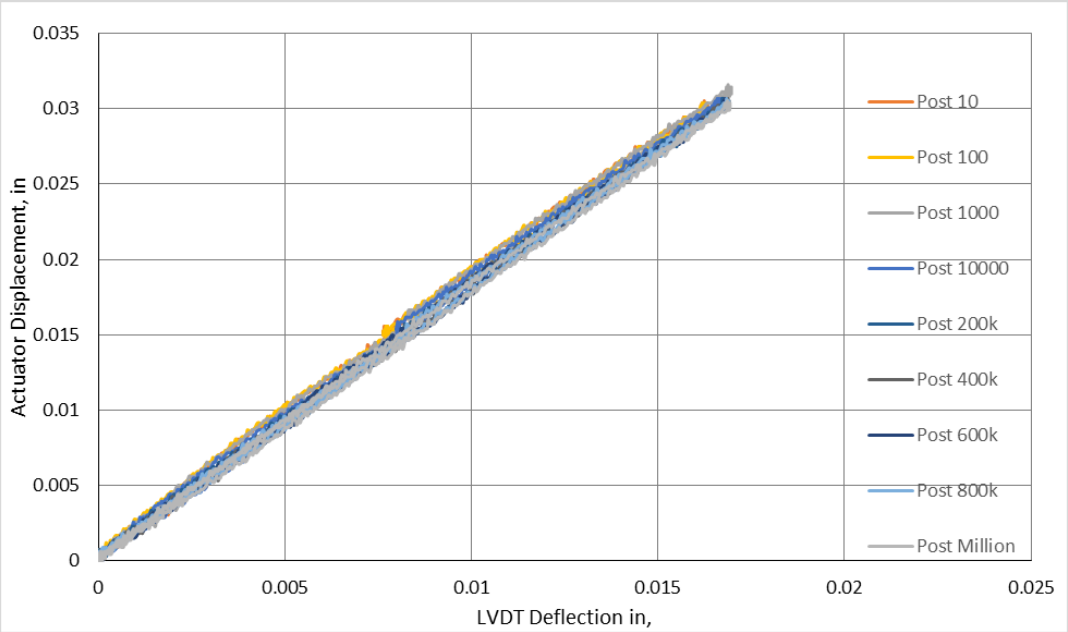

Figure 146: Exterior North vertical LVDT deflection for each cyclic test for specimen 5

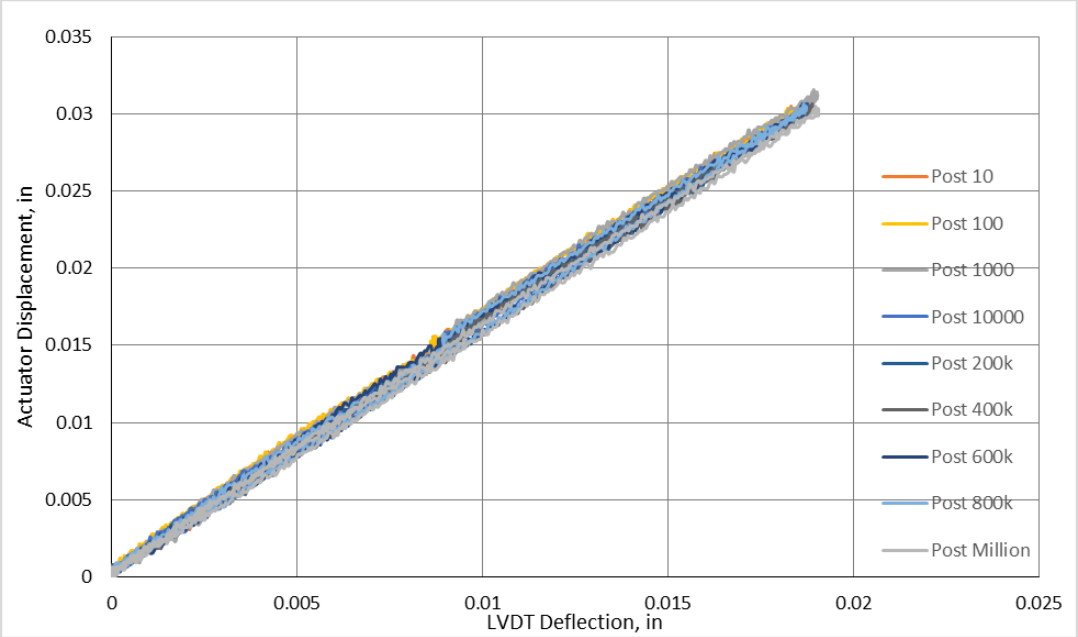

Figure 147: Interior North vertical LVDT deflection for each cyclic test for specimen 5

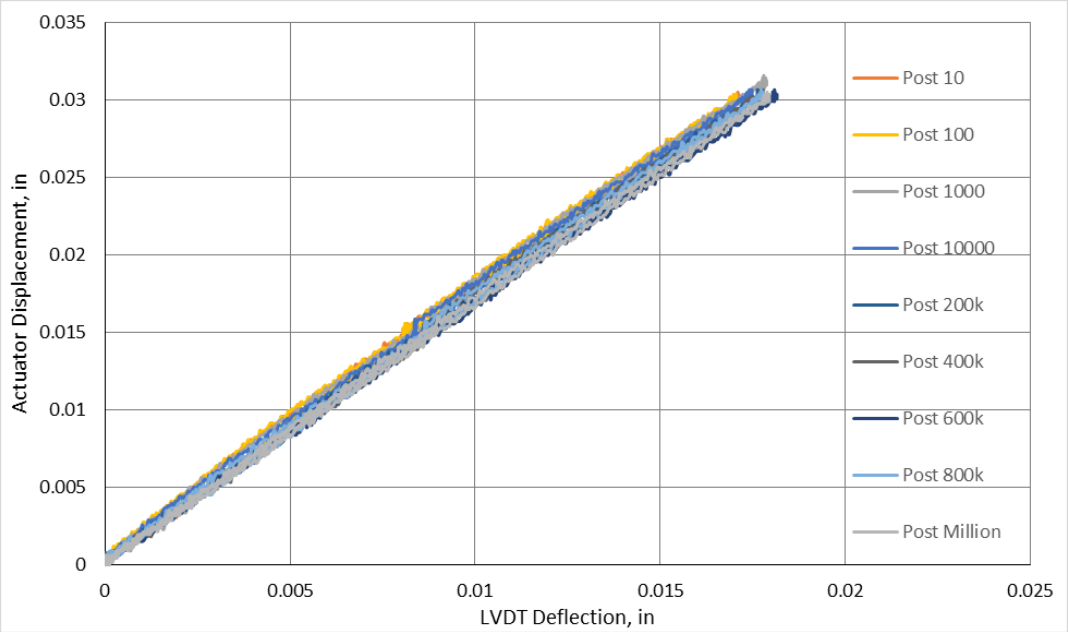

Figure 148: Exterior South vertical LVDT deflection for each cyclic test for specimen 5

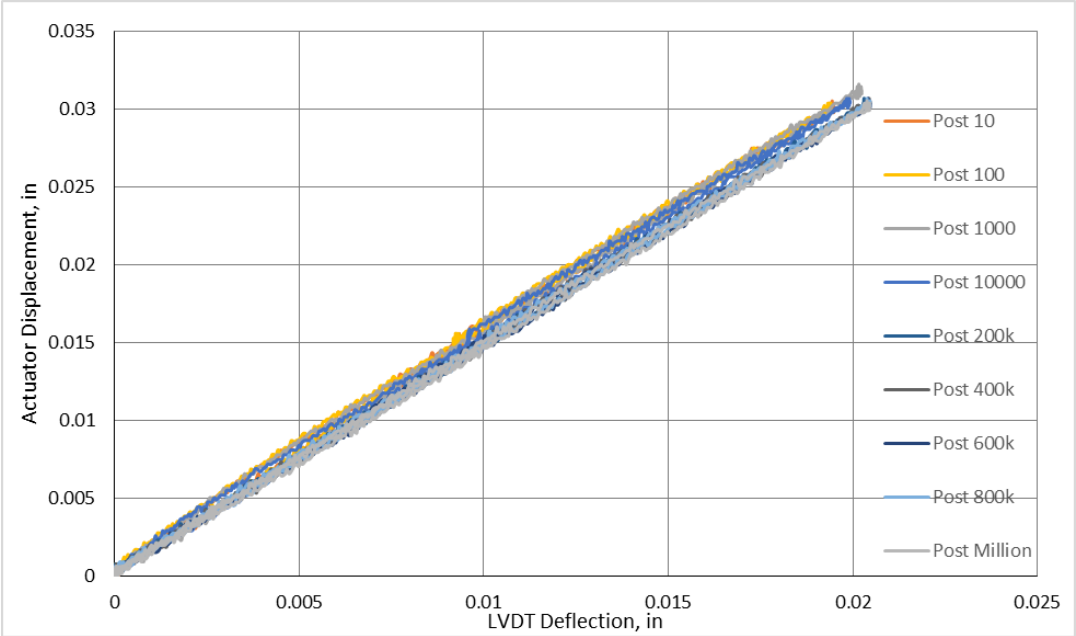

Figure 149: Interior South vertical LVDT deflection for each cyclic test for specimen 5

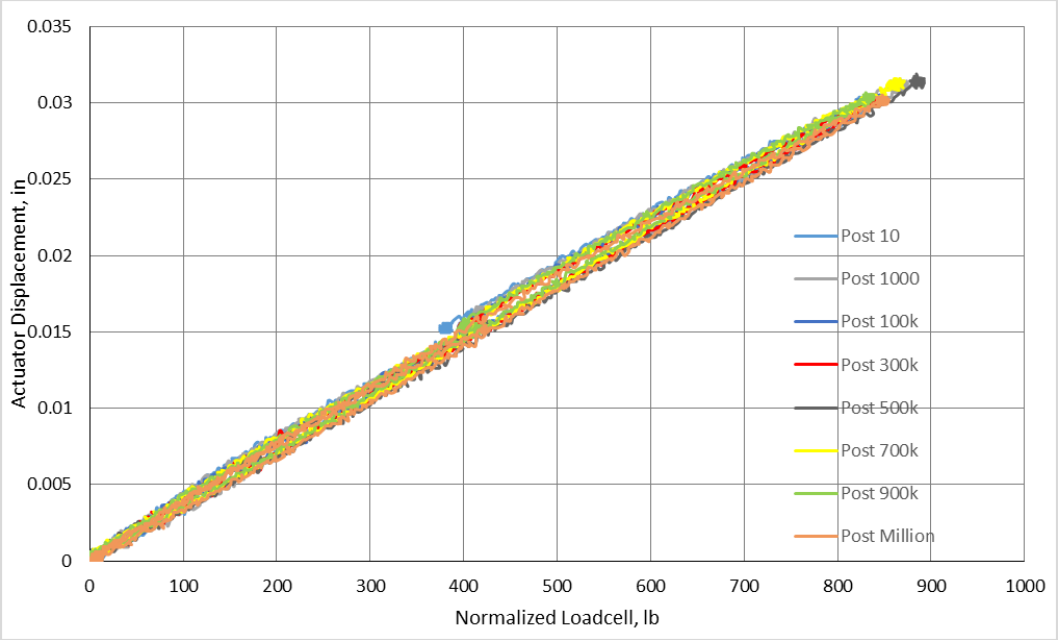

Figure 150: Normalized exterior north load cell following cyclic regimens for specimen 5

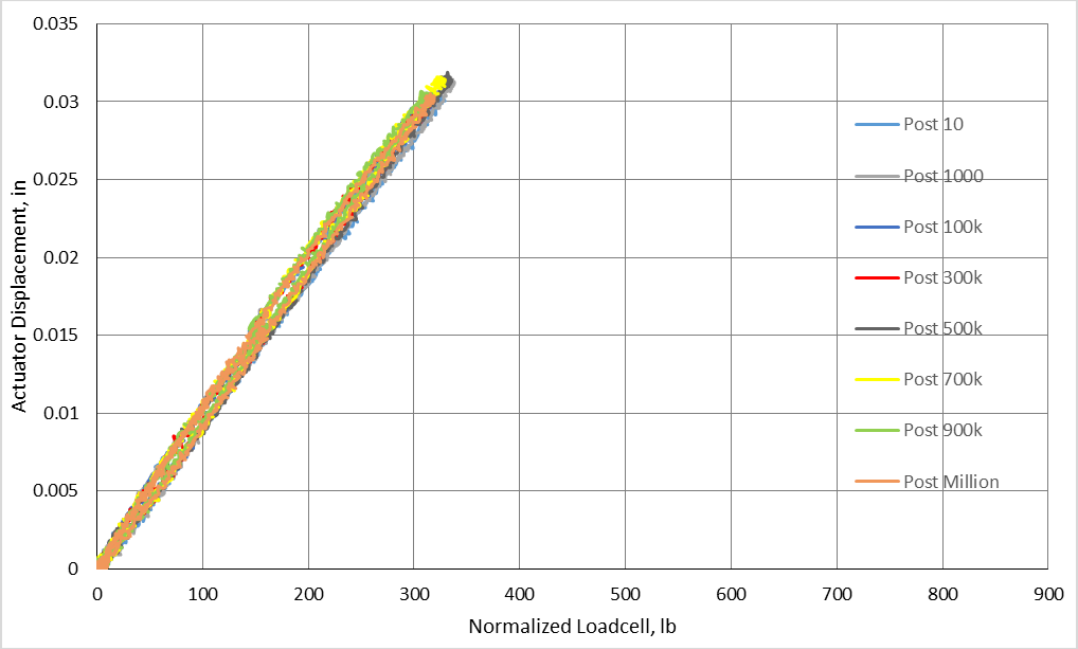

Figure 151: Normalized interior northwest load cell following cyclic regimen for specimen 5

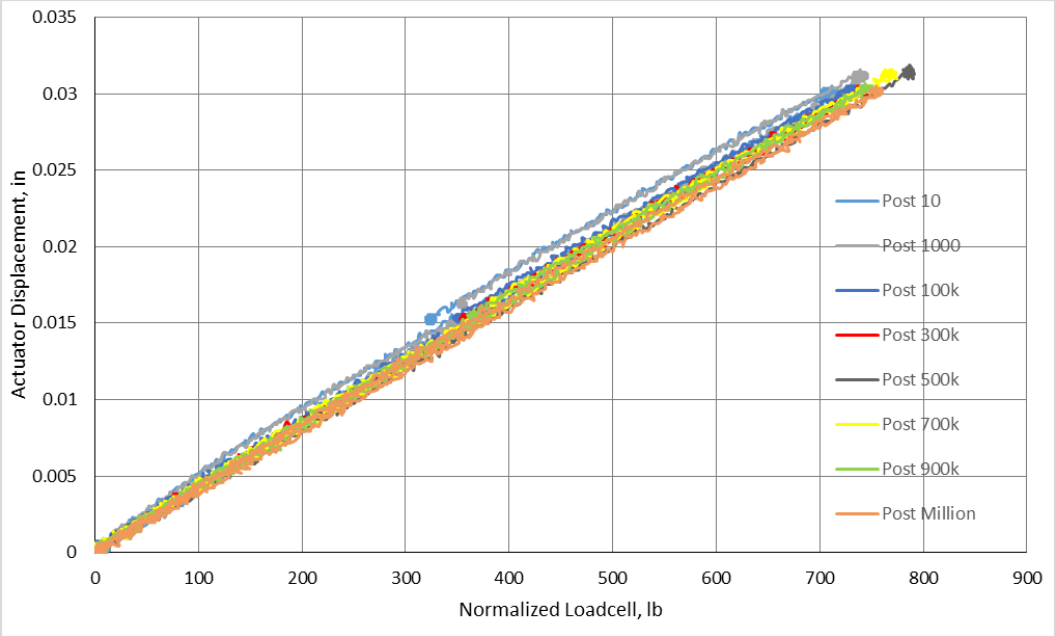

Figure 152: Normalized interior northeast load cell following cyclic regimens for specimen 5

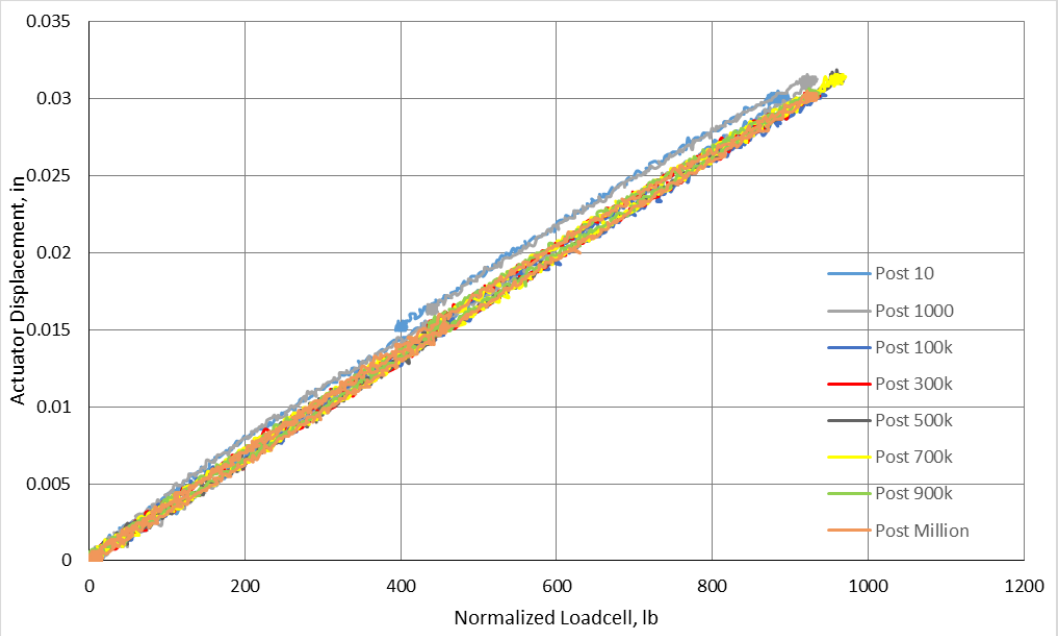

Figure 153: Normalized exterior south load cell following cyclic regimens for specimen 5

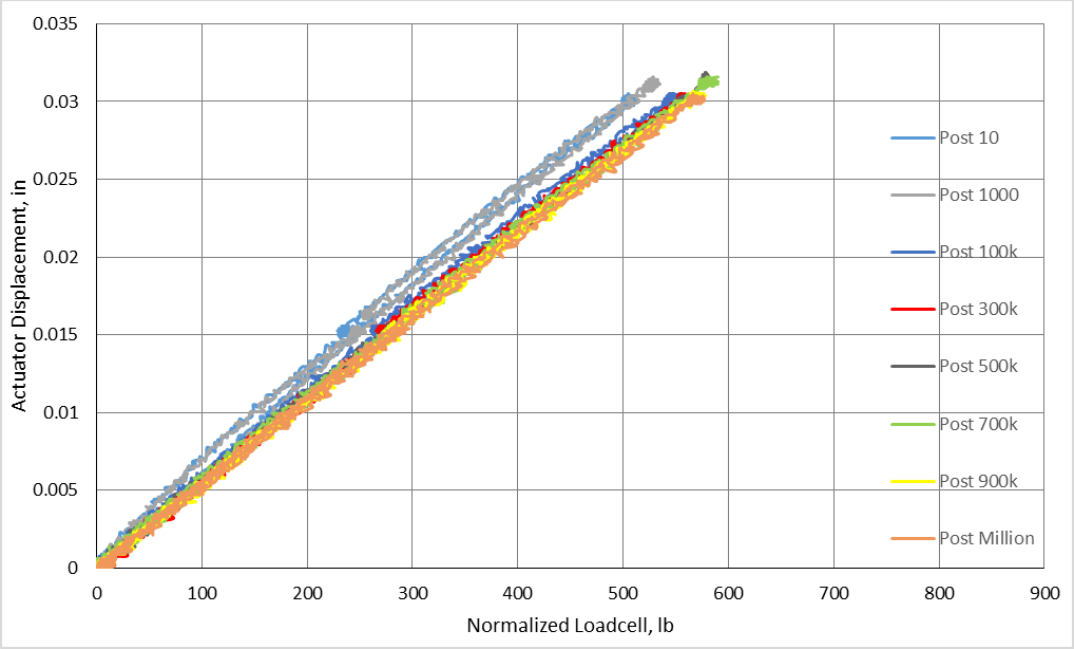

Figure 154: Normalized interior southwest load cell following cyclic regimen for specimen 5

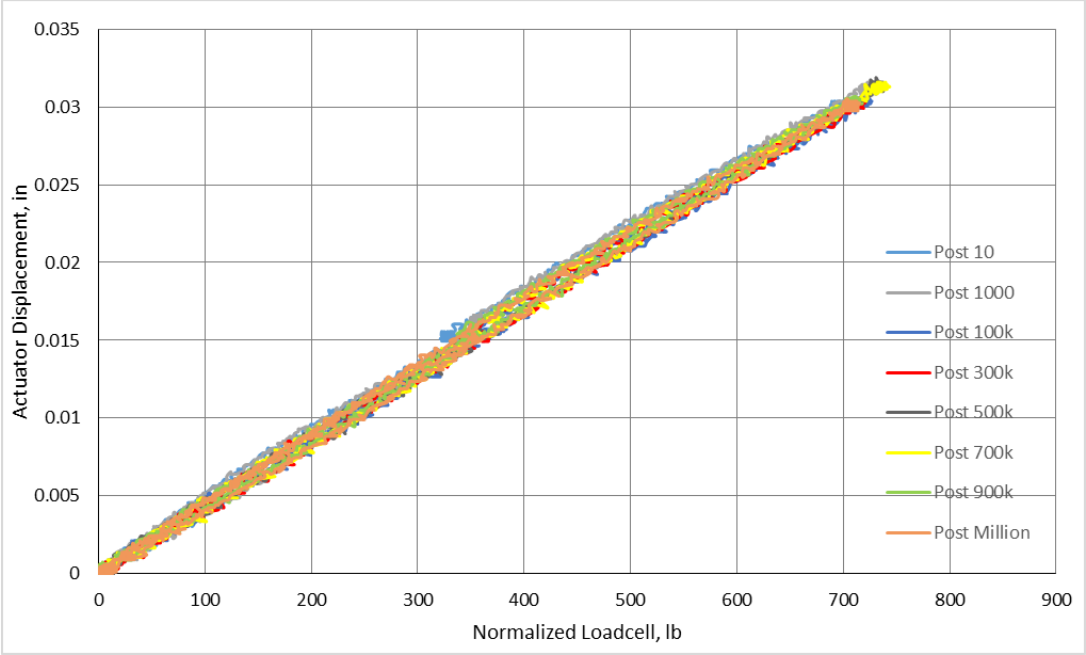

Figure 155: Normalized interior southeast load cell following cyclic regimens for specimen 5

Final Static Test:

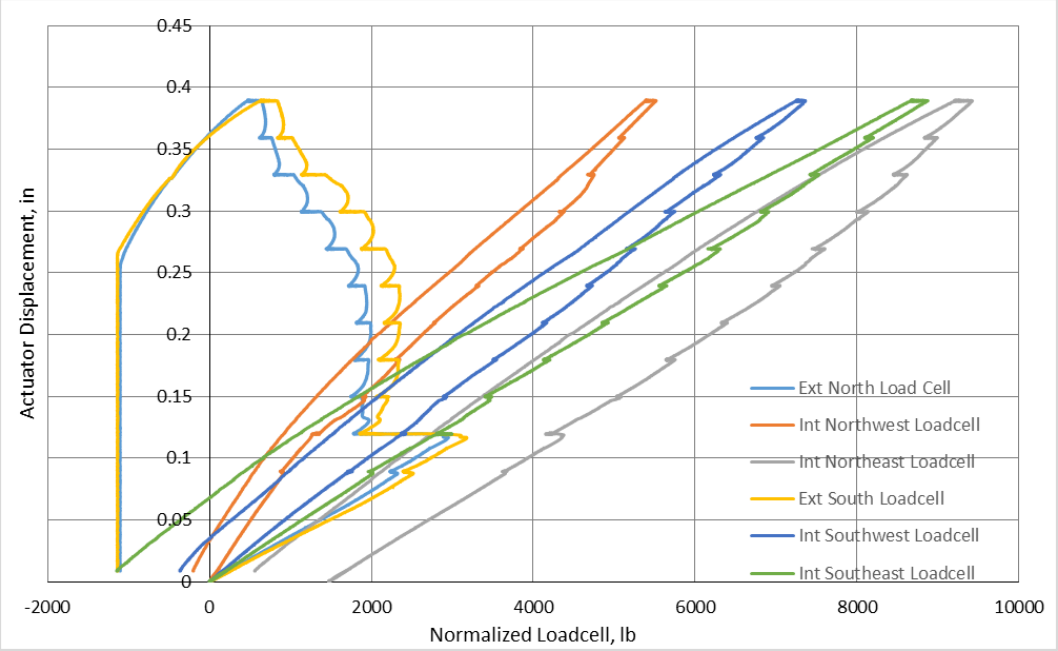

Figure 156: Normalized load cell data for the final static test of specimen 5

Specimen 6: VHPC Connection with Concrete Topping

First Static Test:

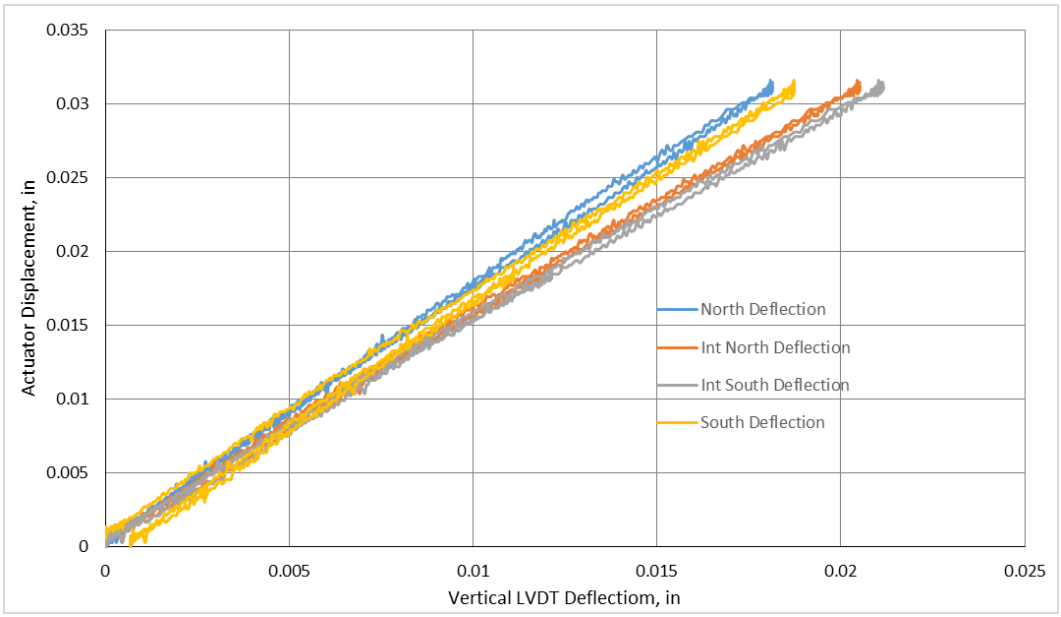

Figure 157: Vertical LVDT deflection during initial static test of specimen 5

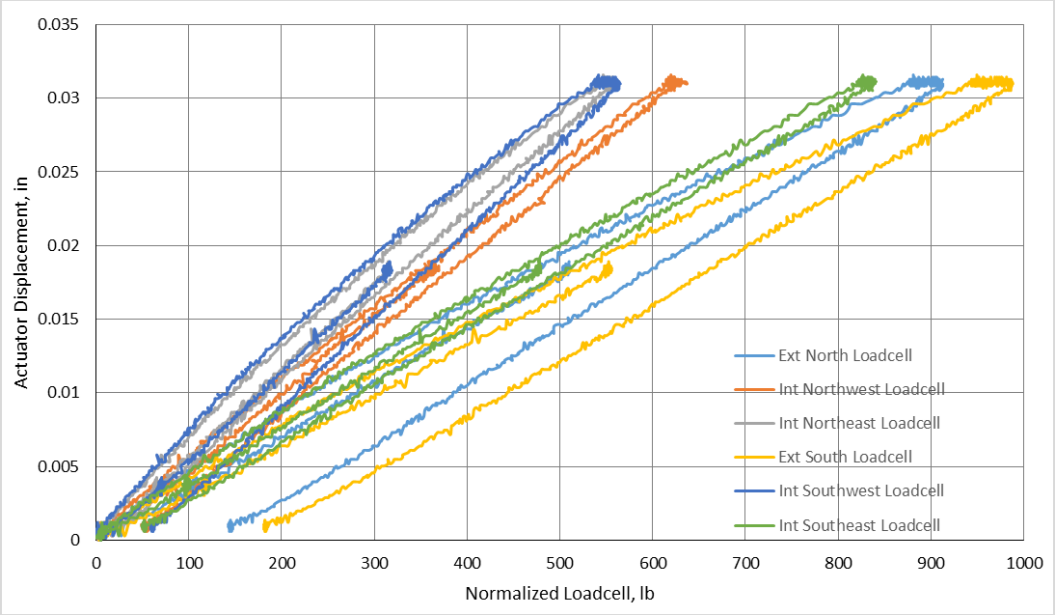

Figure 158: Normalized load cell values during initial static test of specimen 5.

Static Tests following each Cyclic Test:

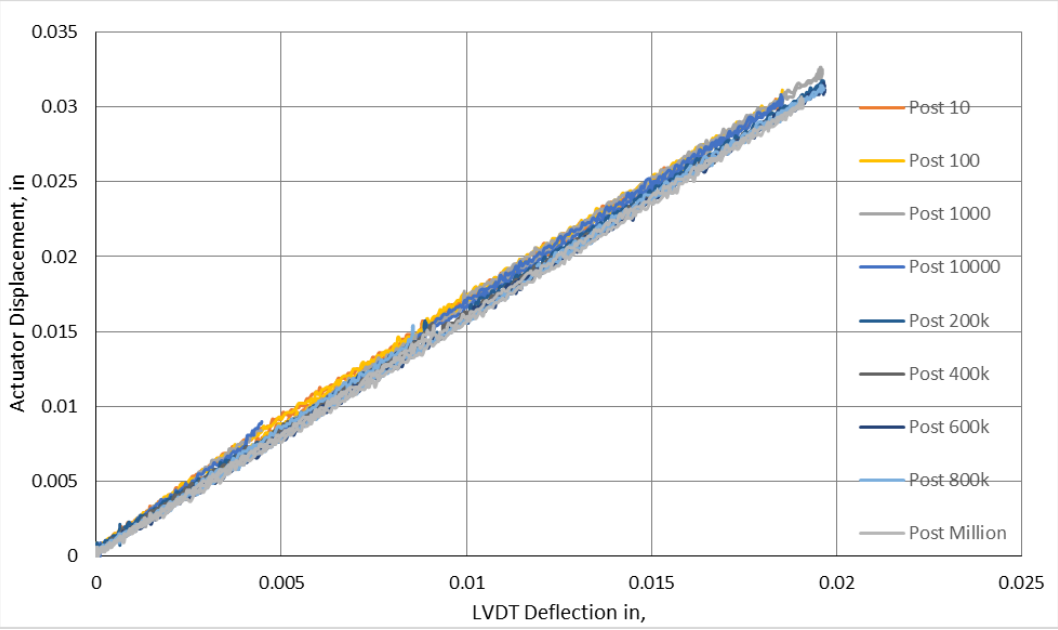

Figure 159: Exterior North vertical LVDT deflection for each cyclic test for specimen 6

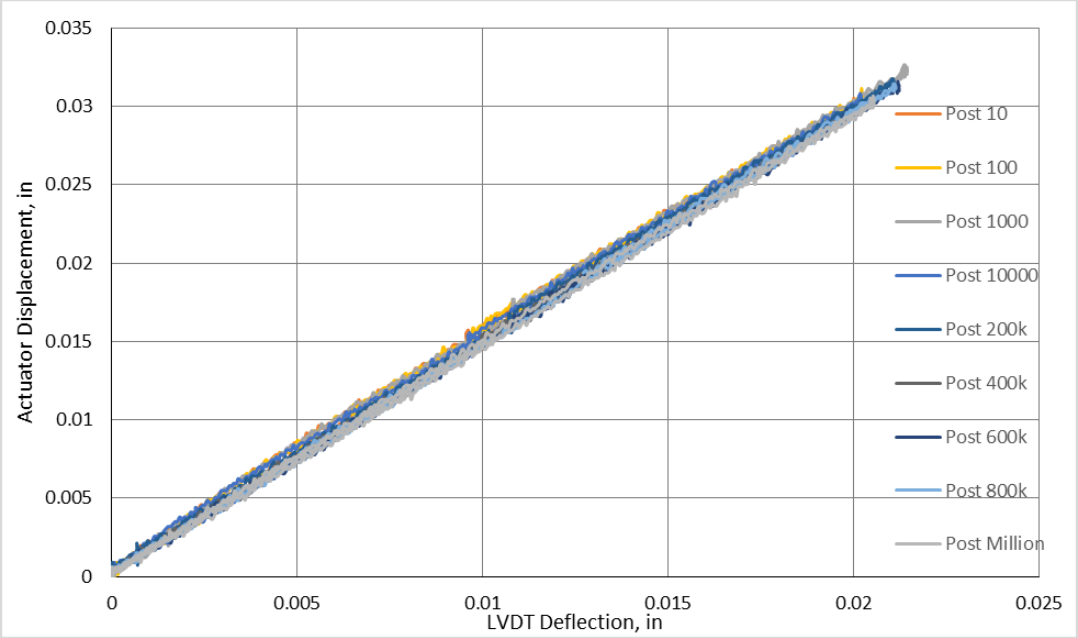

Figure 160: Interior North vertical LVDT deflection for each cyclic test for specimen 6

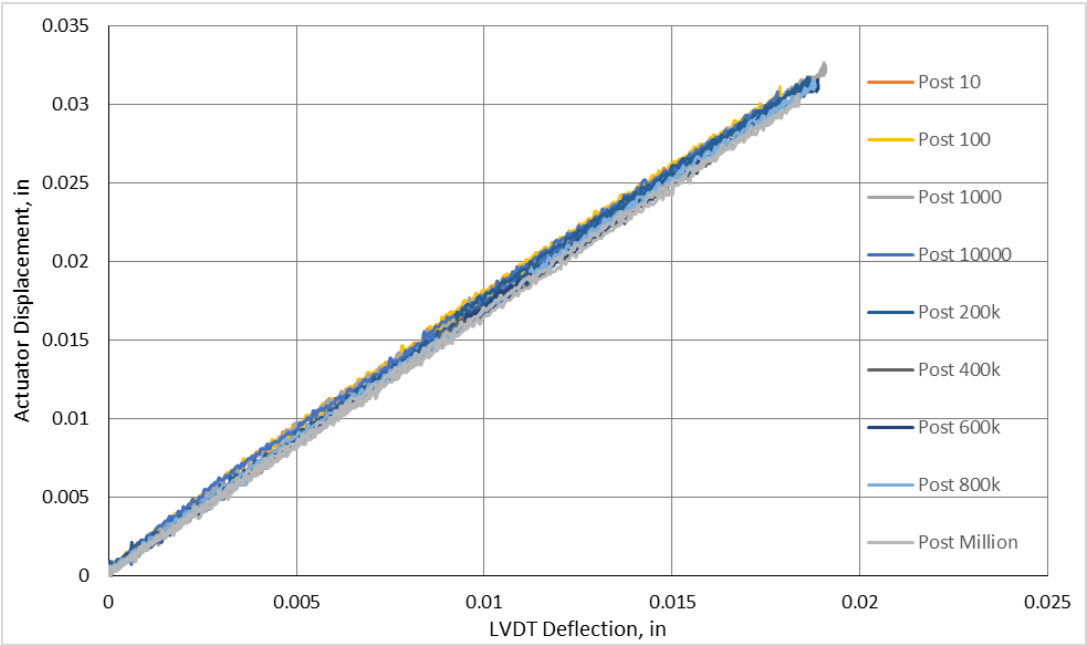

Figure 161: Exterior South vertical LVDT deflection for each cyclic test for specimen 6

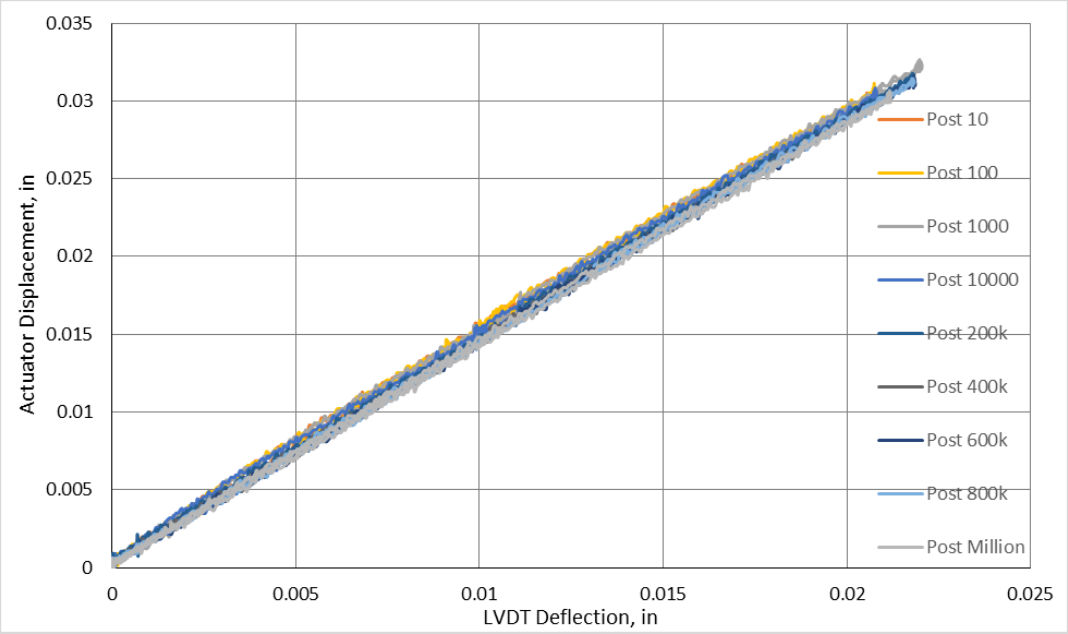

Figure 162: Interior South vertical LVDT deflection for each cyclic test for specimen 6

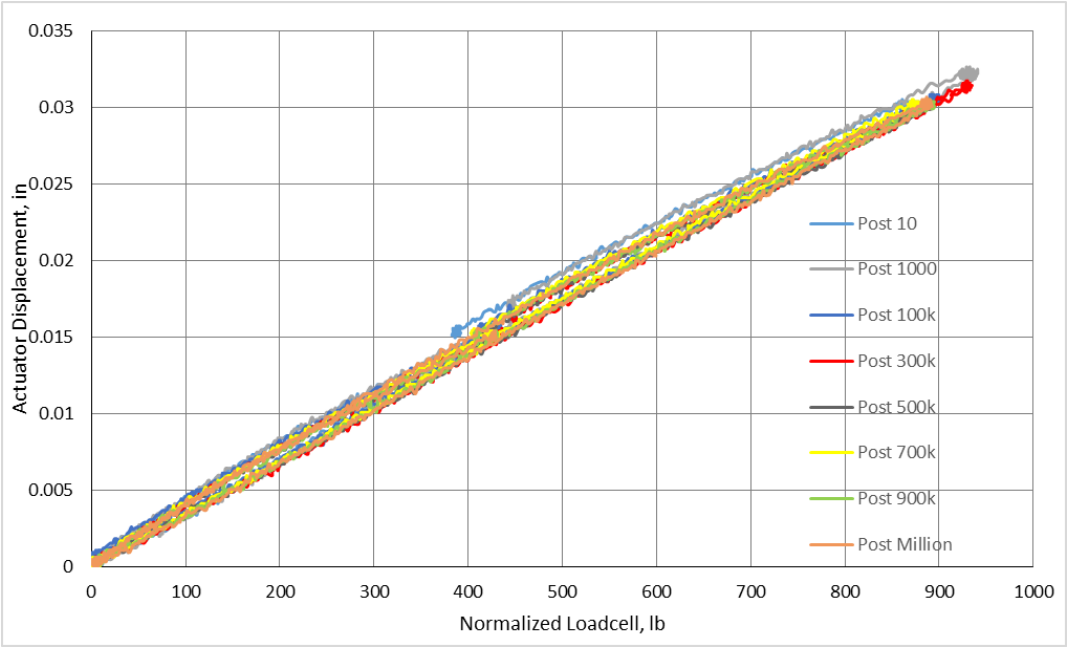

Figure 163: Normalized exterior north load cell following cyclic regimens for specimen 6

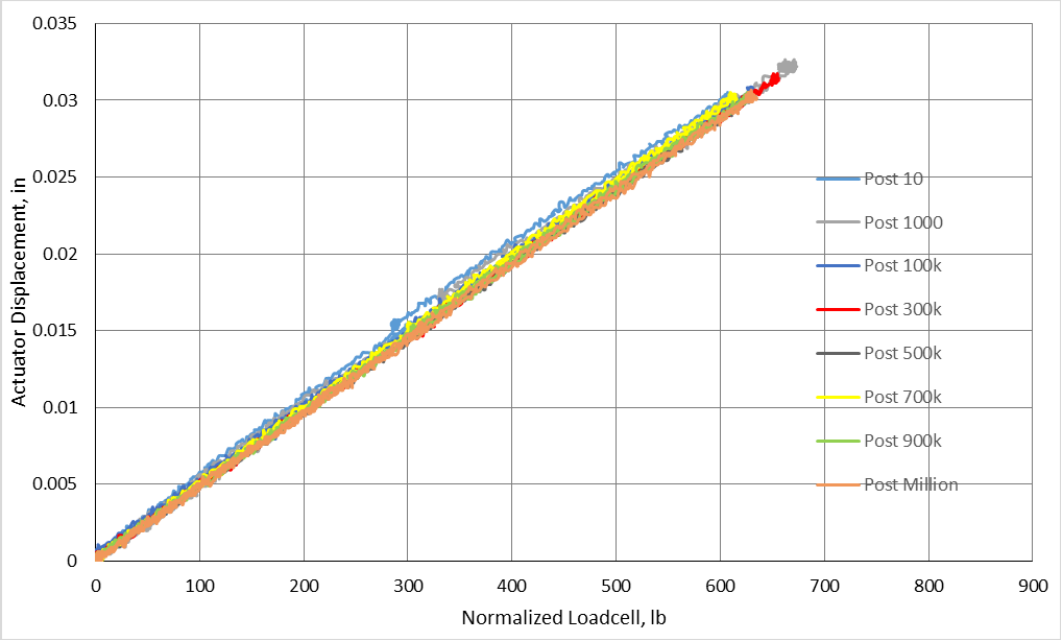

Figure 164: Normalized interior northwest load cell following cyclic regimen for specimen 6

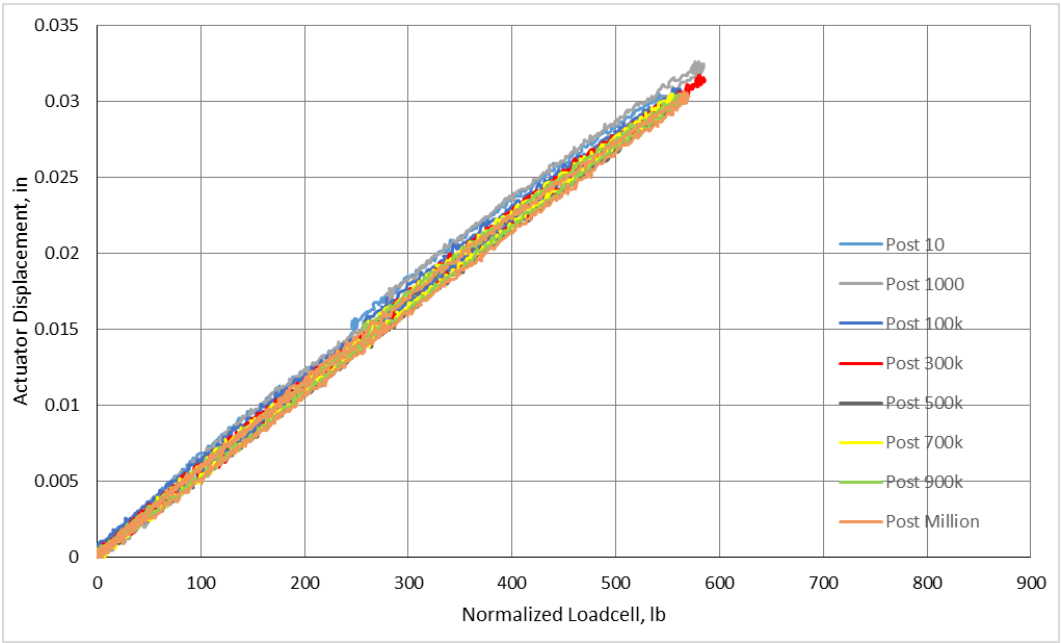

Figure 165: Normalized interior northeast load cell following cyclic regimens for specimen 6

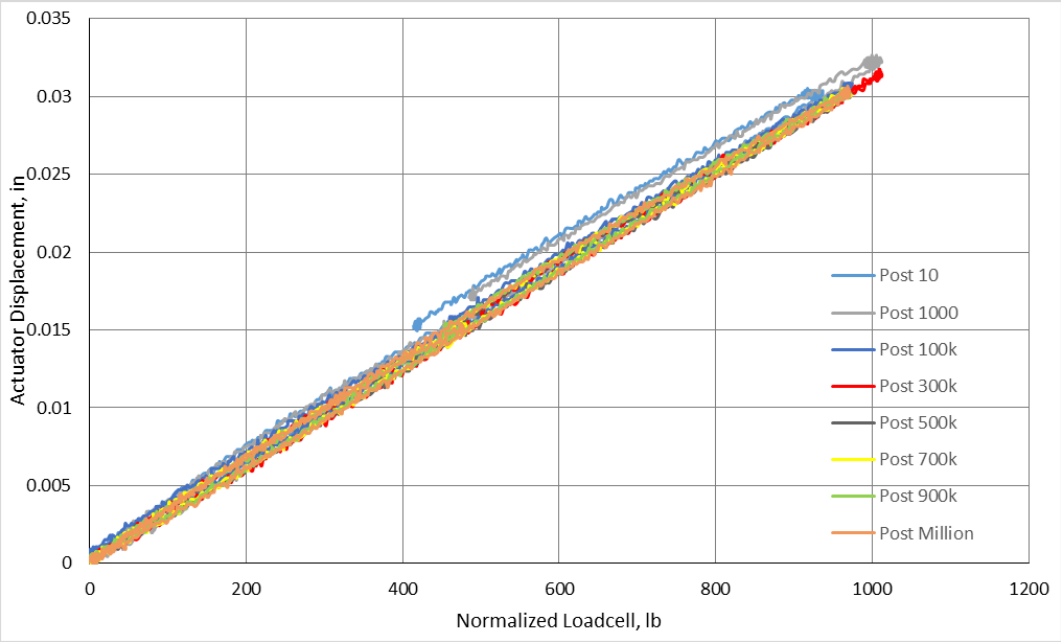

Figure 166: Normalized exterior south load cell following cyclic regimens for specimen 6

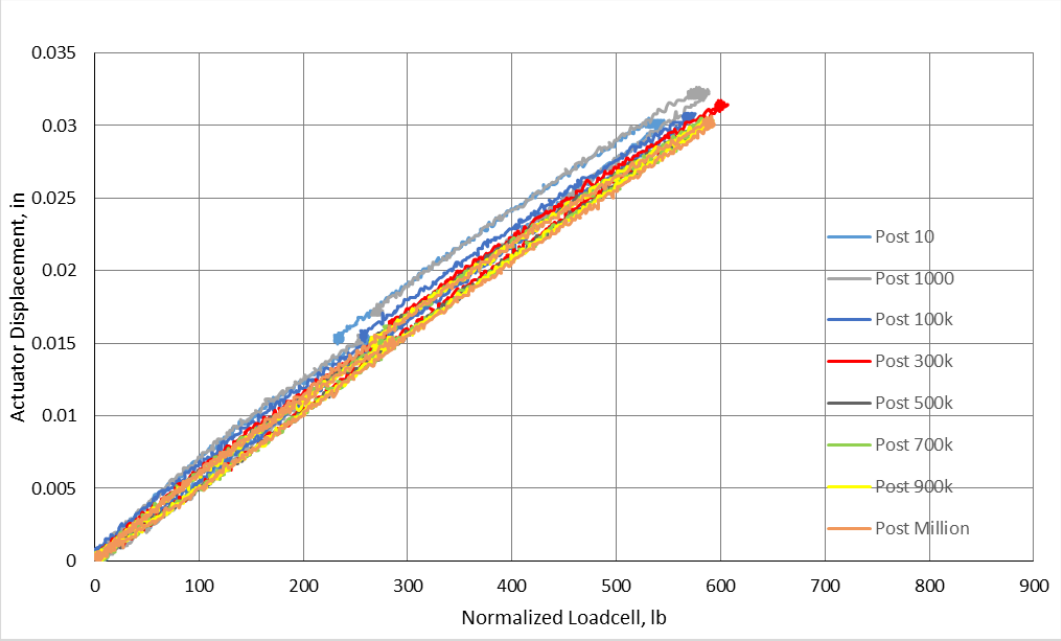

Figure 167: Normalized interior southwest load cell following cyclic regimen for specimen 6

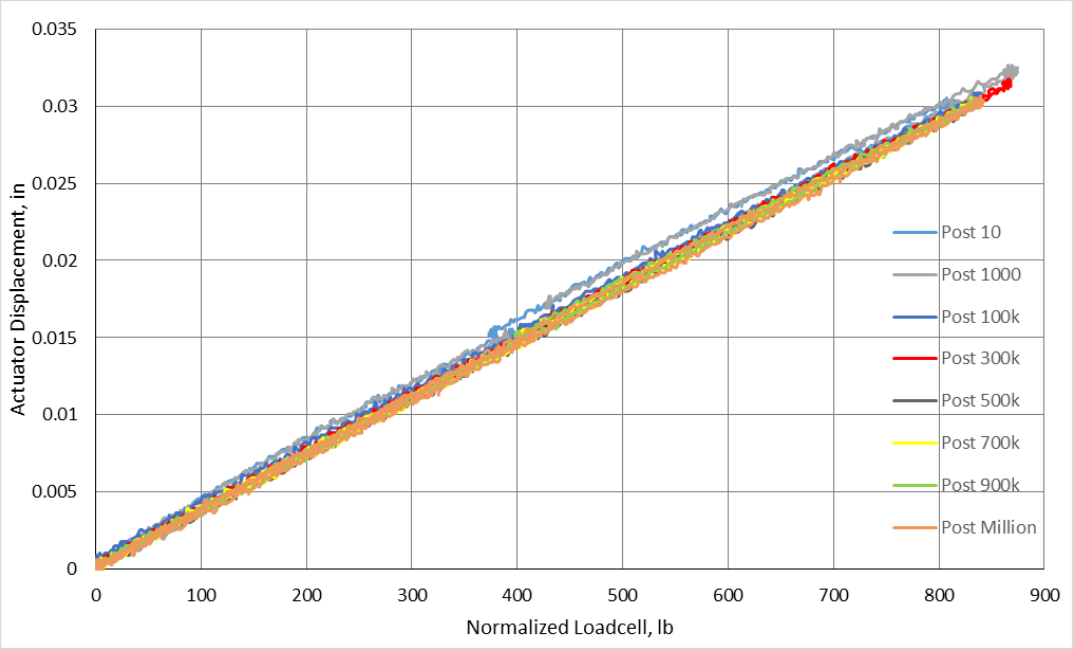

Figure 168: Normalized interior southeast load cell following cyclic regimens for specimen 6

Final Static Test:

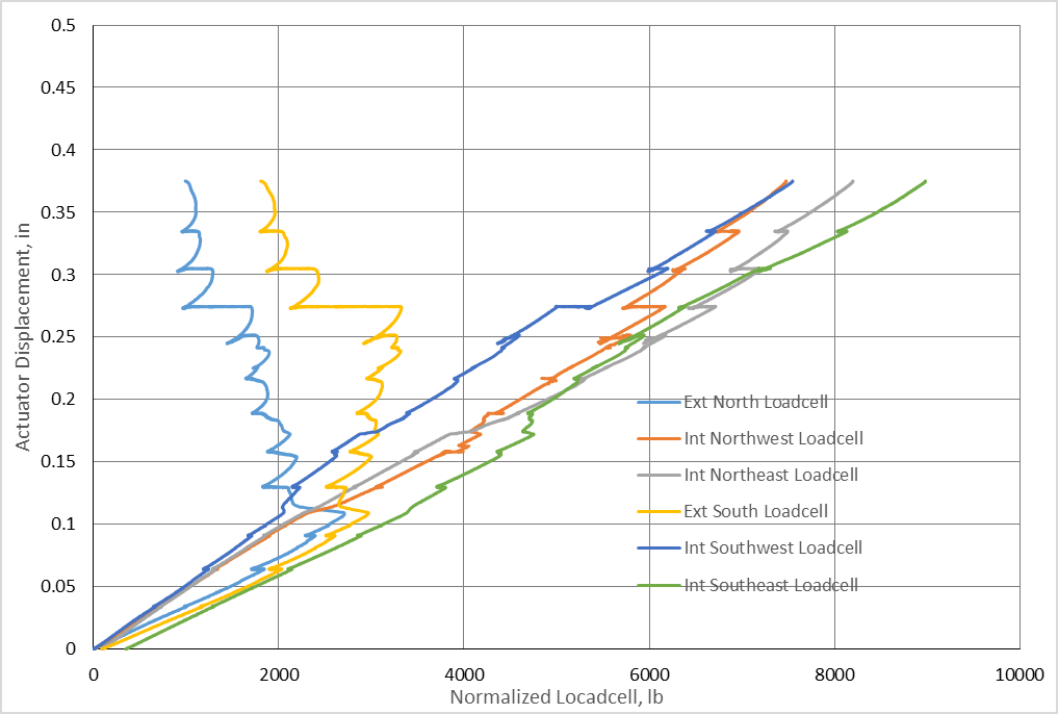

Figure 169: Normalized load cell data for the final static test of specimen 6

Appendix D: Material Testing Data

Specimen 1: Current VDOT Grouted Partial Depth Shear Key

Material Testing was only performed on the first day of testing since the specimen failed on the first day

Table 28: Pull off data for specimen 1

Batch 1				
	Age (days)	Force (lb)	Bond Strength (psi)	Average Bond Strength (psi)
Puck 1	7	170	54.11	49.34
Puck 2	7	140	44.56	
Batch 2				
	Age (days)	Force (lb)	Bond Strength (psi)	Average Bond Strength (psi)
Puck 1	7	60	19.10	22.28
Puck 2	7	80	25.46	

Table 29: Grout strength data for specimen 1

Cube	Age (Days)	Force (kips)	Time (sec)	Strength (ksi)	Average Strength (ksi)
1	7	32	59	8.00	7.71
2	7	30.5	56	7.63	
3	7	30	54	7.50	

Table 30: Grout Shrinkage Data for specimen 1

Age (days)	Bar 1	Bar 1 Avg.	Bar 1 Diff.	Bar 1 Strain	Bar 2	Bar 2 Avg.	Bar 2 Diff.	Bar 2 Strain
4	0.1932	0.1930	N/A	N/A	0.3239	0.3239	N/A	N/A
	0.1929				0.3239			
	0.1929				0.3238			
5	0.1869	0.1869	0.0061	0.0005	0.3180	0.3180	0.0059	0.00052444
	0.1869				0.3180			
	0.1870				0.3179			
6	0.1840	0.1839	0.0091	0.0008	0.3147	0.3146	0.0092	0.00082222
	0.1838				0.3145			
	0.1839				0.3145			
7	0.1813	0.1813	0.0117	0.001037	0.3124	0.3124	0.0115	0.00101778
	0.1814				0.3122			
	0.1813				0.3124			

Table 31: Grout modulus of elasticity data for specimen 1

Cylinder 1						
Load (kip)	Stress (ksi)	Run 1	Run 2	Run 3	Average	Strain
0	0	0	0	0	0	0
2.5	0.20	85	80	65	76.67	6.97E-05
5	0.40	175	170	165	170.00	0.000155
7.5	0.60	260	265	255	260.00	0.000236
10	0.80	355	320	340	338.33	0.000308
12.5	0.99	455	405	435	431.67	0.000392
15	1.19	540	485	525	516.67	0.00047
17.5	1.39	625	580	630	611.67	0.000556
20	1.59	700	665	710	691.67	0.000629
22.5	1.79	805	765	740	770.00	0.0007
25	1.99	895	845	820	853.33	0.000776
27.5	2.19	985	935	910	943.33	0.000858
30	2.39	1070	1020	985	1025.00	0.000932
32.5	2.59	1185	1110	1070	1121.67	0.00102
35	2.79	1295	1200	1170	1221.67	0.001111
Cylinder 2						
Load (kip)	Stress (ksi)	Run 1	Run 2	Run 3	Average	Strain
0	0	0	0	0	0	0
2.5	0.20	55	50	50	51.67	4.7E-05
5	0.40	130	130	125	128.33	0.000117
7.5	0.60	205	200	200	201.67	0.000183
10	0.80	280	280	290	283.33	0.000258
12.5	0.99	360	360	365	361.67	0.000329
15	1.19	445	445	470	453.33	0.000412
17.5	1.39	530	540	560	543.33	0.000494
20	1.59	620	650	650	640.00	0.000582
22.5	1.79	770	755	740	755.00	0.000686
25	1.99	815	835	815	821.67	0.000747
27.5	2.19	920	925	905	916.67	0.000833
30	2.39	1020	1005	980	1001.67	0.000911
32.5	2.59	1135	1095	1055	1095.00	0.000995
35	2.79	1245	1200	1145	1196.67	0.001088
Cylinder 3						
Load (kip)	Stress (ksi)	Run 1	Run 2	Run 3	Average	Strain
0	0	0	0	0	0	0
2.5	0.20	60	65	65	63.33	5.76E-05

5	0.40	135	145	140	140.00	0.000127
7.5	0.60	200	225	235	220.00	0.0002
10	0.80	255	300	300	285.00	0.000259
12.5	0.99	325	405	405	378.33	0.000344
15	1.19	400	485	495	460.00	0.000418
17.5	1.39	470	570	590	543.33	0.000494
20	1.59	555	660	675	630.00	0.000573
22.5	1.79	640	710	755	701.67	0.000638
25	1.99	750	790	865	801.67	0.000729
27.5	2.19	850	880	930	886.67	0.000806
30	2.39	945	960	1000	968.33	0.00088
32.5	2.59	1040	1050	1070	1053.33	0.000958
35	2.79	1150	1155	1160	1155.00	0.00105
	Modulus of Elasticity		Cyl 1	Cyl 2	Cyl 3	Average
			2539.8	2651.1	2733	2641.3

Table 32: Voided Slab Concrete strength data for specimen 1

	Cylinder	Force (kips)	Time (sec)	Strength (ksi)	Average Batch Strength (ksi)
Batch 1	1	83.5	137	6.64	7.00
Batch 1	2	92.5	155	7.36	
Batch 2	1	84.5	144	6.72	6.59
Bacth 2	2	81	125	6.45	

Table 33: Voided Slab Concrete batch 1 modulus of elasticity data for specimen 1

Batch 1-Cylinder 1						
Load (kip)	Stress (ksi)	Run 1	Run 2	Run 3	Average	Strain
0	0	0	0	0	0	0
1	0.08	10	10	10	10	9.09E-06
2	0.16	25	30	25	26.66667	2.42E-05
3	0.24	50	50	50	50	4.55E-05
4	0.32	70	65	70	68.33333	6.21E-05
5	0.40	80	75	80	78.33333	7.12E-05
6	0.48	90	90	90	90	8.18E-05
7	0.56	110	115	105	110	0.0001
8	0.64	135	135	130	133.3333	0.000121
9	0.72	155	145	150	150	0.000136
10	0.80	165	155	160	160	0.000145
11	0.88	180	170	175	175	0.000159
12	0.95	200	200	190	196.6667	0.000179
13	1.03	225	215	215	218.3333	0.000198

14	1.11	240	225	230	231.6667	0.000211
15	1.19	250	240	240	243.3333	0.000221
16	1.27	270	260	255	261.6667	0.000238
17	1.35	295	285	275	285	0.000259
18	1.43	315	300	300	305	0.000277
Batch 1-Cylinder 2						
Load (kip)	Stress (ksi)	Run 1	Run 2	Run 3	Average	Strain
0	0	0	0	0	0	0
1	0.08	5	10	10	8.33	7.58E-06
2	0.16	10	25	30	21.67	1.97E-05
3	0.24	25	45	45	38.33	3.48E-05
4	0.32	40	60	65	55.00	0.00005
5	0.40	60	70	75	68.33	6.21E-05
6	0.48	75	80	85	80.00	7.27E-05
7	0.56	85	95	100	93.33	8.48E-05
8	0.64	95	115	120	110.00	0.0001
9	0.72	110	135	135	126.67	0.000115
10	0.80	125	145	145	138.33	0.000126
11	0.88	150	155	155	153.33	0.000139
12	0.95	160	165	160	161.67	0.000147
13	1.03	170	175	175	173.33	0.000158
14	1.11	180	195	195	190.00	0.000173
15	1.19	200	215	210	208.33	0.000189
16	1.27	220	225	220	221.67	0.000202
17	1.35	235	235	225	231.67	0.000211
18	1.43	245	245	240	243.33	0.000221
		Modulus of Elasticity		Cyl 1	Cyl 2	Average
				5309.80	6320.30	5815.05

Table 34: Voided Slab Concrete batch 2 modulus of elasticity data for specimen 1

Batch 2-Cylinder 1						
Load (kip)	Stress (ksi)	Run 1	Run 2	Run 3	Average	Strain
0	0	0	0	0	0	0
1	0.08	5	10	10	8.33	7.58E-06
2	0.16	20	25	25	23.33	2.12E-05
3	0.24	40	45	50	45.00	4.09E-05
4	0.32	65	65	65	65.00	5.91E-05
5	0.40	70	75	75	73.33	6.67E-05
6	0.48	85	85	85	85.00	7.73E-05
7	0.56	95	95	100	96.67	8.79E-05

8	0.64	115	110	115	113.33	0.000103
9	0.72	140	135	140	138.33	0.000126
10	0.80	150	145	150	148.33	0.000135
11	0.88	160	155	155	156.67	0.000142
12	0.95	170	165	165	166.67	0.000152
13	1.03	185	185	180	183.33	0.000167
14	1.11	210	205	200	205.00	0.000186
15	1.19	230	225	225	226.67	0.000206
16	1.27	240	235	240	238.33	0.000217
17	1.35	250	250	245	248.33	0.000226
18	1.43	270	265	265	266.67	0.000242
Batch 2-Cylinder 2						
Load (kip)	Stress (ksi)	Run 1	Run 2	Run 3	Average	Strain
0	0	0	0	0	0	0
1	0.08	15	10	10	11.67	1.06E-05
2	0.16	35	30	30	31.67	2.88E-05
3	0.24	55	50	50	51.67	4.7E-05
4	0.32	70	60	60	63.33	5.76E-05
5	0.40	80	70	70	73.33	6.67E-05
6	0.48	95	85	85	88.33	8.03E-05
7	0.56	120	105	110	111.67	0.000102
8	0.64	140	125	125	130.00	0.000118
9	0.72	150	135	135	140.00	0.000127
10	0.80	160	145	145	150.00	0.000136
11	0.88	175	160	155	163.33	0.000148
12	0.95	200	180	175	185.00	0.000168
13	1.03	215	195	195	201.67	0.000183
14	1.11	230	215	210	218.33	0.000198
15	1.19	240	225	220	228.33	0.000208
16	1.27	255	240	235	243.33	0.000221
17	1.35	275	255	250	260.00	0.000236
18	1.43	300	275	280	285.00	0.000259
		Modulus of Elasticity		Cyl 1	Cyl 2	Average
				5881.80	5661.30	5771.55

Specimen 2: Current VDOT Grouted Partial Depth Shear Key with Kevlar Reinforcement

Table 35: Pull off data for specimen 2

Batch 1				
	Age (days)	Force (lb)	Bond Strength (psi)	Average Bond Strength (psi)
Puck 1	7	30	9.55	12.73
Puck 2	7	50	15.92	
Puck 3	15	60	19.10	15.92
Puck 4	15	40	12.73	
Batch 3				
	Age (days)	Force (lb)	Bond Strength (psi)	Average Bond Strength (psi)
Puck 1	7	80	25.46	19.10
Puck 2	7	40	12.73	
Puck 3	15	50	15.92	17.51
Puck 4	15	60	19.10	

Table 36: Grout strength data for specimen 2

Cube	Age (Days)	Force (kips)	Time (sec)	Strength (ksi)	Average Strength (ksi)
1	7	39	64	9.75	9.46
2	7	37	61	9.25	
3	7	37.5	66	9.375	
4	15	40.5	76	10.125	9.96
5	15	39.5	77	9.875	
6	15	39.5	72	9.875	

Table 37: Grout shrinkage data for specimen 2

Age (days)	Bar 1	Bar 1 Avg.	Bar 1 Diff.	Bar 1 Strain	Bar 2	Bar 2 Avg.	Bar 2 Diff.	Bar 2 Strain
3	0.3181	0.3179	N/A	N/A	0.2461	0.2460	N/A	N/A
	0.3178				0.2459			
	0.3179				0.2460			
4	0.3150	0.3150	0.0029	0.000261	0.2433	0.2434	0.0026	0.000231
	0.3150				0.2434			
	0.3150				0.2435			
5	0.3125	0.3125	0.0054	0.000483	0.2409	0.2409	0.0051	0.000456
	0.3125				0.2409			
	0.3125				0.2408			

6	0.3098	0.3098	0.0082	0.000726	0.2386	0.2386	0.0074	0.000661
	0.3097				0.2386			
	0.3098				0.2385			
7	0.3084	0.3083	0.0096	0.000853	0.2370	0.2370	0.0090	0.000803
	0.3084				0.2370			
	0.3082				0.2369			
8	0.3071	0.3071	0.0108	0.000960	0.2357	0.2357	0.0103	0.000916
	0.3071				0.2357			
	0.3072				0.2357			
9	0.3055	0.3055	0.0125	0.001108	0.2338	0.2338	0.0122	0.001081
	0.3055				0.2339			
	0.3054				0.2338			
10	0.3042	0.3042	0.0137	0.001218	0.2327	0.2327	0.0133	0.001182
	0.3042				0.2327			
	0.3043				0.2327			
11	0.3034	0.3034	0.0145	0.001289	0.2319	0.2319	0.0141	0.001256
	0.3034				0.2318			
	0.3035				0.2319			
12	0.3031	0.3030	0.0149	0.001324	0.2313	0.2313	0.0147	0.001307
	0.3030				0.2314			
	0.3030				0.2312			
13	0.3027	0.3028	0.0152	0.001348	0.2307	0.2308	0.0152	0.001354
	0.3028				0.2308			
	0.3028				0.2308			

Table 38: Modulus of Elasticity data for the grout on the first day of testing for specimen 2

Cylinder 1						
Load (kip)	Stress (ksi)	Run 1	Run 2	Run 3	Average	Strain
0	0	0	0	0	0	0
2.5	0.20	35	45	40	40.00	0.000036
5	0.40	100	95	100	98.33	0.000089
7.5	0.60	155	150	145	150.00	0.000136
10	0.80	215	215	210	213.33	0.000194
12.5	0.99	285	285	275	281.67	0.000256
15	1.19	350	335	340	341.67	0.000311
17.5	1.39	415	400	410	408.33	0.000371
20	1.59	485	470	465	473.33	0.000430
22.5	1.79	550	540	530	540.00	0.000491
25	1.99	615	610	600	608.33	0.000553
27.5	2.19	680	685	670	678.33	0.000617

30	2.39	725	730	735	730.00	0.000664
32.5	2.59	800	800	800	800.00	0.000727
35	2.79	865	880	870	871.67	0.000792
Cylinder 2						
Load (kip)	Stress (ksi)	Run 1	Run 2	Run 3	Average	Strain
0	0	0	0	0	0	0
2.5	0.20	40	45	50	45.00	0.000041
5	0.40	100	105	110	105.00	0.000095
7.5	0.60	150	150	160	153.33	0.000139
10	0.80	205	210	220	211.67	0.000192
12.5	0.99	275	270	285	276.67	0.000252
15	1.19	340	320	330	330.00	0.000300
17.5	1.39	375	380	390	381.67	0.000347
20	1.59	445	445	455	448.33	0.000408
22.5	1.79	505	510	520	511.67	0.000465
25	1.99	565	555	570	563.33	0.000512
27.5	2.19	625	620	630	625.00	0.000568
30	2.39	690	680	695	688.33	0.000626
32.5	2.59	745	750	765	753.33	0.000685
35	2.79	810	810	815	811.67	0.000738
Cylinder 3						
Load (kip)	Stress (ksi)	Run 1	Run 2	Run 3	Average	Strain
0	0	0	0	0	0	0
2.5	0.20	40	45	50	45.00	0.000041
5	0.40	95	95	100	96.67	0.000088
7.5	0.60	135	150	155	146.67	0.000133
10	0.80	200	200	210	203.33	0.000185
12.5	0.99	250	255	290	265.00	0.000241
15	1.19	305	315	355	325.00	0.000295
17.5	1.39	370	380	410	386.67	0.000352
20	1.59	430	430	470	443.33	0.000403
22.5	1.79	475	485	540	500.00	0.000455
25	1.99	535	550	610	565.00	0.000514
27.5	2.19	605	595	635	611.67	0.000556
30	2.39	655	655	675	661.67	0.000602
32.5	2.59	720	720	730	723.33	0.000658
35	2.79	785	790	790	788.33	0.000717
	Modulus of Elasticity		Cyl 1	Cyl 2	Cyl 3	Average
			3612.1	3846.6	3944.9	3801.2

Table 39: Modulus of Elasticity Data for grout on the last day of testing for specimen 2

Cylinder 4						
Load (kip)	Stress (ksi)	Run 1	Run 2	Run 3	Average	Strain
0	0	0	0	0	0	0
2.5	0.1989437	45	45	40	43.33333	3.94E-05
5	0.3978874	90	100	95	95	8.64E-05
7.5	0.596831	150	150	140	146.6667	0.000133
10	0.7957747	215	215	200	210	0.000191
12.5	0.9947184	265	275	265	268.3333	0.000244
15	1.1936621	320	340	320	326.6667	0.000297
17.5	1.3926058	390	410	370	390	0.000355
20	1.5915494	450	470	440	453.3333	0.000412
22.5	1.7904931	510	535	505	516.6667	0.00047
25	1.9894368	565	600	555	573.3333	0.000521
27.5	2.1883805	630	665	605	633.3333	0.000576
30	2.3873241	695	710	670	691.6667	0.000629
32.5	2.5862678	755	770	715	746.6667	0.000679
35	2.7852115	810	835	790	811.6667	0.000738
Cylinder 5						
Load (kip)	Stress (ksi)	Run 1	Run 2	Run 3	Average	Strain
0	0	0	0	0	0	0
2.5	0.1989437	35	30	30	31.66667	2.88E-05
5	0.3978874	100	90	85	91.66667	8.33E-05
7.5	0.596831	140	135	140	138.3333	0.000126
10	0.7957747	195	185	190	190	0.000173
12.5	0.9947184	245	240	245	243.3333	0.000221
15	1.1936621	310	305	305	306.6667	0.000279
17.5	1.3926058	360	355	355	356.6667	0.000324
20	1.5915494	425	415	415	418.3333	0.00038
22.5	1.7904931	480	470	475	475	0.000432
25	1.9894368	535	525	530	530	0.000482
27.5	2.1883805	595	585	580	586.6667	0.000533
30	2.3873241	660	650	645	651.6667	0.000592
32.5	2.5862678	705	695	705	701.6667	0.000638
35	2.7852115	770	755	755	760	0.000691
Cylinder 6						
Load (kip)	Stress (ksi)	Run 1	Run 2	Run 3	Average	Strain
0	0	0	0	0	0	0
2.5	0.1989437	50	30	35	38.33333	3.48E-05
5	0.3978874	120	90	95	101.6667	9.24E-05
7.5	0.596831	165	160	160	161.6667	0.000147

10	0.7957747	220	220	215	218.3333	0.000198
12.5	0.9947184	285	275	270	276.6667	0.000252
15	1.1936621	335	340	325	333.3333	0.000303
17.5	1.3926058	385	405	390	393.3333	0.000358
20	1.5915494	455	465	440	453.3333	0.000412
22.5	1.7904931	515	515	500	510	0.000464
25	1.9894368	565	570	555	563.3333	0.000512
27.5	2.1883805	630	625	615	623.3333	0.000567
30	2.3873241	695	685	665	681.6667	0.00062
32.5	2.5862678	765	745	730	746.6667	0.000679
35	2.7852115	815	795	790	800	0.000727
	Modulus of Elasticity		Cyl 4	Cyl 5	Cyl 6	Average
			3834	4116.5	3859.9	3936.8

Table 40: Voided slab concrete strength for specimen 2

	Cylinder	Force (kips)	Time (sec)	Strength (ksi)	Average Strength (ksi)
Batch 1	1	90.5	155	7.20	7.10
Batch 1	2	88	161	7.00	
Batch 3	1	120	203	9.55	9.35
Batch 3	2	115	211	9.15	

Table 41: Modulus of elasticity data for batch 1 of voided slab concrete for specimen 2

Batch 1-Cylinder 1						
Load (kip)	Stress (ksi)	Run 1	Run 2	Run 3	Average	Strain
0	0	0	0	0	0	0
1	0.08	5	10	5	6.67	0.000006
2	0.16	25	30	20	25.00	0.000023
3	0.24	40	40	35	38.33	0.000035
4	0.32	50	50	45	48.33	0.000044
5	0.40	65	65	70	66.67	0.000061
6	0.48	75	80	85	80.00	0.000073
7	0.56	95	105	100	100.00	0.000091
8	0.64	115	115	115	115.00	0.000105
9	0.72	130	130	140	133.33	0.000121
10	0.80	140	145	155	146.67	0.000133
11	0.88	155	165	170	163.33	0.000148
12	0.95	175	190	190	185.00	0.000168
13	1.03	200	200	210	203.33	0.000185
14	1.11	210	210	230	216.67	0.000197
15	1.19	220	225	245	230.00	0.000209

16	1.27	235	245	255	245.00	0.000223
17	1.35	260	270	280	270.00	0.000245
18	1.43	280	280	295	285.00	0.000259
Batch 1-Cylinder 2						
Load (kip)	Stress (ksi)	Run 1	Run 2	Run 3	Average	Strain
0	0	0	0	0	0	0
1	0.08	10	5	5	6.67	0.000006
2	0.16	25	15	20	20.00	0.000018
3	0.24	35	25	30	30.00	0.000027
4	0.32	50	40	40	43.33	0.000039
5	0.40	70	55	55	60.00	0.000055
6	0.48	90	80	75	81.67	0.000074
7	0.56	105	95	95	98.33	0.000089
8	0.64	115	105	105	108.33	0.000098
9	0.72	130	115	115	120.00	0.000109
10	0.80	160	140	140	146.67	0.000133
11	0.88	180	160	165	168.33	0.000153
12	0.95	190	170	175	178.33	0.000162
13	1.03	200	180	185	188.33	0.000171
14	1.11	220	200	205	208.33	0.000189
15	1.19	245	230	235	236.67	0.000215
16	1.27	260	240	255	251.67	0.000229
17	1.35	270	255	265	263.33	0.000239
18	1.43	290	275	280	281.67	0.000256
		Modulus of Elasticity		Cyl 1	Cyl 2	Average
				5713.4	5363	5538.2

Table 42: Modulus of elasticity data for batch 3 of voided slab concrete for specimen 2

Batch 3-Cylinder 1						
Load (kip)	Stress (ksi)	Run 1	Run 2	Run 3	Average	Strain
0	0	0	0	0	0	0
1	0.08	5	5	5	5.00	0.000005
2	0.16	10	15	15	13.33	0.000012
3	0.24	25	25	20	23.33	0.000021
4	0.32	40	40	35	38.33	0.000035
5	0.40	60	60	55	58.33	0.000053
6	0.48	70	70	65	68.33	0.000062
7	0.56	80	80	75	78.33	0.000071
8	0.64	95	90	85	90.00	0.000082
9	0.72	105	100	95	100.00	0.000091

10	0.80	120	110	105	111.67	0.000102
11	0.88	135	130	120	128.33	0.000117
12	0.95	150	145	140	145.00	0.000132
13	1.03	160	155	155	156.67	0.000142
14	1.11	170	165	170	168.33	0.000153
15	1.19	180	175	175	176.67	0.000161
16	1.27	195	185	185	188.33	0.000171
17	1.35	205	195	195	198.33	0.000180
18	1.43	215	210	205	210.00	0.000191
Batch 3-Cylinder 2						
Load (kip)	Stress (ksi)	Run 1	Run 2	Run 3	Average	Strain
0	0	0	0	0	0	0
1	0.08	5	5	5	5.00	0.000005
2	0.16	10	10	10	10.00	0.000009
3	0.24	15	20	20	18.33	0.000017
4	0.32	30	30	35	31.67	0.000029
5	0.40	45	45	45	45.00	0.000041
6	0.48	65	65	70	66.67	0.000061
7	0.56	75	80	85	80.00	0.000073
8	0.64	85	90	90	88.33	0.000080
9	0.72	95	100	105	100.00	0.000091
10	0.80	105	115	115	111.67	0.000102
11	0.88	120	135	135	130.00	0.000118
12	0.95	135	155	155	148.33	0.000135
13	1.03	150	165	165	160.00	0.000145
14	1.11	160	175	175	170.00	0.000155
15	1.19	170	185	190	181.67	0.000165
16	1.27	180	205	205	196.67	0.000179
17	1.35	195	230	225	216.67	0.000197
18	1.43	210	240	240	230.00	0.000209
		Modulus of Elasticity		Cyl 1	Cyl 2	Average
				7131	6553.9	6842.45

Specimen 3: Ductal UHPC Connection

Table 43: Pull off data for specimen 3

Batch 1				
	Age (days)	Force (lb)	Bond Strength (psi)	Average
Puck 1	7	720	229.18	224.41
Puck 2	7	690	219.63	
Puck 3	15	500	159.15	213.27
Puck 4	15	840	267.38	
Batch 2				
	Age (days)	Force (lb)	Bond Strength (psi)	Average
Puck 1	7	790	251.46	235.55
Puck 2	7	690	219.63	
Puck 3	15	970	308.76	308.76
Puck 4	15	*N/A	*N/A	

Epoxy bond broke at 600 lb, before the UHPC to concrete bond was broken

Table 44: UHPC strength data for specimen 3

Cube	Age (Days)	Force (kips)	Time (sec)	Strength (ksi)	Average (ksi)
1	7	49.5	73	12.38	11.25
2	7	44.5	81	11.13	
3	7	41	71	10.25	
4	12	62	100	15.50	15.5
5	12	61.5	111	15.38	
6	12	62.5	114	15.63	

Table 45: Shrinkage data for UHPC for specimen 3

Age (days)	Bar 1	Bar 1 Avg.	Bar 1 Diff.	Bar 1 Strain	Bar 2	Bar 2 Avg.	Bar 2 Diff.	Bar 2 Strain
4	0.2708	0.2709	N/A	N/A	0.3317	0.3316	N/A	N/A
	0.2710				0.3316			
	0.2709				0.3315			
5	0.2704	0.2703	0.0006	0.000050	0.3306	0.3307	0.0009	0.000080
	0.2703				0.3308			
	0.2703				0.3307			
6	0.2696	0.2696	0.0013	0.000116	0.3299	0.3300	0.0016	0.000145
	0.2696				0.3300			
	0.2696				0.3300			
7	0.2690	0.2690	0.0019	0.000172	0.3295	0.3294	0.0022	0.000196

	0.2689				0.3294			
	0.2690				0.3293			
	0.2686				0.3289			
8	0.2686	0.2686	0.0023	0.000207	0.3287	0.3287	0.0029	0.000255
	0.2685				0.3286			
	0.2683				0.3281			
9	0.2682	0.2683	0.0026	0.000228	0.3280	0.3280	0.0036	0.000320
	0.2685				0.3279			
	0.2678				0.3277			
10	0.2678	0.2678	0.0031	0.000276	0.3277	0.3277	0.0039	0.000350
	0.2678				0.3276			
	0.2675				0.3274			
11	0.2675	0.2675	0.0034	0.000305	0.3275	0.3275	0.0041	0.000367
	0.2674				0.3275			
	0.2673				0.3274			
12	0.2673	0.2673	0.0036	0.000317	0.3273	0.3273	0.0043	0.000379
	0.2674				0.3273			

Table 46: Modulus of elasticity data for UHPC on the first day of testing for specimen 3

Cylinder 1						
Load (kip)	Stress (ksi)	Run 1	Run 2	Run 3	Average	Strain
0	0	0	0	0	0	0
2.5	0.20	30	25	25	26.67	0.000024
5	0.40	65	55	55	58.33	0.000053
7.5	0.60	85	75	80	80.00	0.000073
10	0.80	130	110	115	118.33	0.000108
12.5	0.99	150	140	140	143.33	0.000130
15	1.19	185	165	170	173.33	0.000158
17.5	1.39	220	205	205	210.00	0.000191
20	1.59	240	225	225	230.00	0.000209
22.5	1.79	275	265	255	265.00	0.000241
25	1.99	300	295	295	296.67	0.000270
27.5	2.19	325	320	320	321.67	0.000292
30	2.39	360	365	360	361.67	0.000329
32.5	2.59	390	385	385	386.67	0.000352
35	2.79	415	415	415	415.00	0.000377
Cylinder 2						
Load (kip)	Stress (ksi)	Run 1	Run 2	Run 3	Average	Strain
0	0	0	0	0	0	0
2.5	0.20	30	30	20	26.67	0.000024

5	0.40	50	65	55	56.67	0.000052
7.5	0.60	75	85	75	78.33	0.000071
10	0.80	110	110	110	110.00	0.000100
12.5	0.99	130	150	145	141.67	0.000129
15	1.19	170	170	165	168.33	0.000153
17.5	1.39	200	210	205	205.00	0.000186
20	1.59	220	240	230	230.00	0.000209
22.5	1.79	260	260	255	258.33	0.000235
25	1.99	285	305	295	295.00	0.000268
27.5	2.19	320	325	315	320.00	0.000291
30	2.39	355	360	360	358.33	0.000326
32.5	2.59	375	390	390	385.00	0.000350
35	2.79	415	415	415	415.00	0.000377
Cylinder 3						
Load (kip)	Stress (ksi)	Run 1	Run 2	Run 3	Average	Strain
0	0	0	0	0	0	0
2.5	0.20	20	15	15	16.67	0.000015
5	0.40	40	40	40	40.00	0.000036
7.5	0.60	85	85	85	85.00	0.000077
10	0.80	110	110	110	110.00	0.000100
12.5	0.99	150	155	155	153.33	0.000139
15	1.19	185	180	180	181.67	0.000165
17.5	1.39	220	215	215	216.67	0.000197
20	1.59	260	250	250	253.33	0.000230
22.5	1.79	290	280	275	281.67	0.000256
25	1.99	330	320	320	323.33	0.000294
27.5	2.19	360	345	345	350.00	0.000318
30	2.39	405	385	380	390.00	0.000355
32.5	2.59	430	420	415	421.67	0.000383
35	2.79	480	455	445	460.00	0.000418
	Modulus of Elasticity		Cyl 1	Cyl 2	Cyl 3	Average
			7404.5	7471	6841.7	7239.067

Table 47: Modulus of elasticity data for UHPC on the last day of testing for specimen 3

Cylinder 4						
Load (kip)	Stress (ksi)	Run 1	Run 2	Run 3	Average	Strain
0	0	0	0	0	0	0
2.5	0.20	15	15	20	16.67	0.000015
5	0.40	50	60	55	55.00	0.000050
7.5	0.60	80	80	75	78.33	0.000071

10	0.80	105	110	100	105.00	0.000095
12.5	0.99	145	145	140	143.33	0.000130
15	1.19	170	170	160	166.67	0.000152
17.5	1.39	205	200	190	198.33	0.000180
20	1.59	235	230	225	230.00	0.000209
22.5	1.79	255	260	250	255.00	0.000232
25	1.99	295	295	285	291.67	0.000265
27.5	2.19	325	320	315	320.00	0.000291
30	2.39	355	350	340	348.33	0.000317
32.5	2.59	390	385	380	385.00	0.000350
35	2.79	420	410	400	410.00	0.000373
Cylinder 5						
Load (kip)	Stress (ksi)	Run 1	Run 2	Run 3	Average	Strain
0	0	0	0	0	0	0
2.5	0.20	20	15	15	16.67	0.000015
5	0.40	55	45	50	50.00	0.000045
7.5	0.60	80	70	75	75.00	0.000068
10	0.80	100	90	90	93.33	0.000085
12.5	0.99	130	125	125	126.67	0.000115
15	1.19	160	155	150	155.00	0.000141
17.5	1.39	180	180	170	176.67	0.000161
20	1.59	220	220	205	215.00	0.000195
22.5	1.79	245	240	235	240.00	0.000218
25	1.99	270	270	255	265.00	0.000241
27.5	2.19	310	305	300	305.00	0.000277
30	2.39	330	330	320	326.67	0.000297
32.5	2.59	365	365	345	358.33	0.000326
35	2.79	400	395	390	395.00	0.000359
Cylinder 6						
Load (kip)	Stress (ksi)	Run 1	Run 2	Run 3	Average	Strain
0	0	0	0	0	0	0
2.5	0.20	20	20	25	21.67	0.000020
5	0.40	60	55	60	58.33	0.000053
7.5	0.60	80	75	80	78.33	0.000071
10	0.80	105	100	95	100.00	0.000091
12.5	0.99	140	140	140	140.00	0.000127
15	1.19	160	160	165	161.67	0.000147
17.5	1.39	185	195	195	191.67	0.000174
20	1.59	225	230	230	228.33	0.000208
22.5	1.79	245	250	250	248.33	0.000226
25	1.99	275	290	290	285.00	0.000259

27.5	2.19	310	315	320	315.00	0.000286
30	2.39	335	340	345	340.00	0.000309
32.5	2.59	375	380	380	378.33	0.000344
35	2.79	395	400	405	400.00	0.000364
	Modulus of Elasticity		Cyl 1	Cyl 2	Cyl 3	Average
			7554	8063	7718	7778.333

Table 48: Voided slab concrete strength data for specimen 3

	Cylinder	Force (kips)	Time (sec)	Strength (ksi)	Average Strength (ksi)
Batch 1	1	98	173	7.80	7.16
Batch 1	2	82	165	6.53	
Batch 2	1	83	162	6.60	7.28
Batch 2	2	100	211	7.96	

Table 49: Modulus of elasticity data for batch 1 of the voided slab concrete for specimen 3

Batch I - Cylinder 1						
Load (kip)	Stress (ksi)	Run 1	Run 2	Run 3	Average	Strain
0	0	0	0	0	0	0
1	0.08	5	5	10	6.67	0.000006
2	0.16	20	25	30	25.00	0.000023
3	0.24	30	50	55	45.00	0.000041
4	0.32	40	65	65	56.67	0.000052
5	0.40	55	80	80	71.67	0.000065
6	0.48	75	100	100	91.67	0.000083
7	0.56	100	130	130	120.00	0.000109
8	0.64	115	145	145	135.00	0.000123
9	0.72	135	160	160	151.67	0.000138
10	0.80	160	180	180	173.33	0.000158
11	0.88	185	210	210	201.67	0.000183
12	0.95	200	225	220	215.00	0.000195
13	1.03	225	240	240	235.00	0.000214
14	1.11	255	260	255	256.67	0.000233
15	1.19	275	285	280	280.00	0.000255
16	1.27	290	305	300	298.33	0.000271
17	1.35	315	315	310	313.33	0.000285
18	1.43	345	335	330	336.67	0.000306
Batch I - Cylinder 2						
Load (kip)	Stress (ksi)	Run 1	Run 2	Run 3	Average	Strain
0	0	0	0	0	0	0

1	0.08	5	5	5	5.00	0.000005
2	0.16	15	15	15	15.00	0.000014
3	0.24	30	25	30	28.33	0.000026
4	0.32	50	45	45	46.67	0.000042
5	0.40	70	70	70	70.00	0.000064
6	0.48	85	85	80	83.33	0.000076
7	0.56	95	95	90	93.33	0.000085
8	0.64	105	105	105	105.00	0.000095
9	0.72	125	120	120	121.67	0.000111
10	0.80	145	140	140	141.67	0.000129
11	0.88	160	160	160	160.00	0.000145
12	0.95	170	170	165	168.33	0.000153
13	1.03	185	180	175	180.00	0.000164
14	1.11	200	190	190	193.33	0.000176
15	1.19	220	205	210	211.67	0.000192
16	1.27	240	230	230	233.33	0.000212
17	1.35	250	245	245	246.67	0.000224
18	1.43	265	255	255	258.33	0.000235
		Modulus of Elasticity		Cyl 1	Cyl 2	Average
				4825.8	5863.4	5344.6

Table 50: Modulus of elasticity data for batch 2 of the voided slab concrete for specimen 3

Batch 2 - Cylinder 1						
Load (kip)	Stress (ksi)	Run 1	Run 2	Run 3	Average	Strain
0	0	0	0	0	0	0
1	0.08	10	10	10	10.00	0.000009
2	0.16	25	25	25	25.00	0.000023
3	0.24	50	50	45	48.33	0.000044
4	0.32	65	65	60	63.33	0.000058
5	0.40	80	75	70	75.00	0.000068
6	0.48	90	90	85	88.33	0.000080
7	0.56	110	105	100	105.00	0.000095
8	0.64	130	125	120	125.00	0.000114
9	0.72	145	145	140	143.33	0.000130
10	0.80	155	155	150	153.33	0.000139
11	0.88	170	165	160	165.00	0.000150
12	0.95	185	175	170	176.67	0.000161
13	1.03	205	195	185	195.00	0.000177
14	1.11	225	215	210	216.67	0.000197
15	1.19	235	230	225	230.00	0.000209

16	1.27	245	240	235	240.00	0.000218
17	1.35	260	250	245	251.67	0.000229
18	1.43	280	265	260	268.33	0.000244
Batch 2 - Cylinder 2						
Load (kip)	Stress (ksi)	Run 1	Run 2	Run 3	Average	Strain
0	0	0	0	0	0	0
1	0.08	15	5	10	10.00	0.000009
2	0.16	35	15	30	26.67	0.000024
3	0.24	45	30	40	38.33	0.000035
4	0.32	60	40	50	50.00	0.000045
5	0.40	75	55	60	63.33	0.000058
6	0.48	100	75	75	83.33	0.000076
7	0.56	115	90	95	100.00	0.000091
8	0.64	125	100	110	111.67	0.000102
9	0.72	135	115	125	125.00	0.000114
10	0.80	155	125	135	138.33	0.000126
11	0.88	175	145	145	155.00	0.000141
12	0.95	190	165	165	173.33	0.000158
13	1.03	205	175	190	190.00	0.000173
14	1.11	215	185	205	201.67	0.000183
15	1.19	225	200	215	213.33	0.000194
16	1.27	245	220	230	231.67	0.000211
17	1.35	270	245	250	255.00	0.000232
18	1.43	280	255	275	270.00	0.000245
		Modulus of Elasticity		Cyl 1	Cyl 2	Average
				5788	5825.7	5806.85

Specimen 4: VHPC Connection

Table 51: Pull off Data for specimen 4

Batch 1				
	Age (days)	Force (lb)	Bond Strength (psi)	Average
Puck 1	7	650	206.90	205.31
Puck 2	7	640	203.72	
Puck 3	15	720	229.18	216.45
Puck 4	15	640	203.72	
Batch 3				
	Age (days)	Force (lb)	Bond Strength (psi)	Average
Puck 1	7	710	226.00	186.21
Puck 2	7	460	146.42	
Puck 3	15	*N/A	*N/A	235.55
Puck 4	15	740	235.55	

Epoxy bond broke at 450 lb, before the VHPC to concrete bond was broken

Table 52: VHPC strength data for specimen 4

Cylinder	Age (Days)	Force (kips)	Time (sec)	Strength (ksi)	Average (ksi)
1	7	149.5	276	11.90	12.40
2	7	166	302	13.21	
3	7	152	299	12.10	
4	12	173	346	13.77	13.90
5	12	168.5	330	13.41	
6	12	182.5	357	14.52	

Table 53: VHPC Shrinkage Data for specimen 4

Age (days)	Bar 1	Bar 1 Avg.	Bar 1 Diff.	Bar 1 Strain	Bar 2	Bar 2 Avg.	Bar 2 Diff.	Bar 2 Strain
4	0.2861	0.2860	N/A	N/A	0.2608	0.2608	N/A	N/A
	0.2859				0.2609			
	0.2860				0.2608			
5	0.2853	0.2853	0.0007	0.000059	0.2601	0.2601	0.0007	0.000062
	0.2853				0.2602			
	0.2854				0.2601			
6	0.2848	0.2848	0.0012	0.000107	0.2596	0.2596	0.0012	0.000110
	0.2849				0.2596			
	0.2847				0.2596			

7	0.2844	0.2844	0.0016	0.000142	0.2593	0.2592	0.0016	0.000142
	0.2844				0.2592			
	0.2844				0.2592			
8	0.2841	0.2841	0.0019	0.000166	0.2589	0.2589	0.0019	0.000172
	0.2842				0.2589			
	0.2841				0.2589			
9	0.2831	0.2831	0.0029	0.000258	0.2580	0.2580	0.0028	0.000252
	0.2832				0.2580			
	0.2830				0.2580			
10	0.2830	0.2830	0.0030	0.000267	0.2580	0.2580	0.0028	0.000252
	0.2830				0.2580			
	0.2830				0.2580			
11	0.2830	0.2830	0.0030	0.000267	0.2580	0.2580	0.0028	0.000252
	0.2830				0.2580			
	0.2830				0.2580			
12	0.2829	0.2829	0.0031	0.000279	0.2579	0.2579	0.0029	0.000258
	0.2827				0.2580			
	0.2830				0.2579			

Table 54: Modulus of Elasticity data for VHPC on the first day of testing for specimen 4

Cylinder 1						
Load (kip)	Stress (ksi)	Run 1	Run 2	Run 3	Average	Strain
0	0	0	0	0	0	0
2.5	0.20	40	45	50	45.00	4.09E-05
5	0.40	90	80	75	81.67	7.42E-05
7.5	0.60	125	120	130	125.00	0.000114
10	0.80	170	160	170	166.67	0.000152
12.5	0.99	205	200	215	206.67	0.000188
15	1.19	250	240	240	243.33	0.000221
17.5	1.39	285	290	290	288.33	0.000262
20	1.59	330	315	315	320.00	0.000291
22.5	1.79	365	360	370	365.00	0.000332
25	1.99	405	390	400	398.33	0.000362
27.5	2.19	440	435	445	440.00	0.0004
30	2.39	490	480	480	483.33	0.000439
32.5	2.59	525	515	520	520.00	0.000473
35	2.79	570	560	555	561.67	0.000511
Cylinder 2						
Load (kip)	Stress (ksi)	Run 1	Run 2	Run 3	Average	Strain
0	0	0	0	0	0	0

2.5	0.20	25	30	35	30.00	2.73E-05
5	0.40	65	75	75	71.67	6.52E-05
7.5	0.60	100	105	110	105.00	9.55E-05
10	0.80	145	155	155	151.67	0.000138
12.5	0.99	185	190	190	188.33	0.000171
15	1.19	230	240	235	235.00	0.000214
17.5	1.39	270	275	265	270.00	0.000245
20	1.59	310	320	315	315.00	0.000286
22.5	1.79	350	355	350	351.67	0.00032
25	1.99	385	395	395	391.67	0.000356
27.5	2.19	430	440	435	435.00	0.000395
30	2.39	475	485	480	480.00	0.000436
32.5	2.59	520	530	525	525.00	0.000477
35	2.79	560	570	555	561.67	0.000511
Cylinder 3						
Load (kip)	Stress (ksi)	Run 1	Run 2	Run 3	Average	Strain
0	0	0	0	0	0	0
2.5	0.20	20	20	25	21.67	1.97E-05
5	0.40	65	75	70	70.00	6.36E-05
7.5	0.60	105	115	110	110.00	0.0001
10	0.80	150	160	160	156.67	0.000142
12.5	0.99	180	195	195	190.00	0.000173
15	1.19	235	245	245	241.67	0.00022
17.5	1.39	275	285	285	281.67	0.000256
20	1.59	315	325	325	321.67	0.000292
22.5	1.79	365	380	385	376.67	0.000342
25	1.99	405	420	420	415.00	0.000377
27.5	2.19	445	470	470	461.67	0.00042
30	2.39	490	500	500	496.67	0.000452
32.5	2.59	540	550	550	546.67	0.000497
35	2.79	580	585	585	583.33	0.00053
	Modulus of Elasticity		Cyl 1	Cyl 2	Cyl 3	Average
			5436.4	5526.6	5294.9	5419.3

Table 55: Modulus of Elasticity data for VHPC on the final day of testing for specimen 4

Cylinder 4						
Load (kip)	Stress (ksi)	Run 1	Run 2	Run 3	Average	Strain
0	0	0	0	0	0	0
2.5	0.20	40	30	30	33.33	3.03E-05
5	0.40	65	60	60	61.67	5.61E-05

7.5	0.60	110	105	105	106.67	9.7E-05
10	0.80	140	135	135	136.67	0.000124
12.5	0.99	185	185	185	185.00	0.000168
15	1.19	220	215	220	218.33	0.000198
17.5	1.39	265	265	265	265.00	0.000241
20	1.59	300	295	295	296.67	0.00027
22.5	1.79	345	340	340	341.67	0.000311
25	1.99	380	370	370	373.33	0.000339
27.5	2.19	425	420	420	421.67	0.000383
30	2.39	460	450	450	453.33	0.000412
32.5	2.59	510	500	500	503.33	0.000458
35	2.79	545	535	530	536.67	0.000488
Cylinder 5						
Load (kip)	Stress (ksi)	Run 1	Run 2	Run 3	Average	Strain
0	0	0	0	0	0	0
2.5	0.20	35	25	20	26.67	2.42E-05
5	0.40	75	60	65	66.67	6.06E-05
7.5	0.60	110	100	100	103.33	9.39E-05
10	0.80	145	135	140	140.00	0.000127
12.5	0.99	195	180	185	186.67	0.00017
15	1.19	240	220	235	231.67	0.000211
17.5	1.39	275	260	270	268.33	0.000244
20	1.59	325	310	325	320.00	0.000291
22.5	1.79	365	345	355	355.00	0.000323
25	1.99	415	400	410	408.33	0.000371
27.5	2.19	445	435	440	440.00	0.0004
30	2.39	500	485	490	491.67	0.000447
32.5	2.59	530	515	525	523.33	0.000476
35	2.79	580	565	555	566.67	0.000515
Cylinder 6						
Load (kip)	Stress (ksi)	Run 1	Run 2	Run 3	Average	Strain
0	0	0	0	0	0	0
2.5	0.20	45	40	40	41.67	3.79E-05
5	0.40	80	75	75	76.67	6.97E-05
7.5	0.60	115	115	115	115.00	0.000105
10	0.80	155	150	150	151.67	0.000138
12.5	0.99	195	195	195	195.00	0.000177
15	1.19	235	230	235	233.33	0.000212
17.5	1.39	280	270	285	278.33	0.000253
20	1.59	320	310	320	316.67	0.000288
22.5	1.79	370	350	370	363.33	0.00033

25	1.99	400	395	400	398.33	0.000362
27.5	2.19	455	450	450	451.67	0.000411
30	2.39	490	480	485	485.00	0.000441
32.5	2.59	540	530	535	535.00	0.000486
35	2.79	575	560	565	566.67	0.000515
	Modulus of Elasticity		Cyl 1	Cyl 2	Cyl 3	Average
			5776.5	5472.4	5424.7	5557.87

Table 56: Voided slab concrete strength data for specimen 4

	Cylinder	Force (kips)	Time (sec)	Strength (ksi)	Average Strength (ksi)
Batch 2	1	94.5	181	7.52	7.58
Batch 2	2	96	189	7.64	
Batch 3	1	117	205	9.31	10.58
Batch 3	2	149	300	11.86	

Table 57: Modulus of elasticity data for batch 2 of the voided slab concrete for specimen 4

Batch 2-Cylinder 1						
Load (kip)	Stress (ksi)	Run 1	Run 2	Run 3	Average	Strain
0	0	0	0	0	0	0
1	0.08	15	10	10	11.67	0.000011
2	0.16	25	20	25	23.33	0.000021
3	0.24	35	30	35	33.33	0.000030
4	0.32	45	45	45	45.00	0.000041
5	0.40	60	60	65	61.67	0.000056
6	0.48	80	80	85	81.67	0.000074
7	0.56	100	95	100	98.33	0.000089
8	0.64	110	105	110	108.33	0.000098
9	0.72	120	115	120	118.33	0.000108
10	0.80	135	130	135	133.33	0.000121
11	0.88	150	150	150	150.00	0.000136
12	0.95	175	170	170	171.67	0.000156
13	1.03	185	180	180	181.67	0.000165
14	1.11	195	190	190	191.67	0.000174
15	1.19	205	200	205	203.33	0.000185
16	1.27	225	220	220	221.67	0.000202
17	1.35	245	245	240	243.33	0.000221
18	1.43	260	260	255	258.33	0.000235
Batch 2-Cylinder 2						
Load (kip)	Stress (ksi)	Run 1	Run 2	Run 3	Average	Strain
0	0	0	0	0	0	0

1	0.08	5	5	5	5.00	0.000005
2	0.16	20	15	15	16.67	0.000015
3	0.24	30	25	30	28.33	0.000026
4	0.32	50	45	45	46.67	0.000042
5	0.40	75	65	65	68.33	0.000062
6	0.48	90	85	85	86.67	0.000079
7	0.56	100	95	95	96.67	0.000088
8	0.64	115	105	105	108.33	0.000098
9	0.72	135	125	120	126.67	0.000115
10	0.80	160	145	140	148.33	0.000135
11	0.88	170	165	165	166.67	0.000152
12	0.95	185	175	175	178.33	0.000162
13	1.03	200	185	185	190.00	0.000173
14	1.11	220	200	200	206.67	0.000188
15	1.19	240	220	220	226.67	0.000206
16	1.27	255	245	240	246.67	0.000224
17	1.35	265	250	250	255.00	0.000232
18	1.43	280	265	265	270.00	0.000245
		Modulus of Elasticity		Cyl 1	Cyl 2	Average
				6307.8	5546.3	5927.05

Table 58: Modulus of elasticity data for batch 3 of the voided slab concrete for specimen 4

Batch 3-Cylinder 1						
Load (kip)	Stress (ksi)	Run 1	Run 2	Run 3	Average	Strain
0	0	0	0	0	0	0
1	0.08	5	10	5	6.67	0.000006
2	0.16	15	25	25	21.67	0.000020
3	0.24	20	30	35	28.33	0.000026
4	0.32	30	40	40	36.67	0.000033
5	0.40	45	55	55	51.67	0.000047
6	0.48	60	75	65	66.67	0.000061
7	0.56	80	95	85	86.67	0.000079
8	0.64	95	105	105	101.67	0.000092
9	0.72	105	115	115	111.67	0.000102
10	0.80	115	125	125	121.67	0.000111
11	0.88	130	140	135	135.00	0.000123
12	0.95	155	160	150	155.00	0.000141
13	1.03	170	180	175	175.00	0.000159
14	1.11	180	190	190	186.67	0.000170
15	1.19	190	200	195	195.00	0.000177

16	1.27	205	210	205	206.67	0.000188
17	1.35	225	230	220	225.00	0.000205
18	1.43	245	250	240	245.00	0.000223
Batch 3-Cylinder 2						
Load (kip)	Stress (ksi)	Run 1	Run 2	Run 3	Average	Strain
0	0	0	0	0	0	0
1	0.08	5	5	5	5.00	0.000005
2	0.16	20	20	20	20.00	0.000018
3	0.24	35	35	35	35.00	0.000032
4	0.32	45	45	45	45.00	0.000041
5	0.40	50	50	50	50.00	0.000045
6	0.48	60	60	60	60.00	0.000055
7	0.56	70	70	70	70.00	0.000064
8	0.64	80	80	80	80.00	0.000073
9	0.72	100	100	100	100.00	0.000091
10	0.80	115	115	115	115.00	0.000105
11	0.88	125	125	125	125.00	0.000114
12	0.95	130	130	130	130.00	0.000118
13	1.03	140	140	140	140.00	0.000127
14	1.11	150	150	155	151.67	0.000138
15	1.19	165	165	170	166.67	0.000152
16	1.27	185	185	190	186.67	0.000170
17	1.35	200	200	205	201.67	0.000183
18	1.43	210	210	215	211.67	0.000192
		Modulus of Elasticity		Cyl 1	Cyl 2	Average
				6310	7419.2	6864.6

Specimen 5: Ductal UHPC Connection with Concrete Topping

Table 59: Pull off Data for specimen 5

Batch 1				
	Age (days)	Force (lb)	Bond Strength (psi)	Average
Puck 1	7	240	76.39	95.49
Puck 2	7	360	114.59	
Puck 3	12	620	197.35	216.45
Puck 4	12	740	235.55	
Batch 2				
	Age (days)	Force (lb)	Bond Strength (psi)	Average
Puck 1	7	540	171.89	178.25
Puck 2	7	580	184.62	
Puck 3	12	980	311.94	267.38
Puck 4	12	700	222.82	

Table 60: UHPC strength data for specimen 5

Cube	Age (Days)	Force (kips)	Time (sec)	Strength (ksi)	Average (ksi)
1	7	50.5	104	12.625	11.63
2	7	41.5	87	10.375	
3	7	47.5	89	11.875	
4	12	58	109	14.5	14.29
5	12	55	106	13.75	
6	12	58.5	112	14.625	

Table 61: UHPC Shrinkage Data for specimen 5

Age (days)	Bar 1	Bar 1 Avg.	Bar 1 Diff.	Bar 1 Strain	Bar 2	Bar 2 Avg.	Bar 2 Diff.	Bar 2 Strain
3	0.2966	0.2965	N/A	N/A	0.3658	0.3657	N/A	N/A
	0.2965				0.3657			
	0.2964				0.3657			
4	0.2958	0.2958	0.0007	0.000062	0.3647	0.3647	0.0010	0.000092
	0.2958				0.3648			
	0.2958				0.3646			
5	0.2951	0.2951	0.0014	0.000127	0.3640	0.3639	0.0018	0.000163

	0.2951				0.3638			
	0.2950				0.3639			
	0.2945				0.3634			
6	0.2944	0.2945	0.0020	0.000181	0.3633	0.3633	0.0024	0.000216
	0.2945				0.3632			
	0.2939				0.3627			
7	0.2937	0.2938	0.0027	0.000243	0.3628	0.3628	0.0029	0.000261
	0.2937				0.3629			
	0.2935				0.3624			
8	0.2936	0.2935	0.0030	0.000264	0.3624	0.3624	0.0033	0.000296
	0.2935				0.3624			
	0.2929				0.3621			
9	0.2930	0.2930	0.0035	0.000308	0.3620	0.3620	0.0037	0.000329
	0.2932				0.3620			
	0.2930				0.3620			
10	0.2930	0.2930	0.0035	0.000311	0.3620	0.3620	0.0037	0.000332
	0.2930				0.3620			
	0.2930				0.3620			
11	0.2929	0.2929	0.0036	0.000317	0.3619	0.3619	0.0038	0.000338
	0.2929				0.3619			
	0.2930				0.3619			
12	0.2929	0.2929	0.0036	0.000317	0.3619	0.3619	0.0038	0.000341
	0.2929				0.3619			

Table 62: Modulus of Elasticity data for UHPC on the first day of testing for specimen 5

Cylinder 1						
Load (kip)	Stress (ksi)	Run 1	Run 2	Run 3	Average	Strain
0	0	0	0	0	0	0
2.5	0.20	10	20	20	16.67	0.000015
5	0.40	40	65	65	56.67	0.000052
7.5	0.60	85	90	90	88.33	0.000080
10	0.80	110	125	135	123.33	0.000112
12.5	0.99	155	160	165	160.00	0.000145
15	1.19	175	190	195	186.67	0.000170
17.5	1.39	210	235	235	226.67	0.000206
20	1.59	245	260	260	255.00	0.000232
22.5	1.79	270	305	300	291.67	0.000265
25	1.99	315	330	330	325.00	0.000295
27.5	2.19	340	370	365	358.33	0.000326
30	2.39	380	405	400	395.00	0.000359

32.5	2.59	405	430	430	421.67	0.000383
35	2.79	440	475	470	461.67	0.000420
Cylinder 2						
Load (kip)	Stress (ksi)	Run 1	Run 2	Run 3	Average	Strain
0	0	0	0	0	0	0
2.5	0.20	40	30	25	31.67	0.000029
5	0.40	80	70	75	75.00	0.000068
7.5	0.60	120	95	95	103.33	0.000094
10	0.80	155	145	140	146.67	0.000133
12.5	0.99	180	170	165	171.67	0.000156
15	1.19	225	220	215	220.00	0.000200
17.5	1.39	255	245	245	248.33	0.000226
20	1.59	300	295	290	295.00	0.000268
22.5	1.79	325	325	315	321.67	0.000292
25	1.99	370	375	330	358.33	0.000326
27.5	2.19	400	405	375	393.33	0.000358
30	2.39	430	415	400	415.00	0.000377
32.5	2.59	475	450	430	451.67	0.000411
35	2.79	505	480	465	483.33	0.000439
Cylinder 3						
Load (kip)	Stress (ksi)	Run 1	Run 2	Run 3	Average	Strain
0	0	0	0	0	0	0
2.5	0.20	15	30	35	26.67	0.000024
5	0.40	70	70	70	70.00	0.000064
7.5	0.60	100	95	95	96.67	0.000088
10	0.80	145	140	140	141.67	0.000129
12.5	0.99	180	165	165	170.00	0.000155
15	1.19	230	210	215	218.33	0.000198
17.5	1.39	270	240	240	250.00	0.000227
20	1.59	315	290	295	300.00	0.000273
22.5	1.79	350	320	315	328.33	0.000298
25	1.99	395	360	355	370.00	0.000336
27.5	2.19	430	390	395	405.00	0.000368
30	2.39	475	430	430	445.00	0.000405
32.5	2.59	505	470	470	481.67	0.000438
35	2.79	550	500	500	516.67	0.000470
	Modulus of Elasticity		Cyl 1	Cyl 2	Cyl 3	Average
			6740	6205	5955	6300

Table 63: Modulus of Elasticity data for UHPC on the final day of testing for specimen 5

Cylinder 1						
Load (kip)	Stress (ksi)	Run 1	Run 2	Run 3	Average	Strain
0	0	0	0	0	0	0
2.5	0.20	15	15	25	18.33	0.000017
5	0.40	55	45	50	50.00	0.000045
7.5	0.60	85	80	90	85.00	0.000077
10	0.80	110	105	110	108.33	0.000098
12.5	0.99	150	135	145	143.33	0.000130
15	1.19	175	175	180	176.67	0.000161
17.5	1.39	205	205	210	206.67	0.000188
20	1.59	245	250	255	250.00	0.000227
22.5	1.79	265	270	280	271.67	0.000247
25	1.99	305	310	320	311.67	0.000283
27.5	2.19	335	340	350	341.67	0.000311
30	2.39	360	370	380	370.00	0.000336
32.5	2.59	405	415	420	413.33	0.000376
35	2.79	425	435	445	435.00	0.000395
Cylinder 6						
Load (kip)	Stress (ksi)	Run 1	Run 2	Run 3	Average	Strain
0	0	0	0	0	0	0
2.5	0.20	25	25	20	23.33	0.000021
5	0.40	50	50	45	48.33	0.000044
7.5	0.60	90	90	85	88.33	0.000080
10	0.80	110	110	105	108.33	0.000098
12.5	0.99	145	140	135	140.00	0.000127
15	1.19	180	180	175	178.33	0.000162
17.5	1.39	205	200	195	200.00	0.000182
20	1.59	245	245	235	241.67	0.000220
22.5	1.79	270	270	260	266.67	0.000242
25	1.99	300	300	290	296.67	0.000270
27.5	2.19	340	345	335	340.00	0.000309
30	2.39	365	370	355	363.33	0.000330
32.5	2.59	410	410	400	406.67	0.000370
35	2.79	435	435	425	431.67	0.000392
Cylinder 5						
Load (kip)	Stress (ksi)	Run 1	Run 2	Run 3	Average	Strain
0	0	0	0	0	0	0

2.5	0.20	35	35	35	35.00	0.000032
5	0.40	65	55	55	58.33	0.000053
7.5	0.60	105	95	90	96.67	0.000088
10	0.80	135	125	125	128.33	0.000117
12.5	0.99	155	145	145	148.33	0.000135
15	1.19	195	185	195	191.67	0.000174
17.5	1.39	220	215	220	218.33	0.000198
20	1.59	245	250	260	251.67	0.000229
22.5	1.79	290	285	295	290.00	0.000264
25	1.99	315	315	335	321.67	0.000292
27.5	2.19	360	360	365	361.67	0.000329
30	2.39	380	380	390	383.33	0.000348
32.5	2.59	415	415	420	416.67	0.000379
35	2.79	450	450	455	451.67	0.000411
	Modulus of Elasticity		Cyl 1	Cyl 2	Cyl 3	Average
			7099.2	7223.1	6825.2	7049.167

Table 64: Voided slab concrete strength data for specimen 5

	Cylinder	Force (kips)	Time (sec)	Strength (ksi)	Average Strength (ksi)
Batch 1	1	93.5	177	7.44	7.60
Batch 1	2	97.5	201	7.76	
Batch 2	1	93	194	7.40	7.24
Batch 2	2	89	167	7.08	

Table 65: Modulus of elasticity data for batch 1 of the voided slab concrete for specimen 5

Batch I - Cylinder 1						
Load (kip)	Stress (ksi)	Run 1	Run 2	Run 3	Average	Strain
0	0	0	0	0	0	0
1	0.08	5	5	10	6.67	0.000006
2	0.16	20	20	30	23.33	0.000021
3	0.24	30	30	40	33.33	0.000030
4	0.32	40	45	50	45.00	0.000041
5	0.40	50	60	65	58.33	0.000053
6	0.48	70	75	80	75.00	0.000068
7	0.56	95	95	105	98.33	0.000089
8	0.64	110	105	115	110.00	0.000100
9	0.72	120	120	125	121.67	0.000111
10	0.80	135	130	140	135.00	0.000123

11	0.88	160	155	155	156.67	0.000142
12	0.95	180	175	175	176.67	0.000161
13	1.03	190	185	190	188.33	0.000171
14	1.11	200	200	200	200.00	0.000182
15	1.19	210	215	210	211.67	0.000192
16	1.27	240	230	230	233.33	0.000212
17	1.35	260	255	250	255.00	0.000232
18	1.43	275	265	270	270.00	0.000245
Batch I - Cylinder 2						
Load (kip)	Stress (ksi)	Run 1	Run 2	Run 3	Average	Strain
0	0	0	0	0	0	0
1	0.08	10	5	10	8.33	0.000008
2	0.16	15	15	20	16.67	0.000015
3	0.24	30	30	30	30.00	0.000027
4	0.32	45	50	55	50.00	0.000045
5	0.40	70	75	75	73.33	0.000067
6	0.48	90	85	90	88.33	0.000080
7	0.56	100	100	100	100.00	0.000091
8	0.64	115	115	120	116.67	0.000106
9	0.72	135	140	140	138.33	0.000126
10	0.80	160	160	160	160.00	0.000145
11	0.88	175	170	170	171.67	0.000156
12	0.95	190	185	185	186.67	0.000170
13	1.03	205	205	205	205.00	0.000186
14	1.11	230	230	230	230.00	0.000209
15	1.19	250	245	245	246.67	0.000224
16	1.27	260	260	260	260.00	0.000236
17	1.35	275	275	275	275.00	0.000250
18	1.43	295	300	300	298.33	0.000271
		Modulus of Elasticity		Cyl 1	Cyl 2	Average
				6080	5112	5596

Table 66: Modulus of elasticity data for batch 2 of the voided slab concrete for specimen 5

Batch 2 - Cylinder 1						
Load (kip)	Stress (ksi)	Run 1	Run 2	Run 3	Average	Strain
0	0	0	0	0	0	0
1	0.08	5	15	10	10.00	0.000009
2	0.16	20	25	20	21.67	0.000020
3	0.24	40	35	30	35.00	0.000032
4	0.32	60	50	45	51.67	0.000047

5	0.40	70	65	65	66.67	0.000061
6	0.48	80	95	85	86.67	0.000079
7	0.56	95	105	100	100.00	0.000091
8	0.64	120	115	110	115.00	0.000105
9	0.72	140	130	125	131.67	0.000120
10	0.80	150	145	145	146.67	0.000133
11	0.88	160	170	165	165.00	0.000150
12	0.95	180	185	175	180.00	0.000164
13	1.03	200	195	185	193.33	0.000176
14	1.11	220	210	200	210.00	0.000191
15	1.19	235	225	215	225.00	0.000205
16	1.27	245	250	240	245.00	0.000223
17	1.35	265	265	255	261.67	0.000238
18	1.43	290	275	265	276.67	0.000252
Batch 2 - Cylinder 2						
Load (kip)	Stress (ksi)	Run 1	Run 2	Run 3	Average	Strain
0	0	0	0	0	0	0
1	0.08	5	5	5	5.00	0.000005
2	0.16	30	30	30	30.00	0.000027
3	0.24	45	45	45	45.00	0.000041
4	0.32	55	50	55	53.33	0.000048
5	0.40	70	65	65	66.67	0.000061
6	0.48	85	75	80	80.00	0.000073
7	0.56	110	95	95	100.00	0.000091
8	0.64	130	115	120	121.67	0.000111
9	0.72	140	130	130	133.33	0.000121
10	0.80	150	140	140	143.33	0.000130
11	0.88	170	150	155	158.33	0.000144
12	0.95	190	165	170	175.00	0.000159
13	1.03	210	190	195	198.33	0.000180
14	1.11	220	205	205	210.00	0.000191
15	1.19	230	215	215	220.00	0.000200
16	1.27	250	230	230	236.67	0.000215
17	1.35	275	245	245	255.00	0.000232
18	1.43	290	270	275	278.33	0.000253
		Modulus of Elasticity		Cyl 1	Cyl 2	Average
				5570	5696	5633.00

Table 67: Topping concrete strength data for specimen 5

Cylinder	Age (Days)	Force (kips)	Time (sec)	Strength (ksi)	Average (ksi)
1	7	47.5	81	3.78	3.78
2	7	48	87	3.82	
3	7	47	83	3.74	
4	12	61	118	4.85	4.50
5	12	56	102	4.46	
6	12	52.5	98	4.18	

Table 68: Modulus data on the first day of testing of the topping concrete for specimen 5

Cylinder 1						
Load (kip)	Stress (ksi)	Run 1	Run 2	Run 3	Average	Strain
0	0	0	0	0	0	0
1	0.08	10	10	15	11.67	0.000011
2	0.16	40	35	45	40.00	0.000036
3	0.24	55	55	60	56.67	0.000052
4	0.32	75	70	75	73.33	0.000067
5	0.40	95	95	100	96.67	0.000088
6	0.48	130	125	130	128.33	0.000117
7	0.56	145	145	145	145.00	0.000132
8	0.64	170	165	170	168.33	0.000153
9	0.72	205	195	200	200.00	0.000182
10	0.80	225	215	220	220.00	0.000200
11	0.88	245	235	235	238.33	0.000217
12	0.95	280	255	265	266.67	0.000242
13	1.03	300	290	290	293.33	0.000267
14	1.11	325	305	305	311.67	0.000283
Cylinder 2						
Load (kip)	Stress (ksi)	Run 1	Run 2	Run 3	Average	Strain
0	0	0	0	0	0	0
1	0.08	10	5	10	8.33	0.000008
2	0.16	30	20	20	23.33	0.000021
3	0.24	45	35	35	38.33	0.000035
4	0.32	55	55	60	56.67	0.000052
5	0.40	80	85	90	85.00	0.000077
6	0.48	110	100	105	105.00	0.000095
7	0.56	125	120	125	123.33	0.000112
8	0.64	150	150	150	150.00	0.000136

9	0.72	180	170	175	175.00	0.000159
10	0.80	205	190	190	195.00	0.000177
11	0.88	225	215	210	216.67	0.000197
12	0.95	255	245	245	248.33	0.000226
13	1.03	280	260	260	266.67	0.000242
14	1.11	305	280	280	288.33	0.000262
Cylinder 3						
Load (kip)	Stress (ksi)	Run 1	Run 2	Run 3	Average	Strain
0	0	0	0	0	0	0
1	0.08	10	10	5	8.33	0.000008
2	0.16	40	40	35	38.33	0.000035
3	0.24	50	55	55	53.33	0.000048
4	0.32	70	70	70	70.00	0.000064
5	0.40	90	95	95	93.33	0.000085
6	0.48	115	125	125	121.67	0.000111
7	0.56	130	140	140	136.67	0.000124
8	0.64	150	160	160	156.67	0.000142
9	0.72	175	185	185	181.67	0.000165
10	0.80	200	210	210	206.67	0.000188
11	0.88	215	225	225	221.67	0.000202
12	0.95	240	250	245	245.00	0.000223
13	1.03	275	280	275	276.67	0.000252
14	1.11	290	295	295	293.33	0.000267
	Modulus of Elasticity		Cyl 1	Cyl 2	Cyl 3	Average
			4001	4436	4281	4239.333

Table 69: Modulus data on the last day of testing for the topping concrete of specimen 5

Cylinder 5						
Load (kip)	Stress (ksi)	Run 1	Run 2	Run 3	Average	Strain
0	0	0	0	0	0	0
1	0.08	5	5	5	5.00	0.000005
2	0.16	20	30	30	26.67	0.000024
3	0.24	50	45	50	48.33	0.000044
4	0.32	70	60	60	63.33	0.000058
5	0.40	80	75	80	78.33	0.000071
6	0.48	95	95	95	95.00	0.000086
7	0.56	115	120	120	118.33	0.000108

8	0.64	140	135	135	136.67	0.000124
9	0.72	155	145	145	148.33	0.000135
10	0.80	170	165	165	166.67	0.000152
11	0.88	185	190	190	188.33	0.000171
12	0.95	210	210	210	210.00	0.000191
13	1.03	230	220	225	225.00	0.000205
14	1.11	245	240	245	243.33	0.000221
Cylinder 6						
Load (kip)	Stress (ksi)	Run 1	Run 2	Run 3	Average	Strain
0	0	0	0	0	0	0
1	0.08	10	10	10	10.00	0.000009
2	0.16	30	35	30	31.67	0.000029
3	0.24	55	45	40	46.67	0.000042
4	0.32	65	60	55	60.00	0.000055
5	0.40	80	75	75	76.67	0.000070
6	0.48	95	100	100	98.33	0.000089
7	0.56	125	120	115	120.00	0.000109
8	0.64	140	135	130	135.00	0.000123
9	0.72	150	155	150	151.67	0.000138
10	0.80	170	180	180	176.67	0.000161
11	0.88	195	205	200	200.00	0.000182
12	0.95	220	215	210	215.00	0.000195
13	1.03	230	235	230	231.67	0.000211
14	1.11	255	265	265	261.67	0.000238
Cylinder 7						
Load (kip)	Stress (ksi)	Run 1	Run 2	Run 3	Average	Strain
0	0	0	0	0	0	0
1	0.08	5	5	5	5.00	0.000005
2	0.16	20	20	25	21.67	0.000020
3	0.24	35	45	50	43.33	0.000039
4	0.32	60	65	65	63.33	0.000058
5	0.40	80	75	75	76.67	0.000070
6	0.48	90	90	90	90.00	0.000082
7	0.56	105	110	115	110.00	0.000100
8	0.64	130	135	135	133.33	0.000121
9	0.72	155	150	150	151.67	0.000138
10	0.80	170	165	160	165.00	0.000150
11	0.88	185	180	180	181.67	0.000165
12	0.95	205	205	210	206.67	0.000188
13	1.03	235	225	230	230.00	0.000209

14	1.11	250	240	245	245.00	0.000223
	Modulus of Elasticity		Cyl 1	Cyl 2	Cyl 3	Average
			5138.5	4942.2	5179	5086.567

Table 70: Shrinkage data for topping concrete of specimen 5

Age (days)	Bar 1	Bar 1 Avg.	Bar 1 Diff.	Bar 1 Strain	Bar 2	Bar 2 Avg.	Bar 2 Diff.	Bar 2 Strain
2	0.2542	0.2540	N/A	N/A	0.2754	0.2752	N/A	N/A
	0.2540				0.2753			
	0.2538				0.2749			
3	0.2535	0.2533	0.0007	0.000062	0.2746	0.2745	0.0007	0.000062
	0.2533				0.2745			
	0.2531				0.2744			
4	0.2529	0.2529	0.0011	0.000098	0.2740	0.2740	0.0012	0.000104
	0.2529				0.2741			
	0.2529				0.2740			
5	0.2523	0.2522	0.0018	0.000157	0.2735	0.2735	0.0017	0.000151
	0.2522				0.2735			
	0.2522				0.2735			
6	0.2517	0.2517	0.0023	0.000204	0.2731	0.2731	0.0021	0.000184
	0.2517				0.2732			
	0.2517				0.2731			
7	0.2516	0.2517	0.0023	0.000207	0.2731	0.2731	0.0021	0.000187
	0.2517				0.2731			
	0.2517				0.2731			
8	0.2514	0.2515	0.0025	0.000225	0.2727	0.2727	0.0025	0.000222
	0.2516				0.2727			
	0.2514				0.2727			

Specimen 6: VHPC Connection with Concrete Topping

Table 71: Pull off Data for specimen 6

Batch 2				
	Age (days)	Force (lb)	Bond Strength (psi)	Average
Puck 1	7	660	210	201
Puck 2	7	600	191	
Puck 3	12	720	229	258
Puck 4	12	900	286	
Batch 3				
	Age (days)	Force (lb)	Bond Strength (psi)	Average
Puck 1	7	740	236	166
Puck 2	7	300	95.5	
Puck 3	12	N/A	N/A	204
Puck 4	12	640	204	

Table 72: VHPC strength data for specimen 6

Cylinder	Age (Days)	Force (kips)	Time (sec)	Strength (ksi)	Average (ksi)
1	7	141	279	11.2	11.2
2	7	135.5	272	10.8	
3	7	147.5	298	11.7	
4	12	149.5	307	11.9	12.1
5	12	159.5	314	12.7	
6	12	146	297	11.6	

Table 73: VHPC Shrinkage Data for specimen 6

Age (days)	Bar 1	Bar 1 Avg.	Bar 1 Diff.	Bar 1 Strain	Bar 2	Bar 2 Avg.	Bar 2 Diff.	Bar 2 Strain
3	0.1763	0.1762	N/A	N/A	0.2815	0.2813	N/A	N/A
	0.1762				0.2813			
	0.1760				0.2812			
4	0.1752	0.1751	0.0011	0.000098	0.2802	0.2802	0.0011	0.000098
	0.1750				0.2803			
	0.1750				0.2802			
5	0.1745	0.1745	0.0017	0.000148	0.2797	0.2797	0.0016	0.000145

	0.1745				0.2797			
	0.1745				0.2797			
6	0.1736	0.1736	0.0026	0.000231	0.2790	0.2790	0.0023	0.000207
	0.1735				0.2790			
	0.1736				0.2790			
7	0.1730	0.1729	0.0032	0.000287	0.2785	0.2785	0.0028	0.000252
	0.1728				0.2785			
	0.1730				0.2785			
8	0.1725	0.1726	0.0036	0.000320	0.2781	0.2780	0.0033	0.000293
	0.1726				0.2780			
	0.1726				0.2780			
9	0.1724	0.1724	0.0038	0.000335	0.2779	0.2779	0.0034	0.000305
	0.1724				0.2779			
	0.1724				0.2779			
10	0.1721	0.1721	0.0041	0.000361	0.2776	0.2775	0.0038	0.000338
	0.1721				0.2775			
	0.1721				0.2775			
11	0.1720	0.1721	0.0041	0.000364	0.2774	0.2774	0.0039	0.000350
	0.1721				0.2774			
	0.1721				0.2774			
12	0.1718	0.1717	0.0045	0.000400	0.2771	0.2771	0.0042	0.000373
	0.1717				0.2772			
	0.1715				0.2771			

Table 74: Modulus of Elasticity data for VHPC on the first day of testing for specimen 6

Cylinder 1						
Load (kip)	Stress (ksi)	Run 1	Run 2	Run 3	Average	Strain
0	0	0	0	0	0	0
2.5	0.20	20	25	30	25.00	0.000023
5	0.40	70	75	80	75.00	0.000068
7.5	0.60	100	110	120	110.00	0.000100
10	0.80	145	155	165	155.00	0.000141
12.5	0.99	180	190	200	190.00	0.000173
15	1.19	235	245	260	246.67	0.000224
17.5	1.39	275	285	295	285.00	0.000259
20	1.59	325	335	325	328.33	0.000298
22.5	1.79	375	385	390	383.33	0.000348
25	1.99	420	430	435	428.33	0.000389
27.5	2.19	475	485	495	485.00	0.000441
30	2.39	520	535	540	531.67	0.000483

32.5	2.59	570	570	580	573.33	0.000521
35	2.79	620	625	640	628.33	0.000571
Cylinder 2						
Load (kip)	Stress (ksi)	Run 1	Run 2	Run 3	Average	Strain
0	0	0	0	0	0	0
2.5	0.20	30	40	30	33.33	0.000030
5	0.40	70	80	70	73.33	0.000067
7.5	0.60	110	130	115	118.33	0.000108
10	0.80	150	170	165	161.67	0.000147
12.5	0.99	210	220	210	213.33	0.000194
15	1.19	265	280	270	271.67	0.000247
17.5	1.39	305	320	310	311.67	0.000283
20	1.59	365	370	360	365.00	0.000332
22.5	1.79	415	425	425	421.67	0.000383
25	1.99	455	470	470	465.00	0.000423
27.5	2.19	500	520	510	510.00	0.000464
30	2.39	500	560	555	538.33	0.000489
32.5	2.59	585	605	595	595.00	0.000541
35	2.79	620	640	635	631.67	0.000574
Cylinder 3						
Load (kip)	Stress (ksi)	Run 1	Run 2	Run 3	Average	Strain
0	0	0	0	0	0	0
2.5	0.20	15	20	20	18.33	0.000017
5	0.40	45	55	65	55.00	0.000050
7.5	0.60	95	100	105	100.00	0.000091
10	0.80	130	160	160	150.00	0.000136
12.5	0.99	175	195	190	186.67	0.000170
15	1.19	220	235	235	230.00	0.000209
17.5	1.39	255	270	270	265.00	0.000241
20	1.59	300	320	320	313.33	0.000285
22.5	1.79	340	355	350	348.33	0.000317
25	1.99	385	400	400	395.00	0.000359
27.5	2.19	425	445	435	435.00	0.000395
30	2.39	475	480	480	478.33	0.000435
32.5	2.59	510	525	520	518.33	0.000471
35	2.79	570	585	575	576.67	0.000524
	Modulus of Elasticity		Cyl 1	Cly 2	Cly 3	Average
			5053	4817	5527	5132.333

Table 75: Modulus of Elasticity data for VHPC on the final day of testing for specimen 6

Cylinder 5						
Load (kip)	Stress (ksi)	Run 1	Run 2	Run 3	Average	Strain
0	0	0	0	0	0	0
2.5	0.20	20	25	30	25.00	0.000023
5	0.40	60	55	65	60.00	0.000055
7.5	0.60	90	95	90	91.67	0.000083
10	0.80	130	135	130	131.67	0.000120
12.5	0.99	160	155	165	160.00	0.000145
15	1.19	190	195	200	195.00	0.000177
17.5	1.39	235	245	240	240.00	0.000218
20	1.59	270	270	275	271.67	0.000247
22.5	1.79	315	310	305	310.00	0.000282
25	1.99	375	365	365	368.33	0.000335
27.5	2.19	420	425	430	425.00	0.000386
30	2.39	470	475	480	475.00	0.000432
32.5	2.59	525	520	525	523.33	0.000476
35	2.79	565	570	580	571.67	0.000520
Cylinder 6						
Load (kip)	Stress (ksi)	Run 1	Run 2	Run 3	Average	Strain
0	0	0	0	0	0	0
2.5	0.20	30	35	30	31.67	0.000029
5	0.40	65	70	60	65.00	0.000059
7.5	0.60	110	120	110	113.33	0.000103
10	0.80	150	165	160	158.33	0.000144
12.5	0.99	200	215	210	208.33	0.000189
15	1.19	255	270	265	263.33	0.000239
17.5	1.39	305	315	310	310.00	0.000282
20	1.59	365	365	360	363.33	0.000330
22.5	1.79	410	405	400	405.00	0.000368
25	1.99	450	455	460	455.00	0.000414
27.5	2.19	490	485	490	488.33	0.000444
30	2.39	520	525	530	525.00	0.000477
32.5	2.59	570	565	565	566.67	0.000515
35	2.79	605	595	600	600.00	0.000545
Cylinder 4						
Load (kip)	Stress (ksi)	Run 1	Run 2	Run 3	Average	Strain
0	0	0	0	0	0	0
2.5	0.20	30	25	20	25.00	0.000023
5	0.40	60	65	55	60.00	0.000055
7.5	0.60	105	115	105	108.33	0.000098

10	0.80	145	155	155	151.67	0.000138
12.5	0.99	195	210	205	203.33	0.000185
15	1.19	245	255	255	251.67	0.000229
17.5	1.39	290	295	295	293.33	0.000267
20	1.59	350	345	350	348.33	0.000317
22.5	1.79	400	395	395	396.67	0.000361
25	1.99	440	440	445	441.67	0.000402
27.5	2.19	485	480	480	481.67	0.000438
30	2.39	515	515	520	516.67	0.000470
32.5	2.59	565	550	555	556.67	0.000506
35	2.79	600	590	595	595.00	0.000541
	Modulus of Elasticity		Cyl 1	Cyl 2	Cyl 3	Average
			5760	4990	5100	5283

Table 76: Voided slab concrete strength data for specimen 6

	Cylinder	Force (kips)	Time (sec)	Strength (ksi)	Average Strength (ksi)
Batch 2	1	82	169	6.53	6.72
Batch 2	2	87	171	6.92	
Batch 3	1	117	229	9.31	9.53
Batch 3	2	122.5	246	9.75	

Table 77: Modulus of elasticity data for batch 2 of the voided slab concrete for specimen 6

Batch 2 - Cylinder 1						
Load (kip)	Stress (ksi)	Run 1	Run 2	Run 3	Average	Strain
0	0	0	0	0	0	0
1	0.08	15	15	15	15.00	0.000014
2	0.16	30	30	30	30.00	0.000027
3	0.24	40	45	45	43.33	0.000039
4	0.32	55	60	55	56.67	0.000052
5	0.40	70	65	75	70.00	0.000064
6	0.48	90	95	95	93.33	0.000085
7	0.56	115	110	115	113.33	0.000103
8	0.64	125	115	125	121.67	0.000111
9	0.72	135	130	135	133.33	0.000121
10	0.80	150	145	145	146.67	0.000133
11	0.88	165	170	160	165.00	0.000150
12	0.95	190	185	185	186.67	0.000170
13	1.03	205	195	195	198.33	0.000180
14	1.11	215	210	205	210.00	0.000191
15	1.19	225	220	225	223.33	0.000203

16	1.27	240	240	245	241.67	0.000220
17	1.35	260	255	260	258.33	0.000235
18	1.43	275	275	280	276.67	0.000252
Batch 2 - Cylinder 2						
Load (kip)	Stress (ksi)	Run 1	Run 2	Run 3	Average	Strain
0	0	0	0	0	0	0
1	0.08	5	10	10	8.33	0.000008
2	0.16	20	25	25	23.33	0.000021
3	0.24	40	45	50	45.00	0.000041
4	0.32	65	65	65	65.00	0.000059
5	0.40	70	75	75	73.33	0.000067
6	0.48	85	85	85	85.00	0.000077
7	0.56	95	95	100	96.67	0.000088
8	0.64	115	110	115	113.33	0.000103
9	0.72	140	135	140	138.33	0.000126
10	0.80	150	145	150	148.33	0.000135
11	0.88	160	155	155	156.67	0.000142
12	0.95	170	165	165	166.67	0.000152
13	1.03	185	185	180	183.33	0.000167
14	1.11	210	205	200	205.00	0.000186
15	1.19	230	225	225	226.67	0.000206
16	1.27	240	235	240	238.33	0.000217
17	1.35	250	250	245	248.33	0.000226
18	1.43	270	265	265	266.67	0.000242
		Modulus of Elasticity		Cyl 1	Cyl 2	Average
				5780	5880	5830

Table 78: Modulus of elasticity data for batch 3 of the voided slab concrete for specimen 6

Batch 3 - Cylinder 1						
Load (kip)	Stress (ksi)	Run 1	Run 2	Run 3	Average	Strain
0	0	0	0	0	0	0
1	0.08	5	5	5	5.00	0.000005
2	0.16	10	10	10	10.00	0.000009
3	0.24	15	20	20	18.33	0.000017
4	0.32	30	30	35	31.67	0.000029
5	0.40	45	45	45	45.00	0.000041
6	0.48	65	65	70	66.67	0.000061
7	0.56	75	80	85	80.00	0.000073
8	0.64	85	90	90	88.33	0.000080

9	0.72	95	100	105	100.00	0.000091
10	0.80	105	110	115	110.00	0.000100
11	0.88	120	125	135	126.67	0.000115
12	0.95	135	145	155	145.00	0.000132
13	1.03	150	160	165	158.33	0.000144
14	1.11	160	170	175	168.33	0.000153
15	1.19	170	180	190	180.00	0.000164
16	1.27	180	195	205	193.33	0.000176
17	1.35	195	210	225	210.00	0.000191
18	1.43	210	220	235	221.67	0.000202
Batch 3 - Cylinder 2						
Load (kip)	Stress (ksi)	Run 1	Run 2	Run 3	Average	Strain
0	0	0	0	0	0	0
1	0.08	5	5	5	5.00	0.000005
2	0.16	10	15	15	13.33	0.000012
3	0.24	25	25	20	23.33	0.000021
4	0.32	40	40	35	38.33	0.000035
5	0.40	60	60	55	58.33	0.000053
6	0.48	70	70	65	68.33	0.000062
7	0.56	80	80	75	78.33	0.000071
8	0.64	95	90	85	90.00	0.000082
9	0.72	105	100	100	101.67	0.000092
10	0.80	120	115	115	116.67	0.000106
11	0.88	135	130	130	131.67	0.000120
12	0.95	150	145	145	146.67	0.000133
13	1.03	160	155	160	158.33	0.000144
14	1.11	170	165	170	168.33	0.000153
15	1.19	180	175	180	178.33	0.000162
16	1.27	195	185	190	190.00	0.000173
17	1.35	205	195	205	201.67	0.000183
18	1.43	220	215	220	218.33	0.000198
		Modulus of Elasticity		Cyl 1	Cyl 2	Average
				6730	6990	6860.00

Table 79: Topping concrete strength data for specimen 6

Cylinder	Age (Days)	Force (kips)	Time (sec)	Strength (ksi)	Average (ksi)
1	7	45.5	94	3.62	3.65
2	7	45.5	92	3.62	
3	7	46.5	97	3.70	
4	12	57.5	105	4.58	4.36
5	12	53	104	4.22	
6	12	54	110	4.30	

Table 80: Modulus data on the first day of testing of the topping concrete for specimen 6

Cylinder 1						
Load (kip)	Stress (ksi)	Run 1	Run 2	Run 3	Average	Strain
0	0	0	0	0	0	0
1	0.08	10	10	15	11.67	0.000011
2	0.16	30	40	40	36.67	0.000033
3	0.24	55	60	60	58.33	0.000053
4	0.32	80	80	80	80.00	0.000073
5	0.40	95	105	100	100.00	0.000091
6	0.48	120	130	130	126.67	0.000115
7	0.56	155	150	145	150.00	0.000136
8	0.64	175	170	170	171.67	0.000156
9	0.72	200	205	205	203.33	0.000185
10	0.80	235	230	225	230.00	0.000209
11	0.88	255	250	245	250.00	0.000227
12	0.95	290	280	280	283.33	0.000258
13	1.03	320	310	310	313.33	0.000285
14	1.11	345	330	325	333.33	0.000303
Cylinder 2						
Load (kip)	Stress (ksi)	Run 1	Run 2	Run 3	Average	Strain
0	0	0	0	0	0	0
1	0.08	10	10	15	11.67	0.000011
2	0.16	25	30	30	28.33	0.000026
3	0.24	45	55	45	48.33	0.000044
4	0.32	70	65	60	65.00	0.000059
5	0.40	90	90	95	91.67	0.000083
6	0.48	110	115	120	115.00	0.000105
7	0.56	145	145	145	145.00	0.000132
8	0.64	170	165	160	165.00	0.000150
9	0.72	195	190	195	193.33	0.000176

10	0.80	235	225	225	228.33	0.000208
11	0.88	255	245	245	248.33	0.000226
12	0.95	290	275	270	278.33	0.000253
13	1.03	320	300	300	306.67	0.000279
14	1.11	345	325	320	330.00	0.000300
Cylinder 3						
Load (kip)	Stress (ksi)	Run 1	Run 2	Run 3	Average	Strain
0	0	0	0	0	0	0
1	0.08	5	15	10	10.00	0.000009
2	0.16	25	35	30	30.00	0.000027
3	0.24	55	60	55	56.67	0.000052
4	0.32	70	75	70	71.67	0.000065
5	0.40	90	100	100	96.67	0.000088
6	0.48	120	125	120	121.67	0.000111
7	0.56	145	150	145	146.67	0.000133
8	0.64	165	170	165	166.67	0.000152
9	0.72	190	200	200	196.67	0.000179
10	0.80	220	230	220	223.33	0.000203
11	0.88	235	240	235	236.67	0.000215
12	0.95	260	270	265	265.00	0.000241
13	1.03	290	295	290	291.67	0.000265
14	1.11	315	325	310	316.67	0.000288
	Modulus of Elasticity		Cyl 1	Cly 2	Cly 3	Average
			3805.2	3896.9	4008	3903.367

Table 81: Modulus data on the last day of testing for the topping concrete of specimen 6

Cylinder 4						
Load (kip)	Stress (ksi)	Run 1	Run 2	Run 3	Average	Strain
0	0	0	0	0	0	0
1	0.08	10	15	10	11.67	0.000011
2	0.16	30	30	25	28.33	0.000026
3	0.24	55	45	45	48.33	0.000044
4	0.32	65	60	60	61.67	0.000056
5	0.40	85	80	75	80.00	0.000073
6	0.48	110	105	95	103.33	0.000094
7	0.56	130	125	120	125.00	0.000114
8	0.64	150	140	130	140.00	0.000127
9	0.72	155	165	155	158.33	0.000144
10	0.80	175	185	185	181.67	0.000165
11	0.88	200	210	205	205.00	0.000186

12	0.95	225	220	215	220.00	0.000200
13	1.03	235	240	235	236.67	0.000215
14	1.11	265	265	260	263.33	0.000239
Cylinder 5						
Load (kip)	Stress (ksi)	Run 1	Run 2	Run 3	Average	Strain
0	0	0	0	0	0	0
1	0.08	5	15	5	8.33	0.000008
2	0.16	25	35	25	28.33	0.000026
3	0.24	55	60	50	55.00	0.000050
4	0.32	70	75	70	71.67	0.000065
5	0.40	90	100	95	95.00	0.000086
6	0.48	125	125	120	123.33	0.000112
7	0.56	145	150	140	145.00	0.000132
8	0.64	165	170	160	165.00	0.000150
9	0.72	185	195	180	186.67	0.000170
10	0.80	205	210	195	203.33	0.000185
11	0.88	225	230	215	223.33	0.000203
12	0.95	250	250	235	245.00	0.000223
13	1.03	270	265	260	265.00	0.000241
14	1.11	290	285	280	285.00	0.000259
Cylinder 6						
Load (kip)	Stress (ksi)	Run 1	Run 2	Run 3	Average	Strain
0	0	0	0	0	0	0
1	0.08	10	5	5	6.67	0.000006
2	0.16	25	20	20	21.67	0.000020
3	0.24	45	30	35	36.67	0.000033
4	0.32	55	55	55	55.00	0.000050
5	0.40	80	80	75	78.33	0.000071
6	0.48	110	100	105	105.00	0.000095
7	0.56	125	120	125	123.33	0.000112
8	0.64	150	150	150	150.00	0.000136
9	0.72	180	170	175	175.00	0.000159
10	0.80	205	190	190	195.00	0.000177
11	0.88	225	215	210	216.67	0.000197
12	0.95	255	245	245	248.33	0.000226
13	1.03	275	265	255	265.00	0.000241
14	1.11	290	280	280	283.33	0.000258
	Modulus of Elasticity		Cyl 1	Cly 2	Cly 3	Average
			4830	4310	4460	4533.333

Table 82: Shrinkage data for topping concrete of specimen 6

Age (days)	Bar 1	Bar 1 Avg.	Bar 1 Diff.	Bar 1 Strain	Bar 2	Bar 2 Avg.	Bar 2 Diff.	Bar 2 Strain
1	0.2526	0.2523	N/A	N/A	0.3054	0.3051	N/A	N/A
	0.2522				0.3050			
	0.2521				0.3048			
2	0.2518	0.2517	0.0006	0.000053	0.3040	0.3041	0.0010	0.000089
	0.2517				0.3041			
	0.2516				0.3041			
3	0.2511	0.2511	0.0012	0.000107	0.3037	0.3034	0.0017	0.000151
	0.2511				0.3033			
	0.2511				0.3031			
4	0.2507	0.2506	0.0017	0.000151	0.3029	0.3028	0.0022	0.000199
	0.2506				0.3027			
	0.2505				0.3029			
5	0.2503	0.2503	0.0020	0.000178	0.3025	0.3025	0.0026	0.000228
	0.2503				0.3025			
	0.2503				0.3025			
6	0.2498	0.2498	0.0025	0.000222	0.3023	0.3022	0.0028	0.000252
	0.2497				0.3022			
	0.2499				0.3022			
7	0.2497	0.2496	0.0027	0.000240	0.3018	0.3018	0.0033	0.000290
	0.2496				0.3018			
	0.2495				0.3018			
8	0.2492	0.2491	0.0032	0.000284	0.3015	0.3015	0.0036	0.000320
	0.2490				0.3014			
	0.2491				0.3015			

Appendix E: Supporting Calculations

Bearing Pad Stiffness Calculations:

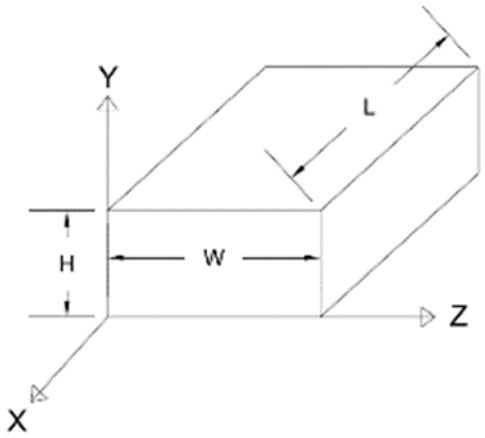

Assuming there is an elastomeric bearing pad at each corner of the beam so four in total. They will be 6"x9" in plan and 0.5" thick. They will be located three inches away from the edges of the beams.

$L := 6\ in \qquad W := 9\ in \qquad H := .5\ in \qquad h_{ri} := .5$

$A := L \cdot W = 54\ in^2 \qquad G := 127.5$

Shape Factor equation from AASHTO:

$$S := \frac{L \cdot W}{2 \cdot h_{ri} \cdot (L + W)} = 3.6$$

$$E_c := 6 \cdot G \cdot S^2$$

$$k_y := \frac{E_c \cdot A}{H \cdot 1000} = 1070.76 \ \frac{kip}{in}$$ vertical stiffness

$$k_x := \frac{G \cdot A}{H \cdot 1000} = 13.77 \ \frac{kip}{in}$$ horizontal stiffness